

Newcastle University

Understanding the Molecular Mechanisms of Mitochondrial Muscle Disease using a Quantitative, Quadruple Immunofluorescent Assay

Syeda Tasnim Ahmed

BSc (Hons) MRes

This thesis is submitted for the degree of Doctor of Philosophy

Wellcome Centre for Mitochondrial Research

Newcastle University; Translational and

Clinical Research Institute

Faculty of Medical Sciences

Newcastle University

December 2019



Author's declaration

This thesis is submitted for the degree of Doctor of Philosophy at Newcastle University. The research detailed within this thesis was conducted in the Wellcome Centre for Mitochondrial Research, Newcastle University and the Translational and Clinical Research Institute, Faculty of Medical Sciences, Newcastle University, under the supervision of Professor Sir Douglass M Turnbull, Professor Robert W Taylor and Dr Sarah J Pickett. Unless stated otherwise, all of the work presented in this thesis is my own and has been undertaken between April 2016 and November 2019.

I certify that none of the material offered in this thesis has been previously submitted by me for a degree or any other qualification at this or any other university.

For my Family,
With love

Abstract

Mitochondrial disease can be caused by pathogenic variants in either nuclear DNA or mitochondrial DNA (mtDNA). Affected patients present with a considerable genetic, clinical and biochemical heterogeneity, thereby complicating the diagnostic pathways. For pathogenic mtDNA variants, this is further compounded by heteroplasmy – the mixture of both wild-type and mutated mtDNA existing within a single cell. When the proportion of mutant mtDNA exceeds a critical threshold of mutated mtDNA molecules, the cell becomes biochemically dysfunctional. This dysfunction can be identified using a recently described quadruple immunofluorescent assay through the assessment of Complex I, Complex IV and porin protein expression in individual fibres within 10µm skeletal muscle sections from patients. The assessment of Complex I dysfunction is crucial, as deficiency of this particular respiratory chain complex is the most common form of mitochondrial dysfunction observed in mitochondrial disease. This thesis describes two studies that have utilised this assay with the aim of i) improving the diagnosis of mitochondrial disease and ii) understanding the molecular mechanisms underlying mitochondrial disease and the expression of a biochemical defect.

Given the lack of histochemical tests to interrogate Complex I in skeletal muscle, the viability of the quadruple immunofluorescent assay in detecting Complex I deficiency was assessed in a heterogeneous cohort of patients with genetically-proven pathogenic variants within mtDNA-encoded or nuclear-encoded (structural Complex I subunits or assembly factors) genes. Clear diagnostic potential was evident, particularly for patients with nuclear-encoded gene defects whilst highlighting the necessity of complete mitochondrial genome sequencing in the diagnostic work up of patients.

The quadruple immunofluorescent assay was also used to characterise –at a single cell level - the biochemical status of skeletal muscle fibres from patients harbouring the m.3243A>G mutation, the most prevalent, pathogenic heteroplasmic mtDNA point mutation. Two groups of patients were identified: those showing a predominance of Complex I deficiency and those expressing no biochemical defect in their skeletal muscle. Isolation of single muscle fibres enabled investigation of the relationship between the biochemical deficiency and single fibre m.3243A>G heteroplasmy, identifying differences in the biochemical threshold for Complex I deficiency between patients.

Acknowledgments

First and foremost, I would like to express my sincere gratitude to my supervisors for their continued support and guidance in getting me to this point. Firstly, my gratitude extends to Professor Sir Doug Turnbull who presented me with the opportunity to undertake this PhD. I would also like to thank him for all his advice on my work. Next, I would like to thank Professor Rob Taylor for being a great teacher and for always pushing me to do my best. Finally, a special thanks to Dr Sarah Pickett for her constant encouragement, unwavering support and for providing me with extremely helpful and insightful discussions throughout the last two years.

I would also like to thank a number of contributors to my work. One key contributor is Dr Conor Lawless who I would like to thank for his fantastic statistical knowledge that helped drive my study. Next, Dr Mariana Rocha whom I would like to thank for all the help and guidance given during the initial stages of this PhD. I would also like to thank Dr John Grady for developing the analysis software which was used during this PhD. I want to express my appreciation to the NHS Highly Specialised Diagnostic Centre for Mitochondrial Disease for providing assistance throughout this PhD – Gavin for always being helpful with the samples and cryostat use and also to Kate, Sarah and Rachel for being the pyrosequencing saviours. I would also like to thank Doug Jerry and Laura Brown for providing me with all the clinical information I had required.

A collective thanks to all the wonderful people at the MRG for making my studies here so enjoyable. To Dan E, Dr Grainne Gorman, Helen, Lyndsey, Amy R, Nicola and Dave, I would like to thank you all for being so lovely. A special thanks to Amy V (also known as boss) for being a source of knowledge, help and advice. Finally, thank you to all my fellow PhD buddies, past and present; Shane, Julia, Ghazelle, Matthew H, Lizzie, Nish, Chen, Ruth, Adam, Hannah L, Yasmin, Megan, Jack, Roisin, Carla, Hannah R and Pav. You guys have been the best group of people to be on this PhD journey with, so thank you all for making work fun for me! Thank you in particular to the recently crowned Dr Charlotte Warren (Char Wazza) for being an awesome write-up buddy/supportive friend!

I would like to thank all of my wonderful family and friends. Firstly, my two best friends Aishah and Rhymee who have been absolutely amazing during this PhD –thank you for providing me with laughter and for always being there for me. I love you both. Thank you also to the Gates family for always encouraging me to do my best in education. Also, I would like to thank my in laws for their understanding and patience during my final year.

To my amazing brothers; Tanvir, Jabir and Abir. If I could write an acknowledgment that was pages and pages long, it would be about you guys! But I can't, so short and sweet it is! Thank you all for pretty much everything; the love (including the tough love!), the patience, the protectiveness and for always having my back. I love you three very much and I hope I have done you all proud. Also, thanks to my sister in laws - Farmin bhabi, you have been a rock for me during this PhD, so thank you for being such a fab big sister. Your enthusiastic nods during my practice presentations and inquisitive questions about my studies were always appreciated. Sabina bhabi, thank you for your kind words and yummy food during the last stages of write up.

A sincere thank you to my dear husband, Sayeed. Thank you for putting up with my stress-tantrums, occasional meltdowns and for convincing me that it would all be worth it in the end. I hate to admit it, but you were right! I love you!

Finally, my parents to whom I dedicate this thesis to. Ammu, your love, prayers and comforting hugs have kept me smiling throughout so thank you for being the most amazing mother ever! Abbu, it's because of you I first became interested in Science, so thank you for being my inspiration. You are an amazing father and I will always endeavour to make you proud. I hope you both can look at this achievement and see it as your own. You always did inspire me by saying "*If you educate a man you educate an individual, but if you educate a woman you educate a family (nation)*". So, thank you both for being fundamental to my achievements in life!

Alhamdulillah for everything.

List of publications

Published:

Ahmed, S. T., Craven, L., Russell, O. M., Turnbull, D. M., & Vincent, A. E. (2018). Diagnosis and Treatment of Mitochondrial Myopathies. *Neurotherapeutics: the journal of the American Society for Experimental NeuroTherapeutics*, 15(4), 943–953. doi:10.1007/s13311-018-00674-4

Ahmed, S. T., Alston, C. L., Hopton, S., He, L., Hargreaves, I. P., Falkous, G., Oláhová, M., McFarland, R., Turnbull, D. M., Rocha, M. C., Taylor, R. W. (2017). Using a quantitative quadruple immunofluorescent assay to diagnose isolated mitochondrial Complex I deficiency. *Scientific reports*, 7(1), 15676. doi:10.1038/s41598-017-14623-2

Hardy, S. A., Blakely, E. L., Purvis, A. I., Rocha, M. C., **Ahmed, S. T.**, Falkous, G., Poulton, J., Rose, M. R., O'Mahony, O., Birmingham, N., Dougan, C. F., Ng, Y. S., Horvath, R., Turnbull, D. M., Gorman, G. S., Taylor, R. W. (2016). Pathogenic mtDNA mutations causing mitochondrial myopathy: The need for muscle biopsy. *Neurology. Genetics*, 2(4), e82. doi:10.1212/NXG.0000000000000082

Courses and conferences attended

Neuromuscular Translational Research Conference -Attended talks. Newcastle, UK, 2019

Cell Symposium: Multifaceted Mitochondria – Poster presentation. San Diego, USA, 2018

Neuromuscular Translational Research Conference - Poster presentation, Cambridge, UK, 2018

Neuromuscular Translational Research Conference - Selected platform presentation, London, UK, 2017

Node Pathology Conference – Platform presentation, Newcastle, UK, 2017

Abbreviations

2D-AGE	2-dimensional agarose gel electrophoresis
A	Adenine
ACL	Anterior cruciate ligament
ADP	Adenosine diphosphate
AIF	apoptosis inducing factor
ATP	Adenosine triphosphate
BN-PAGE	Blue Native Polyacrylamide Gel
Ca ²⁺	Calcium ion
CK	Creatinine kinase
CM	Cristae membrane
CNS	Central nervous system
CoQ10	Ubiquinone
COX	Cytochrome c Oxidase
CPEO	Chronic progressive external ophthalmoplegia
Cryo-EM	Cryomicroscopy
cyt <i>c</i>	Cytochrome <i>c</i>
DAB	Diaminobenzadine
dH ₂ O	Distilled water
DHU	Dihydrouridine
D-Loop	Displacement loop
dNTP	Deoxyribonucleotide Triphosphate
DRP1	Dynammin-related protein 1
dsDNA	Double-stranded DNA
ECG	Electrocardiogram
EGT	Endosymbiotic gene transfer
EM	Electron microscopy
ER	Endoplasmic reticulum
ERR α	Estrogen related receptor alpha
ETC	Electron transport chain
FAD	Flavin adenine dinucleotide
Fe-S	Iron -sulphur cluster
FILA	Fatal infantile lactic acidosis
Fis1	Mitochondrial fission protein1
fMet-tRNA ^{Met}	N-formylmethionine-tRNA
G	Guanine
GI	Gastro-intestinal
GrX	Glutaredoxins
H strand	Heavy strand
H ⁺	Proton
H ₂ O	Water
HCl	Hydrochloric Acid
IBM	Inner boundary membrane
IMM	Inner mitochondrial membrane

IMS	Intermembrane space
IUGR	Intrauterine growth restriction
Kb	Kilobase
KKS	Kearns Sayre Syndrome
L strand	Light strand
Leo	Leucine
LHON	Leber's hereditary optic neuropathy
L-OPA1	Long form OPA1
LS	Leigh Syndrome
Lys	Lysine
m1A	1-methyladenosine
m1G	1-methylguanosine
m2G	2-methylguanosine
m5C	5-methylcytidine
MCIA	Mitochondrial Complex I assembly
MCU	Mitochondrial Ca ²⁺ uniporter
MDOC	Mitochondrial Disease Oversight Committee
MELAS	Mitochondrial encephalomyopathy, lactic acidosis, and stroke-like episodes
MERFF	Myoclonic epilepsy with ragged red fibres
Mff	Mitochondrial fission factor
Mfn1	Mitofusin proteins 1
Mfn2	Mitofusin proteins 2
MIA	Mitochondrial IMS import and assembly
MICOS	Mitochondrial contact site and cristae organising system
MIDD	Maternally inherited diabetes and deafness
MitoCohort	Mitochondrial Disease Patient Cohort
ml	Millilitre
mM	Millimolar
MPP	Mitochondrial processing peptidase
mRNA	messenger Ribonucleic Acid
mtDNA	Mitochondrial DNA
mt-EFG2	Mitochondrial elongation factor G2
MTERF-1	Mitochondrial termination factor 1
mtLSU	Mitochondrial large subunit
MTP-18	Mitochondrial protein 18kDa
MtRF1a	Mitochondrial release factor 1a
mt-RRF1	Mitochondrial release factor 1
mtSSB	Single stranded DNA binding protein
mtSSU	Mitochondrial small subunit
mt-tRNA	Mitochondrial transfer ribonucleic Acid
NaCl	Sodium Chloride
NADH	Nicotinamide adenine dinucleotide
NCR	Non-coding region
NGS	Next generation sequencing
NMDAS	Newcastle Mitochondrial Disease Adult Scale

NRF-1	Nuclear respiratory factor 1
NRF-2	Nuclear respiratory factor 2
O ₂ ^{•-})	Superoxide anion
OD	Optical density
OMM	Outer mitochondrial membrane
OPA1	Optic Atrophy 1
Oriz	Zone of replication
OXPPOS	Oxidative Phosphorylation
PAM	Pre-sequence translocase-associated motor
PBS	Phosphate Buffer Saline
PCR	Polymerase chain reaction
PEO	Progressive external ophthalmoplegia
PFA	Paraformaldehyde
PGC-1 α	Peroxisome proliferator-activated receptor gamma coactivator 1-alpha
P _i	Inorganic phosphate
POLG	Polymerase gamma
PPAR α	Peroxisome proliferator-activated receptor alpha
Q [•]	Semi-ubiquinone radical
QH ₂	Ubiquinol
RITOLS	RNA-incorporated throughout the lagging strand
ROS	Reactive oxygen species
RRF	Ragged-Red Fibres
SAM	Sorting and assembly machinery
SD	Standard deviation
SDH	Succinate Dehydrogenase
SLE	Stroke-like-episodes
SOD	Superoxide dismutase
S-OPA1	Short form OPA1
TAS	Termination-associated sequence
TCA	Tricarboxylic Acid
TFAM	Mitochondrial transcription factor A
TFB2M	Mitochondrial transcription factor B2
TIM	Translocase of the inner membrane
TNF	Tumour necrosis factor
TOM	Translocases of the outer membrane
TWINK	Twinkle helicase
VDAC	Voltage Dependant Anion Channel
WCMR	Wellcome Centre for Mitochondrial Research
WES	Whole exome sequencing
WGS	Whole genome sequencing
μl	Microliter
Mm	Micromolar
tm5U	taurinomethyluridine

Table of Contents

Author's declaration	iii
Abstract.....	v
Acknowledgments	vii
List of publications	ix
Courses and conferences attended	x
Abbreviations	xi
List of Figures.....	xxiii
List of Tables	xxvii
List of Equations.....	xxix
Chapter 1: Introduction.....	1
1.1. Introduction.....	2
1.2. Mitochondrial biology	2
1.2.1. Origins and evolution of mitochondria.....	2
1.2.2. Structure of mitochondria.....	3
1.2.3. The import of mitochondrial proteins.....	6
1.2.4. Mitochondrial dynamics	9
1.2.4.1. Mitochondrial Fission.....	9
1.2.4.2. Mitochondrial fusion	10
1.2.4.3. Mitochondrial biogenesis	11
1.3. Mitochondrial function	12
1.3.1. Oxidative Phosphorylation (OXPHOS) and ATP synthesis	12
1.3.1.1. The tricarboxylic acid (TCA) cycle.....	12
1.3.1.2. Oxidative phosphorylation	13
1.3.1.3. Complex I (NADH: Ubiquinone Oxidoreductase).....	15
1.3.1.4. Complex II - Succinate-ubiquinone oxidoreductase	16
1.3.1.5. Complex III - Ubiquinol-cytochrome c oxidoreductase.....	18
1.3.1.6. Complex IV - Cytochrome c Oxidase	19
1.3.1.7. Complex V - ATP Synthase	21
1.3.1.8. Supercomplexes.....	23
1.3.2. Other functions of Mitochondria	24
1.3.2.1. Reactive oxygen species (ROS) production	24
1.3.2.2. Apoptosis.....	25
1.3.2.3. Haem biogenesis and Fe-S cluster biogenesis.....	25
1.3.2.4. Calcium (Ca ²⁺) signalling and handling	26

1.4.	Mitochondrial DNA	27
1.4.1.	The Mitochondrial genome	27
1.4.2.	Replication of mitochondrial DNA.....	29
1.4.2.1.	The replication machinery	29
1.4.2.2.	Models of mtDNA replication;	30
1.4.3.	Transcription of mitochondrial DNA.....	32
1.4.4.	Translation of mitochondrial DNA	34
1.5.	Mitochondrial Genetics	38
1.5.1.	Heteroplasmy	38
1.5.2.	Threshold effect	38
1.5.3.	Maternal inheritance	40
1.5.4.	The mitochondrial bottleneck	41
1.5.5.	Segregation of mtDNA mutations.....	41
1.5.6.	Clonal expansion.....	42
1.6.	Mitochondrial Disease.....	44
1.6.1.	Mitochondrial DNA pathogenic variants	46
1.6.1.1.	mtDNA point mutations.....	46
1.6.1.2.	Single, large-scale mtDNA deletions.....	47
1.6.2.	Nuclear DNA mutations.....	48
1.7.	Muscle and mitochondria	51
1.7.1.	Structure of skeletal muscle	51
1.7.2.	Mitochondria in skeletal muscle	53
1.7.3.	Skeletal muscle fibre types	53
1.8.	Diagnosis of Mitochondrial Diseases.....	55
1.8.1.	Muscle biopsy and histochemical investigations	55
1.8.2.	Biochemical studies	58
1.8.3.	Molecular genetics studies	58
1.8.4.	Immunofluorescence techniques.....	59
1.9.	The quadruple immunofluorescence Assay	61
1.10.	Overall aims and objectives:.....	62
Chapter 2:	Materials and methods.....	65
2.1.	Equipment	66
2.2.	Consumables	67
2.3.	Chemicals and Reagents.....	68
2.4.	Solutions.....	70

2.5.	Methods	72
2.5.1.	The Newcastle Mitochondrial Research Biobank	72
2.5.2.	Ethical approval and guidelines.....	72
2.5.3.	Clinical Data – Mitochondrial Disease Patient Cohort (UK) (MitoCohort)	72
2.5.4.	Patient Cohort.....	73
2.5.4.1.	Isolated Complex I patients	73
2.5.4.2.	m.3243A>G patients.....	73
2.5.5.	Control Muscle Tissue.....	74
2.5.6.	Newcastle Mitochondrial Disease Adult Scale (NMDAS)	74
2.5.7.	Tissue sectioning	75
2.5.8.	Immunofluorescence	75
2.5.8.1.	Quadruple immunofluorescence.....	75
2.5.8.2.	Fibre type immunofluorescence	77
2.5.9.	Image Acquisition using Zeiss Axio imager MI microscope	78
2.5.10.	Statistical Analysis of OXHPOS deficiency	78
2.5.10.1.	Densitometry measurements using the Quadruple Immuno Analyser Software	78
2.5.10.2.	Data analysis.....	79
2.5.11.	Blue-Native Polyacrylamide gel electrophoresis (BN-PAGE)	81
2.5.11.1.	Muscle homogenisation.....	81
2.5.11.2.	Pierce Assay and BN-PAGE	82
2.5.11.3.	Transfer, blocking and application of antibodies	82
2.5.11.4.	Detecting proteins on BN-PAGE	83
2.5.12.	Laser Microdissection.....	83
2.5.12.1.	Sample preparation.....	83
2.5.12.2.	Single fibre laser microdissection.....	83
2.5.12.3.	Single cell lysis PCR	84
2.5.13.	Pyrosequencing.....	84
2.5.13.1.	Pre-pyrosequencing PCR.....	84
2.5.13.2.	DNA Gel electrophoresis.....	85
2.5.13.3.	Pyrosequencing reaction.....	86
2.5.13.4.	Pre-pyrosequencing PCR – binding of amplicons to the sepharose beads.....	86
2.5.13.5.	Sample clean-up and annealing reaction	86
2.5.13.6.	Preparation of cartridge and pyrosequencing reaction	87
2.5.13.7.	Analysis of Pyrosequencing data.....	87
2.5.14.	Statistics analyses	89

Chapter 3: Using a quantitative quadruple immunofluorescence assay to diagnose isolated mitochondrial Complex I deficiency	91
3.1. Introduction	92
3.1.1. Complex I structure.....	92
3.1.1.1. Determining the structure of Complex I	93
3.1.1.2. Functional modules of Complex I.....	93
3.1.2. Complex I assembly.....	96
3.1.3. Isolated Complex I deficiency in the clinical setting.....	99
3.1.3.1. Pathogenic mutations associated with Complex I deficiency	99
3.1.3.2. Clinical symptoms associated with Complex I deficiency	101
3.1.4. Limitations in the current diagnostic setting for Complex I deficiency	102
3.1.4.1. The Molecular Genetics first approach.....	103
3.1.4.2. The use of muscle biopsy for histopathological and biochemical analyses...	103
3.1.4.3. The Quadruple immunofluorescence assay and Complex I deficiency	104
3.2. Aims	106
3.3. Methods.....	107
3.3.1. Tissue samples and patient cohort	107
3.3.2. Quadruple Immunofluorescence	112
3.3.3. Image Acquisition	114
3.3.4. Statistical Analysis.....	114
3.3.4.1. Densitometry measurements	114
3.3.4.2. Data Analysis	114
3.3.5. Blue Native–Polyacrylamide Gel Electrophoresis (BN-PAGE).....	115
3.4. Results	116
3.4.1. Group 1- Nuclear-encoded Complex I structural subunits	116
3.4.2. Group 2- Nuclear-encoded Complex I assembly factors	120
3.4.3. Assay showed variable results in patients with mutations in mtDNA-encoded Complex I subunits (Group 3)	123
3.4.4. Patients with mutations in mtDNA-encoded CI subunits and normal NDUF8 profile also display normal NDUF3 levels.....	127
3.4.5. BN-PAGE assessing the steady-state levels of assembled Complex I	134
3.5. Discussion	137
3.6. Limitations of this study.....	144
3.7. Conclusion.....	144

Chapter 4: Using the quadruple immunofluorescence assay to determine the OXPHOS biochemical profile of individual skeletal muscle fibres from patients with the m.3243A>G variant.	147
4.1. Introduction.....	148
4.1.1. The m.3243A>G pathogenic variant	148
4.1.2. Epidemiology of the mutation	150
4.1.3. Mechanisms leading to pathogenicity of the mutation.....	150
4.1.4. Clinical phenotypes	154
4.1.5. Muscle involvement in m.3243A>G patients.....	155
4.1.6. Causes of phenotypic variation	156
4.1.7. Biochemical features associated with the m.3243A>G variant.....	159
4.2. Aims.....	161
4.3. Methods	162
4.3.1. Tissue samples and ethics.....	162
4.3.2. Clinical information for cohort.....	162
4.3.3. Tissue sectioning, quadruple immunofluorescence and image acquisition.....	165
4.3.4. Data and statistical analysis	166
4.4. Results.....	167
4.4.1. Immunoreactivity of NDUFB8 and COX-1 in m.3243A>G patients	167
4.4.2. Quantifying the quadruple immunofluorescence assay biochemical findings .	170
4.4.2.1. Biochemical findings for control group;	170
4.4.2.2. Biochemical findings in m.3243A>G patient muscle;	170
4.4.3. Two distinct groups of patient muscle biopsies.....	172
4.4.4. The mitochondrial respiratory chain expression profiles of m.3243A>G patient skeletal muscle section	172
4.4.5. Correlating the quadruple immunofluorescence data with the clinical data	174
4.4.5.1. Biochemical data (Z_scores) vs homogenate m.3243A>G heteroplasmy levels	174
4.4.5.2. Biochemical deficiency vs homogenate m.3243A>G heteroplasmy levels ...	176
4.4.5.3. Correlating the biochemical findings with clinical phenotypes	178
4.5. Discussion.....	180
4.5.1. The biochemical status of m.3243A>G patients is heterogeneous based on Complex I interrogation	180
4.5.2. Complex I deficiency correlates with homogenate heteroplasmy levels	181
4.5.3. No correlation is observed between the biochemical deficiency and clinical phenotypes.....	182
4.5.4. What is causing the difference in the biochemical status between patients in Group A and Group B?	182

4.6. Limitations of this study.....	184
4.7. Conclusion.....	185

Chapter 5: A single cell approach to estimate the heteroplasmic threshold for biochemical deficiency of Complex I in skeletal muscle sections from patients harbouring the m.3243A>G pathogenic variant 187

5.1. Introduction	188
5.2. Aims	190
5.3. Methods.....	191
5.3.1. Selecting patients for the single cell study.....	191
5.3.2. Single muscle fibre work flow	191
5.3.3. Tissue sectioning for fibre typing	191
5.3.4. Fibre Typing.....	191
5.3.5. Matching fibres to OXHOS defect and fibre type:	191
5.3.6. Section preparation for single muscle fibre isolation.....	193
5.3.7. Isolation of single muscle fibres	193
5.3.8. Assessing the m.3243A>G heteroplasmy levels in single muscle fibres with quantitative pyrosequencing	193
5.3.9. Selection of single muscle fibres for single cell study.....	195
5.3.10. Analysis.....	198
5.3.10.1. LOESS profiles	198
5.3.10.2. Hierarchical clustering	200
5.3.10.3. Kernel density estimate plots	201
5.4. Results	202
5.4.1. Optimisation of the single cell study.....	202
5.4.1.1. Investigating the sampling method for single cell study.....	202
5.4.2. Heteroplasmy level and respiratory chain deficiency	205
5.4.2.1. m.3243A>G heteroplasmy levels increase in deficient fibres	205
5.4.2.2. The relationship between single cell m.3243A>G heteroplasmy levels and homogenate heteroplasmy levels	210
5.4.2.3. Investigating the difference in porin levels between the two patient groups ..	210
5.4.2.4. Muscle fibre types and m.3243A>G heteroplasmy levels	211
5.4.3. Estimating the biochemical threshold for Complex I in the skeletal muscle of m.3243A>G patients.....	214
5.4.3.1. LOESS profiles using single fibre Z-scores and heteroplasmy level data.....	214
5.4.3.2. Control-free classifications using hierarchical clustering:.....	218
5.4.3.3. The heteroplasmy levels in the biochemically normal and deficient fibres...	223

5.4.3.4. Kernel density estimate for threshold levels.....	226
5.5. Discussion.....	231
5.5.1. Increased m.3243A>G heteroplasmy levels in deficient fibres.....	231
5.5.2. Type II fibres harbour higher levels of m.3243A>G heteroplasmy levels.....	232
5.5.3. Difference in tissue segregation of the m.3243A>G mutation between patients in Group A and Group B;.....	232
5.5.4. Differences in the estimated heteroplasmic threshold for Complex I deficiency between patients.....	236
5.6. Limitations of this study.....	236
5.7. Conclusion.....	238
Chapter 6: Final discussion and future work	241
6.1. Conclusions.....	242
6.1.1. The quadruple immunofluorescence assay is a beneficial tool in the diagnosis of Complex I deficiency:.....	242
6.1.2. Skeletal muscle sections of patients harbouring the m.3243A>G pathogenic variant show variable biochemical status based on Complex I expression.....	243
6.1.3. m.3243A>G heteroplasmy distribution differs in biochemically normal fibres between patients in Group A and B	244
6.1.4. Patients showed a difference in their biochemical threshold	244
6.2. Future work and potential studies.....	245
6.3. Final conclusion.....	248
Chapter 7: Appendices.....	249
Appendix 1: Newcastle Adult Mitochondrial Disease scale (NMDAS) questionnaire which is used to assess mitochondrial disease severity and progression in the Newcastle Mitochondrial disease cohort.....	250
Appendix 2:.....	260
Appendix 3:.....	261
Appendix 4:.....	262
Appendix 5:.....	264
Appendix 6:.....	266
Appendix 7:.....	270
Chapter 8: References	274

List of Figures

Figure 1.1: The mitochondrial structure.	5
Figure 1.2: Import pathways for nuclear encoded mitochondrial proteins.	8
Figure 1.3: Regulation of mitochondrial fission.	10
Figure 1.4: Regulation of mitochondrial fusion.	11
Figure 1.5: The TCA (Krebs) Cycle.	13
Figure 1.6: Oxidative Phosphorylation.	14
Figure 1.7: The movement of electrons through Complex I.	16
Figure 1.8: A schematic structure and function of Complex II.	17
Figure 1.9: A schematic structure and function of Complex III.	19
Figure 1.10: A schematic structure and function of Complex IV.	21
Figure 1.11: A schematic diagram of Complex V (ATP synthase).	22
Figure 1.12: Crystal structure of ovine supercomplex.	24
Figure 1.13: The Human Mitochondrial Genome.	28
Figure 1.14: A schematic diagram of the mitochondrial DNA replication machinery.	30
Figure 1.15: The current models of replication of mammalian mitochondrial DNA.	32
Figure 1.16: Mitochondrial translation.	36
Figure 1.17: Heteroplasmy and the threshold effect.	39
Figure 1.18: The clinical spectrum of mitochondrial diseases.	45
Figure 1.19: List of genes currently associated with mitochondrial disease. Genes have been listed according to their function.	50
Figure 1.20: A schematic figure of the structure of skeletal muscle and sarcomere.	52
Figure 1.21: Histochemical investigations showing hallmarks of mitochondrial dysfunction in skeletal muscle.	57
Figure 1.22: Comparison of the quadruple immunofluorescence assay to the traditional histopathology techniques.	60
Figure 2.1: Schematic diagram of the quadruple immunofluorescence assay detecting respiratory chain enzymes.	76
Figure 2.2: Schematic diagram of the immunofluorescence assay detecting different fibres types in skeletal muscle section.	77
Figure 2.3: Analysis of single muscle fibres using the Quadruple Immuno Analyser.	79
Figure 2.4: An illustrated representation of the Mitochondrial Respiratory Chain plot.	81
Figure 2.5: Isolation of single muscle fibres by laser capture microdissection.	84

Figure 2.6: A schematic diagram showing the layout of cartridge during experimental preparation for the pyrosequencing reaction.....	87
Figure 2.7: Pyro-gram outputs from the PyroMark software.	88
Figure 3.1: A 3.3 Å resolution modular structure of mouse heart Complex I.	95
Figure 3.2: Subunit composition of Complex I.	95
Figure 3.3: A comprehensive model of Complex I assembly.....	98
Figure 3.4: A schematic diagram highlighting the study design and the quadruple immunofluorescence protocol.....	112
Figure 3.5: Images of Complex I, IV and porin expression in skeletal muscle sections from patients with isolated Complex I deficiency caused by defects on nuclear-encoded Complex I subunits using the immunofluorescence assay.....	118
Figure 3.6: Mitochondrial respiratory chain expression profile linking Complex I, Complex IV and porin levels in patients with isolated Complex I deficiency caused by defects in nuclear-encoded Complex I subunits.	119
Figure 3.7: Images of Complex I, IV and porin expression in skeletal muscle sections from patients with isolated Complex I deficiency caused by defects on nuclear-encoded Complex I assembly factors using the immunofluorescence assay.	121
Figure 3.8: Mitochondrial respiratory chain expression profile linking Complex I, Complex IV and porin levels in patients with isolated Complex I deficiency caused by defects in nuclear-encoded Complex I assembly factors.	122
Figure 3.9: Images of Complex I, IV and porin expression in skeletal muscle sections from patients with isolated Complex I deficiency caused by defects on mtDNA-encoded CI subunits using the immunofluorescence assay.....	124
Figure 3.10: Images of Complex I, IV and porin expression in skeletal muscle sections from patients with isolated Complex I deficiency caused by defects on mtDNA-encoded Complex I subunits using the immunofluorescence assay.....	125
Figure 3.11: Mitochondrial respiratory chain expression profile linking complex I (NDUFB8), complex IV and porin levels in patients with isolated Complex I deficiency caused by defects in mtDNA-encoded Complex I subunits.	127
Figure 3.12: Immunofluorescent images of Complex I targeted with ND1 and NDUFB8 alongside porin expression in skeletal muscle sections from A) control case and B) an isolated Complex I deficiency case – P6 (NDUFS6, Homozygous c.316_319delGAAA, p.(Glu106Glnfs*41)).	129

Figure 3.13: Immunofluorescent images of Complex I targeted with NDUFS3 and porin expression in skeletal muscle sections from A) control case and B) an isolated Complex I deficiency case.....	130
Figure 3.14: Images of Complex I, IV and porin expression in skeletal muscle sections from patients with isolated Complex I deficiency caused by defects on mtDNA-encoded Complex I subunits using the immunofluorescence assay.	132
Figure 3.15: Mitochondrial respiratory chain expression profile linking complex I (NDUFS3), complex IV and porin levels in patients with Isolated complex I deficiency caused by defects in mtDNA-encoded Complex I subunits.	133
Figure 3.16: Analysis of Complex I assembly by BN-PAGE.	135
Figure 3.17: The assembly of Complex I with indication of where the subunits affected in the cohort of patients enter the complex.	139
Figure 3.18: A schematic flowchart designating the role of the quadruple immunofluorescence assay in the current diagnostic process for Mitochondrial disease.	143
Figure 4.1: A schematic diagram of the cloverleaf secondary structure of mitochondrial tRNA ^{Leu (UUR)}	149
Figure 4.2: A schematic diagram highlighting the study design and quadruple immunofluorescent protocol.	165
Figure 4.3: Images of Complex I, IV and porin expression in skeletal muscle sections of m.3243A>G patients.....	169
Figure 4.4: Mitochondrial respiratory chain (MRC) expression profile linking Complex I (NDUFB8), Complex IV (COX-1) and porin levels in m.3243A>G muscle sections.....	173
Figure 4.5: Relationship between homogenate heteroplasmy and the Z-scores determined for a) Complex I and b) Complex IV deficiency in individual muscle fibres.....	175
Figure 4.6: Relationship between homogenate heteroplasmy and the percentage of A) Complex I and B) Complex IV deficiency.	177
Figure 4.7: Boxplots showing the proportion of Complex I-deficient and Complex IV-deficient fibres (%) within patients who fall below (absent) and above thresholds (present) scores:	179
Figure 5.1: A schematic diagram of the single cell study experimental workflow.....	192
Figure 5.2: Matching OXHPOS status and fibre type.....	194
Figure 5.3: The OXPHOS status groups seen in m.3243A>G patient mitochondrial respiratory chain profiles.	195
Figure 5.4: Mitochondrial respiratory chain profiles highlighting sampled fibres.	197
Figure 5.5: A schematic diagram of the LOESS regression and bootstrapping.....	199

Figure 5.6: Schematic illustration of two-dimensional scatter plot (2Dmito plot) after hierarchical clustering for fibre classification.....	201
Figure 5.7: Schematic illustration of kernel density estimate.....	201
Figure 5.8: Heteroplasmy levels in fibres accessing inter and intra variability of pyrosequencing.	204
Figure 5.9: Distribution of heteroplasmy levels in the three controls in all pyrosequencing experiments.	205
Figure 5.10: Distribution of single fibre heteroplasmy levels in each OXPHOS group observed in patients in Group A.	208
Figure 5.11: Distribution of single fibre heteroplasmy levels from Group B patient muscle sections.....	208
Figure 5.12: Boxplot showing log(Porin) levels in muscle fibres from each patient muscle section.	211
Figure 5.13: Boxplot of m.3243A>G heteroplasmy level in Type I and Type II muscle fibres.	212
Figure 5.14: LOESS profiles showing the Z_score and heteroplasmy level distribution of single fibres and the estimated heteroplasmic threshold for deficiency.	217
Figure 5.15: Two-dimensional scatterplots (2Dmito plots) comparing Complex I protein expression with mitochondrial mass.	219
Figure 5.16: 2Dmito plots and mitochondrial respiratory chain profiles representing the data for P05 and P06.....	221
Figure 5.17: Boxplot distribution of heteroplasmy levels in biochemically normal and deficient fibres from patients in Group A and B.....	225
Figure 5.18: Kernel density estimate plot showing heteroplasmic threshold estimates of Complex I deficiency in all patients.	227
Figure 7.1: Mitochondrial respiratory chain profiles highlighting sampled fibres from all patients.	263
Figure 7.2: LOESS profiles showing the Z_score and heteroplasmy level distribution of single fibres and the estimated heteroplasmic threshold for deficiency.	269
Figure 7.3: Two-dimensional scatterplots (2Dmito plots) comparing Complex I protein expression with mitochondrial mass.	272

List of Tables

Table 1.1: Muscle fibre type, function and characteristics.....	54
Table 2.1: List of equipment.....	66
Table 2.2: List of consumables.....	67
Table 2.3: List of chemicals and reagents.....	68
Table 2.4: Characteristics of the non-disease control skeletal muscle biopsies (taken from distal region of hamstring following ACL surgery).....	74
Table 2.5: Primary antibodies used in the Quadruple immunofluorescence assay.....	76
Table 2.6: Secondary antibodies used in the Quadruple immunofluorescence assay.....	77
Table 2.7: Primary antibodies used in fibre type immunofluorescence and associated dilutions.....	78
Table 2.8: Secondary antibodies used in fibre type immunofluorescence and associated dilutions.....	78
Table 2.9: Fibre classifications based on Z_scores.....	80
Table 2.10: Antibodies used for BN-PAGE.....	83
Table 2.11: Primers used for pre-pyrosequencing PCR.....	85
Table 2.12: Pre-pyrosequencing PCR and conditions.....	85
Table 2.13: Primers used for Pyrosequencing annealing reaction.....	86
Table 3.1: List of Complex I subunits and assembly factors and first report of pathogenic mutations associated with each.....	100
Table 3.2: Clinical, biochemical and molecular genetic characteristics of the patient cohort with isolated Complex I deficiency.....	108
Table 3.3: Genes affected in the cohort of confirmed Isolated Complex I deficiency patients; their known/postulated function and assembly intermediate.....	111
Table 3.4: Primary and secondary antibodies used for immunofluorescence.....	113
Table 3.5: Percentage of Complex I- deficient fibres detected with the quadruple immunofluorescence assay.....	117
Table 3.6: A summary of all experimental data for the cohort of patients with isolated Complex I deficiency.....	136
Table 4.1: Proposed mechanisms for the pathogenicity of the m.3243A>G mutations and key findings from the studies undertaken.....	152
Table 4.2: Clinical and molecular genetic characteristics of the patient cohort harbouring the m.3243A>G pathogenic variant on the MT-TL1 gene.....	163

Table 4.3: Quantification of Complex I (NDUFB8) and Complex IV (COX-I) deficiency in skeletal muscle fibres from patients with the m.3243A>G point mutation	171
Table 4.4: Age, homogenate heteroplasmy and total Complex I and Complex IV deficiency in skeletal muscle sections	174
Table 5.1: The number of fibres targeted for selection per OXHPOS status and fibre type	196
Table 5.2: Overall number of fibres actually sampled per case per group of OXPHOS status in each patient and the final number included in the molecular genetics investigation.....	196
Table 5.3: Random sampling compared to current sampling method	203
Table 5.4: The range of heteroplasmy level determined in single fibres per OXPHOS group from all patient skeletal muscle sections.....	209
Table 5.5: Median, W and P-value showing differences in m.3243A>G heteroplasmy levels between the different muscle fibre types	213
Table 5.6: Threshold estimates and upper and lower confidence intervals for selected patients using LOESS model fitted to the bootstrapped data	215
Table 5.7: Differences in the proportion of fibres (%) classified as Complex I and Complex IV deficient through Z_scores classification and Complex I deficient with hierarchical clustering.....	222
Table 5.8: Summary data for heteroplasmic threshold estimates (%) as plotted on kernel density estimate plot (Figure 5.18)	228
Table 5.9: Probability-based estimates of the difference in threshold between the seven patients in Group A. The top half shows probability estimates and the bottom half shows the corresponding magnitude of the difference (%).	229
Table 7.1: NMDAS scores and thresholds for clinical phenotypes assessed in cohort.....	260
Table 7.2: Quantification of Complex I (NDUFB8) and Complex IV (COX-I) deficiency in skeletal muscle fibres from non-disease controls	261
Table 7.3: The m.3243A>G heteroplasmy levels through inter and intra-variability testing of pyrosequencing	264

List of Equations

Equation 1.1: Glycolysis	12
Equation 1.2: Pyruvate decarboxylation	12
Equation 1.3: The TCA (Kreb's) cycle overall reaction	12
Equation 1.4: Complex I reaction	15
Equation 1.5: Complex II reaction	16
Equation 1.6: Complex III reaction	18
Equation 1.7: Complex IV reaction	20

Chapter 1: Introduction

1.1. Introduction

Mitochondria are essential intracellular organelles which are present in the cytoplasm of all nucleated mammalian cells. They are predominantly known for their principle role of generating cellular energy in the form of adenosine triphosphate (ATP) (Hatefi, 1985). However, mitochondria are also involved in multiple biological processes and pathways for example, the regulation of cell death via apoptosis, cytosolic calcium handling, iron-sulphur (Fe-S) cluster and haem biogenesis and the generation of reactive oxygen species. Most interestingly, mitochondria are unique in that they are the only organelle, other than the nucleus, that contain their own genome; the mitochondrial DNA (mtDNA). This genome accommodates the essential genes required for the production of ATP and mitochondrial function. However, the vast majority of mitochondrial proteins (1,158 proteins according to the MitoCarta2.0) (Calvo et al. 2016), are encoded for by the nuclear DNA. Such, the mitochondria is under the dual control of both the nuclear DNA and mtDNA, thereby any defects occurring in these genomes can lead to complicated disease. One particular tissue that is frequently affected by mitochondrial disease in patients is the skeletal muscle – a post-mitotic tissue that has high metabolic demand due to its critical function in controlling voluntary movement. Therefore, skeletal muscle is a major source of resource for both diagnostic investigation and research into mitochondrial disease.

This section of the thesis will introduce basic mitochondrial biology and genetics, linking the latter to mitochondrial disease and current diagnostic processes. Areas of this introduction which are of particular interest and relevance to the studies described in this thesis, will be highlighted and detailed further in the relevant Results chapters (**Chapters 3, 4 and 5**).

1.2. Mitochondrial biology

1.2.1. Origins and evolution of mitochondria

The first identification of mitochondria dates back to the 1800s, where intracellular structures known as “bioblasts” were founded in the cytoplasm of nucleated cells (Altmann 1894). Thereafter, the organelle was named mitochondria (singular; mitochondrion), taken from the Greek terms “mito” which means thread and “khondrion” meaning granule.

The origins of mitochondria in eukaryotic cells has been proposed by two theories. The first and most well-known theory is the endosymbiotic theory. The mitochondria was said to have an endosymbiotic origin, whereby a free living Eubacteria (believed to be a prokaryotic ancestor related to alpha-proteobacteria) was engulfed by a primordial eukaryotic cell

(Margulis 1971). It was proposed that the endosymbiosis event occurred after the emergence of the cell nucleus (Margulis 1971). The second theory which has been proposed is known as the “hydrogen hypothesis”, in which it was postulated that both the nucleus and mitochondria were formed after the fusion of a hydrogen dependent Archaeobacterium and a hydrogen-producing Eubacterium (Martin and Muller 1998). Both of these theories are in agreement that during the expansive and reductive evolution process, most of the genes from the bacterial genome were lost or transferred to the nuclear genome of the eukaryotic host cell, leaving a compact mtDNA, during a process called the endosymbiotic gene transfer (EGT) during mitochondrial evolution (Gray et al. 1999).

Mitochondria have retained features of a bacterial ancestry which is reflected in the double membrane, circular genome (mtDNA), machinery for protein synthesis in the matrix and the ability to move, divide and fuse. Additionally, the respiratory chain complexes involved in Oxidative Phosphorylation (OXPHOS) is evident of the evolutionary conservation between the mitochondrion and the primitive Eubacterium (Gray et al. 1999).

1.2.2. Structure of mitochondria

With the use of electron microscopy (EM), two pioneering studies in the 1950s were able to show that the mitochondria was a double membraned organelle, containing the outer mitochondrial membrane (OMM) and the inner mitochondrial membrane (IMM) (Palade 1952; Sjostrand 1953). However, these studies differed in their proposed models of mitochondrial structures. Palade proposed the “baffle model” of cristae structure in which the inner membrane formed baffles that projected into the matrix, termed cristae mitochondriales. Sjostrand’s alternative model proposed a third membrane forming septa that divided the matrix into many compartments. Both theories were proven to be inaccurate when a study using EM tomography and isolated mitochondria from rat liver, showed that narrow tubular invaginations of the IMM form the cristae (Mannella et al. 1997).

As shown in **Figure 1.1 (A and B)**, the membranes of the mitochondrion confine two aqueous compartments; the intermembrane space (IMS) and the matrix. The IMS is a ~20nm gap between the OMM and the IMM. Within the matrix, mtDNA is present alongside proteins involved in DNA replication, transcription and translation as well as proteins involved in biosynthetic reactions, namely the Tricarboxylic acid cycle (TCA cycle) or fatty acid (β) oxidation. The mitochondrial matrix has been found to have a pH of 7.8 which is believed to have a role in creating a transmembrane electrochemical gradient that drives ATP synthase (Complex IV) to produce ATP (Llopis et al. 1998).

The OMM is smooth and porous as it contains a high abundance of the beta-barrel protein called porin (also known as VDAC), a voltage gated anion which allows for the passage of low molecular weight molecules (under 10KDa) from the cytoplasm to the IMS. These molecules include lipid, sugars, amino acids and ions (Szabo and Zoratti 2014; Villinger et al. 2010). Larger molecules, such as proteins, require translocases to be transported across the membrane.

The IMM is much less permeable than the OMM. This ion selectivity leads to an electrochemical membrane potential of approximately 180 millivolts (mV) to build across the membrane. Additionally, in comparison to the OMM, the IMM has a high amount of membrane associated proteins with studies stating a 3:1 ratio for protein: lipid association (Shaikh et al., 2012). This high protein content is largely due to the proteins involved in OXPHOS. The IMM is rich in the phospholipid cardiolipin, which accounts for 20% of the lipid constitution. Cardiolipin has been shown to have an important role in the architecture of the IMM, as well as having a role in the maintenance of the membrane potential and providing an essential structural and functional support to the OXPHOS proteins (Bazan et al. 2013).

The IMM forms invaginations called cristae that extend deeply into the matrix. Cristae can be found in different morphologies including lamellar sheets and tubular enlarged bag-like-extensions (Frey and Mannella 2000). The cristae are connected to the IMS by the tubular cristae junctions (Daems and Wisse 1966; Mannella et al. 1997). The IMM can be subdivided into two parts; the inner boundary membrane (IBM) and the cristae membrane (CM). The IBM is found adjacent to the outer membrane and is enriched with proteins which are responsible for mitochondrial fusion and nuclear-encoded protein transport. The CM is enriched in proteins including the fully assembled complexes of the electron transport chain (ETC) and other proteins involved in OXPHOS, protein synthesis, mtDNA- encoded protein transport and Fe-S cluster biogenesis (Gilkerson et al. 2003; Vogel et al. 2006). At the junction between the IBM and CM is the large protein complex known as the 'Mitochondrial contact site and cristae organising system' (MICOS), which serves to anchor the cristae (the cristae junctions) to the outer membrane (Korner et al. 2012; Zerbes et al. 2012) (**Figure 1.1 (C)**).

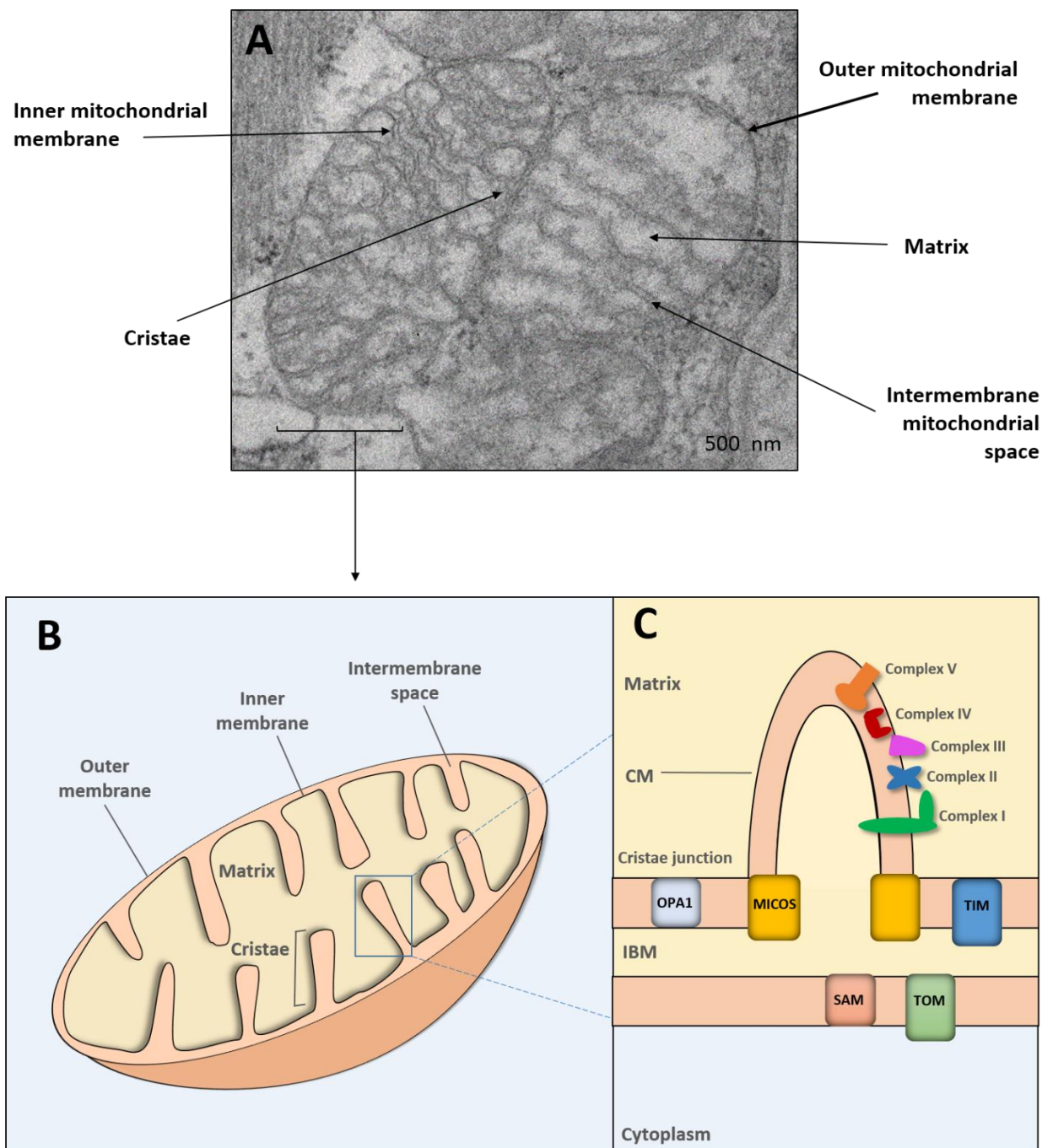


Figure 1.1: The mitochondrial structure.

A) Transmission electron microscopy image of a mitochondrion (provided by Dr Amy Vincent, Wellcome Centre for Mitochondrial Research, Newcastle University) and **B)** a schematic diagram showing the key structures of mitochondria. **C)** The proteins associated with the inner boundary membrane (IBM) and the cristae membrane (CM) that are involved with mitochondrial fusion (OPA1), nuclear- encoded protein transport complexes (TIM, SAM, TOM), the fully assembled complexes of the electron transport chain (ETC) which include Complex I, II, III, IV which then in conjunction with Complex V completes the oxidative phosphorylation (OXPHOS) system. The 'Mitochondrial contact site and cristae organising system' (MICOS) which anchors the CM to OMM.

1.2.3. The import of mitochondrial proteins

According to the recently published MitoCarta2.0, the mitochondria contains 1,158 proteins of which 99% are encoded by the nDNA (Calvo et al. 2016; Pagliarini et al. 2008; Sickmann et al. 2003). Therefore, these proteins are synthesised by the cytosolic ribosomes in a precursor form and then subsequently imported into the mitochondria (Schmidt et al. 2010). These cytosolic ribosomes have been found to be in close proximity to the OMM (Kellems et al. 1975). The import of the precursors and the following intra-mitochondrial sorting is mediated by membrane protein complexes, termed translocases, founded in the outer and inner membranes. Further soluble factors are found within the cytosol, intermembrane space and matrix.

The precursors contain targeting signals that are recognised by receptors on the mitochondrial surface, which assist in directing them to their functional destinations in the mitochondrial sub-compartments. There are 2 main groups of targeting signals and the first is the amino-terminal cleavable pre-sequence which is found in 60% of all precursors (Schatz and Dobberstein 1996; Schulz et al. 2015). These sequences are usually proteolytically cleaved off after import. The remaining 40% of precursors are termed non-cleavable precursor proteins as they contain an internal targeting signal that remains part of the mature protein (Chacinska et al. 2009).

All precursors must be translocated into or across the outer membrane of the mitochondria. The translocases responsible for most precursors are the translocases of the outer membrane (TOM), consisting of Tom40, Tom22, Tom5, Tom6, Tom7, Tom20 and Tom70 (Endo and Yamano 2010; Ryan et al. 2000; Schmidt et al. 2010). Once translocated through the TOM complex, precursors follow four different protein import pathways dependent on their sub-compartment role. **Figure 1.2** highlights the pathways by which the nuclear-encoded proteins are imported into the mitochondria.

Pre-sequence Pathway

The first pathway is the pre-sequence pathway which leads cleavable precursors from the TOM complex to the translocase of the inner membrane (TIM) complex – indicated by 3 in **Figure 1.2** (Schmidt et al. 2010; Straub et al. 2016; Vogtle et al. 2009). The mitochondrial processing peptidase (MPP) cleaves the pre-sequence (Hawlitschek et al. 1988; Mossmann et al. 2012). The precursors are imported to the inner membrane and matrix with the assistance of the pre-sequence translocase-associated motor (PAM) (Schmidt et al. 2010).

Carrier pathway

The second pathway is the carrier pathway (indicated by 7 in **Figure 1.2**) which involves the import of non-cleavable precursors of metabolite carriers (ADP and ATP carriers). The precursors are imported firstly through the TOM complex then transferred to chaperone complexes of the IMS - the small TIM complex (Rehling et al. 2003). From this, the precursors are inserted into the inner membrane through the translocases of the TIM22 complex (Schmidt et al. 2010).

Oxidative pathway for intermembrane space precursors

The third pathway is the oxidative pathway of the IMS precursors (indicated by 5 in **Figure 1.2**). Many of the IMS precursors contain cysteine motifs and these precursors are imported through the TOM complex. They then interact with the mitochondrial IMS import and assembly (MIA) machinery which oxidises the cysteine motifs (Chacinska et al. 2004; Straub et al. 2016).

Beta-barrel protein pathway

The final pathway is the transport pathway of beta-barrel proteins of the OMM (indicated by 6 in **Figure 1.2**). The precursors for these proteins are translocated through the TOM complex and transported to the small TIM chaperones (Tim9-Tim10 and Tim8-13). They are then inserted into the outer membrane by the sorting and assembly machinery (SAM) which is embedded in the OMM. Beta-barrel proteins are the most abundant type of proteins of the OMM including porin. Sam50, the core component of the complex, recognises beta-barrel proteins through an amino acid sequence near their C-termini leading to the folding and insertion into the OMM (Dudek et al. 2013; Riezman et al. 1983; Schmidt et al. 2010; Walther et al. 2009).

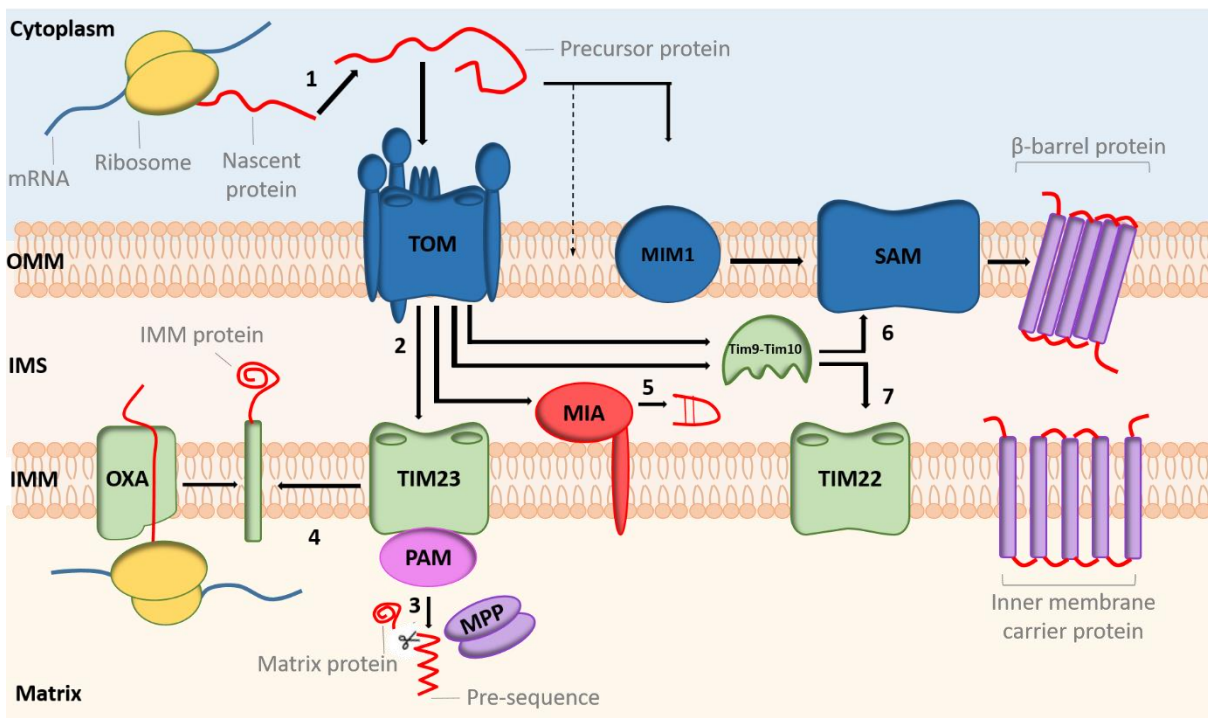


Figure 1.2: Import pathways for nuclear encoded mitochondrial proteins.

(1-2) 99% of proteins in the mitochondrial proteome are encoded for by nuclear DNA and synthesised on cytosolic ribosomes. Proteins are imported to the mitochondria through the translocase of outer membrane (TOM) complex. Thereafter, precursors can use different sorting machineries. (3) Pre-sequence pathway – pre-sequence precursors belonging to the matrix are imported by the translocase of the inner membrane (TIM23) complex and the pre-sequence translocase-associated motor (PAM). The mitochondrial processing peptidase (MPP) removes the pre-sequence. (4) Some precursors are laterally released from the TIM23 complex into the inner membrane. (5) Precursors which are for the intermembrane space are imported by the mitochondrial intermembrane space assembly (MIA). (6) Hydrophobic precursor proteins are transferred by the Tim9-Tim10 chaperones complex through the intermembrane space to the sorting and assembly machinery (SAM) in the case of the beta-barrel proteins of the outer membrane complex or (7) through the carrier pathway to the TIM22 complex. Figure has been adapted from (Schmidt et al. 2010).

1.2.4. Mitochondrial dynamics

Mitochondria are dynamic organelles that are continually undergoing fission and fusion (Westermann 2010). These act concurrently to allow the mitochondrial network to be remodelled in terms of morphology, size, number and content in accordance to the metabolic demand and changes (Westermann 2012).

1.2.4.1. Mitochondrial Fission

Fission involves the separation of both the outer and inner mitochondrial membrane and so the organelle becomes two separate entities (**Figure 1.3**). DRP1 (Dynamin-related protein 1), predominantly found in the cytosol of the cell, is the protein regulating the fission of the OMM (Smirnova et al. 2001). It is recruited to the mitochondria by four integral membrane proteins found in the OMM; mitochondrial fission protein 1 (Fis1 – an adapter protein anchored to the membrane by a c-terminal transmembrane domain), mitochondrial fission factor (Mff), MiD49 and MiD50 (Loson et al. 2013; Otera et al. 2010; Palmer et al. 2011; Scott and Youle 2010). Once translocated from the cytoplasm to the OMM, DRP1 oligomerises into ring-like structures at the sites of division which are marked by endoplasmic reticulum (ER) and actin cytoskeleton. GTP binding and hydrolysis promotes a conformational change in DRP1, resulting in constriction and severing of the OMM (Friedman et al. 2011; Mears et al. 2011; Smirnova et al. 2001). The fission of the IMM remains unclear, however recent studies have suggested two IMM proteins; S-OPA1 (short form OPA1 - generated from the proteolytic cleavage of L-OPA1 at sites S1 or S2) (Anand et al. 2014; Belenguer and Pellegrini 2013; Mishra et al. 2014) and MTP-18 (mitochondrial protein 18kDa) (Tondera et al. 2004; Tondera et al. 2005).

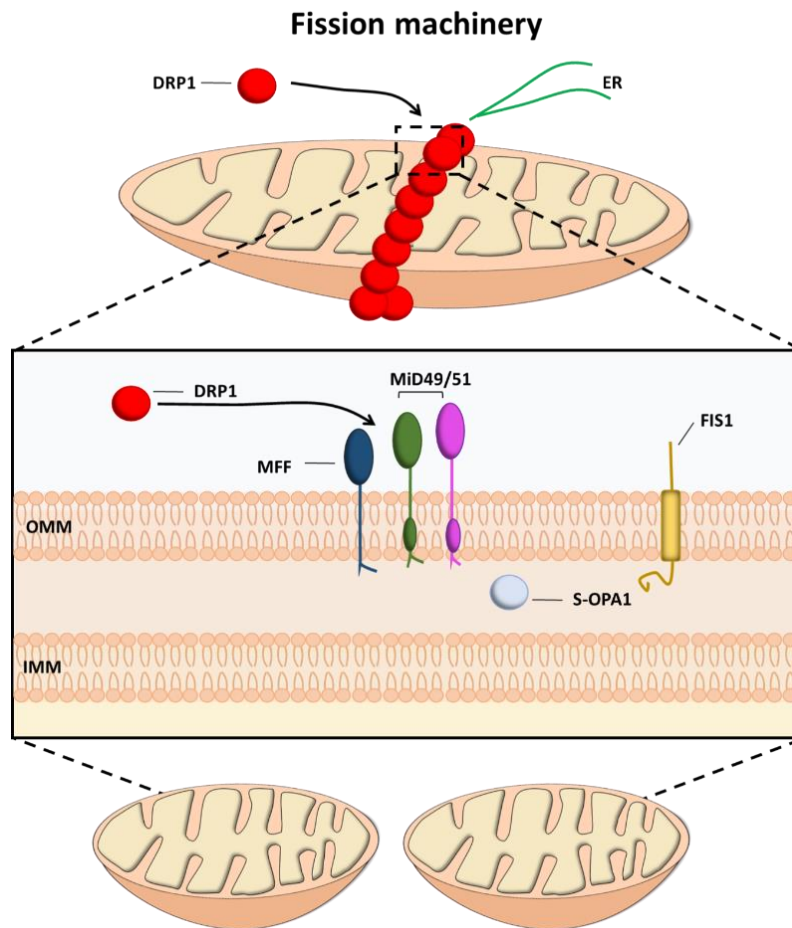


Figure 1.3: Regulation of mitochondrial fission.

Dynamamin-related protein 1 (DRP1; red) is recruited from the cytosol to the outer mitochondrial membrane (OMM) by MFF (dark blue), MiD49 (dark green) and MiD59 (pink) and Fis1 (yellow). DRP1 oligomerises into ring-like structures at the site of division which are marked by endoplasmic reticulum (ER - green). The binding and hydrolysis promotes a conformational change in DRP1, resulting in constriction and severing of the outer membrane. Figure has been adapted from (Wai and Langer 2016).

1.2.4.2. Mitochondrial fusion

Fusion is the process by which two mitochondria and their outer and inner membrane merge to result in one large mitochondria (**Figure 1.4**). The fusion of the OMM is regulated by the mitofusin proteins 1 and 2 (Mfn1 and Mfn2) which are localised to the OMM and have a role in tethering two mitochondria during the early stage of fusion. OPA1 mediates the fusion of the IMM (Meeusen et al. 2004; Meeusen et al. 2006). OPA1 exists in two forms, a long OPA1 (L-OPA1) and a short form (S-OPA1). Both are localised in the IMS, however L-OPA1 is anchored to the IMM whereas S-OPA1 is not (Mishra et al. 2014). It was found that both isoforms are required in combination for efficient mitochondrial fusion activity (Song et al. 2007).

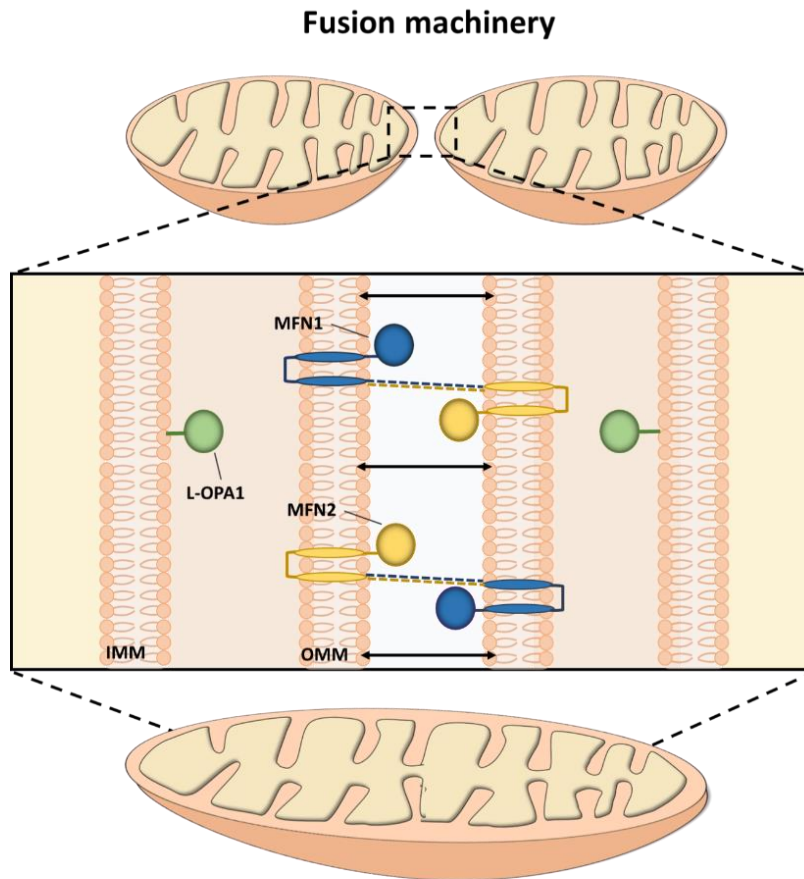


Figure 1.4: Regulation of mitochondrial fusion.

Mitochondrial fusion is facilitated by interactions between MFN1 (blue) and MFN2 (yellow) at the outer mitochondrial membrane (OMM) and L-OPA1 (green) in the inner mitochondrial membrane (IMM). Black arrows represent the emergence of two mitochondria. Figure has been adapted from (Wai and Langer 2016).

1.2.4.3. Mitochondrial biogenesis

Mitochondrial biogenesis is the process by which the mitochondrial copy number and activity increases within a cell as a response to metabolic stress (such as exercise) or an environmental stimuli, such as caloric restriction (Kelly and Scarpulla 2004). A major regulator of mitochondrial biogenesis is the peroxisome proliferator-activated receptor gamma coactivator 1-alpha (PGC-1 α) (Puigserver et al. 1998). It is a co-transcriptional regulator factor that induces biogenesis through the activation of different transcription factors including both nuclear respiratory factor 1 and 2 (NRF-1 and NRF-2), which promote the expression of TFAM, thus driving the replication and transcription of mtDNA (Virbasius and Scarpulla 1994). Other transcription factors include estrogen related receptor alpha (ERR α) and peroxisome proliferator-activated receptor alpha (PPAR α).

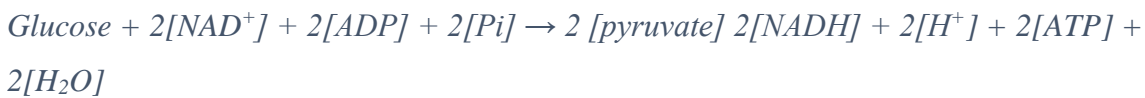
1.3. Mitochondrial function

1.3.1. Oxidative Phosphorylation (OXPHOS) and ATP synthesis

Mitochondria are the principle generators of cellular energy in the form of ATP, hence why they are commonly known as the “powerhouse of the cells” (Hatefi 1985).

1.3.1.1. The tricarboxylic acid (TCA) cycle

The generation of ATP is a multistep process which begins with glycolysis in the cytosol of the cell, where glucose is broken down into two molecules of pyruvate and two molecules of water (H₂O), as shown by **Equation 1.1** (Berg 2011). Pyruvate can also be a by-product of fatty acid β-oxidation.



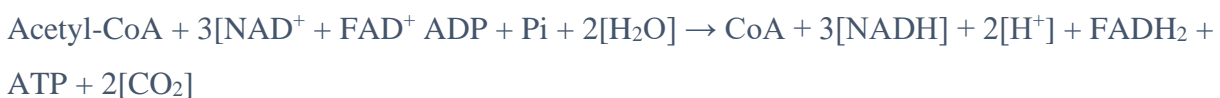
Equation 1.1: Glycolysis

The pyruvate is imported into the mitochondria via the mitochondrial pyruvate carrier (MPC) and is converted to acetyl-coenzyme (CoA) by the enzyme pyruvate decarboxylation (**Equation 1.2**).



Equation 1.2: Pyruvate decarboxylation

Acetyl-coenzyme (CoA), alongside NAD⁺ and FAD are major substrates in the tricarboxylic acid (TCA) cycle, also known as the Krebs’s cycle (Krebs and Johnson 1937) – highlighted by **Figure 1.5**. Here, the carbon atoms of the acetyl group of CoA are oxidized, producing citrate (catalysed by citrate synthase). Oxaloacetate is also converted to citrate. The TCA cycle is a series of reactions that produces one molecule of ATP and CO₂, as well as NADH (nicotinamide adenine dinucleotide) and FADH₂ (flavin adenine dinucleotide) which are electron carriers that are subsequently involved in the initial stage of OXPHOS. It also returns citrate to oxaloacetate (Berg 2011). **Equation 1.3** highlights the complete TCA cycle.



Equation 1.3: The TCA (Krebs's) cycle overall reaction

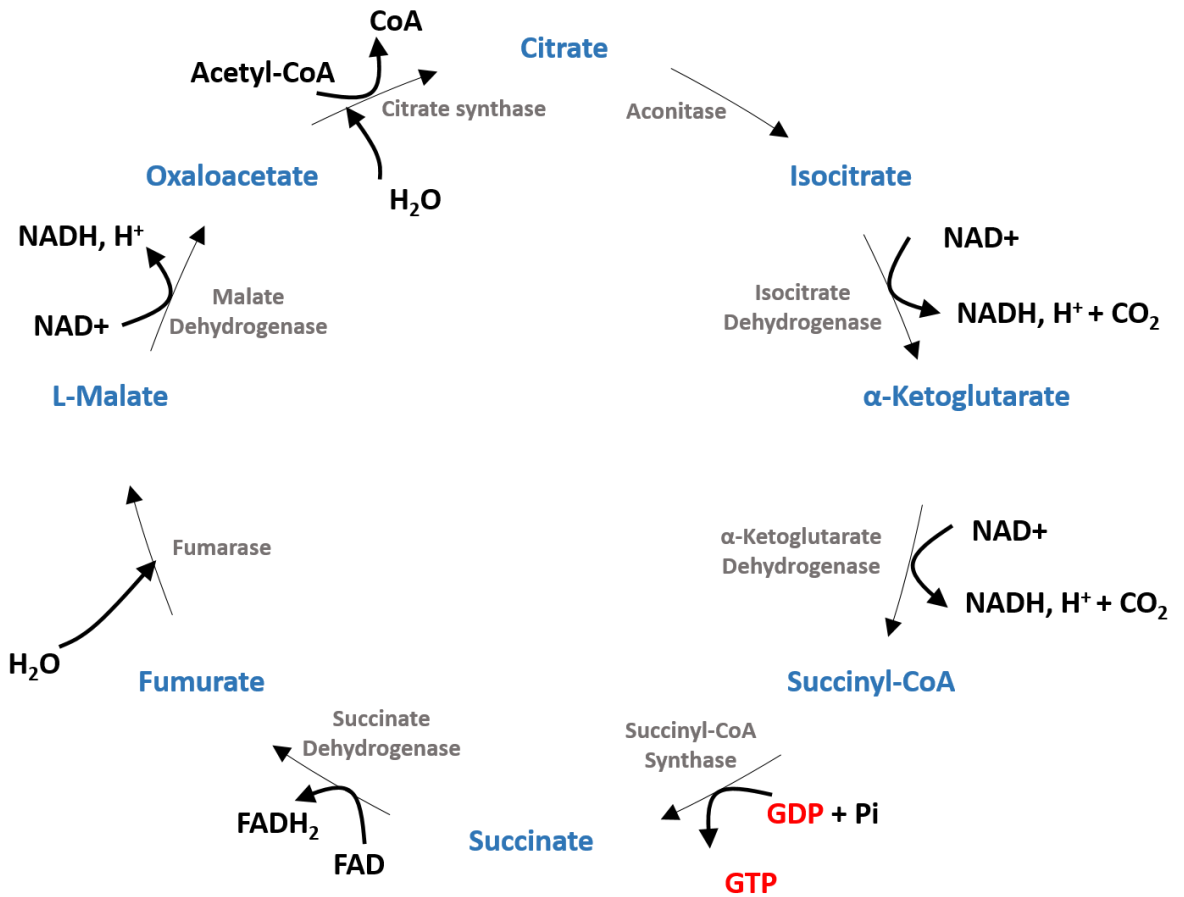


Figure 1.5: The TCA (Krebs) Cycle.

Eight intermediate redox reactions required for the conversion of Acetyl-CoA to CoA. A single molecule of GTP (red) or ATP is generated when inorganic phosphate (Pi) is transferred from Succinyl-CoA to either GDP or ADP. Essential electron carriers for the electron transfer chain are also produced; NADH and FADH₂.

1.3.1.2. Oxidative phosphorylation

The final stage of cellular respiration is OXPHOS where the vast majority of ATP is synthesised. The OXPHOS system is embedded in the IMM. At the core of the OXPHOS system is the ETC (also known as the mitochondrial respiratory chain) which consists of a series of complexes (Complex I -IV) in conjunction with ATP synthase (Complex V), which completes the OXPHOS system. Approximately 90 protein components make up OXPHOS – 13 of which are coded for by the mtDNA. The four complexes of the ETC catalyse the movement of electrons along the chain, as well as the translocation of protons from the matrix into the IMS, creating a proton motive force which drives the synthesis of ATP from ADP via complex V (Smeitink et al. 2001). The proton gradient across the IMM of the mitochondria is

180mV. This proton motive force is also essential for other processes such as ion transport across the inner membrane, protein import and Fe-S cluster biogenesis.

As shown in **Figure 1.6**, the electron carrying substrates NADH and FADH₂ enter the ETC via Complex I and II and are reduced to NAD/FAD. The electrons are transferred to ubiquinone (Q), a soluble electron carrier found within the IMS. Ubiquinone is reduced to ubiquinol (QH₂) by Complex III and the electrons are transferred to cytochrome *c* (cyt *c*), a water-soluble carrier. Complex IV then catalyses the final transfer of electrons to produce molecular oxygen (O₂) and water (H₂O). During this series of electron transfer, protons are translocated from the matrix into the IMS by complex I, III and IV. This coupled movement of electrons and translocation of protons creates the proton motive force which then drives the production of ATP from ADP and P_i via Complex V. This coupling of electron transfer and ATP production is known as the chemiosmotic theory, as first described by Mitchell (1961).

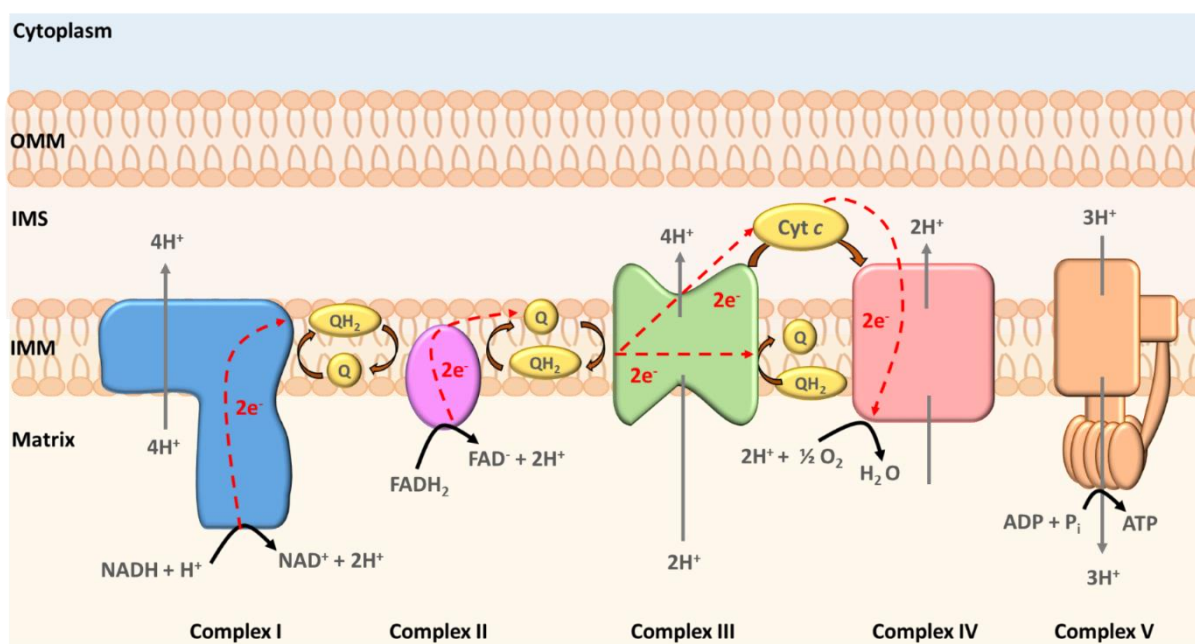


Figure 1.6: Oxidative Phosphorylation.

The five protein complexes (CI-CV) are embedded in the inner membrane of the mitochondria. Oxidative phosphorylation couple's electron transport and proton translocation to generate ATP. Electrons (in red) enter the electron transport chain through either Complex I or Complex II and are moved along to Complex III and Complex IV, via cytochrome *c*. This transfer of electrons generates the proton transfer from the matrix to the intermembrane space (IMS). Complex V utilises the proton gradient to produce ATP. The direction of electron movement is indicated by white arrows.

1.3.1.3. Complex I (NADH: Ubiquinone Oxidoreductase)

With a relative molecular mass of 1MDa, the mitochondrial Complex I (also known as NADH: ubiquinone oxidoreductase), is the first and largest complex of the ETC. This complex is the first entry point for electrons in the OXPHOS system (Brandt 2006; Hirst 2013). The main function is to oxidize NADH (derived from the breakdown of carbohydrates, amino acids and fatty acids) to NAD^+ , as well as playing a central role in both electron transfer and in ATP production through establishing the proton motive force (also known as the mitochondrial electrochemical proton gradient ($\Delta\Psi$)).

The movement of electrons through Complex I, as shown in **Figure 1.7**, is initiated when NADH is oxidised to NAD^+ . Two electrons and two hydrogen ions are released from this reaction and are transferred to the primary electron acceptor known as flavin mononucleotide (FMN) protein which is consequently reduced to FMNH_2 . The two electrons from FMNH_2 are then shuttled through a series of eight Fe-S clusters, each of which have an increased reduction potential. When electrons reach the final Fe- S cluster (N2 Fe-S cluster), they are transferred to the final electron acceptor known as ubiquinone (CoQ_{10}) which is reduced to ubiquinol (QH_2). This electron carrier is able to diffuse within the IMM to the next electron acceptor within Complex III of the ETC. The reduction reaction of CoQ_{10} is coupled with the translocation of four protons (H^+) from the mitochondrial matrix into the IMS (Ripple et al. 2013). This proton movement coupled with the electron movement contributes to the proton motive force, which leads to the eventual synthesis of ATP via ATP synthase (Complex IV) (Guerrero-Castillo et al. 2017; Lazarou et al. 2009; Mitchell 1961; Stroud et al. 2016). To summarise, with every two electrons which are transferred from NADH to ubiquinone, four protons are translocated (Galkin et al. 2006) - (**Equation 1.4**). It has been found that Complex I provides 40% of the proton motive force to drive the energy production (Giachin et al. 2016), hence it's importance in the synthesis of ATP.



Equation 1.4: Complex I reaction

(Berg 2011)

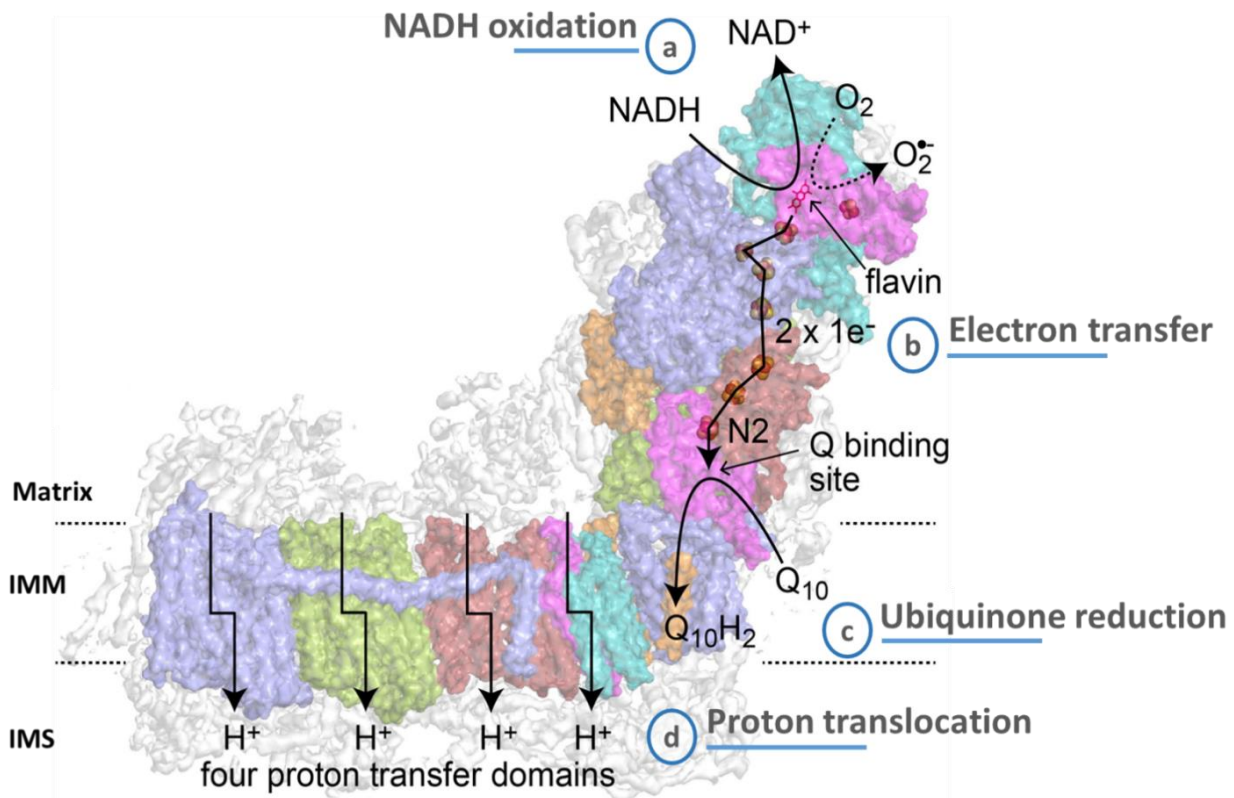
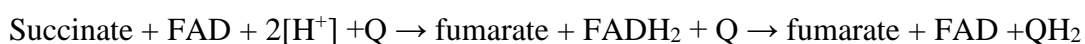


Figure 1.7: The movement of electrons through Complex I.

A-D indicate the order in which electrons move through the complex. **A)** Two electrons accepted from NADH **B)** and transferred to the flavin mononucleotide (FMN) and then shuttled through a series of eight iron-sulphur (Fe-S) clusters (black). **C)** They are passed to the final acceptor ubiquinone (Q_{10}) which is reduced to ubiquinol ($Q_{10}H_2$), **D)** consequently causing the release of 4 protons (H^+) into the intermembrane space of the mitochondria. Figure adapted from (Hirst and Roessler 2016).

1.3.1.4. Complex II - Succinate-ubiquinone oxidoreductase

Complex II, is the only complex which is completely encoded by the nDNA. At ~260 kDa in size, the complex has a dual role in ATP synthesis; firstly, within the TCA cycle where it oxidises the metabolite succinate to fumarate, generating $FADH_2$ in the process (**Equation 1.5**) and secondly within the ETC where it transfers electrons from $FADH_2$ to ubiquinone which is reduced to ubiquinol (Cecchini 2003; Sun et al. 2005). Therefore, with its involvement with the TCA cycle, Complex II links the TCA cycle to the respiratory chain.



Equation 1.5: Complex II reaction

(Berg 2011).

Complex II consists of four nuclear encoded subunits – the two hydrophilic catalytic subunits SDHA (flavoprotein (Fp); 70 kDa) and SDHB (iron-sulphur (Ip); 35 kDa) and the two hydrophobic subunits SDHC and SDHD (**Figure 1.8**). SDHA and SDHB project into the matrix of the mitochondria whilst SDHC and SDHD are embedded within the inner membrane, helping to stabilise the complex (Sun et al. 2005). SDHA harbours a covalently bound prosthetic group called flavin adenine dinucleotide (FAD) which acts as the initial acceptor of electrons donated by FADH_2 that is then consequently oxidised to FAD^+ , releasing two electrons. These electrons are then sequentially transferred through three Fe-S clusters within SDHB to ubiquinone at the Q binding site found between SDHC and SDHD (Lee et al. 1995). Ubiquinone is consequently reduced to ubiquinol. The haem group (heme b moiety) within SDHD stabilises the electrons adjacent to ubiquinol in the reduction process. Ubiquinol dissociates from SDHC to transfer electrons to Complex III (McNeil and Fineran 2013; Quinlan et al. 2012). The movement of electrons from FADH_2 to ubiquinone does not contribute towards the proton motive force.

There are two main assembly factors associated with Complex II; SDHAF1 which inserts the Fe-S clusters into SDHB (Ghezzi et al. 2009) and SDHAF2 which inserts FAD into SDHA (Hao et al. 2009).

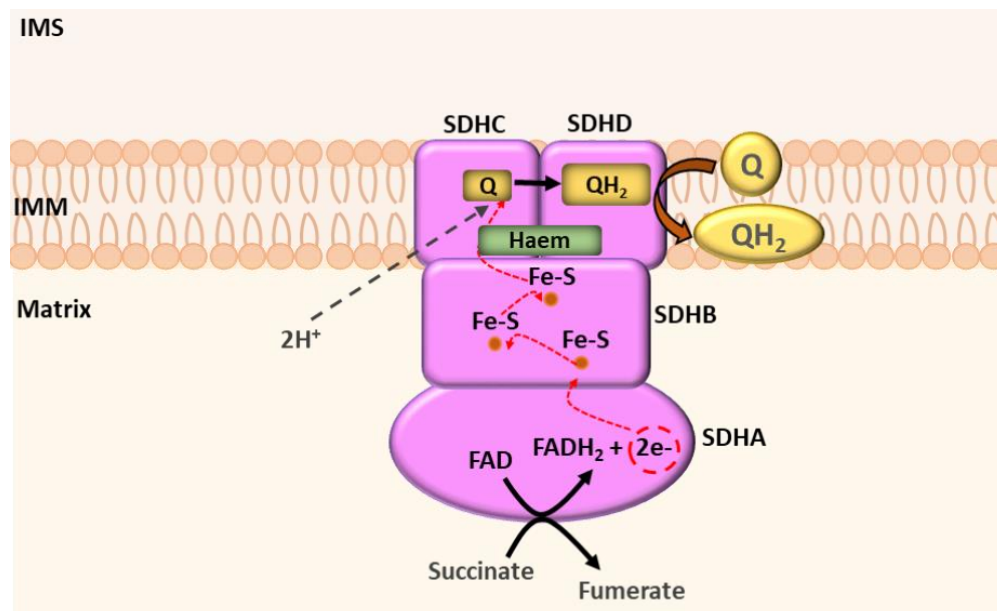


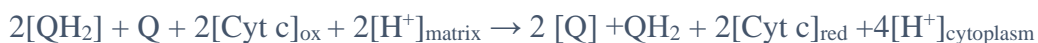
Figure 1.8: A schematic structure and function of Complex II.

The two hydrophilic catalytic subunits SDHA and SDHB project into the matrix of the mitochondria. The two hydrophobic subunits SDHC and SDHD are embedded within the inner membrane. The FADH_2 is oxidised to FAD^+ , releasing two electrons. Fe-S clusters in SDHB transfer the electrons to the haem group in SDHD and to ubiquinone in SDHC which is reduced to ubiquinol (QH_2). This dissociates from SDHC to transfer to CIII.

1.3.1.5. Complex III - Ubiquinol-cytochrome *c* oxidoreductase

Complex III is ~480 kDa in size and consists of 11 subunits. Cytochrome *b* is the only mtDNA encoded subunit whilst the remaining 10 are encoded by the nuclear DNA (Iwata et al. 1998; Xia et al. 1997; Yu et al. 1999). The catalytic centre of the complex is comprised of cytochrome *b* (MTCYB), cytochrome *CI* (CYC1), two haem moieties (cytochrome b_L and cytochrome b_H) and a Fe-S cluster known as the Rieske Fe-S cluster (UQCRFS1). The complex functions as a homodimer and has the role of catalysing the transfer of electrons from the reduced ubiquinol (QH₂), from Complex I and II, to cytochrome *b* and then to cytochrome *c* (Figure 1.9), as part of the process known as the ‘Q cycle’ (Mitchell 1975, 1976; Rieske 1976) – which processes two QH₂ molecules in succession, as shown in **Equation 1.6** and **Figure 1.9**.

The ‘Q cycle’ starts with the transfer of two electrons from ubiquinol (QH₂) to the Q₀ site. One electron is passed to the Rieske Fe-S cluster and cytochrome C₁ which in turn leads to the reduction of one cytochrome *c* (cyt *c*) molecule. During this, two hydrogen protons are pumped from the mitochondrial matrix to the IMS. The alternative electron is passed to haem b_L and haem b_H and then to the Q₁ site where ubiquinone is reduced to semi-ubiquinone radical (Q^{•-}). This process is repeated, allowing haem b_H to reduce the semi-ubiquinone to ubiquinol and in doing so removes an additional two protons from the matrix to the IMS. In total, this process is therefore coupled with the translocation of four hydrogen ions into the intermembrane space, thus contributing the proton motive force.



Equation 1.6: Complex III reaction

(Berg 2011)

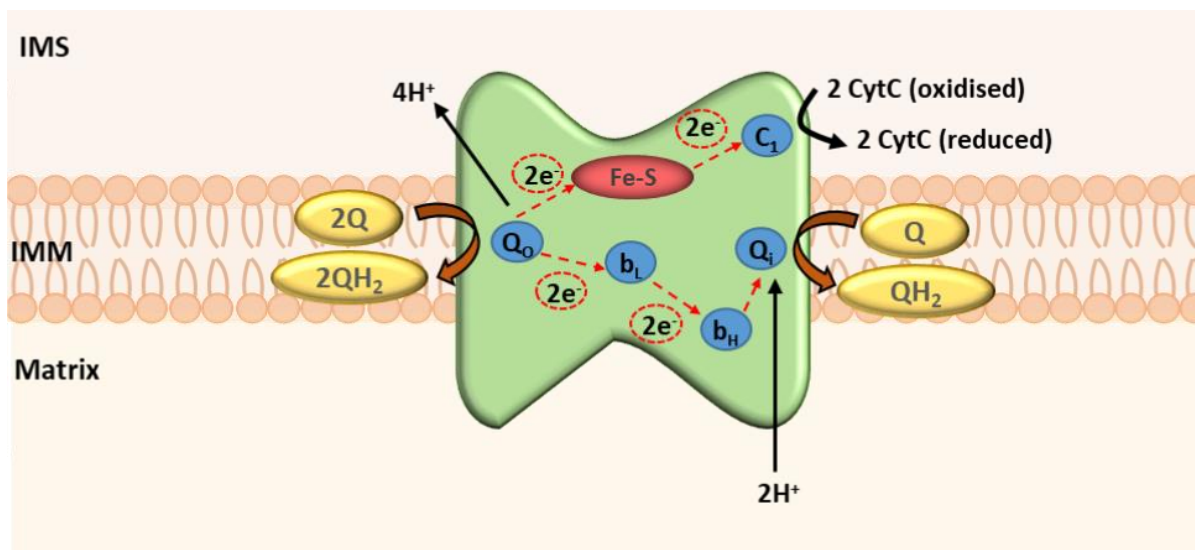


Figure 1.9: A schematic structure and function of Complex III.

The transfer of electrons in Complex III (process known as the *Q* cycle). Overall, four electrons ($2 \times 2e^-$) are required for the reduction of two cytochrome *c* (2CytC). 4 hydrogen protons (H^+) are pumped into the intermembrane space (IMS). The path of electrons is shown with red dashed line and the Rieske Fe-S cluster (red oval), cytochrome C_1 , haem moieties B_L and B_H and the two binding sites Q_0 and Q_1 .

1.3.1.6. Complex IV - Cytochrome *c* Oxidase

Complex IV, also known as cytochrome *c* oxidase (COX), is the terminal complex of the ETC and is embedded into the IMM. The complex has a molecular weight of 204 kDa and comprises of 13 subunits, of which three are mtDNA encoded (Tsukihara et al. 1996). These three subunits – COX-I, COX-II and COX-III are the largest subunits and form the functional core of Complex IV (Capaldi 1990; Rubin and Tzagoloff 1973). The complex is active as a dimer and has the role in oxidising cytochrome *c* (cyt *c*) and transferring the electrons to molecular oxygen (O_2) (Shoubridge 2001). The oxygen molecule is subsequently reduced to H_2O . Overall, four cytochrome *c* molecules are oxidised, thereby four electrons are required for one molecule of oxygen to be reduced to H_2O .

The crystal structure of Complex IV was resolved by Tsukihara and colleagues in 1996 and showed that the core subunits contain the prosthetic groups which are required for the catalytic function of the complex. COX-I contains the two haem moieties; a and a_3 and copper centre Cu_B . COX-II contains the copper centre Cu_A . It also contains a magnesium and zinc ion (Tsukihara et al. 1996). COX-III is also associated with proton translocation (Wilson and Prochaska 1990).

The electron movement through Complex IV is shown in the schematic **Figure 1.10** and is as follows; each electron from reduced cytochrome *c* is transferred to the binuclear Cu_A site and haem a. They are then transferred to haem a₃ and Cu_B site which forms the oxygen binding site (binuclear site) known as haem a₃-Cu_B. This is reduced, consequently producing in total, two molecules of H₂O (Capaldi et al. 1995; Faxen et al. 2005). The transfer of electrons is coupled with the translocation of four protons from the matrix to the IMS, per oxidised molecule (**Equation 1.7**) (Belevich et al. 2006).

The nuclear-encoded subunits are known as the accessory subunits and have been found to have a role in the regulation and stability of the fully assembled complex (Galati et al. 2009). They also have the role of protecting the core subunits from oxidative damage (Diaz et al. 2006; Shoubridge 2001; Soto et al. 2012).

Briefly, the assembly of Complex IV has been found to initiate with the synthesis of COX-1, followed by COX-II and COX-III. The assembly factor Surf-1 has a role in inserting the haem groups (Pacheu-Grau et al. 2015).



Equation 1.7: Complex IV reaction

(Berg 2011)

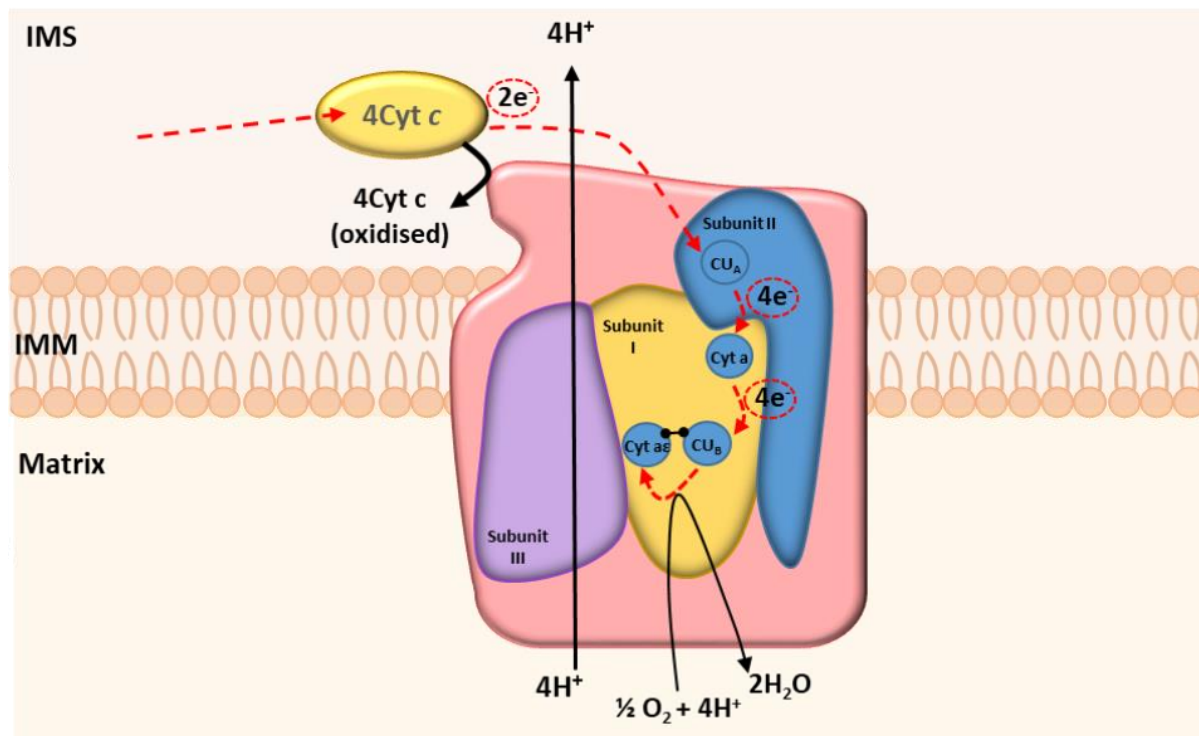


Figure 1.10: A schematic structure and function of Complex IV.

A simplified structure of Complex IV showing the movement of electrons and translocation of protons. The three mitochondrial DNA encoded subunits contain the prosthetic groups – COX-1 (yellow) contains the two haem moieties, COX-2 (subunit II - blue) contains the copper centre Cu_A and COX-3 (subunit III = purple) is involved in proton translocation. Electrons reduced from cytochrome c are transferred to the Cu_A site, then to haem (cyt) a, and lastly to the oxygen binding site haem (cyt) a_3 - Cu_B , producing H_2O . The transfer of electrons is coupled with the translocation of four protons from the matrix to the intermembrane space, per oxidised molecule. Figure is taken from (Nelson et al. 2008).

1.3.1.7. Complex V - ATP Synthase

Complex V (ATP synthase), utilises the proton motive force generated by Complex I, III and IV to drive the conversion of ADP and inorganic phosphate (P_i) to ATP. The complex is ~600 kDa in size and comprises of 13 structural subunits, of which two are mtDNA encoded (ATPase 6 and 8) (Pogoryelov et al. 2009).

The structure, as schematically shown in **Figure 1.11**, is divided into two functional regions - the F_0 and F_1 regions, which are joined together by a central and peripheral stalk. The F_1 region protrudes into the matrix and is the catalytic unit of Complex V. It is formed by five polypeptide chains; β (x3), α (x3), δ , γ and ϵ . Both α and β chains form a hexameric $\alpha_3\beta_3$ ring structure which catalyses the synthesis of ATP through binding ADP and P_i . However only the β subunits have catalytic activity (Abrahams et al. 1994). The δ and γ polypeptides form

the central stalk of Complex V and connects both regions together. The F_0 region is embedded into the IMM and is organised into a c-ring structure (12 'c' subunits) that forms a proton channel, allowing for the movement of protons across the IMS to the matrix.

The proton gradient generates a proton motive force. The movement of protons through the c-ring is coupled with the rotation of the rotary motors; c ring and δ , γ and ϵ subunits. As F_1 rotates, the β subunit undergoes a structural conformational change (Noji et al. 1997). The complete 360° rotation catalyses ATP synthesis in a proton dependent manner (Abrahams et al. 1994) – a full rotation is coupled to the transfer of eight protons and the production of three ATP molecules (Watt et al. 2010).

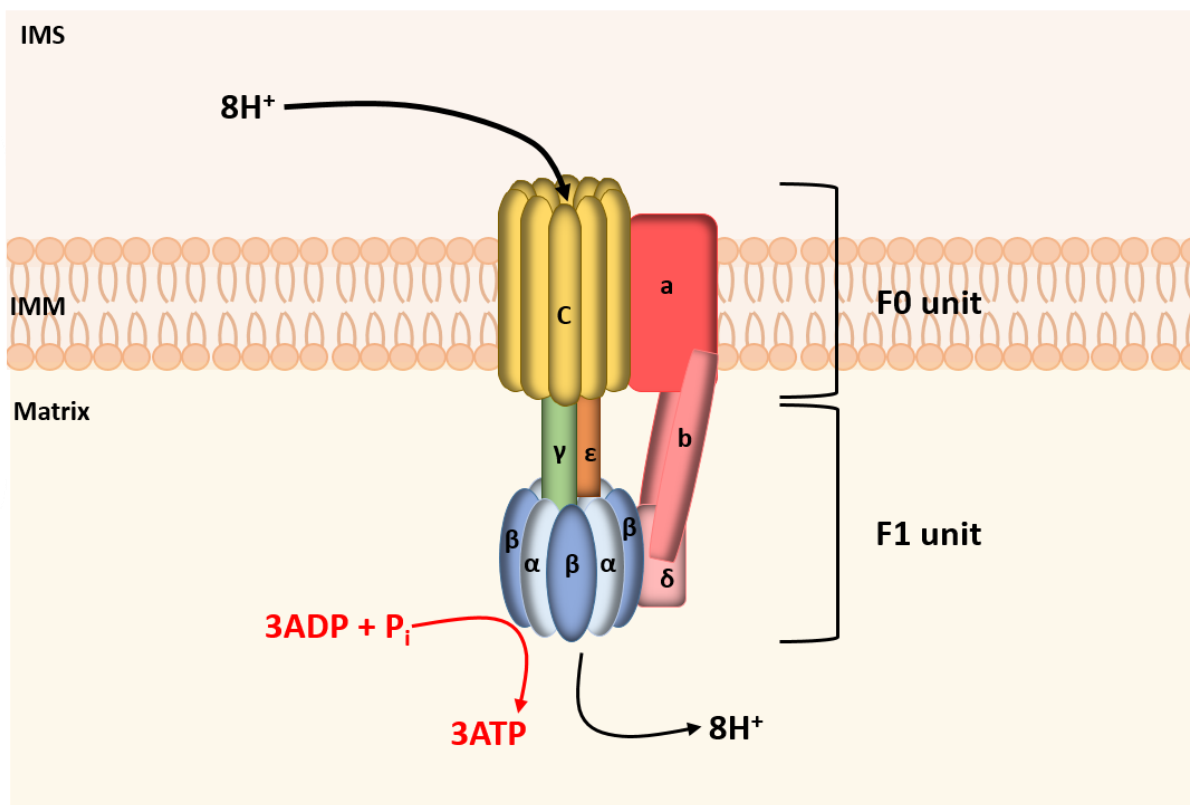


Figure 1.11: A schematic diagram of Complex V (ATP synthase).

The diagram illustrates the structural arrangement of subunits of Complex V. The complex has the role of generating ATP from ADP and inorganic phosphate (P_i) which is achieved through the use of the electrochemical gradient generated from Complexes I-IV. Protons flow through the C-ring along the electrochemical gradient, leading to the rotation of the $\alpha\beta$ ring of the F1 unit. This causes the formation of ATP.

1.3.1.8. Supercomplexes

Individual respiratory chain complexes can be organised into supercomplexes, which are also known as ‘respirasomes’. These were first postulated following the analysis of yeast and bovine heart mitochondria using Blue Native Polyacrylamide gel (BN-PAGE) (Schagger and Pfeiffer 2000, 2001) and were further confirmed using EM (Dudkina et al. 2005). There are various types of supercomplexes which are found in co-existence with single ETC complexes in the IMM; CI/CIII₂/CIV, CI/CIII₂, and CIII₂/CIV₁₋₂. The most well studied of these is the CICI₂CIV supercomplex (Complex I monomer, Complex III dimer and Complex IV monomer) for which the spatial arrangement has been deduced as shown in **Figure 1.12** (Dudkina et al. 2005; Gu et al. 2016; Letts et al. 2016; Wu et al. 2016). It has been estimated that approximately 85%–100% of Complex I molecules are found in supercomplexes, 55%–65% of Complex III and only 15%–25% of Complex IV (Greggio et al. 2017; Schagger and Pfeiffer 2001). The three individual complexes pass electrons from NADH to O₂ (NADH:O₂ oxidoreduction) through the ETC, contributing to the proton motive force, therefore, the supercomplex can undertake respiration in the presence of ubiquinone and cytochrome *c*, hence the term ‘respirasomes’. Supercomplexes have been found to be important for the stability of ETC complexes (Acin-Perez et al. 2008) and protecting the complexes from ROS (Maranzana et al. 2013). In terms of assembly, it was believed that the supercomplex provided a scaffolding for the completion of Complex I assembly whereby the final part of the peripheral arm of the complex (the N module) was added only when the remainder of the complex had been assembled into the supercomplex. The theory behind this notion was so that Complex I was not activated before the supercomplex was completely assembled (Moreno-Lastres et al. 2012). However, this has been proven otherwise by Guerrero-Castillo and colleagues (2017), who showed that Complex I was fully assembled in a stepwise manner before it combined with Complex III and IV into a supercomplex. The assembly of Complex I is described in detail in **Chapter 3**.

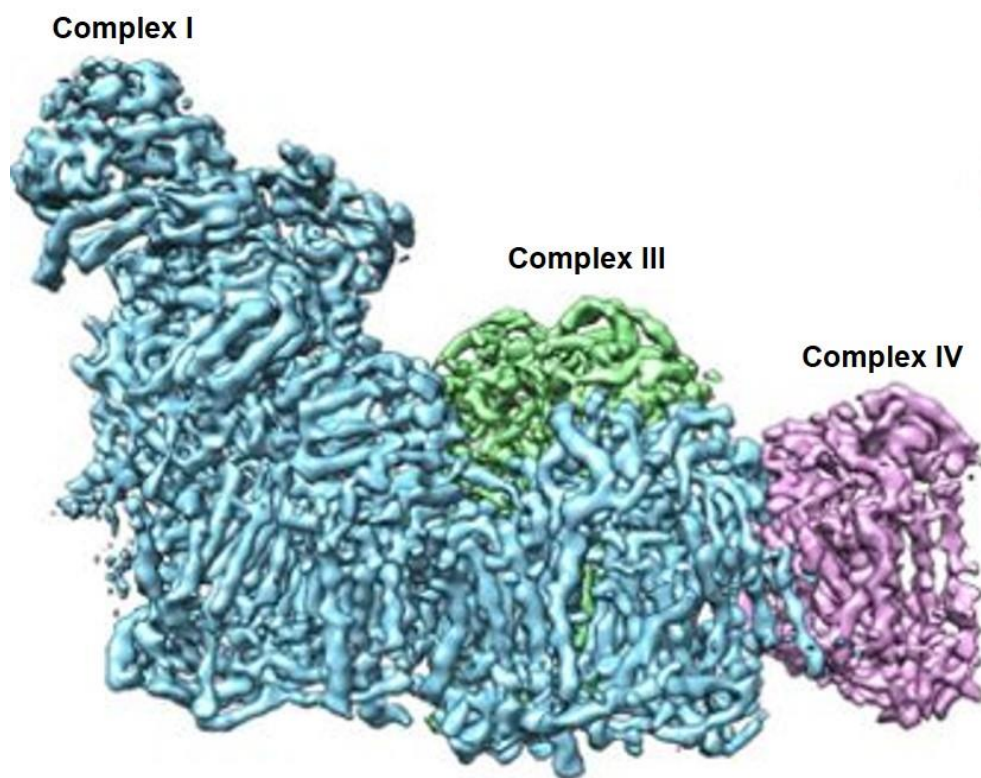


Figure 1.12: Crystal structure of ovine supercomplex.

The CI/CIII₂/CIV respirasome supercomplex. Complex I: blue, Complex III: green, Complex IV: pink.

Figure has been adapted from Letts et al. (2016).

1.3.2. Other functions of Mitochondria

1.3.2.1. Reactive oxygen species (ROS) production

It was initially believed that ROS production was a major cause of cell damage, however it has now been shown that ROS signalling has roles in cell differentiation, regulation of autophagy (Scherz-Shouval et al. 2007), apoptosis (Pierce et al. 1991) and immune cell activity (Sena et al. 2013; West et al. 2011).

The ETC, in particular Complex I–III, is a major source of ROS in cells (Boveris et al. 1972; Turrens and Boveris 1980). This was first reported in 1966 (Jensen 1966), followed by the work presented by Chance and colleagues who demonstrated the production of H₂O₂ in isolated mitochondria (Loschen et al. 1971). During the movement of electrons along the ETC, some electrons leak out and react with O₂ leading to the production of the most common ROS; superoxide anion (O₂^{•-}) – the precursor for other ROS, through partial reduction. Complex I produces O₂^{•-} in the matrix and Complex III produces O₂^{•-} on both sides of the IMM. Complex I is a vast producer of O₂^{•-}, influenced by either a high proton gradient caused by a decrease in ATP synthesis or a high NADH/NAD⁺ ratio in the matrix

(Murphy 2009). The $O_2^{\bullet-}$ is converted to hydrogen peroxide (H_2O_2) by superoxide dismutase (SOD) in the matrix (catalysed by SOD2) and IMS (catalysed by SOD1) (Sabharwal and Schumacker 2014). H_2O_2 is usually converted to H_2O by the antioxidant molecule glutathione peroxidase (Turrens 2003). However, when there is an excessive production of ROS or the antioxidant system fails to counteract the ROS, H_2O_2 can leak into the IMS and cytosol where it can oxidise proteins, lipids or mtDNA, leading to eventual cell death (Murphy et al. 2011).

1.3.2.2. Apoptosis

Apoptosis, or programmed cell death is a critical process for tissue homeostasis in multicellular organisms. First described by Kerr et al. (1972), the process is defined by the morphological changes which occur in dying cells including blebbing, chromatin condensation, nuclear fragmentation and cell shrinkage.

There are two major apoptotic pathways; the intrinsic pathway and the extrinsic pathways. Firstly, the intrinsic pathway, also known as the mitochondrial pathway due to the essential role of mitochondria (Wang and Youle 2009). This role was first established by biochemical studies identifying several mitochondrial proteins that can activate apoptosis directly, particularly cytochrome *c* and the mitochondrial apoptosis inducing factor (AIF) (Liu et al. 1996; Susin et al. 1999). These proteins reside in the IMS but in response to variable apoptotic signals, they are released into the cytosol of the cells. Cytochrome *c*, released after signal from Bid, initiates the activation of procaspase-9 which activates downstream caspases such as caspase-3, leading to the eventual apoptotic changes in the cell after further cleavage of substrates. Chromatin and large scale DNA fragmentation occurs due to the AIF protein, which translocate from the mitochondria to the nucleus of the cell (Liu et al. 1996; Susin et al. 1999; Wang 2001). The alternative apoptotic pathway is independent of mitochondria, known as the extrinsic pathway (or the death receptor-dependent pathway) and is activated by death receptors of the tumour necrosis factor (TNF) receptor superfamily.

1.3.2.3. Haem biogenesis and Fe-S cluster biogenesis

Haem is the major functional form of iron and is synthesised in mitochondria. The molecule is found within a tetrapyrrole which allows for the haem to function as an electron carrier and a catalyst for redox reactions. The mitochondrial membrane associated enzyme ferrochelatase catalyses the insertion of the ferrous iron into the protoporphyrin IX (a tetrapyrrole) to form haem (Ajioka et al. 2006; Wu et al. 2001).

Fe-S clusters are essential for the movement of electrons through the ETC and it has been shown that the mitochondria is the main site of Fe-S cluster assembly (Lill et al. 2012). For

biogenesis to occur, there is a requirement for a supply of iron which is imported from the cytosol, involving monothiol glutaredoxins (GrX) as iron donors and the inner membrane iron carrier Mrs3 and Mrs4. These carriers require the proton motive force to allow for membrane passage. The Fe-S cluster biogenesis is initiated by the mitochondrial iron sulphur cluster (ISC) complex which comprises 17 mitochondrial proteins including the following; IscU which acts as a scaffold protein for Fe-S cluster synthesis, NFS1 (cysteine desulfurase) which is a sulphur donor, GRP75 (mitochondrial Hsp70 chaperone) which transfer Fe-S cluster from the scaffold protein and FXN (frataxin) which is an iron donor in the initial stage of biogenesis (Lill et al. 2012; Stehling and Lill 2013).

1.3.2.4. Calcium (Ca^{2+}) signalling and handling

Calcium (Ca^{2+}) is an important cellular signal and mitochondria have been shown to have an important role in cytosolic Ca^{2+} homeostasis due to their ability to uptake and buffer Ca^{2+} (Carafoli 2003; Cohen and Fields 2004; Rossi and Lehninger 1964). Calcium enters the mitochondrion through porin found in the OMM and the mitochondrial Ca^{2+} uniporter (MCU) (De Stefani et al. 2011). In the process of entering the mitochondrion through both the OMM and IMM, it travels down an electrochemical gradient leading to the reduction of cytoplasmic calcium.

Calcium is a major modulator of many cellular functions. For example, an increase in the uptake of Ca^{2+} has been shown to stimulate the function of the electron transport chain and thereby increasing ATP production (Denton and McCormack 1980; Griffiths and Rutter 2009). But an excessive accumulation of Ca^{2+} is toxic for the mitochondria and can lead to the induction of apoptosis (Mattson and Chan 2003; Orrenius et al. 2003).

In addition, the control of intracellular Ca^{2+} is important for the normal function of skeletal muscle. This is due to the fact that Ca^{2+} is the signalling messenger that triggers all processes underlying muscle excitation-contraction, particularly in neuromuscular junctions (MacIntosh 2003).

1.4. Mitochondrial DNA

1.4.1. The Mitochondrial genome

Aside from the nucleus, mitochondria are the only other organelle which contains genomic information. The human mitochondrial genome (mtDNA), as schematically shown in **Figure 1.13**, is found in the matrix of the mitochondria and is organised into a compact circular, double-stranded DNA (dsDNA) with a heavy (H strand – outer circle) and a light (L-strand – inner circle) strand. These two strands are distinguished by their nucleotide composition (G and T base) which result in the different buoyant densities. The H strand is guanine rich whilst the L strand is cytosine rich.

The genome was originally sequenced by Anderson et al. (1981) and later revised by Andrews et al. (1999), which is known as the Revised Cambridge Reference Sequence (rCRS). The genome is comprised of 16,569 base pairs and contains 37 genes; 28 genes on the H strand and nine genes on the L strand. Of these 37 genes, 13 encode essential hydrophobic proteins of the OXPHOS system and the remaining 24 genes encode the RNA machinery consisting of two RNAs (16S RNA (the large ribosome) and 12S RNA (the small ribosome)) and 22 tRNAs (Anderson et al. 1981).

In comparison to the nuclear genome, the genome is highly compact with no introns within the mtDNA genes, nor any intergenic regions between the encoded proteins. However, the only exception to this is the major non-coding region (NCR) which spans 1.1kb of the molecule and includes the displacement loop (D-loop) which extends from the O_H to the termination-associated sequence (TAS) (Nicholls and Minczuk 2014). The D-loop contains the origin of heavy strand replication (O_H) and the H strand transcription promoters HSP1 and HSP2 – the sites at which replication and transcription are initiated from respectively.

The mitochondrial genome is a multi-copy genome meaning there are numerous copies of the molecule in a mitochondrion. It has been estimated that mammalian cells can contain between 5,000 to 10,000 copies of the genome; the exact number varying on a cell-type specific basis depending on the cellular energy demand of the cell (Lightowlers et al. 1997; Miller et al. 2003). For example, a mature oocyte contains between 100,000 to 600,000 copies of mtDNA (Shoubridge and Wai 2007; Wai et al. 2010) whilst fibroblasts contain very few due to their capability of relying on anaerobic glycolysis for ATP. In addition, cardiomyocytes and skeletal muscle have been shown to have approximately 7,000 and 3,600 mtDNA molecules respectively (Miller et al. 2003). Unlike the nuclear genome which is organised in

1.4.2. Replication of mitochondrial DNA

Replication of the mtDNA genome occurs in the matrix of the mitochondria. Unlike the replication of nuclear DNA which occurs only once during cell division, the replication of the mtDNA occurs continuously and is independent of the cell cycle in replicative and post-mitotic cells such as skeletal muscle and nerve cells of the central nervous system (Bogenhagen and Clayton 1977). This is known as a relaxed replication and this process has been found to take approximately 60-75 minutes (Clayton 1982; Korr et al. 1998). Another difference between the replication of the nuclear DNA and mtDNA is that the proteins included in the mtDNA replication machinery (as described below) are distinct and many are related to replication factors founded in bacteriophages (Shutt and Gray 2006).

1.4.2.1. The replication machinery

Mitochondria contain their own DNA replication machinery comprising of at least four key proteins - often referred to as the 'mitochondrial DNA minimal replisome' (Korhonen et al. 2004). These proteins include the mitochondria DNA polymerase gamma (POLG), mtDNA helicase TWINKLE and mitochondrial single stranded DNA binding protein (mtSSB) and the mitochondrial DNA polymerase POLRMT which is likely to synthesise the RNA primers needed for replication (Falkenberg et al. 2007; Fuste et al. 2010; Gustafsson et al. 2016; Milenkovic et al. 2013; Wanrooij et al. 2008). This is schematically shown in **Figure 1.14**.

At the core of the machinery is POLG which is the only replicative polymerase in the mitochondria. This heterometric protein consists of a catalytic subunit POLG-A which contains a 3' to 5' exonuclease domain, allowing for an efficient proofreading of the newly synthesised DNA strand. The two identical POLG-B (also called POLG2) subunits have dsDNA binding activity as well as the ability to increase the catalytic and processing activity of POLG-A through enhancing the interaction with the DNA substrates (Gray and Wong 1992; Gustafsson et al. 2016; Milenkovic et al. 2013). TWINKLE is a hexameric protein which catalyses the 5' to 3' nucleotide triphosphate dependent unwinding of the dsDNA to a single stranded DNA (ssDNA) molecule (Korhonen et al. 2004; Spelbrink et al. 2001). It has been shown that POLG requires TWINKLE to synthesise dsDNA (Korhonen et al. 2004). TWINKLE moves with POLG to the replication fork where it initiates the unwinding of the DNA (Gustafsson et al. 2016). The tetrameric mtSSB protein has a role in stabilising the single stranded regions of the mtDNA at the replication fork and protects it from nucleolysis. It also enhances primer recognition during replication and has a stimulatory effect on TWINKLE unwinding activity (Korhonen et al. 2004; Milenkovic et al. 2013). Finally, the

POLRMT protein forms primers to initiate DNA synthesis of the heavy strand (Chang and Clayton 1985).

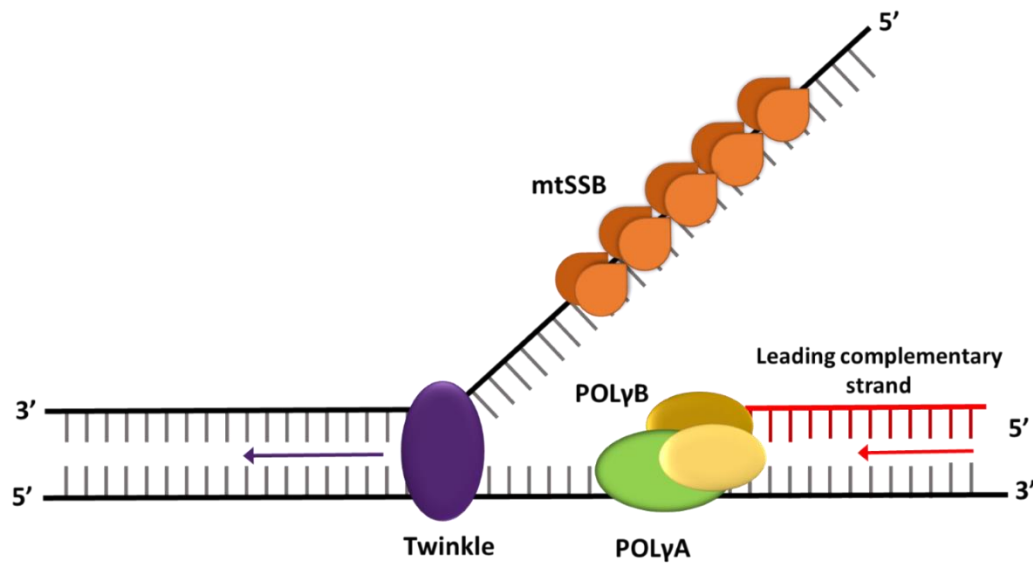


Figure 1.14: A schematic diagram of the mitochondrial DNA replication machinery.

Twinkle (purple) unwinds the mtDNA into a single stranded DNA which is stabilised by mtSSB (orange). PolyA and B (green and yellow respectively) synthesises the nascent leading complementary strand (red, direction shown by red arrow). Figure is adapted from Tsai and John, 2016.

1.4.2.2. Models of mtDNA replication;

There is currently no scientific consensus on a single mechanism for the mode of replication of mtDNA, therefore there are several models that exist. Currently, there are two prevailing models that are proposed; strand-displacement (asynchronous) and strand-couple (synchronous) replication (Holt and Reyes 2012).

The Strand-displacement model

One model is the ‘Strand-displacement model’ which is also known in the literature as the ‘asynchronous strand displacement’ model. This was first described by Robberson et al. (1972) and later refined by Clayton (1982) who used EM images to demonstrate that replication is initiated at the O_H within the D- loop, causing a displacement of the L strand. As shown schematically in **Figure 1.15(A)**, the H strand is replicated from 5’ to 3’ and during the synthesis of the new H strand, mtSSB covers the displaced parental H strand and blocks POLRMT, preventing random initiation of RNA primer synthesis. Replication of the H strand is 70% completed before the origin of replication of the L strand (O_L) is exposed, thus initiating the replication of the L strand which occurs from 3’ to 5’ (Clayton 1982; Gustafsson

et al. 2016; Robberson et al. 1972). Replication is terminated once the H strand is complete. Since the H strand is first replicated, this is often called the leading strand and thus, the L strand is termed the lagging strand.

The Strand Coupled model

The second model was suggested by Holt et al., 2000 and is called the ‘Strand couple model’ (also known as the coupled leading lagging strand model) – shown in **Figure 1.15(B)**. The analysis of 2-dimensional agarose gel electrophoresis (2D-AGE) showed partially single stranded replication intermediates and so the model suggested that replication is initiated at the zone of replication (O_{RIZ}) which is a stretch of mtDNA encompassing the genes *MT-ND5*, *MT-ND6* and *MT-CYTB*. In contrast to the strand displacement model, replication terminates at the O_H . The replication of the H strand is followed by replication of the L strand in the same direction, hence why the model is referred to as ‘Strand coupled’ (Bowmaker et al. 2003; Holt et al. 2000).

The RITOLS model

The third model is the ‘RNA-incorporated throughout the lagging strand’ – RITOLS – model which is based on the findings of extended RNA tracts incorporated into replication intermediates and RNA hybridised to the parental H strand (Yang et al. 2002; Yasukawa et al. 2006) – shown in **Figure 1.15(C)**. In the RITOLS model, replication is initiated at either within the non-coding region close to the O_H or at the O_H . The replication of the H strand progresses until O_L is exposed and the replication of the L strand is initiated with the simultaneous incorporation of RNA onto the L strand. The RNA is either replaced by DNA or converted to DNA (maturation) – this either occurs when the entire strand is incorporated with RNA or two-thirds completed (Yasukawa et al. 2006). The replication is unidirectional. The RITOLS model is essentially similar to the strand displacement model whereby both models suggest that replication is initiated at the O_H and the two strands are replicated separately. However, a major difference in the models is that within the RITOLS model, the parental H strand is coated with RNA rather than mtSSB (Gustafsson et al. 2016).

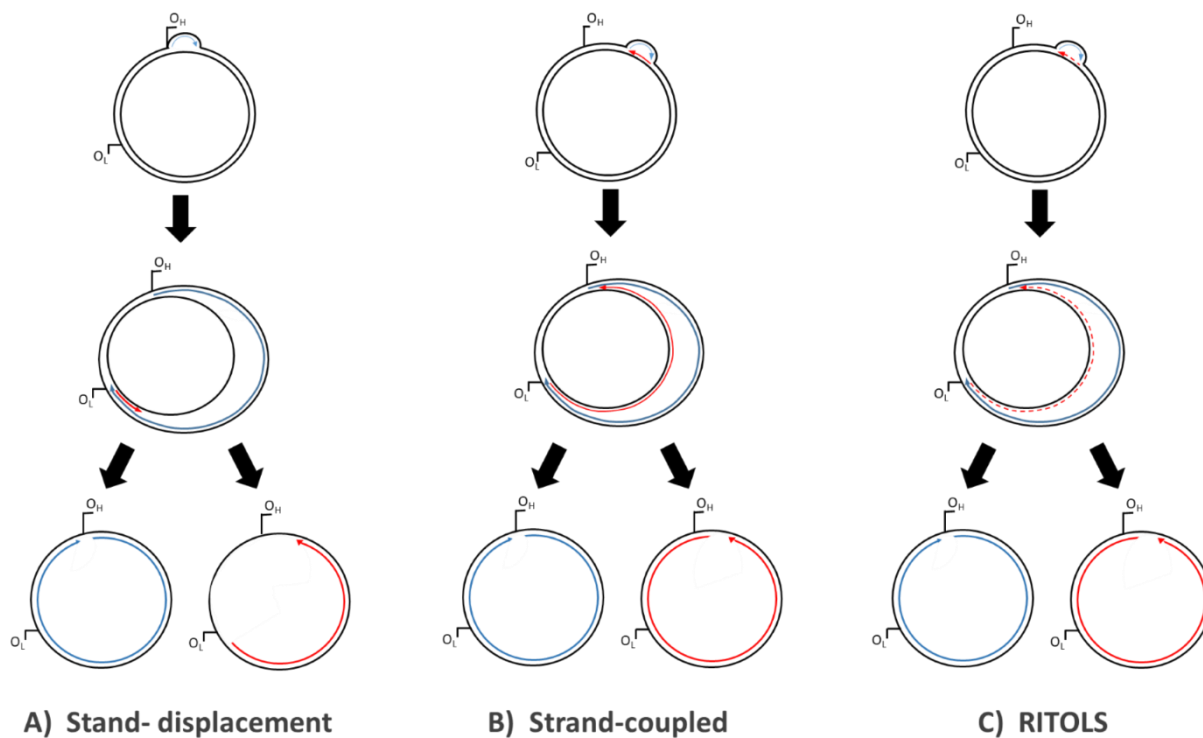


Figure 1.15: The current models of replication of mammalian mitochondrial DNA.

Three models of replication have been proposed starting with the (A) Strand-displacement model - replication of mtDNA starts at the origin of replication for H strand (O_H) within the D-Loop. Displacement of light strand occurs. 70% into replication of nascent H strand, origin of light stand (O_L) is exposed and replication can commence in the opposite direction until both strands have been replicated. (B) The strand couple model - replication begins from the zone of replication ($Oriz$) on the genome and replication of both strands occur bidirectionally. (C) The RNA incorporation throughout the lagging strand (RITOLS) model - replication is initiated at or close to the O_H , displacing the L strand. The model is very similar to the strand-displacement model only RNA intermediates are incorporated into the L strand (dashed lines) which are then replaced by or converted (matured) to DNA. Figure has been adapted from (Krishnan et al. 2008).

1.4.3. Transcription of mitochondrial DNA

The D-loop contains three promoters required for the transcription of mtDNA; HSP1, HSP2 and LSP (Chang and Clayton 1984; Montoya et al. 1982; Zollo et al. 2012). Transcription occurs bi-directionally and gives rise to polycistronic transcripts – mRNA transcripts which encode several genes. Transcription of mtDNA is mediated by at least four key proteins; POLMRT (Ringel et al. 2011; Tiranti et al. 1997), mitochondrial transcription factor A (TFAM) (Fisher and Clayton 1988; Shi et al. 2012), mitochondrial transcription factor B2 (TFB2M) (Falkenberg et al. 2002) and the mitochondrial termination factor 1 (MTERF-1)

(Gaspari et al. 2004; Kruse et al. 1989; Yakubovskaya et al. 2010). Promoter recognition and transcription initiation requires the simultaneous presence of the first three factors.

The transcription of the H strand is initiated at HSP1 and HSP2 and the L strand transcription occurs from LSP. HSP1 is located upstream from the *tRNA^{Phe}* gene and the transcripts of this H strand promoter contain two tRNA genes (*tRNA^{Phe}* and *tRNA^{Val}*) and two rRNA genes (12S rRNA and 16S rRNA). The HSP2 promoter is located approximately 100 base pairs (bps) further downstream within the D loop at the boundary between *tRNA^{Phe}* and the 12S rRNA genes. Transcription from this promoter proceeds along almost the entire length of the H strand and so contains majority of the genes located on the strand. Transcription from LSP generates a single transcript containing all genes contained on the L strand – *MTND6* and 8 tRNAs (Kuhl et al. 2016; Montoya et al. 1982).

The sequence of transcription can be briefly described as the following. Firstly, TFAM initiates transcription by sequence specific binding to a region 10 to 15bp upstream of the HSP and LSP (Fisher et al. 1987), causing the DNA to unwind and a structural alteration of the promoter region to occur (Hallberg and Larsson 2011). This recruits POLRMT to the promoters where it binds to TFAM and subsequently recruits TFB2M, completing the transcription complex (Rebelo et al. 2011). TFB2M executes the elongation step after initiation. The termination of transcription (characterised for HSP1 transcripts) is executed by MTERF-1 which binds to a specific 28bp region in the *tRNA^{Leu (UUR)}*, resulting in DNA helix unwinding and base flipping leading to termination (Roberti et al. 2006; Yakubovskaya et al. 2010).

The resulting transcripts undergo post-transcriptional processing through the process of ‘tRNA punctuation model’ (Ojala et al. 1981), which states that tRNAs flanking the transcripts provide the signals for the endonucleolytic excision of the tRNAs, leading to the release of individual tRNAs, rRNAs and mRNAs. It has been shown that processing takes place in distinct speckles named the mitochondrial RNA granules (Antonicka et al. 2013; Jourdain et al. 2013) and these contain the enzyme RNase P (consisting of 3 subunits – mitochondrial RNase P proteins (MRPP) 1 -3). RNase P cleaves the transcript at the 5’ end of the tRNAs (Rossmannith and Karwan 1998). On the other hand, the enzyme RNase Z (coded by the *ELAC2* gene) which cleaves the 3’ end of the tRNAs (Schiffer et al. 2002) are not found in the mitochondrial RNA granules but within the mitochondrial matrix (Jourdain et al. 2013).

1.4.4. Translation of mitochondrial DNA

The mitochondrial genome only encodes for 13 proteins, all of which are components of the OXPHOS system. These genes are translated by the mitochondrial ribosomes at the matrix face of the inner membrane (Hallberg and Larsson 2014; Herrmann et al. 2013; Lightowlers et al. 2014).

Mitochondrial ribosomes (known as mitoribosomes), contain two mtDNA- encoded proteins, the *12S rRNA* and the *16S rRNA* alongside a further 80 nDNA-encoded proteins.

Mitoribosomes have a sedimentation coefficient of 55s and are comprise of a large subunit (mtLSU, also known as 39S) and a small subunit (mtSSU, also known as 28S). The 39S subunit is involved in the catalysis of peptidyl-transferase and the 28S subunit binds the mRNA and is involved in the initiation of translation and decoding. This subunit also undergoes a conformational change during the elongation stage of translation. The 12S rRNA is found in the 28S subunit and the 16S rRNA is found in the 39S subunit. The mitoribosomes differ from the cytoplasmic ribosomes as they are characterised by a higher protein content rather than rRNA (ratio of rRNA/protein) (Amunts et al. 2015; Brown et al. 2014; Greber et al. 2014; Kaushal et al. 2014).

The translation process includes three phases – initiation, elongation and termination, as shown by **Figure 1.16**.

Initiation:

Initiation occurs through two mitochondrial initiation factors; MtIF2 and MtIF3 (Koc and Spremulli 2002; Ma et al. 1995). MtIF3 aligns the start codon (AUG or AUA) of the mRNA at the peptidyl (P) site of the mitochondrial small subunit (mtSSU or 28S). MtIF3 also prevents the association of the mtSSU to the mitochondrial large subunit (mtLSU – 39S) (Bhargava and Spremulli 2005; Haque and Spremulli 2008). Following this, MtIF2 directs the N-formylmethionine-tRNA (fMet-tRNA^{Met}) to also bind to the start codon of the mRNA, forming a stable complex. MtIF2 also stimulates the recombination of mtSSU and mtLSU by directing the dissociation of the mtIF3 and GTP hydrolysis complex (GTP-bound IF2mt). This then allows for the re-association of the mitoribosome subunits.

Elongation:

Following this, translation thereby enters the elongation phase in which the elongation factor MtEFTu (Ling et al. 1997) forms a ternary complex with GTP and an aminoacylated- tRNA. MtEFTu transfers the tRNA to the aminoacyl/acceptor (A) site in the mitoribosome – the site

at which mtDNA is decoded through codon-anticodon recognition on the 28S subunit. The recognition causes GTP hydrolysis of mtEFTu instigating the release of the elongation factor from the mitoribosome. The 3' end of the aminoacylated tRNA moves into the peptidyl transferase centre (P site) in the 39S subunit where peptide bond formation is catalysed, adding one amino acid to the growing peptide. The movement of the tRNA from the A and P site to the P and exit (E) site occurs after conformational changes in both the second elongation factor mtEFG1 and the mitoribosome. The mRNA is advanced by one codon and the tRNA leaves the mitoribosome, initiating a new elongation cycle.

Termination:

The elongation of the polypeptide continues until a stop codon (either UAA or UAG) is reached and thereafter the termination of translation is undertaken by the mitochondrial release factor 1a (MtRF1a) which recognises the stop codons (Soleimanpour-Lichaei et al. 2007; Zhang and Spremulli 1998). MtRF1a triggers a hydrolysis cleavage of the ester bond between the terminal tRNA in the P-site and the last amino acid of the nascent polypeptide chain causing the release of the polypeptide from 39S subunit. Following this step, the dissociation of the mitoribosome and release of the uncharged mt-tRNA and mRNA occurs through two mitoribosome recycling factors; mitochondrial release factor 1 (mt-RRF1) and mitochondrial elongation factor G2 (mt-EFG2) (Rorbach et al. 2008).

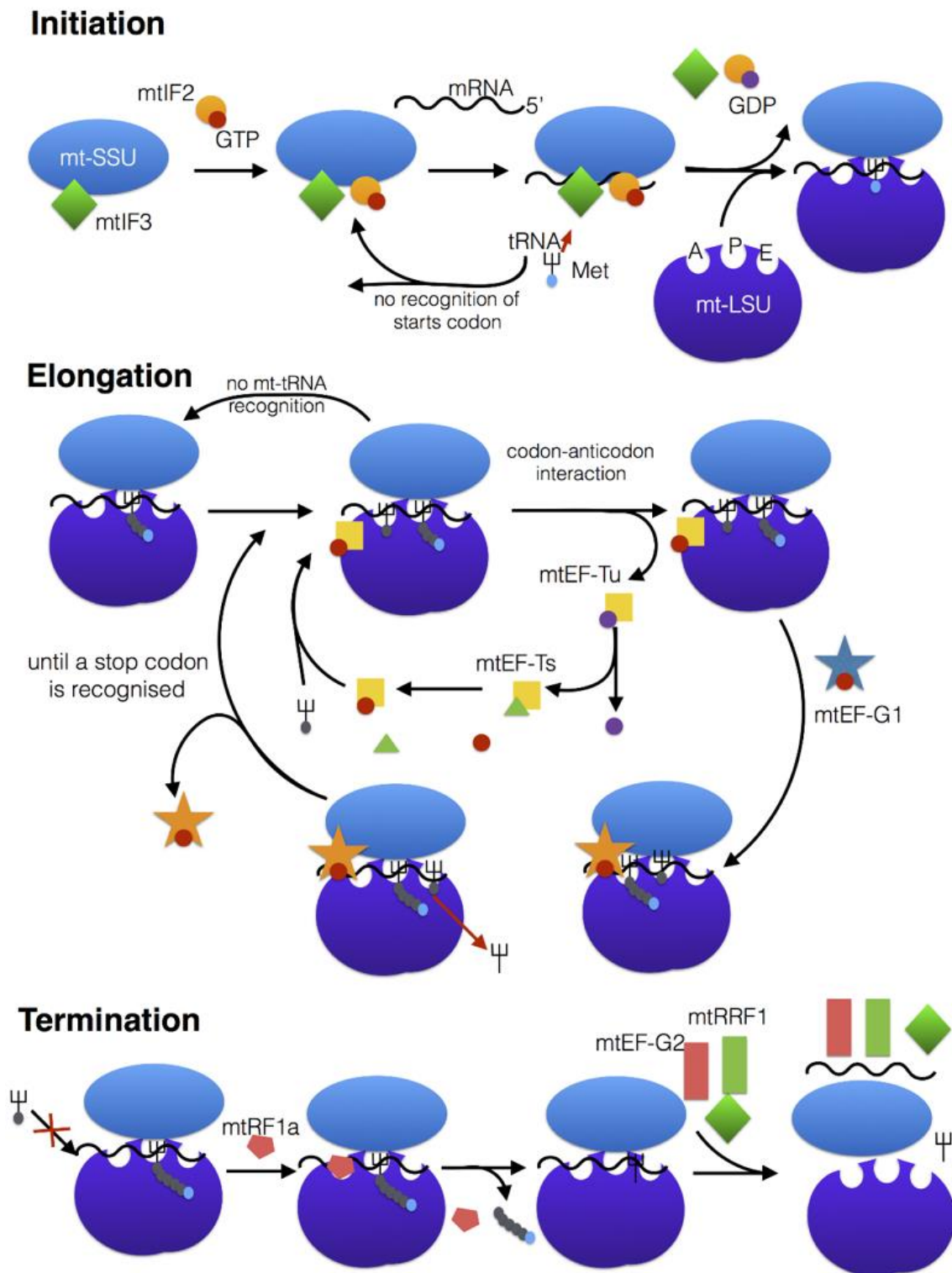


Figure 1.16: Mitochondrial translation.

Translation is undertaken in 3 steps; initiation, elongation and termination. Prior to the start of the initiation stage, ribosomal recycling occurs and the mitochondrial small subunit (mt-SSU in blue) remains bound to the initial factor 3 (mt-IF3 in green). The first step of initiation involves the bindings of mtIF2 (light orange) to a GTP molecule (red) which now joins the previous complex. The recruitment of mt-mRNA occurs to the mt-SSU and fMet-tRNA^{Met} in the P-site anchors it to the start codon. This causes GTP is hydrolysed to GDP (purple) and the initiation factors are released. The

mitochondrial large subunit (*mt-LSU* in darker blue) associates. During the elongation stage (centre illustration), the nascent polypeptide chain is bound to the P-site and the A-site hold charged *mt-tRNAs* which are delivered by the mitochondrial elongation factor-Tu (*mtEF-Tu* in yellow). When GTP is hydrolysed and *mtEF-Tu* is released, the GDP is replaced by another GTP molecule mediated by *mtEF-Ts* (red). The charged A-site *mt-tRNA* changes its conformation which facilitates peptide bond formation and transferring the polypeptide chain onto the A-site *mt-tRNA*. The elongation factor *mtEF-G1* (dark orange) promotes ribosome movement that repositions the *mt-mRNA* within the 55S so that the *mt-tRNAs* move from the A- and P-sites to the P- and E-sites. This cycle repeats until the completion of the polypeptide initiated by a stop codon at the A site. This termination step occurs after the recognition of the stop codon by a release factor protein (*mtRF1a* in pink), which after undergoing conformational change, promotes hydrolysis of the ester bond anchoring the nascent chain to the final *mt-tRNA*. After the release of the polypeptide chain, the two recycling factors, *mtRRF1* (dark red) and *mtRRF2* (red), promote the dissociation of the ribosomal subunits and premature re-association is prevented by the formation of an *mtIF3/mt-SSU* complex. Figure has been provided by Dr Amy Vincent (Wellcome Centre for Mitochondrial Research, Newcastle University) - legend and figure adapted from (Mai et al. 2017).

1.5. Mitochondrial Genetics

Given that both the nuclear DNA and mtDNA are involved in the mitoproteom, mitochondrial dysfunction can be caused by defects on either of the genomes. This dual genetics introduces the unique features of mitochondrial genetics which forms an essential basis for the understanding of the aetiology and pathogenesis of mitochondrial disease. For example, the unique inheritance patterns and the effects of having multiple copies of mtDNA in different cells and tissues.

1.5.1. Heteroplasmy

The polyploid nature of the mtDNA means that there are multiple copies of the genome in each individual cell (Holt et al. 1988; Zeviani et al. 1988). This gives rise to fundamental aspect of mitochondrial genetics; the state of homoplasmy and heteroplasmy within a cell.

Homoplasmy refers to the state in which all copies of the mtDNA are identical in their genotype -either all normal (wild-type) or all mutated. Conversely, heteroplasmy, which is further described in **Chapters 4** and **5**, refers to the co-existence of the two mtDNA genotypes (wild-type and mutated) in the same single cell (Holt et al. 1988). The proportion of mutated mtDNA in the total mtDNA population is known as the heteroplasmy level, which is generally expressed as a percentage (can vary between 0-100%). This heteroplasmy level can vary between different tissues and organs within the same patient (Shanske et al. 2004) and it is an important feature of mitochondria genetics in terms of phenotypic expression of the causative mtDNA mutation. This will be described further in the next section of this chapter.

1.5.2. Threshold effect

Most heteroplasmic mutations exist in low levels and therefore do not typically cause an observable biochemical dysfunction or phenotype, due to the compensatory effect of the high proportion of wild-type mtDNA. Thereby, a minimum percentage of mutated mtDNA must be present in a cell for OXPHOS dysfunction to occur – termed the critical threshold level, which is highlighted in **Figure 1.17**. When the pathogenic mutation reaches this critical threshold and beyond, the wild-type mtDNA population can no longer act as a compensatory mechanism in upholding a normal mitochondrial function against the mutated mtDNA (Rossignol et al. 2003). Thereby a biochemical defect and associated clinical phenotype is observed due to respiratory chain deficiency. This is referred to as the ‘threshold effect’ (Rossignol et al. 2003).

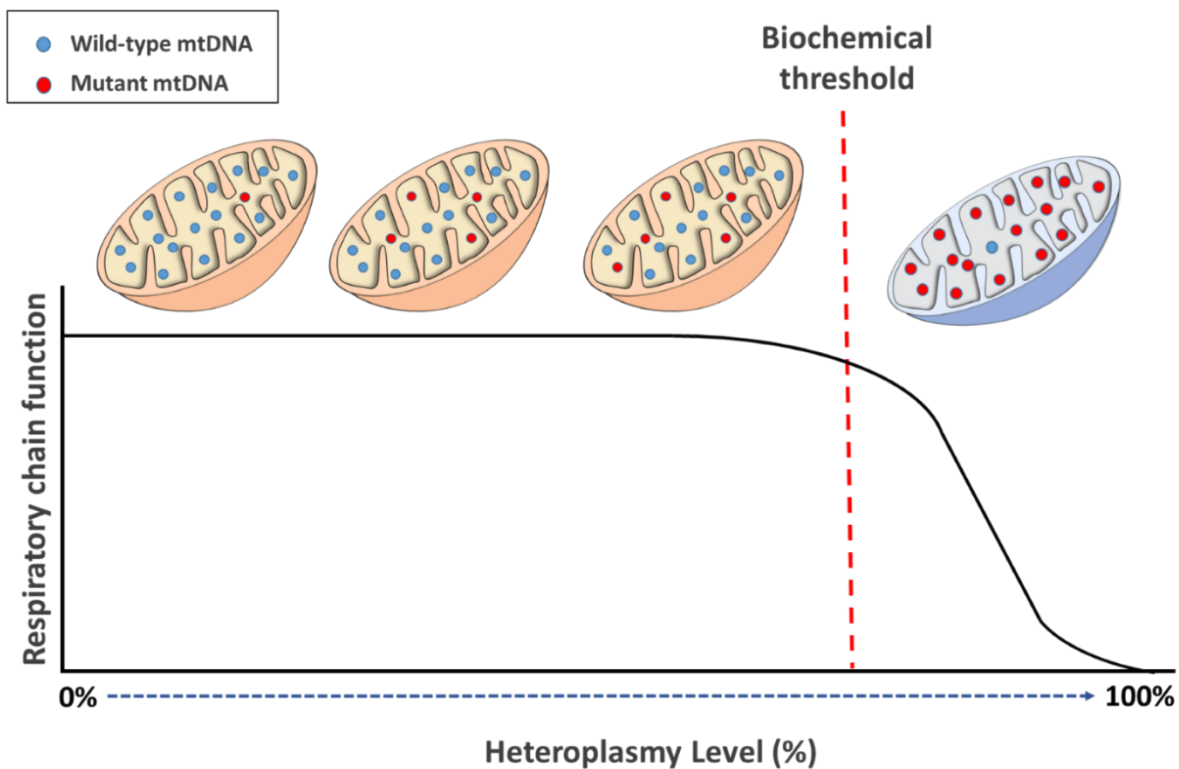


Figure 1.17: Heteroplasmy and the threshold effect.

The polyploidy nature of mitochondria means there are multiple copies of mtDNA. A mix of both wild-type and mutant mtDNA is termed heteroplasmy, which can be between 0 to 100% (as indicated by the blue dotted arrow on X-axis). The mitochondria remains biochemically normal (beige mitochondria) until a particular heteroplasmy level is reached (red dashed line), after which the cell becomes biochemically deficient due to OXPHOS dysfunction (grey mitochondria). This heteroplasmy level is called the critical threshold (red dashed line).

Threshold levels vary greatly amongst different tissues and between different mutation types. Tissues which are highly dependent on OXPHOS, such as skeletal muscle, are reported to have threshold levels between 50% (Porteous et al. 1998) and 90% (Sciacco et al. 1994). Although, threshold levels have been found to vary across different regions of the skeletal muscle due to variation in COX-deficiency across the myofibre (Elson et al. 2007; Murphy 2009).

The threshold level for point mutations involving mt-tRNA genes has been estimated as 90%, according to studies using *transmitochondrial* cybrids cell lines – described further in **Chapter 4** (Chomyn et al. 1992; Yoneda et al. 1992). Studies using patient muscle fibres have also shown threshold levels of approximately 80% - 90% for the m.8344A>G (*MT-TK* gene) and m.3243A>G (*MT-TL1* gene) (Jeppesen et al. 2017; Shoffner et al. 1990). However, a

lower estimate of 50% heteroplasmy has been suggested as the threshold level for m.3243A>G in skeletal muscle (Jeppesen et al. 2006) and 60% in cells (Miyabayashi et al. 1992). This variation highlights that the threshold level is not entirely known for the different tRNA pathogenic variants, particularly with regard to the m.3243A>G mutation. This aspect will be described in further details in **section 1.5.5** of this current chapter as well as in **Chapters 4 and 5**.

In comparison, single large scale mtDNA deletions are thought to cause biochemical defect at a lower threshold level of 50-60% based on *transmitochondrial* cybrid cell lines (Hayashi et al. 1991; Porteous et al. 1998). Although, higher threshold levels of 70-90% have been reported in patient skeletal muscle (Sciacco et al. 1994).

1.5.3. Maternal inheritance

It is widely accepted that mtDNA is inherited strictly through the maternal line – referred to as maternal inheritance (Giles et al. 1980). There are a few processes which can be used to explain this uniparental inheritance, which involve the elimination of the paternal mitochondria. The sperm contains only 50-70 copies of mtDNA compared to 100,000 to 600,000 in the unfertilised egg (Jacobs et al. 2006; Lopez-Lluch et al. 2008; Shoubridge and Wai 2007; Wai et al. 2010). Once fertilisation has occurred, the paternal mtDNA (from sperm) is diluted away by the excessive oocyte (maternal) mtDNA – this model is termed the ‘simple dilution model’ (Ankel-Simons and Cummins 1996; Gyllensten et al. 1991).

Moreover, maternal inheritance is also driven by the active destruction of paternal mitochondria after fertilisation by proteosomal degradation. It has been shown that ubiquitin tagging of the paternal mitochondrial membrane occurs within the fertilised egg, resulting in selective degradation by lysosomes and/or proteasomes (Sutovsky et al. 2000). Lastly, a significant downregulation of mtDNA copy number occurs during spermatogenesis (Larsson et al. 1997).

Cases of paternal inheritance have been reported in patients. Evidence of paternal inheritance was found in a patient with muscle specific mitochondrial disease, caused by a 2-base pair (bp) deletion in the *MTND2* gene. The muscle biopsy showed that 90% of the mtDNA was paternally derived and also contained the mutation on the *MTND2* gene. This findings suggested that this occurrence was likely to be resulting from the failure of eliminating the mtDNA within the sperm (Schwartz and Vissing 2002). A recent study has shown evidence for biparental transmission of mtDNA in three unrelated families (Luo et al. 2018). By undertaking whole mtDNA sequencing using Next Generation Sequencing (NGS) of seventeen individuals, Lou and colleagues identified high levels of heteroplasmic and

homoplasmic non-pathogenic mtDNA variants that were likely to be transmitted from the father. This paternal transmission of the variants was also observed in the siblings and the mother. The study concluded that whilst maternal inheritance remained dominant, the mechanisms driving bilateral transmission needs to be investigated to further understand mitochondrial inheritance, most particularly the potential paternal inheritance and its contribution to the disease pathogenicity of mitochondrial disease (Luo et al. 2018).

1.5.4. The mitochondrial bottleneck

During mitosis, both wild type and mutated mtDNA from the maternal mtDNA pool are believed to be randomly distributed to the daughter cells, resulting in a large amount of variability in the number of mutated mtDNA molecules passed on to offspring's. Thus, siblings from the same mother can end up with very different heteroplasmy levels. This variation is due to a phenomena termed 'the mitochondrial bottleneck'; the restriction and then re-amplification of mtDNA copy number that leads to random shifts of heteroplasmy from one generation to the next (Cree et al. 2008; Jenuth et al. 1996; Taylor and Turnbull 2005). Genetic bottleneck is a result of the rapid replication that occurs after fertilisation (Cree et al. 2008; Howell et al. 2003).

Heteroplasmy levels in offspring's are thought to be determined by random genetic drift during replication in the oocyte (Brown et al. 2001).

1.5.5. Segregation of mtDNA mutations

As a result of continuous replication, the segregation of mtDNA mutations is possible in both mitotic and post mitotic tissues. Macmillan et al. (1993) proposed random segregation to explain the tissue specific segregation observed in many mutations. However, evidence that segregation is not random has been shown and rather that nuclear genes influence segregation pattern (Raap et al. 2012). In addition, Chinnery et al. (1999) showed that specific tissues demonstrate consistent alteration from the average heteroplasmy level of an individual, for example, the m.3243A>G heteroplasmy level is found to be higher in muscle and urine than blood or hair. The tissue specific segregation of the m.3243A>G mutation in embryogenesis was later exemplified by Frederiksen et al. (2006). Specific nuclear encoded mitochondrial proteins that affect this segregation are beginning to be identified, for example the GIMAP3, an outer mitochondrial membrane GTPase (Jokinen et al. 2010).

An offspring would inherit a proportion of mutated mtDNA from their mother, but this load may not be enough to cause an immediate OXPHOS deficiency in cells. As the individual ages, a genetic drift occurs during cell proliferation which results in variable levels of mutated

mtDNA between cells. Only the cells or tissues that reach the threshold and above exhibit a biochemical defect (Mishra and Chan 2014). Thus, mutation segregation can influence and affect both the disease expression as well as inheritance.

1.5.6. Clonal expansion

Clonal expansion is the term used to describe the process by which a single mutated mtDNA (caused by either a point mutation or deletions), expands in proportion in a given cell, thus increasing the level of heteroplasmy. Eventually, this accumulation leads to the mutated mtDNA population outnumbering the wild-type mtDNA population, subsequently exceeding the necessary threshold required to induce a biochemical respiratory chain deficiency and the consequent functional impairment of a cell. Therefore the clonal expansion of mutated mtDNA may play an important role in both inherited diseases and ageing (Greaves et al. 2014).

A number of models have been proposed in aid of explaining how clonal expansion occurs within a cell. The first model was called the “survival of the smallest” by Wallace (1992) in which it was hypothesised that a smaller mtDNA genome, caused by a deletion, replicated faster than the wild-type, allowing for a selective and replicative advantage which leads to an accumulation of the mutated mtDNA. This model was initially supported by studies in which it was shown that cells containing high levels of mtDNA deletions replicated faster or were able to repopulate their mtDNA copy number faster than wild-type cell lines, although these studies were undertaken in non-physiological conditions (Diaz et al. 2002; Fukui and Moraes 2009; Hayashi et al. 1991). Opposing studies refuted the hypothesis by showing that there was no replicative advantage of smaller genomes (Campbell et al. 2014). It was also apparent that the theory did not offer an explanation for the clonal expansion of mtDNA molecules damaged due to point mutations, as these did not alter the size of the genomes, yet significantly increased in frequency with age (Greaves et al. 2014).

The second theory was termed the “survival of the slowest” by de Grey (1997). Also based on the notion of selective advantage, the theory proposed that mutated mtDNA produce a reduced level of ROS after a reduction in the OXPHOS process, compared to wild type mtDNA which are consequently degraded at a higher rate. However, this theory was not accepted as a sufficient explanation of clonal expansion because in order to impact the respiratory capacity of the mitochondria, there would need to be a sufficient amount of mutated mtDNA present in the mitochondria via clonal expansion.

Unlike the first two theories, which were based on the selective advantages of mutated mtDNA, the third hypothesis proposed was termed “random genetic drift” by Elson et al. (2007), where no selective advantage is required for clonal expansion. The hypothesis was based on the theory of relaxed replication by Bogenhagen and Clayton, 1997 (theory in which the mtDNA replication occurs independently to the nuclear DNA, which is linked to the cell cycle) and it was argued to be sufficient to explain clonal expansion. A population of mtDNA molecules in non-dividing cells were stimulated, with relaxed replication, over the maximum accepted human life span of 120 years. It was shown that the vast majority of mutations present after 80 years were found to have occurred before 30 years of ages, with 46% occurring before the age of 15. The study concluded that any mutation events which occurred after this, would not have sufficient time to accumulate. This study defined a COX-deficient fibre (described in **section 1.8.1** of this chapter) as cells that contained more than 60% mutated mtDNA at the end of the simulation. Although this model is supported by mathematical models, there is some dispute between the predictions of COX-deficiency and physiological observations (Campbell et al. 2014).

A more recent model has been proposed to explain clonal expansion, particularly within skeletal muscle fibres (Vincent et al. 2018). The study performed in depth imaging and molecular studies of skeletal muscle from patients with genetically confirmed mitochondrial disease (multiple mtDNA deletions) to determine how clonal expansion proceeded through highly organised and spatially restricted mitochondrial populations within these cell types (see **section 1.7.2** of this chapter). The clonal expansion model by Vincent and colleagues proposes that mtDNA deletions, which first arise in the perinuclear region of the cell (opposite the myonuclei), preferentially accumulate due to an increase in mitochondrial biogenesis in the region. This gives rise to the first visible signs of a focal mitochondrial respiratory chain deficiency in the cell, indicating that the mtDNA have exceeded the biochemical threshold in this region. The mutant mitochondria then expand transversely from the site of the foci through to the remainder of the muscle fibre, driven by increased mitochondrial biogenesis. Whilst this study was unable to investigate the clonal nature of the deletions and the role of mtDNA replication, it has provided an insight into how fully COX-deficient cells are derived from the spread of small proliferative perinuclear foci.

1.6. Mitochondrial Disease

Mitochondrial disease is the umbrella term used for a group of disorders that are characterised by a chronic loss of cellular energy and this failure to meet the energy demands consequently results in a clinical phenotype. The clinical spectrum for the diseases is extremely heterogeneous in terms of age of onset, the clinical manifestations, inheritance and prognosis. Tissues which have a high-energy demand, such as the brain, skeletal muscle, heart and the central nervous system (CNS) are typically most affected. Mitochondrial diseases can affect a single organ in isolation, such as pure myopathy, cardiomyopathy or optic neuropathy. Alternatively, they can be multisystem, in which several organs are affected. Due to this clinical heterogeneity, the prevalence of mitochondrial diseases is hard to quantify. However, it has been recently shown that approximately 12.5 per 100,000 adults (Gorman et al. 2015a) and 4.7 per 100,000 children are affected (Koenig 2008; Skladal et al. 2003).

Common clinical features of mitochondrial disease, as shown in **Figure 1.18** include ptosis, proximal myopathy, exercise intolerance, cardiomyopathy, external ophthalmoplegia, deafness, optic atrophy and diabetes (Gorman et al. 2016). Owing to the high metabolic demand, muscle is commonly affected in mitochondrial patients, either exclusively or predominantly.

As mitochondria are under the dual control of both the mitochondrial genome and nuclear genome, genetic lesions can lie in either, giving rise to either defects caused by mtDNA mutations (primary defect) or defects of the nDNA-encoded mitochondrial protein (secondary defect). For mitochondrial disease in general, pathogenic variants have been reported in all 37 mtDNA genes and more than 300 nDNA-encoded genes (as reviewed by (Thompson et al. 2019) (**Figure 1.19**).

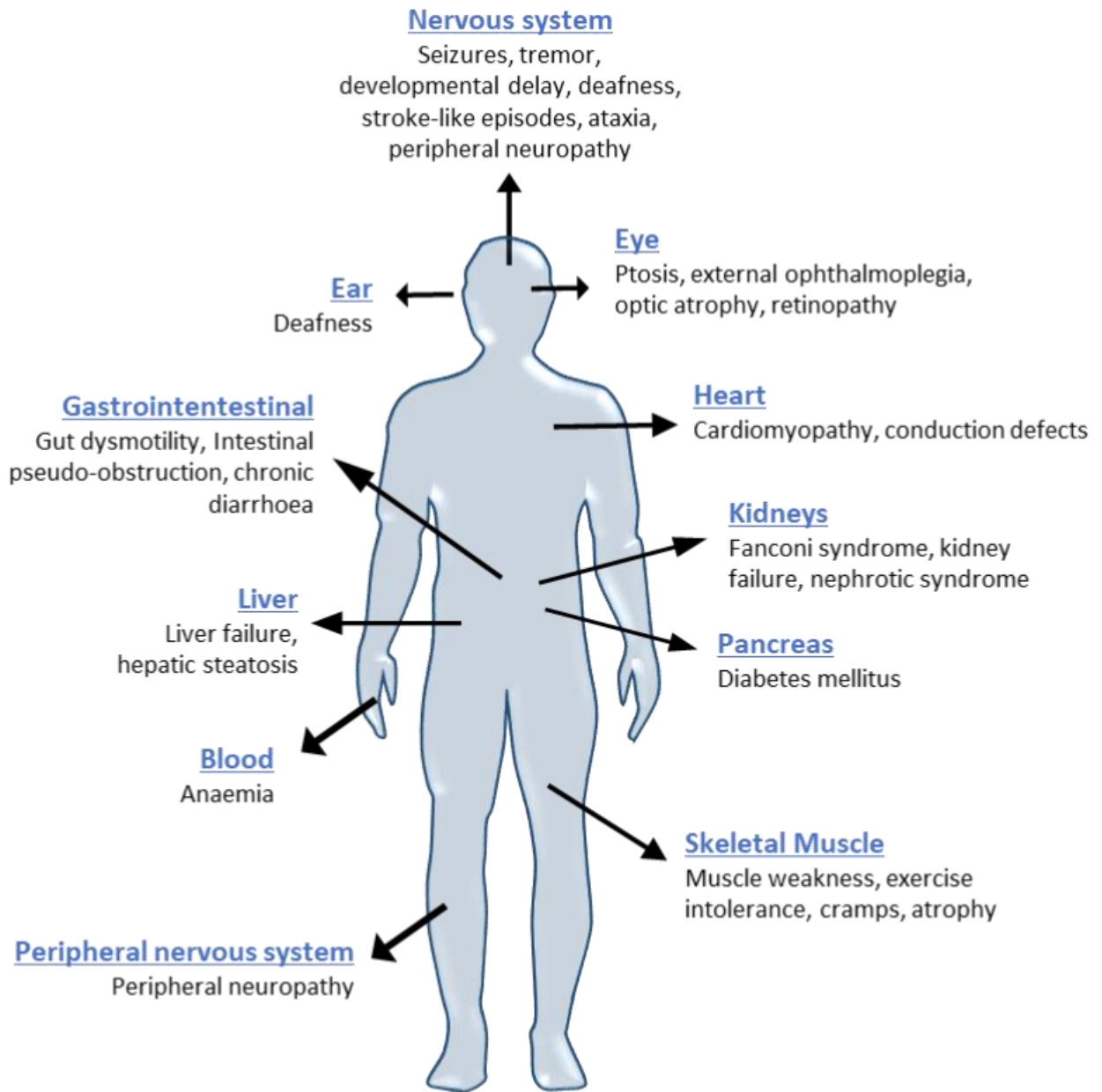


Figure 1.18: The clinical spectrum of mitochondrial diseases.

Schematic diagram showing the organs affected in mitochondrial disease and the corresponding clinical manifestations. Organs that require a high-energy demand, such as the brain, heart, nervous system and skeletal muscle are the most regularly affected.

1.6.1. Mitochondrial DNA pathogenic variants

The mtDNA is significantly more vulnerable to mutations than the nuclear DNA, with a mutation rate that is 10-20 times higher (Brown et al. 1979; Richter et al. 1988). This is thought to be for a number of reasons; i) the mtDNA genome consists almost entirely of coding regions and therefore mutations are more likely to occur in a coding region, ii) the lack of protective histones found on the mtDNA molecule, iii) the close proximity to damaging ROS produced by the ETC within the IMM, iv) a nucleotide imbalance in the mitochondria results in the mtDNA polymerase POLG having a much lower fidelity and higher mtDNA mutation rates than that of the nuclear polymerase (Kunkel and Loeb 1981; Song et al. 2005) and v) the continuous replication of mtDNA which leads to the increase in the chances of error being made during the process (Bogenhagen and Clayton 1977).

Primary mtDNA mutations are due to two common causes; point mutations (a single base pair substitution) and mtDNA rearrangements (typically single large-scale deletions but can also be insertions). These were first reported in 1988 when a point mutation in the *ND4* gene was found to cause Leber's hereditary optic neuropathy (LHON) (Wallace et al. 1988) and a deletion of up to ~7kb was reported in patients with mitochondrial myopathy (Holt et al. 1988). Both point mutations and single large-scale deletions can be maternally inherited or arise as a *de novo* during embryonic development.

1.6.1.1. mtDNA point mutations

Mitochondrial DNA point mutations (occurring in mt-tRNA, mt-rRNA and mt-mRNA) have become a significant cause of mitochondrial disease, with a prevalence of approximately 1 in 5,000 in the adult population (Schaefer et al. 2008). The majority of defects have been reported in tRNA genes (accounting for 50%), which consequently cause an overall reduction in mitochondrial protein synthesis, a decline in oxygen consumption rate and a decreased activity of multiple respiratory chain complexes (Mariotti et al. 1994). The remaining mutations are founded in structural genes with only 2% in rRNA genes (Schon et al. 2012).

Point mutations are heritable and follow a strict maternal inheritance pattern. They are usually highly recessive and heteroplasmic, however homoplasmic mutations have also been reported, for examples the m.11778G>A mutation in the *ND4* gene and the m.4300A>G mutation in the *mt-tRNA^{Leu}* gene (Nakamura et al. 1993; Taylor et al. 2003; Yen et al. 2002). In heteroplasmic cases, point mutations have been shown to require a high threshold to induce a biochemical defect (Chomyn et al. 1992; Mariotti et al. 1994). However, some mutations have been shown to cause a biochemical defect, thereby clinical disease, with substantially lower thresholds as proposed. For example, Sacconi et al. (2008), reported a young patient harbouring the

m.5545C>T mutation within the *MT-TW* gene (tryptophan tRNA - tRNA^{trp}), which caused severe multisystemic disorder and marked respiratory chain deficiency at low levels of heteroplasmy (25%) in clinically affected tissue (muscle). Additionally, the m.14723T>C within the tRNA^{Glu} (*MT-TE*) gene (glutamic acid tRNA) was shown to cause CPEO at low levels of heteroplasmy in muscle tissue of the patient (7% in initial biopsy, 34% in second biopsy) (Alston et al. 2010).

The most common point mutation in mitochondrial disease is the m3243A>G mutation – a transition of A to G nucleotide at position 3243 of the mtDNA, within the dihydrouridine loop (D-loop) of the mt-tRNA Leu^(UUR) (*MT-TLI* gene) (Goto et al. 1990). This pathogenic variant is a key topic for interest in this thesis and will be described in greater detail in **Chapters 4** and **5**. Another common point mutation is the m.8344A>G in the *MT-TK* gene (mitochondrial tRNA lysine (Lys)), which was first identified in patients with MERFF (myoclonic epilepsy with ragged red fibres) (Shoffner et al. 1990). The prevalence for this point mutation within the North East of England has been shown to be 0.7 in 100,000 (Gorman et al. 2015a), therefore is much rarer in comparison to the m.3243A>G mutation.

Further pathogenic point mutations that have been identified in mtDNA genes encoding subunits of Complex I, IV and V. For example, the three most commonly found mutations causing LHON; m.3460G>A within the *MTND1* gene (Howell et al. 1991), m.11778G>A within the *MTND4* gene (Wallace et al. 1988) and m.14484T>C within the *MTND6* gene (Johns et al. 1992; Mackey and Howell 1992). These last three pathogenic variants, along with other variants related to Complex I, will be described again in **Chapter 3**.

1.6.1.2. Single, large-scale mtDNA deletions

The second cause of primary mitochondrial disease is single, large-scale mtDNA deletions, which Gorman et al., 2015, estimated the frequency to be 1.5 in 100,000 (12% of adult mitochondrial disease cases). These mutations are not heritable and instead usually occur sporadically during embryogenesis due to errors in either mtDNA replication or repair (Chinnery et al. 2004). In comparison to point mutations, patients affected show a lower threshold of approximately 50-60% (Rossignol et al. 2003). Deletions have been found to result from defects in mtDNA replication, maintenance and repair and occur frequently between O_H and O_L (origin of replication) and regions flanked by tandem repeats (Krishnan et al. 2008; Rossignol et al. 2003; Schon et al. 1989; Spelbrink et al. 2001). Deletions vary in size (1.3-10kb), however the most frequently reported deletion size is the so called “common deletion” which spans 4,977bp (approximately 5kB); extending from base 8,470 in *MT-AT8* to base 13,477 in *MT-ND5* genes and flanked by a 13bp direct repeat (Pitceathly et al. 2012;

Zeviani et al. 1988). A study by Grady et al. (2014), showed that there is a correlation between deletion size, heteroplasmy and severity of disease. Using a single cell approach (single muscle fibres), Rocha et al. (2018), provided an insight into the pathological mechanism underlying single large –scale deletions by showing that the removal of mtDNA genes is directly linked to the expression and severity of the consequential respiratory chain deficiency.

Single large-scale deletions predominantly cause syndromes which comprise of; CPEO (Chronic progressive external ophthalmoplegia) which is present in ~ 65% of cases, KKS (Kearns Sayre Syndrome) accounting for 30% of cases and Pearson syndrome in the remaining ~ 5% of cases (Mancuso et al. 2015). Pearson syndrome is the most severe disorder, affecting the bone marrow and pancreas thereby leading to the characteristic sideroblastic anaemia and exocrine pancreas diabetes. Neutropenia (low white blood cells) and thrombocytopenia (low platelets) are also observed. The disorder is often associated with death occurring at infancy. KKS is defined by clinical onset before the age of 20 years and affects mainly the eyes through a progressive external ophthalmoplegia (weakness or paralysis of the eye muscles - extraocular). This consequently leads to the impairment of eye movement and patients often present with ptosis. Pigmentary retinopathy is also observed in patients and additional features for KKS include cerebellar ataxia, impaired cognitive function such as dementia, muscle weakness, deafness, liver and kidney involvements. Finally, CPEO is characterised by ptosis, impaired eye movement due to paralysis of the extraocular. Proximal limb muscle weakness and exercise intolerance are also important findings in these patients.

1.6.2. Nuclear DNA mutations

As stated, the nDNA encodes 99% of mitochondrial proteins (1,158) and to date, over 300 genes have now been reported to cause mitochondrial disease (Thompson et al. 2019), owed to the progress and application of high-throughput molecular genetic analysis. Mutations follow a Mendelian inheritance pattern which include autosomal dominant, recessive and X-linked (Fernandez-Moreira et al. 2007; Harel et al. 2016; Sperl et al. 2015; Tang et al. 2011).

The nuclear DNA encodes genes that are crucial for multiple mitochondrial functions, such as the structure and assembly of complexes in the OXPHOS system, the regulation of mitochondrial dynamics through fusion and fission, the import of nuclear-encoded RNA and proteins into the mitochondria, the proteins required for the maintenance of the mtDNA and also protein synthesis (Schon et al. 2012). Therefore, pathogenic variants can potentially disrupt any of these complexes and functions. **Figure 1.19** highlights a list of nuclear DNA

genes (and mtDNA genes) that are currently known to be associated with mitochondrial disease.

Nuclear DNA mutations often have secondary effects on the mtDNA which results in multiple mtDNA deletions of varying size and position to occur. This is predominantly due to pathogenic variants on nuclear genes encoding proteins involved in mtDNA transcription, replication and maintenance machinery (Kaukonen et al. 2000; Spelbrink et al. 2001; Van Goethem et al. 2001).

The first nuclear gene mutation that was found to give rise to mitochondrial disease involved *SDHA* in two sisters with Complex II deficiency and Leigh syndrome (LS) (Bourgeron et al. 1995). This particularly mutation was found to be recessive. Other examples include mutations in *POLG* which leads to mtDNA depletion syndrome or PEO (progressive external ophthalmoplegia) (Naviaux et al. 1999; Van Goethem et al. 2001). Another example would be mutations in *PEO1* which is the gene encoding TWINKLE and pathogenic variants have also been associated with mtDNA depletion and multiple deletions (Spelbrink et al. 2001).

Nuclear mutations can lead to an isolated disorder where only one complex of the respiratory chain is affected or a combined dysfunction of several complexes. The latter is usually a consequence of defects in mtDNA maintenance, protein synthesis or mitochondrial protein import.

mtDNA pathogenic variants: 36/37 genes																
OXPHOS subunits	(C1) MT-ND1, MT-ND2, MT-ND3, MT-ND4, MT-ND4L, MT-ND5, MT-ND6; (CIII) MT-CYB; (CIV) MT-CO1, MT-CO2, MT-CO3; (CV) MT-ATP6, MT-ATP8															
Ribosomal RNA	MT-RNR1															
Transfer RNA	MT-TA, MT-TC, MT-TD, MT-TE, MT-TF, MT-TG, MT-TH, MT-TI, MT-TK, MT-TL1, MT-TL2, MT-TM, MT-TN, MT-TP, MT-TQ, MT-TR, MT-TS1, MT-TS2, MT-TT, MT-TV, MT-TW, MT-TY															
Nuclear pathogenic variants: 295 genes																
	<table border="1"> <thead> <tr> <th>Complex I</th> <th>Complex II</th> <th>Complex III</th> <th>Complex IV</th> <th>Complex V</th> </tr> </thead> <tbody> <tr> <td>NDUFA1, NDUFA2, NDUFA6, NDUFA9, NDUFA10, NDUFA11, NDUFA12, NDUFA13, NDUFB3, NDUFB8, NDUFB9, NDUFB10, NDUFB11, NDUFS1, NDUFS2, NDUFS3, NDUFS4, NDUFS6, NDUFS7, NDUFS8, NDUFV1, NDUFV2</td> <td>SDHA, SDHB, SDHD</td> <td>CYC1, UQCRB, UQCRCQ, UQCRC2</td> <td>COX4I1, COX4I2, COX5A, COX6A1, COX6B1, COX7B, COX8A, NDUFA4</td> <td>ATP5F1A, ATP5F1D, ATP5F1E</td> </tr> <tr> <td>ACAD9, FOXRED1, NDUFAF1, NDUFAF2, NDUFAF3, NDUFAF4, NDUFAF5, NDUFAF6, NDUFAF8, NUBPL, TIMMDC1, TMEM126B</td> <td>SDHAF1</td> <td>BCS1L, LYRM7, TTC19, UQCC2, UQCC3</td> <td>CEP89, COX14, COX20, COA3, COA5, COA7, PET100, PET117, SURF1</td> <td>ATPAF2, TMEM70</td> </tr> </tbody> </table>	Complex I	Complex II	Complex III	Complex IV	Complex V	NDUFA1, NDUFA2, NDUFA6, NDUFA9, NDUFA10, NDUFA11, NDUFA12, NDUFA13, NDUFB3, NDUFB8, NDUFB9, NDUFB10, NDUFB11, NDUFS1, NDUFS2, NDUFS3, NDUFS4, NDUFS6, NDUFS7, NDUFS8, NDUFV1, NDUFV2	SDHA, SDHB, SDHD	CYC1, UQCRB, UQCRCQ, UQCRC2	COX4I1, COX4I2, COX5A, COX6A1, COX6B1, COX7B, COX8A, NDUFA4	ATP5F1A, ATP5F1D, ATP5F1E	ACAD9, FOXRED1, NDUFAF1, NDUFAF2, NDUFAF3, NDUFAF4, NDUFAF5, NDUFAF6, NDUFAF8, NUBPL, TIMMDC1, TMEM126B	SDHAF1	BCS1L, LYRM7, TTC19, UQCC2, UQCC3	CEP89, COX14, COX20, COA3, COA5, COA7, PET100, PET117, SURF1	ATPAF2, TMEM70
Complex I	Complex II	Complex III	Complex IV	Complex V												
NDUFA1, NDUFA2, NDUFA6, NDUFA9, NDUFA10, NDUFA11, NDUFA12, NDUFA13, NDUFB3, NDUFB8, NDUFB9, NDUFB10, NDUFB11, NDUFS1, NDUFS2, NDUFS3, NDUFS4, NDUFS6, NDUFS7, NDUFS8, NDUFV1, NDUFV2	SDHA, SDHB, SDHD	CYC1, UQCRB, UQCRCQ, UQCRC2	COX4I1, COX4I2, COX5A, COX6A1, COX6B1, COX7B, COX8A, NDUFA4	ATP5F1A, ATP5F1D, ATP5F1E												
ACAD9, FOXRED1, NDUFAF1, NDUFAF2, NDUFAF3, NDUFAF4, NDUFAF5, NDUFAF6, NDUFAF8, NUBPL, TIMMDC1, TMEM126B	SDHAF1	BCS1L, LYRM7, TTC19, UQCC2, UQCC3	CEP89, COX14, COX20, COA3, COA5, COA7, PET100, PET117, SURF1	ATPAF2, TMEM70												
OXPHOS subunits																
OXPHOS assembly factors																
Protein import & processing	AFG3L2, AIFM1, CLPB, CLPP, DNAJC19, GFER, HSPD1, HTRA2, LONP1, MIPEP, PITRM1, PMPCA, PMPCB, SACS, SPG7, TIMM22, TIMM50, TIMM8A, XPNPEP3, YME1L															
mtDNA replication & maintenance	ABAT, DGUOK, DNA2, MGME1, MPV17, POLG, POLG2, RNASEH1, RRM2B, SAMHD1, SLC25A4, SSBP1, SUCLA2, SUCLG1, TFAM, TK2, TOP3A, TWNK, TYMP															
RNA maturation/modification	ELAC2, ERAL1, FASTKD2, GTPBP3, HSD17B10, LRPPRC, MRM2, MTFMT, MTO1, MTPAP, NSUN3, PNPT1, PUS1, TRIT1, TRMT10C, TRMT5, TRMU, TRNT1															
Mitochondrial aminoacyl tRNA synthetases	AARS2, CARS2, DARS2, EARS2, FARS2, GARS, GATB, GATC, IARS2, KARS, LARS2, MARS2, NARS2, PARS2, QRSL1, RARS2, SARS2, TARS2, VARS2, WARS2, YARS2															
Mitoribosome	MRPS2, MRPS7, MRPS14, MRPS16, MRPS22, MRPS23, MRPS28, MRPS34, MRPL3, MRPL12, MRPL44, PTCO3															
Translation	C12orf65, GFM1, GFM2, RMND1, TACO1, TSFM, TUFM															
Membrane dynamics & composition	AGK, CHKB, DNM1L, GDAP1, MFF, MFN2, MSTO1, NME3, OPA1, OXA1L, PGA2G6, PNPLA4, PNPLA8, QIL1, SERAC1, SLC25A46, STAT2, TAZ, TRAK1, VPS13C															
β-oxidation	ACADM, ACADS, ACADSB, ACADVL, ACAT1, CPT1A, CPT2, ETFA, ETFB, ETFDH, HADH, HADHA, HADHB, HMGCL, HMGCS2, OXCT1, SLC22A5, SLC25A20															
TCA cycle	ACO2, ALDH18A1, CA5A, DLAT, FH, HAAO, IDH3A, IDH3B, KYNU, MDH2, MPC1, PC, PDHA1, PDHB, PDHX, PDK3, PDP1, PPA2, SLC25A12, SLC25A13, SLC25A3															
Cofactors	ABCB7, BOLA3, C19ORF12, COA6, COASY, COQ2, COQ4, COQ5, COQ6, COQ7, COQ8A, COQ8B, COQ9, COX10, COX15, CYCS, DLD, FDX1L, FDXR, FLAD1, FXN, GLRX5, HCCS, IBA57, ISCA1, ISCA2, ISCU, LIAS, LIPT1, LIPT2, LYRM4, MECR, MICU1, MICU2, NADK2, NAXE, NFS1, NFU1, PANK2, PDSS1, PDSS2, SCO1, SCO2, SFXN4, SLC19A2, SLC19A3, SLC25A19, SLC25A24, SLC25A26, SLC25A32, SLC25A42, SLC39A8, TPK1															
Other	APOPT1, ATAD3A, C1QBP, CHCHD10, D2HGDH, ECHS1, ETHE1, FBXL4, HIBCH, IARS, L2HGDH, OPA3, RTN4IP1, SLC25A1, TMEM65, TXN2															

Figure 1.19: List of genes currently associated with mitochondrial disease. Genes have been listed according to their function.

To date, pathogenic variants have been founded in 36/37 mitochondrial-encoded genes and 295 nuclear-encoded mitochondrial genes which are associated with a wide range of mitochondrial functions. This figure has been taken from (Thompson et al. 2019) who has used broad categories of mitochondrial functions in order to appropriately assign these genes with more than one function to their most appropriate one. The list also takes into account the causative genes that have been shown to have a primary or secondary impact on OXPHOS and does not include genes where variants have been described in cancer, but not a mitochondrial disorder (e.g. SDHC).

1.7. Muscle and mitochondria

The primary function of the skeletal muscle is to generate force and movement through contraction, for which it requires mitochondria to continuously synthesise ATP. The muscle is therefore known to be a tissue which has a high demand for energy, thus clinical phenotypes associated with the muscle are commonly found in mitochondrial patients.

1.7.1. Structure of skeletal muscle

Skeletal muscle has a highly organised architecture, as depicted in **Figure 1.20**. The smallest contractile unit is the multinucleated elongated cell which is called the muscle fibre (also known as a myofibre). Each of these muscle fibres are formed from densely arranged, parallel array of cylindrical elements called myofibrils. These myofibrils are formed by repetitive units called sarcomeres which are approximately 2.5 μ m to 3 μ m in length and are the functional units of muscle (Hopkins 2006). Sarcomeres are separated by the Z bands and consist of smaller contractile filaments (myofilaments), actin which is the thin myofilament and myosin which is the thick myofilament as well other support proteins such as troponin and tropomyosin. The thick myofilament is anchored to the Z-band by an elastic protein called titin, which regulates the spatial relationships between the two myofilaments (Dubowitz 2007). Each muscle fibre is then organised into linearly aligned bundles called a fascicle and a bundle of these fascicles then form the muscle.

There are three layers of connective tissue that enclose and provide structure to skeletal muscle and also providing compartmentalization of the muscle fibres. The first is the external sheath called the epimysium which envelopes the muscle and allows the muscle to maintain its structural integrity during contraction and movement. The middle layer of connective tissue is the perimysium which covers the fascicles and acts a way of holding muscle fibres in these bundles. This layer also provides the pathway for the capillarity network and the innervating motor neurons. The third layer is the endomysium which encases each individual muscle fibre within each fascicle (Gillies and Lieber 2011).

The plasma membrane of the muscle fibre is known as the sarcolemma (also known as the plasmalemma), which is found under the endomysium. The sarcolemma is an excitable membrane that can activate the contractile machinery in response to signals from the motor neuron. When the motor nerve axon innervates the muscle fibre, it forms a synapse which is neuromuscular junction. The region at which the sarcolemma makes contact with the presynaptic nerve terminal is known as the motor end plate. This is characterised by the deep

folding of the sarcolemma. A single motor neuron can innervate a few or numerous muscle fibres and this collectively becomes known as the motor unit.

Skeletal muscle fibres are multinucleated cells. The nuclei accumulate in the periphery of the individual muscle fibre adjacent to the sarcolemma.

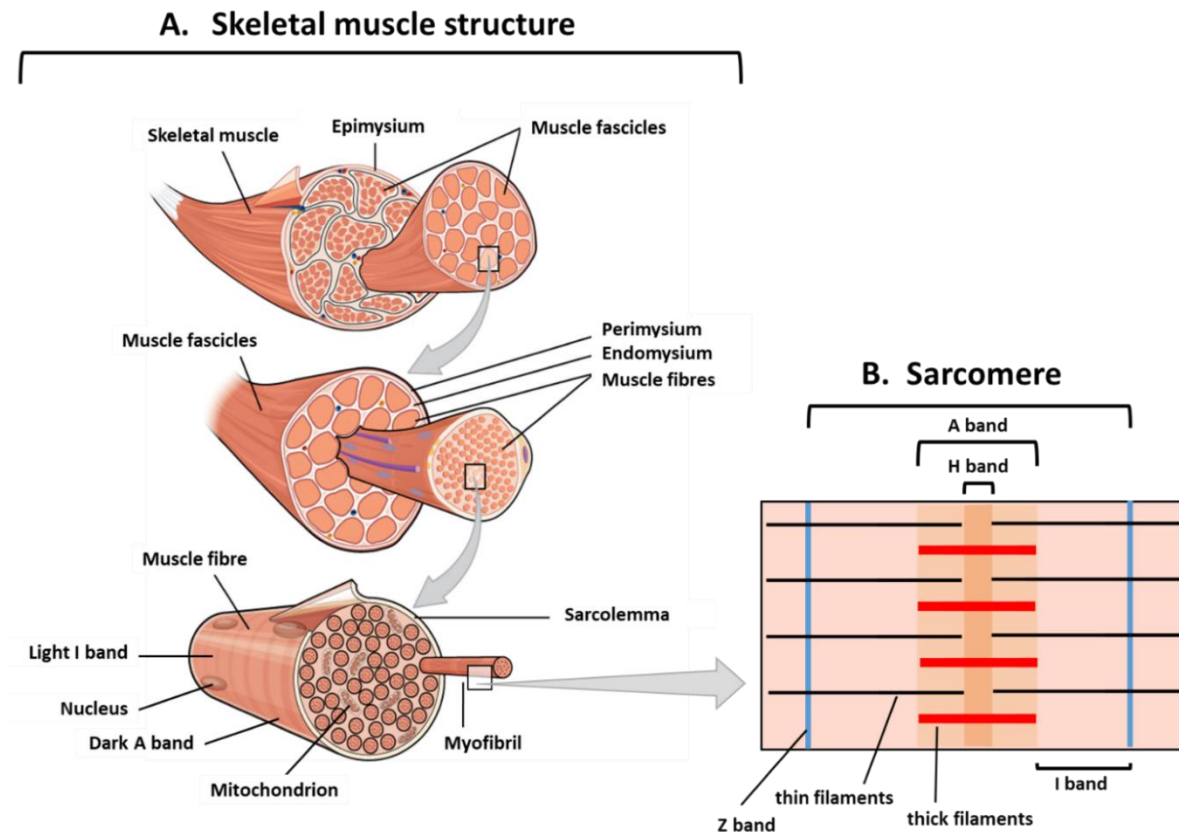


Figure 1.20: A schematic figure of the structure of skeletal muscle and sarcomere.

A) Skeletal muscle is enclosed by the epimysium and arranged into muscle fascicles which are surrounded by the perimysium. Within in each fascicle are muscle fibres which are surrounded by the endomysium and each muscle fibre is composed of the myofibril. The sarcolemma is the plasma membrane of the muscle fibre. **B)** Each myofibril is composed of repetitive units called sarcomeres, which are separated by Z bands. These Z bands consist of smaller contractile myofilaments – thin (actin) and thick (myosin).

1.7.2. Mitochondria in skeletal muscle

There are two subpopulations of mitochondria within skeletal muscle fibres that differ in their subcellular localization, morphology, function and biochemical properties. The first population is found in small, perinuclear clusters below the sarcolemmal membrane and thus are known as the subsarcolemmal (SS) mitochondria. These mitochondria make up for 20% of the complete population of skeletal muscle mitochondria and are important in providing ATP for membrane transport and gene transcription (Ferreira et al. 2010; Hoppeler 1986). Morphologically, SS mitochondria appear punctate. The second population of mitochondria (accounting for the remainder of 80% of mitochondrial population) are found in parallel rows between the myofibrils adjacent to the Z line of the sarcomere and are called intermyofibrillar (IMF) mitochondria. These mitochondria play a prominent role in providing ATP to the contractions myofilaments (actin and myosin) to assist contraction (Kirkwood et al. 1986; Ogata and Yamasaki 1997). The IMF mitochondria are more elongated in structure as they must extend between myofibrils and have a higher oxidative capacity (efficiency in ATP production) (Ferreira et al. 2010).

1.7.3. Skeletal muscle fibre types

In mammals, skeletal muscle is composed of different types of muscle fibres, grouped according to their diverse morphology, functional and metabolic capabilities and contraction rates. They are characterised by the expression of specific isoforms of myosin heavy chain (MHC) which determine their contractile strengths. These fibre types can be distinguished by myofibrillar actomyosin ATPase histochemistry, immunoblot or immunofluorescence labelling of MHC isoforms. Motor neurons influence the phenotype of the fibre types and in human skeletal muscle, there are three types of motor units; slow, fast fatigable and fast fatigue resistant motor unit. This leads to the three different fibre types; Type I (slow twitch fatigue resistance), Type IIa (fast twitch fatigue resistance) and Type IIx (fast twitch fatigue sensitive) (Burke et al. 1973; Smerdu et al. 2005). Electrical impulses from the nervous system influence the growth and differentiation of the different phenotypes of the fibre types. Discharge rates at 10 and 100Hz result in changes in gene expression that consequently cause the development of the fast and slow fibre types (Schiaffino et al. 1989). **Table 1.1** highlights the main differences between each of the fibre types. However briefly, Type I fibres are the most oxidative and so have a high oxidative capacity, higher mitochondrial content but lower ATP consumption due to a longer contraction and relaxation time. Type II fibres are split into further two types; Type IIa and Type IIx. Firstly, Type IIa fibres are defined as being fast oxidative glycolytic, have a high mitochondrial content and a high ATP consumption due to a

quicker contraction rate. Type IIb fibres are known as fast glycolytic with low mitochondrial content and higher ATP consumption due to a fast contraction rate (Lieber 2010).

Most human skeletal muscles have a mosaic of different fibre types, with the ratio of Type I and Type II differing within the same muscle and between different muscles. The human vastus lateralis muscle (quadriceps) from young healthy adults have approximately equal proportions of type II (fast twitch) and Type I (slow twitch). However, sedentary adults over the age of ~60 years have been shown to have an increased proportion of hybrid fibres which express more than one MHC isoform (St-Jean-Pelletier et al. 2017). Additionally, a study by Gehrig et al. (2016), found that in patients with mitochondrial myopathy, there is a shift in the fibre type composition from Type I to type II, possibly acting as a compensatory mechanism. The decrease in oxidative capacity means a switch from an oxidative to a more glycolytic phenotype. This shift will allow for the partial restoration of muscle strength and energy production but also a higher lactic acid production, which is characteristic in patients with mitochondrial disease (Gehrig et al. 2016).

Table 1.1: Muscle fibre type, function and characteristics

	Slow Type I	Type IIa Fast-resistant	Type IIb Fast-fatigable
Morphological properties			
Fibre diameter	Small	Medium	Large
Capillary density	Rich	Rich/ medium	Sparse
Mitochondria	Rich	Rich	Poor
Oxidative activity	High	High	Low
Glycolytic activity	Low	High/ intermediate	High
Myoglobin	High	High/ Intermediate	Low
Myosin heavy chain	Type I	Type IIa	Type IIb
Functional properties			
Recruitment	1	2	4
Ca ²⁺ sequestration(SR)	Slow	Slow/ rapid	Rapid
ATP consumption	Low	High	High
Contraction speed	Slow	Fast	Fast
Twitch force	Small	Intermediate	Large
Fatigues resistance	High	Low/ Intermediate	Low

1.8. Diagnosis of Mitochondrial Diseases

The diagnosis of mitochondrial diseases requires a multidisciplinary approach, owing to factors including mtDNA heteroplasmy, wide genetic and clinical heterogeneity and a clinical spectrum which often overlaps with other neurological disorders. With the growing knowledge of mitochondrial and nuclear genes responsible for mitochondrial disease, as well as a progress in the recognition of phenotype - genotype correlations, the current diagnostic procedure has shifted from the “biopsy first approach” to the “genetics first approach” because of the advances being made with next generation sequencing (NGS).

The process of diagnosis first includes a detailed clinical examination from a number of specialist clinicians. Despite the vast clinical heterogeneity of mitochondrial disease, the identification of certain clinical features alone can lead to targeted mtDNA or nuclear gene screening, prior to a muscle biopsy. For example, a child presenting with classic MELAS (Mitochondrial Encephalomyopathy, Lactic acidosis, and Stroke-like episodes) phenotypes would be tested for the m.3243A>G mutation (usually through sampling blood from the patient) whilst a visual failure in a young male adult may prompt targeted sequencing of the three common point mutations associated with LHON, as listed previously in **section 1.6.1.1** (Nesbitt et al. 2013; Yu-Wai-Man et al. 2003).

Despite the impact of NGS in the diagnostic setting for mitochondrial disease, there is still a requirement for clinically affected tissue samples that are used for histological, immunohistochemical and biochemical investigations. An example for such requirement would be the identification of novel pathogenic variants with unknown function that would require further investigation of affected tissue through enzymatic activity assays and steady state levels of OXPHOS complexes, undertaken with BN-PAGE.

1.8.1. Muscle biopsy and histochemical investigations

Skeletal muscle biopsy plays an important role in the diagnostic work up for mitochondrial disease, principally because it is commonly clinically affected in patients with pathogenic mutations in either mtDNA or nuclear DNA. This is owed to the fact that muscle is a mitochondrial rich tissue with a high energy demand, thus is likely to exhibit a respiratory chain defect in the presence of a pathogenic variant. This is also true for the brain and heart which are also commonly affected in patients, however muscle is an accessible tissue in comparison hence its role in the diagnostic pathway. With the ongoing shift towards the “genetics first approach”, the question of when to perform a muscle biopsy arises. It is becoming less common to obtain biopsies from young children, however in some adults, the

procedure is still undertaken following clinical assessments. For example, this could be due to further investigation required for a novel variant with unknown function.

Many patients manifest distinct histopathological alterations in their skeletal muscle which indicate mitochondrial dysfunction. One such hallmark feature observed in muscle histology is the presence of Ragged-Red Fibres (RRF) which are detected through the modified Gomori trichrome stain (**Figure 1.21**) (Engel and Cunningham 1963). These fibres present when there is an accumulation of mitochondrial aggregates in the subsarcolemmal region of the fibre due to mitochondrial proliferation as a result of mitochondrial OXPHOS dysfunction (Moraes et al., 1992). Amongst the normal blue stained fibres, RRF are visualised as being red in colour with cracking of fibre edges. Whilst it is recognised that RRF is a feature of mitochondrial disease, the fibres are also observed in normal ageing muscle (Cao et al. 2001), Duchenne and Becker muscular dystrophy and other chronic myopathies (Paizner et al., 1991; Calere et al., 1994). To distinguish from these disorders, Bernier et al. (2002), suggested that the presence of RRF in over 2% of all fibres on the muscle sections of individuals under 50 years of ages should be indicative of mitochondrial disease.

Another canonical pathological feature of mitochondrial disease is the presence of COX-deficient fibres. A number of diagnostic protocols have been established in distinguishing these fibres in patient muscle biopsies. The most universally used protocol is the sequential COX/SDH histochemical assay (**Figure 1.21**) – often referred to as being the ‘gold standard method’. The enzymatic reactions include the loss of oxidized 3,3’ diaminobenzidine (DAB) tetrahydrochloride and the electron acceptor nitroblue tetrazolium (NBT). The oxidation of DAB results in a brown reaction product whilst NBT forms a blue reaction product known as formazan (Old and Johnson 1989; Sciacco and Bonilla 1996) (Ross 2011). Fibres are either coloured brown which signifies healthy fibres or blue which identifies the COX-deficient fibres. A global loss of COX-activity, indicated by all blue fibres on the skeletal muscle section, is observed in cases where the mitochondrial disease is caused by a pathogenic variant on a nuclear-encoded gene affecting COX assembly or homoplasmic mt-tRNA mutations (Taylor et al. 2003; Tiranti et al. 1998; Zhu et al. 1998). However, in the case of the mutation being on the mtDNA, a mosaic pattern is frequently observed on the muscle section - COX-deficient fibres appearing blue amongst the brown normal COX-positive fibres. This mosaic pattern is due to the differing levels of heteroplasmy (due to mitotic segregation and clonal expansion) by which fibres where heteroplasmy has exceeded the threshold for deficiency appear as COX-deficient (Bua et al. 2006; Campbell et al. 2014). It is important to also consider that clonal expansion leads to healthy aged individuals accumulating a low

frequency of COX-deficient fibres (Baines et al. 2014; Bua et al. 2006; Rygiel et al. 2016). A suggestive diagnosis of mitochondrial disease is only made when an individual's (under 50 years of age) muscle section harbours COX-deficiency fibres at a frequency of >5%.

More recently, Simard and colleagues (2018), established the nitrotetrazolium blue exclusion assay (NBTx assay) as an alternative enzymatic histochemical reaction for the detection of COX-deficient fibres. Unlike COX/SDH, the single colour reaction only requires the reduction of NBT without the use of DAB and thus the protocol provides a rapid time processing during diagnosis. The assay utilises the redox reactions between cytochrome *c* oxidase, NBT and the potent electron carrier phenazine methosulphate (PMS). PMS carries electrons from Complex II to NBT which is localised in COX subunits, however PMS only favourably transfers electrons when COX activity is intact. Upon accepting the electrons, NBT forms formazan. This only occurs in COX-deficient fibres, therefore, the assay allows for the direct visualization of deficient cells. Unlike COX/SDH, NBTx is capable of revealing low levels of COX-deficiency in single cells. The assay has also the potential for automated and quantifiable analysis (Simard et al. 2018).

Whilst skeletal muscle is commonly used for these investigations, in some cases, cardiac muscle, liver and brain (post-mortem) can also be used.

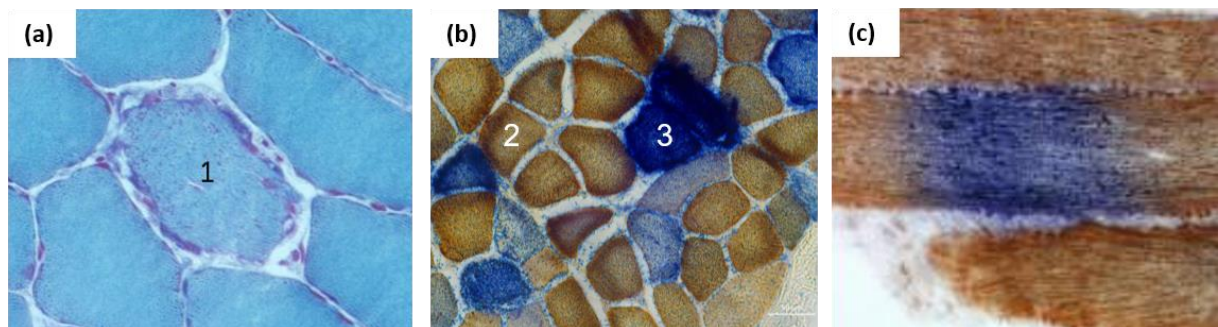


Figure 1.21: Histochemical investigations showing hallmarks of mitochondrial dysfunction in skeletal muscle

A) Gomori trichrome stain to detect ragged red fibres which show an accumulation of mitochondrial aggregates in the subsarcolemmal region of the fibre due to mitochondrial proliferation, indicated by the red in colour (fibre 1). **B)** Sequential COX/SDH histochemistry showing a mosaic pattern of unaffected (COX-positive – fibre 2) and affected (COX-deficient – fibre 3) muscle fibres in transverse sections. **C)** When muscle biopsies are examined longitudinally, COX-deficiency can be seen restricted to small segments along the length of the fibre surrounded by COX-positive regions.

1.8.2. Biochemical studies

Spectrophotometric evaluation of individual respiratory chain complex activities is an important approach to the biochemical investigation and diagnosis of mitochondrial diseases. It can be performed in either fresh or frozen muscle homogenate (~50mg of skeletal muscle required), however the latter is more common in diagnostic centres due to cross-continental or national referral of patients. Each complex can be analysed in isolation following the oxidation/reduction of specific substrates or substrate analogues. The spectrophotometric enzyme assays are as follows; NADH:ubiquinone oxidoreductase for complex I, succinate:CoQ₁ oxidoreductase for complex II, ubiquinol- cytochrome *c* oxidoreductase for complex III, cytochrome *c* oxidase for complex IV and oligomycin sensitive ATP synthase for complex V. Bernier et al. (2002), recommended a 20-30% of normal complex activities as a criterion for the diagnosis of mitochondrial disease.

Alongside the spectrophotometric assays, another useful assay includes the BN-PAGE assay which is used to assess the relative abundance of fully assembled respiratory chain enzyme complexes. Similarly, measurements of protein subunits of complexes are assessed through western blots and gel electrophoresis. These two techniques are often used to validate suspected pathogenic variants (Parikh et al. 2015).

1.8.3. Molecular genetics studies

A confirmed defect in the respiratory chain complexes, through both histochemical and biochemical testing, can facilitate appropriate molecular genetic testing to elucidate the underlying genetic cause. However, as previously discussed, the advent and application of NGS has changed the diagnostic approach to a “genetics first approach”.

Prior to the expansion and application of NGS, first generation sequencing, primarily Sanger sequencing (Sanger et al. 1977), was utilised to identify pathogenic variants, however the technique was only able to sequence short DNA reads. This led to the development of Shotgun *de novo* sequencing which was able to sequence larger DNA regions such as whole chromosomes or genomes. NGS techniques were developed thereafter, classed as second-generation sequencing techniques. The application of NGS is effective for heterogeneous conditions such as mitochondrial diseases as it allow for the interrogation of a large number of genes simultaneously. Moreover, it provides a rapid, high throughput sequencing which is much more cost effective than Sanger sequencing. Over the past decade, the screening of the mitochondrial genome and the high throughput analysis of Mendelian candidate genes has been achieved with the following NSG approaches; targeted gene panels for example the targeted Complex I panel (Alston et al. 2016), targeted exome sequencing (“MitoExome”)

(Calvo et al. 2012) whole exome sequencing (WES) (Haack et al. 2010; Taylor et al. 2014; Wortmann et al. 2015), whole genome sequencing (WGS) (Hartmannova et al. 2016) and RNA-seq (Kremer et al. 2017).

If the diagnostic pathway follows the “biopsy first approach” and the evidence from the histopathological and biochemical algorithms indicate a defect in a mtDNA gene, the entire mitochondrial genome can be analysed. NGS allows for deep coverage across mtDNA and thus detection of low levels of heteroplasmy, point mutations and breakpoints of single, large-scale mtDNA deletions. Alternatively, if evidence is inferring to a defect located in the nuclear DNA, either WES, WGS or a targeted multi-gene panel of candidate genes can be employed to identify the causative gene.

In the case of novel variants that have not been previously reported, functional tests must be undertaken to confirm the pathogenicity of the defect. These typically include looking at pathogenicity predictions based on protein structure and “rescue” experiments where patient cells are transfected with a wild type copy of the suspected gene and is shown to rescue the disease phenotype. Additionally, protein expression can also be investigated through BN-PAGE and SDS-PAGE as well as the quadruple immunofluorescence assay (Thompson et al. 2019).

1.8.4. Immunofluorescence techniques

Immunofluorescence techniques using specific monoclonal antibodies targeting the subunit of mitochondrial OXPHOS complexes have also been used in investigating biochemical defects in skeletal muscle sections. One advantage of this is the direct visualisation of the antigen-antibody binding sites and therefore a direct protein expression. Another is that immunofluorescence techniques allow for the quantification of several subunits of the respiratory chain complexes on one muscle section. Rahman et al. (2000) utilised the technique to identify specific staining patterns associated with the different subunits of Complex IV. The study recognised specific staining patterns/subunit loss associated with patients with COX-deficiency secondary to mtDNA mutations whilst most patients did not have this particular staining pattern and therefore were thought to harbour nuclear gene defects. Another study utilised the technique to determine the expression of the targeted proteins in the frontal cortex, cerebellum and medulla on autopsied brain biopsy from a MERFF patient and found decreased expression of COX-II in these regions (Sparaco et al. 1995). Likewise, COX-deficiency was detected using a monoclonal antibody against COX-I to show Complex IV deficiency in the small intestine of a patient with MERFF (Tanji et al. 2001). In addition, De Paepe et al. (2009) developed an immunofluorescence approach to

identify all five complexes in skeletal muscle sections of patients with mitochondrial tRNA gene defects and was able to stain for Complex I in two tRNA patients who had previously been undetected in the routine histochemical diagnostic process.

As further described in **section 1.9** below and also **Chapter 2**, Rocha et al, developed the quadruple immunofluorescence assay and validated the technique using skeletal muscle cryosections from patients with various pathogenic variants (Rocha et al. 2015) - **Figure 1.22(B)**. The technique has since been applied routinely in a diagnostic setting at the Newcastle NHS Highly Specialised Service for Rare Mitochondrial Disorders, located within the Wellcome Centre for Mitochondrial Research at Newcastle University.

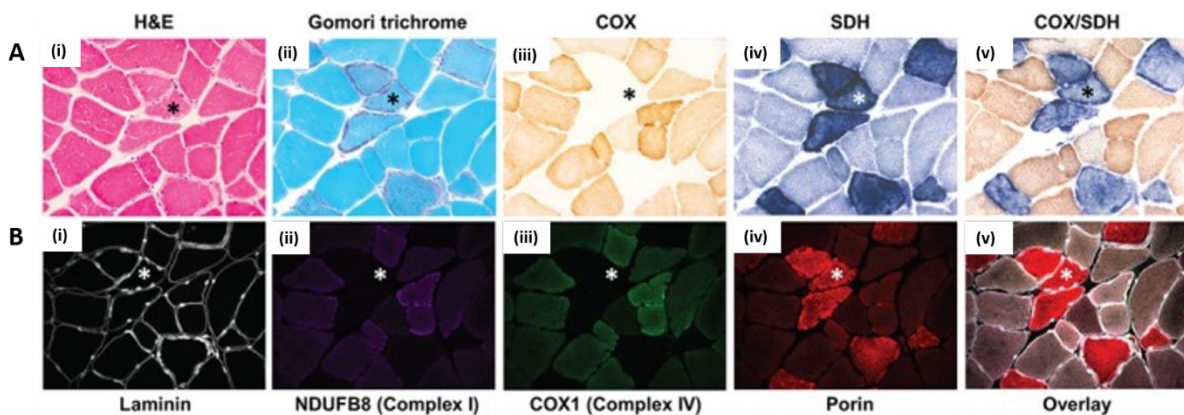


Figure 1.22: Comparison of the quadruple immunofluorescence assay to the traditional histopathology techniques.

(A) The traditional standard histopathology techniques used in serial skeletal muscle sections from a patient with a single, large- scale mtDNA deletion (i) H&E used to assess fibre size variation, abnormal infiltrations and central nuclei. (ii) Gomori trichrome (iii) Individual staining of COX (fibre marked with asterix (*) indicating loss of Complex IV), (iv) SDH (fibre marked with asterix (*) indicating normal Complex II) and (v) sequential COX/SDH staining showing mosaic COX deficiency.

(B) the application of the quadruple immunofluorescence assay (i) Laminin staining used as a myofibre boundary marker (ii) NDUFB8 targeting Complex I (iii) COX-1 targeting complex IV (iv) Porin used for mitochondrial mass marker and (v) is the overly of all antibodies used. Fibre marked with the * indicate focal accumulation of sub-sarcolemma mitochondria and the down regulated immunoreactivity of both NDUFB8 and COX-1, therefore a downregulation in the expression of CI and CIV. Figure has been taken and amended from Alston et al., 2016.

1.9. The quadruple immunofluorescence Assay

The quadruple immunofluorescence assay, as developed by Rocha et al., 2015, targets the two most commonly affected complexes in mitochondrial disease; Complex I and Complex IV.

The assay utilises monoclonal antibodies targeting NDUFB8 (Complex I), COX-1 (Complex IV), porin (VDAC- mitochondrial mass) and laminin (myofibre boundary) on a 10µm skeletal muscle tissue section. The assay allows for an objective and reliable quantitative method which allows for the assessment of Complex I and Complex IV protein abundance relative to the mitochondrial mass in each individual muscle fibre within a 10µm transverse skeletal muscle tissue sections of patients with different genotypes causing mitochondrial disease (Rocha et al. 2015). The analysis of the single muscle fibres is undertaken using an automated analysis software (described further in **Chapter 2, section 2.5.10.1**), where staining intensity of NDUFB8, COX-1 and porin is determined.

A major advantage of the assay is the ability to target Complex I, therefore providing an alternative histopathological technique to COX/SDH, for Complex I deficient patients in particular. Furthermore, through targeting COX-1, a core catalytic subunit of Complex IV, which is essential for the function and assembly of the complex, the assay is targeting a subunit which is responsible for the integrity of the complex.

The assay has been utilised in research, for example the technique has been shown to have important implications for the diagnosis of mitochondrial diseases (Ahmed et al. 2017) which is expanded upon in **Chapter 3**. Additionally, the assay has been used to investigate the underlying molecular mechanisms of disease, for example gaining a mechanistic insight into single large-scale deletions through utilising both the assay and single cell (fibre) approach (Rocha et al. 2018). Further muscle related diseases which involve the mitochondria have also been investigated using the assay for instance disorders caused by mutations in the *DYSF* gene (dysferlin) (Vincent et al. 2016b) and myofibrillar myopathies caused by mutations in *DES*, *MYOT*, *CRYAB*, *FLNC*, *BAG3*, *DNAJB6* and *ZASP* genes (Vincent et al. 2016a).

1.10. Overall aims and objectives:

The aims of this PhD can be divided into two themes; i) improving the diagnosis of mitochondrial diseases and ii) improving the understanding of molecular mechanisms underlying mitochondrial disease and the expression of a biochemical defect. The principle methodology of this work will be the use of patient skeletal muscle sections and the quadruple immunofluorescence assay, to achieve the following aims;

- 1) Firstly, with regards to the first theme, the aim will be to investigate whether the quadruple immunofluorescence assay can be utilised in a diagnostic setting for patients with Complex I deficiency. This will be specifically achieved through assessing the Complex I expression in the skeletal muscle sections of patients who have proven pathogenic mutations in either nuclear encoded subunits or assembly factors or mtDNA encoded subunits of Complex I. Given the vast clinical and genetic heterogeneity associated with Complex I deficiency, it will be important to assess how effectively and accurately this assay is able to detect Complex I deficiency in this group of patients (**Chapter 3**).

The second theme is specifically exploring the heteroplasmic m.3243A>G pathogenic variant located within the *MT-TL1* gene. This mutation is associated with a vast clinical heterogeneity and complexity. This study has the overarching aim of deducing the heteroplasmic threshold for individual patients, how this may differ and how this biochemical phenotype may correlate with the clinical phenotype. Therefore, the aims for this part of the thesis (**Chapters 4 and 5**) are as following;

- 1) To characterise the biochemical profile of skeletal muscle sections from patients harbouring the m.3243A>G mutation from the MitoCohort. The study will utilise the assay in a larger cohort of patients to capture this heterogeneity and to better characterise the protein expression of Complex I and Complex IV in single muscle fibres.
- 2) Taking forward the data attained from the quantitative immunofluorescence assay, the next aim will be to assess the relationship between this data and the clinical data available for each patient, specifically the homogenate m.3243A>G heteroplasmy level and the clinical assessments scoring the phenotypic severity (NMDAS scores).

This paves way for the final aims of this project which are the following;

- 1) Using a single fibre approach, fibres will be sampled from skeletal muscle sections of these patients for downstream molecular genetic testing to determine the heteroplasmy level in each individual fibre. The relationship between the biochemical respiratory chain defect (Complex I and Complex IV) and heteroplasmy level will be assessed at the cellular level.
- 2) To determine the threshold level at which Complex I and Complex IV deficiency occur in each patient skeletal muscle section. Using the appropriate statistical input, the estimated threshold will be determined and to ascertain whether there is a difference in these thresholds between patients

Chapter 2: Materials and methods

2.1. Equipment

Table 2.1: List of equipment

Equipment	Company
3510 pH meter	Jenway
ABI Step one software v.2	Applied Biosystems
ABI StepOnePlus™ Real-Time PCR system	Applied Biosystems
ABI verti 96 well Thermo Cycler	Applied Biosystems
Apoptome Axio Imager Z2 microscope	Carl Zeiss
Autoclave	Prior Clave
Axio Imager M1 microscope	Carl Zeiss
AxioCam MRc colour digital camera	Carl Zeiss
AxioCam MRm monochrome digital camera	Carl Zeiss
AxioVision (release.4.8.2) image capture software	Carl Zeiss
Balance	VWR
Benchtop Centrifuge, 5417	Eppendorf
Benchtop Centrifuge, 5418	Eppendorf
Benchtop Heat Block – OBD2	Grant
BioRad ChemiDoc MP imaging system	Bio-Rad
Cary WinUV Software (Version 3.00)	Agilent Technologies
CCD colour camera	Olympus
Cryostat (Cryo-star) HM 560M	Microm International
Cryostat	Bright – OTF5000
DNA Gel Electrophoresis Tray	PeQlab
Excel	Microsoft
Image J – image analysis software	Public domain – NIH
Image Lab (version 4.0.1, build 6)	Bio-Rad Laboratories
Laminar flow hood	Jencons-PLS
Leica Laser Microdissection Microscope System	Leica
Microwave, Jet convection and Grill	Sharp
NANOpurell Water Purification System	Elga Veolia
Olympus BX51 light microscope	Olympus
Optima Max – XP Ultracentrifuge	Beckman Coulter
Orbital Shaker (SSL1)	Stuart
Palm Robo Software (version 4.6)	Carl Zeiss
Platform Shaker STRG	Stuart Scientific
Power Supply – MP 250 volts	Cleaver Scientific
Prism 5	GraphPad Software Inc
PyroMark Q24	Qiagen

PyroMark Q24 Cartridge ε 3, Version 2	Qiagen
PyroMark Q24 System (version 2.0.7)	Qiagen
PyroMark Q24 Workstation	Qiagen
Quadruple Immunofluorescence Analyser	Dr John Grady (Kinghorn Centre for Clinical Genomics Garvan Institute Sydney NSW Australia)
R (version 3.5.0 (2018-04-23) -- "Joy in Playing")	R
R Studio (Version 1.1.447)	R Studio
ThermoMixer Comfort	Eppendorf
UV hood	Bioair Instruments
UV Visible Spectrophotometer Cary 300	Agilent Technologies
Vortex Genie	Scientific Industries
Vortex genie 2	Scientific industries
Vortex Genie 2	Scientific Industries
Zeiss Axioimager	Zeiss
Zen (blue edition) image capture software	Carl Zeiss

2.2. Consumables

Table 2.2: List of consumables

Consumable	Company
0.2ml thin-walled PCR tubes	Starlab UK Ltd
10µl Multichannel Pipette	Ergo One
25 well, 1.5mm DNA Gel electrophoresis combs	PeQlab
8-Strip PCR Caps, Domed	StarLab
Aerosol resistance pipettes	Starlab UK Ltd
Centrifuge Tubes – 7/1 x 13/8 (11x34mm)	Beckman Coulter
Certified Thin Wall 24 x 0.2ml PCR Plates – Elevated Wells	StarLab
Coverslips (22x50mm)	Merck (MSD)
Eppendorf tubes (1.5ml, 2.0ml)	Starlab UK Ltd
Falcon tubes (15ml, 50ml)	BD Biosciences
Filtered Pipette Tips (10µl, 20µl, 200µl, 1ml), Tip One	StarLab
Gilson pipette (P1, P10, P20, P200, P1000)	Gilson Scientific
Gloves	StarLab
Hydrophobic pen	Daido Sangyo
MicroAmp®Optical 96- Well reaction plate	Fisher Scientific
Native 4-16% BisTris Gel	Life Technologies
Pasteur pipette (3ml)	VWR international Ltd

Pipette tips (10µl, 20µl, 200µl, 1ml)	Starlab UK Ltd
Polyvinylidene fluoride (PVDF) membrane	Immobilon-P, Millipore Co
PyroMark Q24 Plate – 100	Qiagen
Scalpels	Swann Morton
StarSeal advanced polyolefin film	Starlab UK Ltd
Superfrost Glass slides	Merck (MSD)
Teflon Glass Dounce Homogenizer	Thomas Scientific
Weigh boats	VWR International Ltd
Whatman filter paper	Fisher Scientific
X-Cell SURE Lock apparatus	Thermo Fisher

2.3. Chemicals and Reagents

Table 2.3: List of chemicals and reagents

Chemicals	Company
Ethanol (absolute)	Fisher Chemicals
Methanol (99.9%)	Fischer Chemicals
Liquid Nitrogen	Boc
<i>Reagents: Immunofluorescence staining</i>	
Sodium Chloride (NaCl)	Sigma Aldrich Company Ltd
Trizma Base	Sigma Aldrich Company Ltd
Tween-20	Sigma Aldrich Company Ltd
Hydrochloric Acid (HCl)	VWR International
Paraformaldehyde (PFA), 4%	Santa Cruz
Methanol (99.9%)	Fisher Chemicals
Normal Goat Serum (NGS)	Sigma Aldrich Company Ltd
Avidin and Biotin Kit	
Prolong Gold Mounting Media	Life Technologies
<i>Reagents: Primary Antibodies</i>	
Mouse IgG1 NDUFB8 (100µg at 1 mg/ml)	Abcam (Ab110242)
Mouse IgG1 NDUF3 (100 µl at 0.5 mg/ml)	Abcam (Ab197971)
Mouse IgG2a MTCO1 (100µg at 1 mg/ml)	Abcam (Ab14705)
Mouse IgG2b VDAC (Porin) (100µg at 1 mg/ml)	Abcam (Ab14734)
Polyclonal Rabbit IgG Laminin α-1 (500 µl at 0.5 mg/ml)	Sigma Aldrich (L9393)
Mouse IgG2b Ba-F8-s (26µg/ml)	DSHB (3/3/16)
Mouse SC-71-s IgG1 (26µg/ml)	DSHB (3/3/16)
6H1-s (IgM) = MHC type IIx (64µg/ml)	DSHB (4/7/16)
Polyclonal Rabbit ND1	Gifted by Professor Anne Lombés (Institut Cochin, France)
<i>Reagents: Secondary Antibodies</i>	
Goat Anti- mouse IgG1 Alexa fluor – 488nm	Life Technologies (A21121)
Goat Anti-mouse IgG 2a-Alexa fuor - 488nm	Life Technologies (A21141)
Goat Anti- mouse IgG2b Alexa fluor – 546nm	Life Technologies (A21143)

Goat Anti- mouse IgG1-Alexa Fluor - 546nm
Goat Anti-rabbit IgG Alexa fluor - 750nm
Streptavidin – 647nm
Anti-mouse IgM Alexa fluor – 647nm
XX Goat Anti-mouse IgG1 Biotin

Life Technologies (A21123)
Life Technologies (S31556)
Life Technologies (S32357)
Invitrogen (A21238)
Life Technologies (A10519)

Reagents: DNA extraction

Nuclease Free Water
Tween-20
Tris- HCl
Proteinase K Solution (20mg/ml), RNA grade
DNA Away

Promega
Sigma Aldrich Company Ltd
Sigma Aldrich Company Ltd
Thermo Fisher Scientific
Molecular Bio Products

Reagents: Polymerase Chain Reaction (PCR)

GoTaq® G2 DNA Polymerase (5u/μl)
5X Colorless GoTaq® Reaction Buffer
Deoxyribonucleotide Triphosphate (dNTP) A
Deoxyribonucleotide Triphosphate (dNTP) C
Deoxyribonucleotide Triphosphate (dNTP) G
Deoxyribonucleotide Triphosphate (dNTP) T
PCR primers
Nuclease Free water
DNA Away

Promega
Promega
Roche Diagnostics Ltd
Roche Diagnostics Ltd
Roche Diagnostics Ltd
Roche Diagnostics Ltd
IDT
Promega
Molecular Bio Products

Reagents: Gel Electrophoresis

Agarose (Molecular Grade)
Tris Acetate EDTA (TAE), 10x
Syber Safe DNA Gel Stain, 10,000
Bromophenol Blue
Glycerol
PCR Ranger 100bp Ladder

Bioline Reagents
Sigma Aldrich Company Ltd
Invitrogen
Sigma Aldrich Company
Sigma Aldrich Company
Norgen

Reagents: Pyrosequencing
Streptavidin Sepharose High Performance beads
PyroMark Binding Buffer
PyroMark Annealing Buffer
PyroMark Wash Buffer, Concentrate
Ethanol
Sodium Hydroxide Pellets
PyroMark Enzyme Mixture
PyroMark Substrate Mixture
PyroMark dATPaS
PyroMark dCTP
PyroMark dGTP
PyroMark dTTP
Pyrosequencing reverse Primer

GE Healthcare
Qiagen
Qiagen
Qiagen
Fisher Chemicals
VWR
Qiagen
Qiagen
Qiagen
Qiagen
Qiagen
Qiagen
IDT

Reagents: Real- Time PCR

Taqman PCR Mastermix
Real-Time PCR probes
Real-Time PCR primers
Nuclease Free Water

Applied Biosystems
Eurofins
Eurofins
Promega

Reagents: Muscle Homogenisation and Solubilisations

Phosphate Buffer Saline (PBS)	OXOID
Sucrose	BDH
Imidazole	Sigma Aldrich Company Ltd
HCl	Fisher Scientific
Native Page 4 x Sample Buffer	Invitrogen
20% n-Dodecyl β -D-Maltoside (DDM)	Sigma Aldrich Company Ltd
Glycerol	Sigma Aldrich Company Ltd
Phenylmethylsulphonyl Fluoride (PMSF)	Sigma Aldrich Company Ltd
Isopropanol	Sigma Aldrich Company Ltd

Reagents: Blue Native Polyacrylamide Gel (BN-PAGE)

Pierce BCA Protein Assay Kit	Thermo Scientific
BN-PAGE Marker	
20 x Native Page Running Buffer	Novex by Life Technologies
20 x Native Page Cathode Buffer	Novex by Life Technologies
20 x Native Page Transfer Buffer	Novex by Life Technologies
Marvel Original Dried Skimmed Milk	Marvel
Amersham TM ECL TM Prime Luminol Enhancer Solution	GE Healthcare Life Sciences
Amersham TM ECL TM Prime Peroxide Solution	GE Healthcare Life Sciences

2.4. Solutions

1 x PBS (100ml)	1 x PBS tablet 100ml deionised water (dH ₂ O)
70% Ethanol (500ml)	350ml Ethanol 150ml dH ₂ O
70% Methanol (400ml)	280ml Methanol 120ml dH ₂ O
95% Methanol (400ml)	380ml Methanol 20ml dH ₂ O
50% Glycerol (30ml)	15ml Glycerol 15ml dH ₂ O
5 x TBST – pH 7.4 (2 litres)	121g Trizma Base 90g NaCl 2L dH ₂ O 5ml Tween 20 HCl to pH 7.6
DNA Loading Buffer (50ml)	0.125 (0.25% w/v) Bromophenol Blue (BpB) 35ml dH ₂ O 15ml (30%) Glycerol
Gel pouring buffer/running buffer (1 litre)	100ml 10 x TAE 900ml NANOpure water

2% Agarose Gel	2g Agarose 100ml 10 x TAE
Single Cell Lysis Buffer	250µl 1% Tween 20 50µl 0.5M TrisHCL at pH 8.5 5µl Proteinase K 190µl dH ₂ O
PMSF, 100mM (10ml)	192mg PMSF Dissolve in 10ml Isopropanol
Muscle Homogenisation Buffer (30ml)	5.13g sucrose (250mM) 600µl Imidazole/HCl (20mM) 30ml dH ₂ O 300µl PMSF (1mM)
Muscle Solubilisation Buffer (50µl)	1.75µl Native Page 4x Sample buffer 20% DDM 50% Glycerol 26.25µl dH ₂ O
1 x Wash Buffer (500ml) (Pyrosequencing)	50ml 10x wash buffer 450ml dH ₂ O
Denaturation Solution (Pyrosequencing)	4g NaOH 500ml dH ₂ O
1 x Cathode Buffer (200ml) (BN-PAGE)	10ml 20 x Native Page cathode buffer 10ml 20 x Native Page running buffer 180ml dH ₂ O
1 x Anode Buffer (2L) (BN-PAGE)	50ml 20 x Native Page running buffer 950ml dH ₂ O
10 x Transfer Buffer (1L) (BN-PAGE)	50ml 20x Native Page Transfer Buffer 200ml Methanol 750ml dH ₂ O
Tris- HCl, pH 8.5, 3.75M	45.45g Trisma Base 100ml dH ₂ O HCl to pH 8.5

2.5. Methods

2.5.1. The Newcastle Mitochondrial Research Biobank

The Newcastle Mitochondrial Research Biobank is a UK REC approved Research Tissue Bank which received ethical approval from the North East – Newcastle and North Tyneside 1 Research Ethics Committee in 2016. The Biobank is sponsored by the Newcastle Upon Tyne Hospitals NHS Foundation Trust and is based within the NHS Highly Specialised Service for Rare Mitochondrial Disorders, located within the Wellcome Centre for Mitochondrial Research (WCMR) at Newcastle University

The Biobank consists of tissue samples from mitochondrial patients and their family members. Samples are either excess to diagnostic requirements or were collected exclusively for research purposes.

2.5.2. Ethical approval and guidelines

Skeletal muscle tissue samples used throughout this PhD project were made available for access after requesting from the Newcastle Mitochondrial Research Biobank (Research Ethics Committee reference: 16/NE/0267). Ethical approval and guidelines for the projects were issued under either the Newcastle and North Tyneside Local Research Ethics Committees (reference 09/H0906/76) as complied with the declaration of Helsinki (as revised in 2013), or by the generic research tissue bank approval for the Newcastle Mitochondrial Research Biobank. Any clinical information linked to the samples was also provided under the approval of the latter committee with support from the Wellcome Centre for Mitochondrial Research Patient Cohort: A natural history study and Patient registry - the MitoCohort, (research ethics committee reference: 13/NE/0326). See the below section (2.5.3) for further information on the MitoCohort.

2.5.3. Clinical Data – Mitochondrial Disease Patient Cohort (UK) (MitoCohort)

The Wellcome Centre for Mitochondrial Research Patient Cohort: A natural history study and patient registry (the MitoCohort) received ethical approval from the North East – Newcastle and North Tyneside 2 research Ethics Committee in 2013. It replaced the MRC Centre Mitochondrial Disorders Patient Cohort (UK) Database (REC Ref 08/H0402/72). The MitoCohort is sponsored by The Newcastle Upon Tyne Hospitals NHS Foundation Trust and is managed by Newcastle University. The main collaborating centres are Newcastle, University College London Hospitals and Oxford University Hospitals. There are a total of 1675 patients across all these sites. All patients included are clinically, genetically and biochemically confirmed as having mitochondrial disease.

The clinical data within the MitoCohort is stored in a secure database which can only be accessed by authorised individuals. An MDOC (Mitochondrial Disease Oversight Committee) application is required to be submitted in order to allow access for research purposes. The clinical data attained for patients included in **Chapter 4** and **5** was attained via an approved MDOC application.

2.5.4. Patient Cohort

All patient samples were obtained and used for research purposes with informed consent from all participants prior to the start of the projects. All experiments were carried out in accordance with the approved guidelines.

2.5.4.1. Isolated Complex I patients

In **Chapter 3**, 25 skeletal muscle biopsies (quadriceps muscle) of patients were used. Measurements of the enzymatic activities of respiratory chain complexes were undertaken at one of two approved Mitochondrial Diagnostic laboratories; the NHS Highly Specialised Service for Rare Mitochondrial Disorders located within the WMCR at Newcastle University or the Neurometabolic Laboratory at University College London Hospitals (UCLH). Muscle biopsy referral, enzyme measurements and genetic studies were all undertaken as part of the diagnostic work-up of these patients for suspected mitochondrial disease. This study was approved and performed under the ethical guidelines issued by the Newcastle and North Tyneside Local Research Ethics Committees (reference 09/H0906/75) and complied with the Declaration of Helsinki (as revised in 2013).

2.5.4.2. m.3243A>G patients

A cohort of patients (n=17) who harbour the m.3243A>G mutation were selected from the MitoCohort UK database for investigation in **Chapter 4** (further investigated at in **Chapter 5**). Of the total 1,775 patients (as of October 2019) across all of the sites included in the MitoCohort, 455 patients have their genotype recorded as m.3243A>G. Within Newcastle, there are 292 patients who are registered as being carriers of m.3243A>G, of which 28 are deceased. For this study, 19 muscle biopsy samples (either quadriceps muscle or tibialis anterior (TA)) were requested from the Newcastle Mitochondrial Research Biobank (Research Ethics Committee reference: 16/NE/0267). Two further patient biopsies were included in this study who were not part of the MitoCohort but were provided by the Neuromuscular Centre, Institute for exercise and Environmental medicine at the University of Texas, Dallas.

Unless stated, the muscle biopsy referrals, clinical, histochemical, molecular genetics and enzymatic investigations were all undertaken as part of the diagnostic work up of these patients for suspected mitochondrial disease at the NHS Highly Specialised Service for Rare Mitochondrial Disorders (located within the Wellcome, Centre for Mitochondrial Research) at Newcastle University.

2.5.5. Control Muscle Tissue

The control muscle tissues used throughout these studies were obtained from patients who underwent anterior cruciate ligament (ACL) surgery, with prior informed consent and approval from the Newcastle biobank (NAHPB reference: 042). Biopsies were obtained from the distal part of the hamstring of these individuals. They were made available from the NHS Highly Specialised Mitochondrial Diagnostic Service for Rare Mitochondrial Disorders, for research purposes and were shown to have normal respiratory activities (both protein expression and enzymatic activity). The characteristics of the five controls used in the studies are shown in **Table 2.4**.

Table 2.4: Characteristics of the non-disease control skeletal muscle biopsies (taken from distal region of hamstring following ACL surgery)

Control ID	Gender	Age (years) at biopsy
C1	M	17
C2	M	33
C3	F	25
C4	F	23
C5	M	28

2.5.6. Newcastle Mitochondrial Disease Adult Scale (NMDAS)

The Newcastle Mitochondrial Disease Adult Scale (NMDAS) was first published in 2006 (Schaefer et al. 2006) with the aim of standardising assessment of patients both within our centre and internationally. The clinically validated method allows for a quantitative measure of patients which is important due to the multi-systemic nature of mitochondrial disease and the varied severity of clinical symptoms observed by clinicians. The scale also allows for assessing patient disease progression.

An example of the NMDAS assessment is given in the Appendix (**Appendix 1**). Briefly, the assessment is split into three separate sections with 29 questions in total. Section 1 includes ten questions completed by the patient or the caregiver, assessing the current function and the impact of the disease on a day to day basis. Section 2 entails nine questions which are

completed by the clinician and allows for the assessment of system specific involvements over the past 12 months. Section 3 includes ten questions which score the current clinical examination performed on the day of the clinic.

A score is obtained between 0 (normal function) and 5 (poorest form of function) for each of the 29 clinical questions, giving a maximum scoring total of 145. The total score for each patient is referred to as the 'Total NMDAS'. These observations are stored in the secure MitoCohort database. Further reference to the NMDAS scale will be in **Chapter 4**.

2.5.7. Tissue sectioning

Serial transverse sections were obtained from frozen skeletal muscle blocks using a Cryo-star HM 560M cryostat (Microm International), at a temperature of -20°C. The sections were cut to either 10µm or 20µm-thickness and two sections were collected per superfrost slides (Merck). Sections were dried at room temperature (RT) for approximately 1 hour and then stored at -80°C until relevant use.

2.5.8. Immunofluorescence

2.5.8.1. Quadruple immunofluorescence

Tissue sections were removed from -80°C storage and air dried for approximately 1 hour. Each section was drawn around with wax pen (to keep liquid on section and to ensure no mixing of solutions) and labelled appropriately as either OXPPOS primary or no primary control (NPC). Sections were fixed with cold 4% paraformaldehyde for three minutes followed by washes in 1% TBST three times for a period of five minutes each. Sections underwent permeabilization in a methanol gradient; 70% methanol for 10 minutes, 95% methanol for 10 minutes, 100% methanol for 20 minutes, 95% methanol for ten minutes and lastly 70% methanol for ten minutes. Slides were washed again three times for a period five minutes each, followed by a 10% normal goat serum (NGS – diluted in 1% TBST) protein block for one hour at RT to block non-specific binding. This was followed by a further biotin-avidin blocking step – avidin for 15 minutes, washed in TBST twice for five minutes each time followed by biotin for 15 minutes and again washes in TBST. Approximately 100µl of corresponding primary antibodies diluted in 10% NGS (**Figure 2.1**) were added to each section. Primary antibody concentrations can be found in **Table 2.5**. Sections were then incubated in a humidified and dark chamber overnight at 4°C.

Sections were washed in TBST three times for ten minutes with gentle agitation using the Orbital Shaker (SSL1). Following this, sections were incubated with secondary antibodies (diluted in 10% NGS) for 2 hours at 4°C. Secondary antibody dilutions can be found in **Table**

2.6. Sections were washed again as previously stated and incubated with 100µl of the streptavidin conjugated with Alexa 647 for a further 2 hours at 4°C. The sections were washed in TBST three times for 15 minutes and mounted in prolong gold mounting medium (Life Technologies) to preserve the fluorescence.

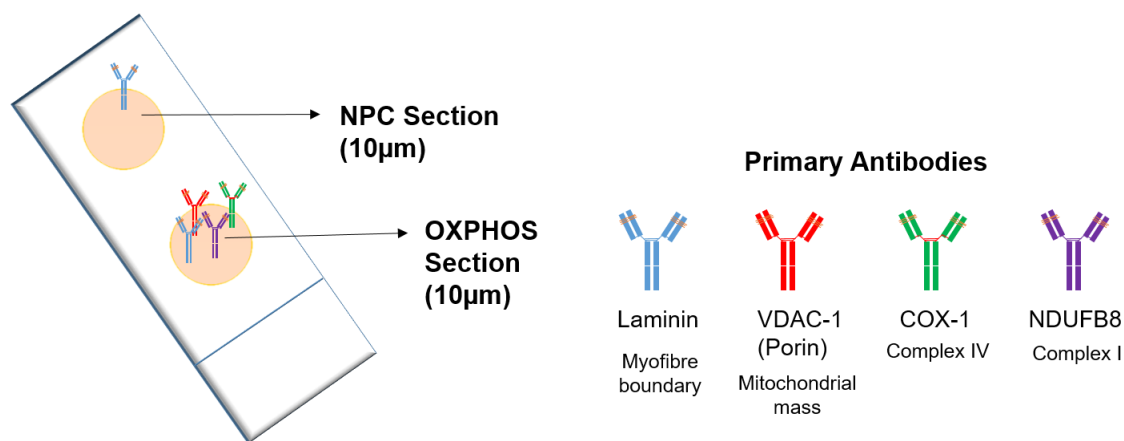


Figure 2.1: Schematic diagram of the quadruple immunofluorescence assay detecting respiratory chain enzymes.

Two sections of skeletal muscle (OXPHOS and NPC) are on glass slides. OXPPOS section undergoes labelling with antibodies targeting Complex I (NDUFB8), Complex IV (COX-1), mitochondrial mass (Porin, VDAC1) and laminin for highlighting myofibre boundary. The NPC section is labelled only with the laminin.

Table 2.5: Primary antibodies used in the Quadruple immunofluorescence assay

Antibody	Target	Supplier	Catalogue	Dilution
Mouse IgG1 NDUFB8	Subunit of Complex I	Abcam	Ab110242	1:100
Mouse IgG2a MTCO1	Subunit of Complex IIV	Abcam	Ab14705	1:100
Mouse IgG2b VDAC (Porin)	Voltage gated anion on outer membrane of mitochondria	Abcam	Ab14734	1:100
Polyclonal Rabbit IgG Laminin α-1	Protein of the extracellular matrix	Sigma Aldrich	L9393	1:50

Table 2.6: Secondary antibodies used in the Quadruple immunofluorescence assay

Antibody (Alexa fluor)	Wavelength	Supplier	Catalogue	Dilution
Goat Anti- mouse IgG1	488nm	Life Technologies	A21121	1:200
Goat Anti- mouse IgG2b	546nm	Life Technologies	A21143	1:200
Goat Anti-rabbit IgG	750nm	Life Technologies	A21039	1:100
Streptavidin	647nm	Life Technologies	S32357	1:100
XX Goat Anti-mouse IgG1 Biotin	n/a	Life Technologies	A10519	1:200

2.5.8.2. Fibre type immunofluorescence

Muscle fibre types were determined using an immunofluorescent protocol targeting the different myosin heavy chain isoforms. Transverse 20 μ m tissue sections were removed from 80°C storage and air dried for 1 hour. Sections were briefly washed with TBST followed by an hour of incubation with 10% NGS at room temperature. A cocktail of antibodies (**Table 2.7**) diluted in 5% NGS were added onto the sections and left to incubate overnight at 4°C (**Figure 2.2**). Following washes in TBST three times for 10 minutes, a cocktail of secondary antibodies, listed in **Table 2.8**, all at a dilution of 1:200 diluted in 5% NGS were added to the sections and incubated for 1 and a half hours in the dark at room temperature. Sections were then washed in TBST and mounted in prolong gold mounting medium for fluorescence. After the completion of imaging (see **section 2.5.9**), sections were stored at 4°C.

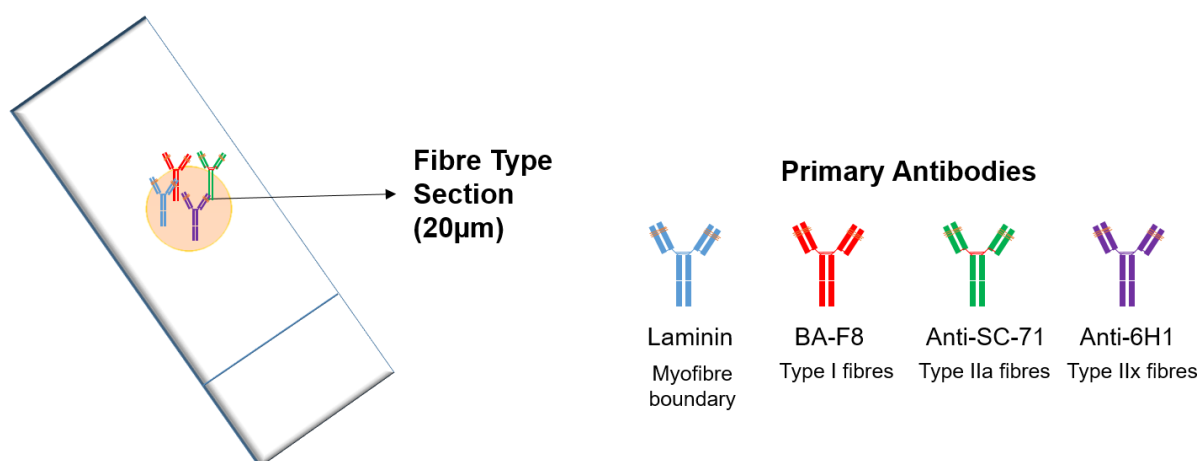


Figure 2.2: Schematic diagram of the immunofluorescence assay detecting different fibres types in skeletal muscle section.

A 20 μ m section is labelled with antibodies detecting different myosin chains associated with fibre types. Laminin allows for detection of the myofibre boundary.

Table 2.7: Primary antibodies used in fibre type immunofluorescence and associated dilutions

Antibody	Target	Supplier	Catalogue	Dilution
Mouse BA-F8-s (IgG2b)	Myosin heavy chain (MHC) slow Type I	DSHB	(11/5/15-43µg/ml)	1:200
Mouse SC-71-s (IgG1)	MHC Type IIa	DSHB	(3/3/16-26µg/ml)	1:200
6H1-s (IgM)	MHC Type IIx	DSHB	(4/7/16-64µg/ml)	1:50
Polyclonal Rabbit IgG Laminin α-1	Protein of the extracellular matrix	Sigma Aldrich	L9393	1:50

Table 2.8: Secondary antibodies used in fibre type immunofluorescence and associated dilutions

Antibody (Alexa fluor)	Wavelength	Supplier	Catalogue	Dilution
Anti-IgG 2b	488nm	Life Technologies	A21141	1:200
Anti-IgG1	546nm	Life Technologies	A21123	1:200
Anti-IgM	647nm	Invitrogen	A21238	1:200
Goat Anti-rabbit IgG	750nm	Life Technologies	A21039	1:200

2.5.9. Image Acquisition using Zeiss Axio imager MI microscope

Fluorescent images of the muscle sections were captured at x20 magnification using the Zen 2011 (blue edition) software and Zeiss Axio imager MI microscope. This microscope was equipped with a motorised stage, an AxioCam digital camera and filter cubes which detected light at the wavelengths of 488nm, 546nm, 647nm and 750nm. The motorised stage and a tiling function on the software allowed for automated scanning of a full muscle section on the slide. Exposure times were set for each channel to avoid over saturation and to minimise the background fluorescence in the NPC sections. The same exposure times were then maintained across all cases (controls and patients) for the experiment. Following this imaging process, tiled .zvi files were stitched to generate a .czi file for subsequent image analysis. Snapped images at 20x magnification were also captured for purposes of this thesis, publication and PowerPoint presentations.

2.5.10. Statistical Analysis of OXHPOS deficiency

2.5.10.1. Densitometry measurements using the Quadruple Immuno Analyser Software

Analysis of the single muscle fibres was undertaken using an in-house analysis software called the Quadruple Immuno Analyser. The software is coded for by MatLab 2015a and was designed by Dr John Grady (Kinghorn Centre for Clinical Genomics Garvan Institute Sydney

NSW Australia) in 2016. Fluorescent stitched .czi images were first uploaded into the software and the scanning option allowed for the generation of low resolution .jpg images to be created per channel (channel 1-4 in accordance to the wavelengths; 488nm (Porin), 546nm (COX-1), 647nm (NDUFB8) and 750nm (laminin) respectively), as well as merged images for channels 1, 2 and 3 and channels 2, 3 and 4. The laminin immunofluorescence (channel 4) was used to detect muscle fibres automatically (setting the parameters which include threshold and area for muscle fibre boundary contours to be set) (**Figure 2.3**). Any contours over unwanted muscle fibre and areas including those over background fluorescence, fibres with poor morphology or areas of the section which were folded were removed. Any fibres which were not detected automatically were drawn around manually. The muscle fibre contours were applied to all .jpg images and thus allowed for the measurement of the mean intensity/optical density (OD) of 488 (COX-1), 546 (Porin) and 647 (NDUFB8) in each individual fibre. The same procedure was repeated for each NPC to determine the levels of non-specific binding. Following image analysis, the software created a Microsoft Excel file containing the mean OD data for each case. This was then merged into one Excel file and the data was saved as a .csv file format using the merged processing on the software. The data was then uploaded to the Mitochondrial Immunofluorescence Analysis online tool (<http://research.ncl.ac.uk/mitoresearch/>).

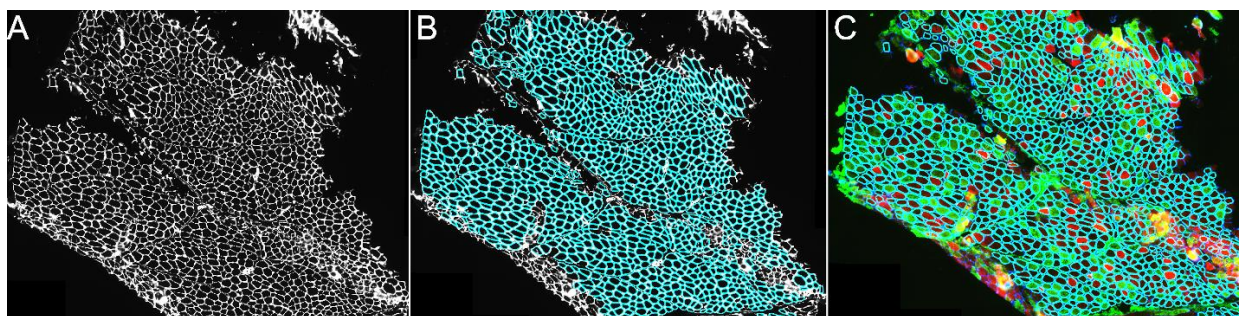


Figure 2.3: Analysis of single muscle fibres using the Quadruple Immuno Analyser.

A) A low resolution .jpg image of section is uploaded onto the analysis software and visualised using channel 4 (laminin myofibre boundary). B) Surfaces are created based on the detection of fibres using channel 4 and C) switching to view the combined .jpg image of Channel 2,3 and 4 allowed for the analysis of fibres according to morphology of fibres.

2.5.10.2. Data analysis

The Mitochondrial Immunofluorescence Analysis online tool can be found on the following link; <http://research.ncl.ac.uk/mitoresearch/>), uses an R-script written and developed by Dr John Grady (2016). Briefly, the script is encoded to correct the background in each channel for each myofibre by subtracting the average OD for each channel in the NPC from the values

generated from the OXPHOS section. The background corrected values were then log transformed to normalise the data. The VDAC (porin) distribution in the non-disease control population of fibres were checked to be plotted as a normal distribution and following this, the mean and standard deviation (SD) were obtained. The Z _scores were determined for VDAC, Complex I (NDUFB8) and Complex IV based on the predicted level of each based on the porin level (as mitochondrial mass marker). Subsequently the Z _scores for all non-disease control and patient fibres were determined. Each individual fibres were classified based on Z _score boundaries which are based on standard deviation limits. The Z _scores allowed each fibre to be classified as positive (Pos), intermediate positive (Int +), intermediate negative (Int -) and negative (Neg) for Complex I and Complex IV. The categories of the fibres are highlighted in **Table 2.9**. Fibres were also classified into levels of porin according to Z scores (Z -score: "very low" (porin_Z < - 3SD), "low" (porin_Z between - 3SD and - 2SD), "normal" (porin_Z between - 2SD and + 2SD), "high" (porin_Z between + 2SD and + 3SD) and "very high" (porin_Z above + 3SD)). These boundaries were tested and validated by Rocha et al., 2015.

Table 2.9: Fibre classifications based on Z _scores.

Classifications	Z_score boundaries (SD limits)
Positive (Pos)	>-3
Intermediate positive (Int +)	-3 and - 4.5
Intermediate negative (Int -)	-4.5 and -6
Negative (Neg)	< -6

The Z scores of COX-1 and NDUFB8 (in conjunction with mitochondrial mass – porin) in individual fibres were then plotted against each other to produce a mitochondrial respiratory chain profile (also known as a Z -plot), providing a coherent visualisation of the type and extent of deficiency (**Figure 2.4**).

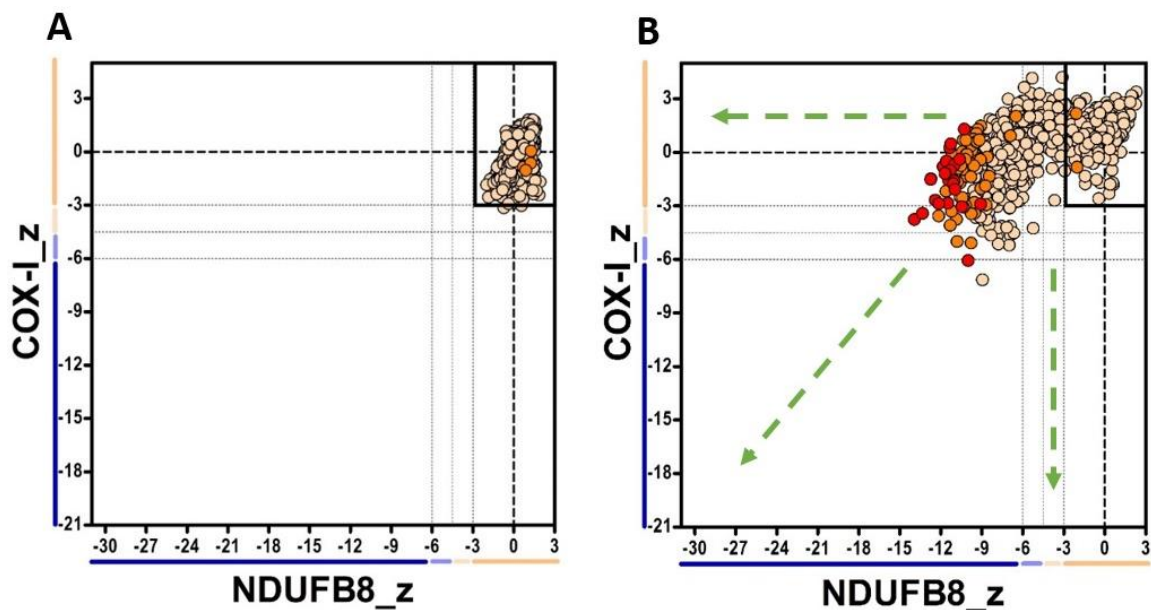


Figure 2.4: An illustrated representation of the Mitochondrial Respiratory Chain plot.
 The Z-scores of NDUFB8 and COX-1 in conjunction with mitochondrial mass in individual muscle fibres, as represented by each individual dot. A) A normal profile where all fibres are above -3 Z score for both Complex I (NDUFB8_z on the x-axis) and Complex IV (COX-I_z on the y axis). B) A deficient profile where fibres have shifted out of the normal range (fibres are now below -3 Z score). As indicated by the arrows, a left shift in fibres denotes Complex I deficiency, downward shift represents Complex IV deficiency and a diagonal shift represents a deficiency of both complexes.

2.5.11. Blue-Native Polyacrylamide gel electrophoresis (BN-PAGE)

2.5.11.1. Muscle homogenisation

Skeletal muscle biopsies of approximately 20 to 30mg in size (from both patients and controls) were cut up and homogenized using a Teflon glass Dounce homogenizer at 4°C (15-20 gentle strokes) in homogenization buffer (containing 250mM sucrose powder, 20mM imidazole/HCl pH 7.4 and 1mM PMSF). The muscle homogenates were centrifuged at 20,000g for 10 minutes at 4°C. Pellets were re-suspended and washed twice with 1ml of homogenization buffer and centrifuged at 20,000g for 5 minutes at 4°C each time. The final pellet for each sample was then solubilized in a solubilisation buffer (containing 13.75µl of Native page x4 sample buffer, 5.0µl of 20% n-dodecyl β-D maltoside (DDM), 26.25µl of dH₂O and 5.0µl of 50% glycerol) and were further homogenized on ice for 20 minutes using a small glass spatula. Samples were then transferred into Beckman Ultracentrifuge tubes. This was followed by centrifugation of the samples at 100,000g (53,000rpm) for 15 minutes at 6°C. The supernatants were transferred into a fresh 1.5ml Eppendorf tube, snap frozen in liquid nitrogen and stored at -80°C for BN-PAGE.

2.5.11.2. Pierce Assay and BN-PAGE

The protein concentration of each sample was determined using the Pierce BCA protein assay kit, according to the manufacturer's instructions (Pierce Thermo Scientific) and the UV-Vis-NIR spectrophotometer (Cary WinUV Software v.3.00). A minimum of 150µg of muscle mitochondria extract was required for each sample

The X-Cell SURE lock apparatus was set up according to the manufacturer's instructions and the native 4-16% BisTris gel (Life technologies) was placed inside. The apparatus was filled with both the 1x Cathode buffer (180ml dH₂O, 10 ml 20x Native Page running buffer and 10ml 20x Native Page cathode buffer) and the 1 x Anode buffer (50ml Running buffer and 950ml dH₂O). Subsequently, calculated volumes (containing a minimum of 150µg of muscle mitochondria extract) for each sample, mixed with 5µl of 5% coomassie blue, and were loaded into the native 4-16% BisTris gel. A volume of 2µl of BN-PAGE marker was also added into the first lane of the gel. Samples were electrophoretically separated in first dimension according to the NOVEX NativePAGE™ Bis-Tris Gel system instructions (2-3 hours, 250 volts).

2.5.11.3. Transfer, blocking and application of antibodies

The proteins from the gel were then transferred onto a PVDF membrane. Firstly, the membrane was cut to necessary size, activated in 100% methanol for 30 seconds, placed in dH₂O for 30 seconds and then in transfer buffer. The proteins were then transferred onto the PVDF membrane according to the BIO-RAD manufacturer's instructions (minimum 1 hour at 100 volts, 350 mA). Thereafter, the membrane was fixed in 8% acetic acid for 15 minutes at room temperature followed by quick washes with dH₂O. The membrane was blocked with 5% milk (in 1x TBST) for 1 hour at room temperature and then incubated in primary antibody diluted to 1:1000 in 5% milk (in 1xTBST), overnight at 4°C (Table 2.5). Following this, the membrane was washed 3 times for 10 minutes each with 1x TBST and incubated in secondary antibody diluted to 1:2000 in 5% milk for 1 hour at room temperature (**Table 2.10**). The membrane was washed with 1 x TBST for a further 3 times for 10 minute each.

Table 2.10: Antibodies used for BN-PAGE

Antibody	Supplier	Catalogue	Dilution
<i>Primary antibody</i>			
Monoclonal Anti-NDUFB8 IgGI	Novex by Life Technologies	459210 (100µg)	1:1000
Monoclonal Anti- SDHA IgGI	Novex by Life Technologies	459200 (100µg)	1:1000
<i>Secondary antibody</i>			
Rabbit Anti-mouse IgG	Dako	P02260	1:200

2.5.11.4. Detecting proteins on BN-PAGE

The membrane was incubated in the Amersham ECL prime detecting reagents for 5 minutes in the dark at room temperature. The proteins were then detected using the BioRad ChemiDoc MP imaging system and Image lab software (set to Blots, Colorimetric).

Complex II was used as a loading control, so the membrane was incubated in primary antibody labelling SDHA either overnight at 4°C or 3 hours at room temperature. The steps were repeated for the secondary antibody and detection of bands.

2.5.12. Laser Microdissection

2.5.12.1. Sample preparation

The 20µm sections previously stained for fibre typing were left to soak in PBS at 4°C overnight which allowed for coverslips to be easily removed. The slides were dehydrated in an ethanol gradient – 70% for 10 minutes, 95% for 10 minutes, 100% for 10 minutes and a further 10 minutes in 100% ethanol. Sections were stored at -20°C for later use for laser microdissection (or at 4°C on ice if being used imminently).

2.5.12.2. Single fibre laser microdissection

Sections were left to dry at room temperature for one hour. Laser microdissection was undertaken using the PALM microbeam system (Zeiss). An empty membrane slide was used for the initial laser setting. Using the PALM RoboSoftware 4.6 (Zeiss), the selected fibres were drawn around at x20 magnification (**Figure 2.5**). Laser microdissected fibres were captured into individual 0.2ml PCR tubes containing 15µl single cell lysis buffer (250µl of 1% Tween20, 50µl of 0.5M TrisHCl at pH8.5, 5µl proteinase K and 195µl dH₂O). Samples were kept on ice during the procedure and were subsequently centrifuged for approximately 8 seconds, reaching a speed of approximately 7000rcf (relative centrifugal field), to allow for lysis buffer to fall to the bottom of the PCR tubes.

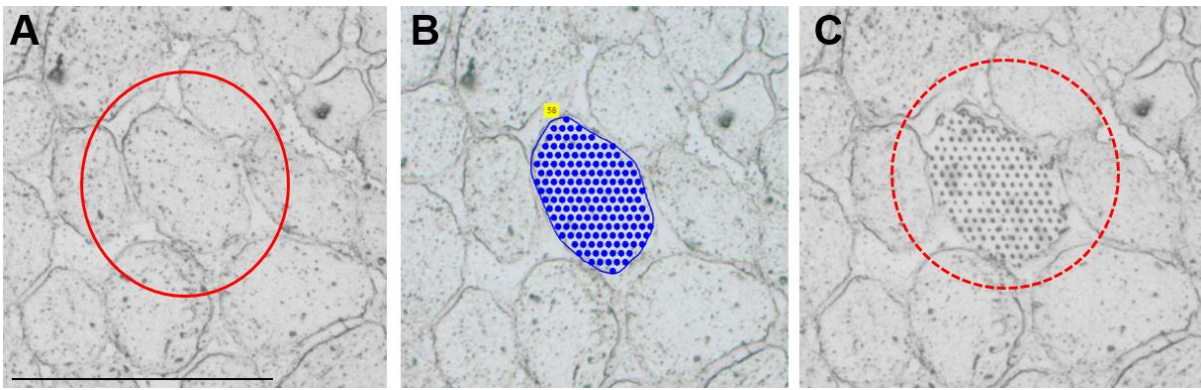


Figure 2.5: Isolation of single muscle fibres by laser capture microdissection.

A) Muscle section of interest was viewed and located (encircled) using the PALM microbeam system, **B)** Muscle fibre traced around, blue dots represent the cut path of the laser, **C)** Fibre has been removed with the laser into the cap of a 0.2ml PCR tube containing lysis buffer. Scale bars are measuring 150µm at x20 magnification.

2.5.12.3. Single cell lysis PCR

The lysis reaction was as follows: activation of the proteinase K enzyme occurred at 55°C for 3 hours and the deactivation of proteinase K enzyme was at 95°C for 10 minutes. This was undertaken using the ABI Veriti 96-well thermal cycler (Applied Biosystems). Samples were stored at -20°C following the lysis, ready for molecular genetic procedures.

2.5.13. Pyrosequencing

2.5.13.1. Pre-pyrosequencing PCR

PCR was used to amplify a fragment of 210bp length of mtDNA, spanning the mutation site. The PCR mastermix consisted of: 5µl of 5x GoTaq Buffer, 2.5µl of 10x dNTP mix, 1.25µl of 10µmol/L m.3243A>G forward primer, 1.25µl of 10µmol/L m.3243A>G reverse primer, 0.2µl of GoTaq polymerase, all diluted in 13.8µl autoclaved dH₂O. Primer details are as listed in **Table 2.11**. 1µl of template DNA was added to the 24µl master mix per well of a 24-well PCR plate.

With each experiment, one blank control containing no template DNA (master mix with no DNA) and three positive controls (with known heteroplasmy levels of 18%, 48% and 78% respectively) were included alongside the single fibres, to provide internal quality control procedures. The PCR was undertaken with the ABI Veriti 96-well thermal cycler (Applied Biosystems) is listed in **Table 2.12**.

Table 2.11: Primers used for pre-pyrosequencing PCR

Primer	Sequence	Length (bp)	T _m (°C)
Forward (m.3243A_G_FBio)	5' /5Biosg/ TAA GGC CTA CTT CAC AAA GCG 3'	21	55
Reverse (m.3243A_G_R)	5' GCG ATT AGA ATG GGT ACA ATG AG 3'	23	53.5

Table 2.12: Pre-pyrosequencing PCR and conditions

Process	Temperature	Duration	Cycles
GoTaq activation	95°C	2 minutes	1
Denaturation	95°C	30 seconds	
Primer annealing	63°C	30 seconds	35-38 cycles
Extension	72°C	30 seconds	
Final extension	72°C	10 minutes	1
Hold	4°C	∞	-

2.5.13.2. DNA Gel electrophoresis

To verify the amplification of the target DNA sequence, the PCR products were visualised using a 2% agarose gel. Gels were prepared by dissolving 2.0g of agarose in 100ml of 1x TAE buffer by heating in a microwave until boiling. After cooling the conical flask, 4.0µl of SYBR Safe DNA Gel stain were added and gently mixed into the agarose/TAE buffer mix. The gel mix was then poured into a cassette containing a comb for 25 x 1.5mm wells and left to set for 30 minutes at room temperature. The gel was then placed into an electrophoresis tank filled with 1x TAE running buffer, immersing the gel completely. Following this, 5µl of each PCR product was mixed with 1µl of bromophenol blue (BpB) DNA loading dye and added into the wells of the agarose gel subsequently. A 100bp DNA ladder and the negative control were also loaded into the gel. The gel was electrophoresed for 50 minutes using a benchtop power supply set at 120 volts (V). The bands were detected using the BioRad ChemiDoc MP imaging system and the SYBR safe protocol, according to the manufacturer's guidelines. The remaining PCR products (20µl) were placed at 4°C for the following stage.

2.5.13.3. Pyrosequencing reaction

Following detection of amplicons showing positive amplification of the target DNA sequence in each PCR, quantitative pyrosequencing was undertaken using the PyroMark Q24 system from Qiagen (UK), to determine the heteroplasmy levels of the m.3243A>G mutation. Prior to the pyrosequencing reaction, a pyrosequencing run file was produced containing the plate layout information using the PyroMark software (Version 2.0.7, Build 3). The instrument used for the reactions was the “PyroMark Q24 Method 0015”.

2.5.13.4. Pre-pyrosequencing PCR – binding of amplicons to the sepharose beads

For each sample, 10µl of the PCR products (referred to as amplicons) were added into a 24 well PCR plate with 70µl of binding buffer mixture (40µl of binding buffer, 2µl of streptavidin sepharose beads and 28µl of dH₂O per sample), giving a final volume of 80µl. Domed caps were used to seal the 24 well plate before being placed on a shaking platform for 10 minutes which allowed the binding of the streptavidin sepharose beads to the amplicons.

2.5.13.5. Sample clean-up and annealing reaction

Once samples had been agitated for 10 minutes, a handheld vacuum pump tool (VPT) with filter probes attached was used to capture the beads from the 24 well plate (held in wells for approximately 15 seconds) and was moved through a series of sequential steps: 5 seconds in 70% ethanol, 5 seconds in denaturation buffer and 10 seconds in wash buffer. The handheld VPT was deactivated and then placed into a 24-shallow well plate containing 25µl of annealing buffer in each well (24.25µl of annealing buffer and 0.75µl of 10µmol/L sequencing primer), releasing the beads. **Table 2.13** highlights the detail for sequencing primer. The plate was heated at 80°C for 2 minutes to denature the templates, before placing into the PyroMark Q24 system and left to stand at room temperature for a minimum of 5 minutes to allow for the annealing of the pyrosequencing primer to the amplicon strand.

Table 2.13: Primers used for Pyrosequencing annealing reaction

Primer	Sequence	Length (bp)	T _m (°C)
Sequencing m.3243A_G_Rev_Seq	5' ATG CGA TTA CCG GGC 3'	15	52.3

2.5.13.6. Preparation of cartridge and pyrosequencing reaction

The PyroMark 24 cartridge was first rinsed with dH₂O and then loaded with the appropriate volumes of the enzyme, substrate and dNTPs, as illustrated in the **Figure 2.6**. Volumes were determined via the 'Pre-run information' on the PyroMark software, according to the pyrosequencing run file,

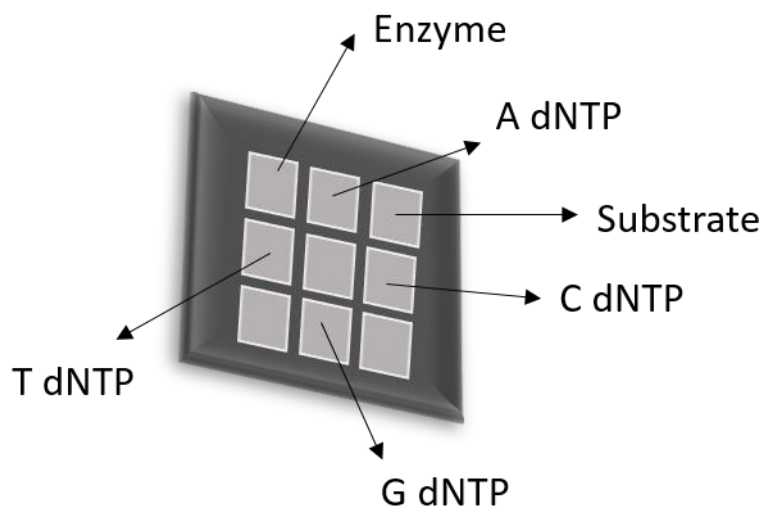


Figure 2.6: A schematic diagram showing the layout of cartridge during experimental preparation for the pyrosequencing reaction.

Individual reagents, as indicated by the annotations, are placed into the designated wells in the cartridge. Volumes of each was determined via the PyroMark Software.

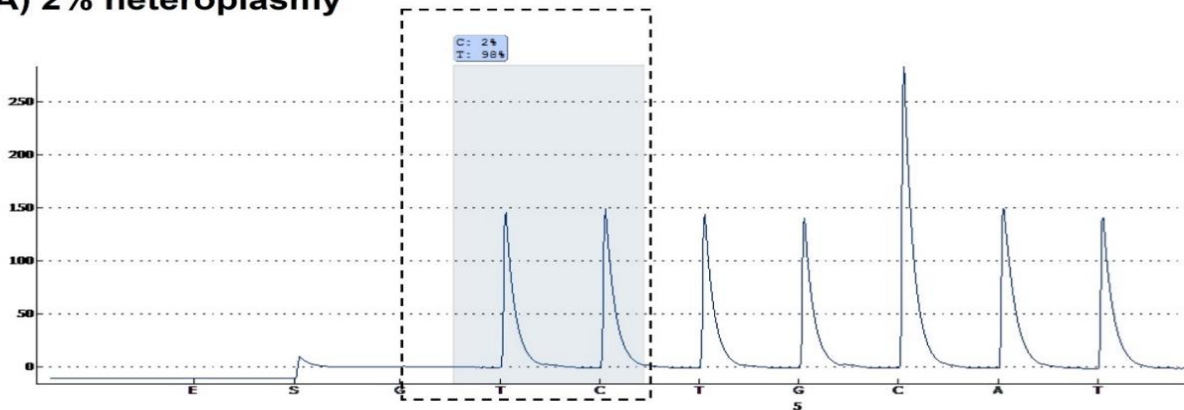
2.5.13.7. Analysis of Pyrosequencing data

On completion of the pyrosequencing reaction, the PyroMark software was used to automatically calculate the m.3243A>G heteroplasmy level in each sample. Wells marked as blue showed a pass, yellow indicated uncertainty in the calculations thus indicating a repeat of the sample was required and red indicated a failed calculation of the sample. Negative controls were seen to be red as no DNA was added.

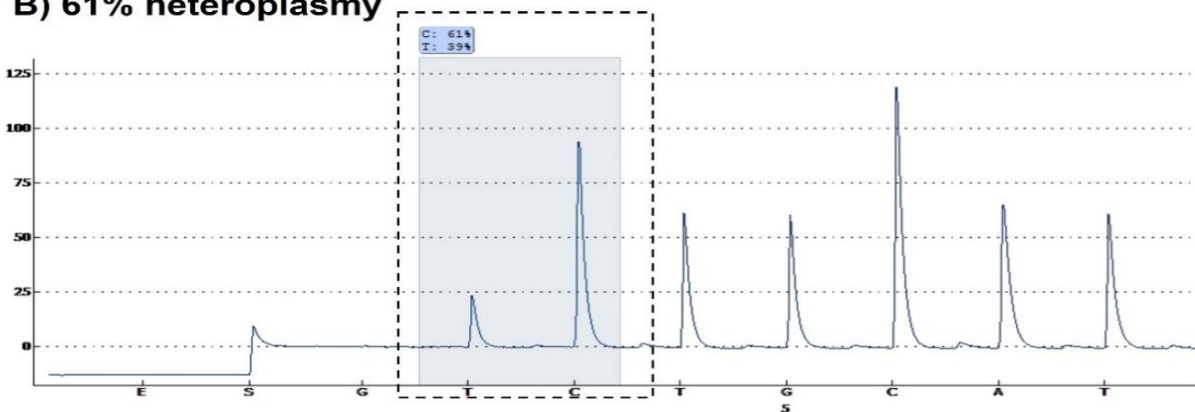
The interpretation of the pyro-gram data is demonstrated by **Figure 2.7**. Firstly, because a biotinylated forward primer was used, the pyrosequencing reaction was undertaken on a reverse strand and so the wild-type allele will be a T (due to the pairing with wild-type allele A) and the mutant allele will be a C (paring with mutant allele G). Therefore, the sequence to analyse was; T/CCTGCCATCTT as shown at the x-axis of the pyro-gram. Fibres which are wild-type showed the peak at the C allele (underlined and corresponding to the wild-type allele) at the same height as the T allele – thus the same ratio. But fibres with the m.3243A>G mtDNA mutation showed a clear skewing of the C: T allele ratio on the pyro-gram, due to the

mutant allele C. The amount of dTTP and dCTP incorporated at position 3243 during the pyrosequencing reaction was determined and from this the percentage of heteroplasmy was calculated. A heteroplasmy below 3% would be considered a wild-type. When peaks are below 50 on the y-axis, the read-out is considered not a pass. The blank control should have a peak below 10.

A) 2% heteroplasmy



B) 61% heteroplasmy



C) 95% heteroplasmy

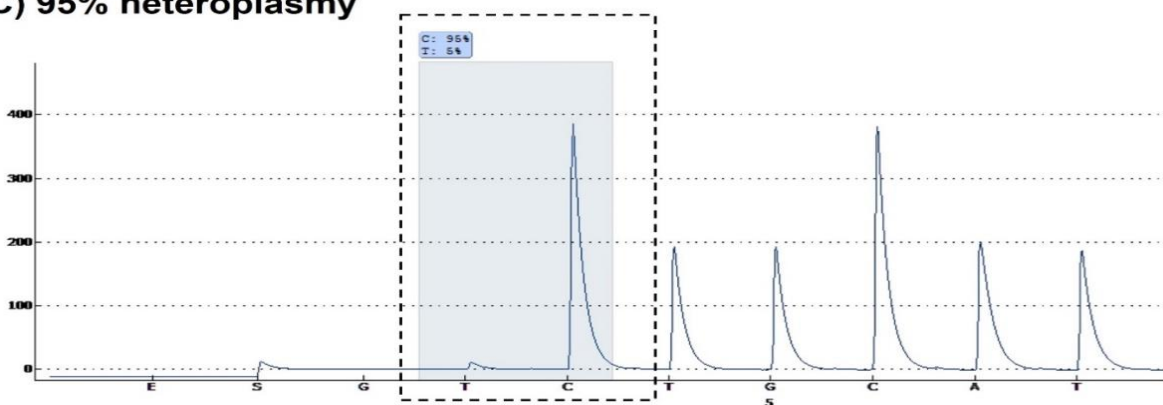


Figure 2.7: Pyro-gram outputs from the PyroMark software.

A) Fibre with 2% heteroplasmy and **C:** T nucleotide ratio very similar **B)** sample showing 61% **C)** 96% *m.3243A>G* heteroplasmy level.

2.5.14. Statistics analyses

Statistical analysis was performed using R v3.3.0 and Mini tab 17. Graphs were produced in GraphPad Prism v7.0 (GraphPad Software Inc.) or R, using ggplot. A p value of <0.05 was used to consider a result as being statistically significant. Specific tests are specified in the methods and results sections of each individual chapters.

Chapter 3: Using a quantitative quadruple immunofluorescence assay to diagnose isolated mitochondrial Complex I deficiency

3.1. Introduction

This chapter is based on the first theme of this thesis; the diagnosis of mitochondrial disease. It is specifically based on the diagnosis of Complex I deficiency in isolated Complex I deficient cases. Thereby, this section will first introduce Complex I structure and assembly, followed by the discussion of isolated Complex I deficiency in a clinical setting. Finally, the current limitations in the diagnostic work-up for the identification of Complex I deficiency will also be highlighted in the context of the aim of this study.

3.1.1. Complex I structure

The function of Complex I is detailed in **section 1.3.1.3, Chapter 1**. In terms of structure, the complex constitutes of 45 structural subunits. Of these subunits, 14 are known as the ‘core subunits’ which are highly conserved between both human and bacterial Complex I. Seven of the 14 core subunits are encoded by the nDNA (nuclear core subunits) whilst the remainder are mtDNA encoded (ND1-ND6 and ND4-L). Overall, these core subunits have a critical role in the biogenetic functions of Complex I; containing co-factors (FMN and Fe-S clusters) and proton pumping (Baradaran et al. 2013; Berrisford and Sazanov 2009; Sazanov and Hinchliffe 2006; Vinothkumar et al. 2014; Zickermann et al. 2015). The remaining 30 mammalian subunits are known as the “supernumerary” or “accessory” subunits. These accessory subunits have now been localised according to the architecture of the bovine Complex I through the use of electron cryomicroscopy (Cryo-EM) (Zhu et al. 2016). This study revealed that these accessory subunits bind peripherally around the core subunits. Whilst the roles of these subunits have not yet been entirely determined, they are believed to be critical for OXPHOS function through the following roles; assisting in the assembly of Complex I, allowing for structural stability, regulation of biogenesis and importantly, the protection of core subunits against oxidative stress through forming a cage-like structure around them (Fiedorczuk et al. 2016; Sazanov 2015; Stroud et al. 2016; Vinothkumar et al. 2014; Zhu et al. 2016; Zickermann et al. 2015). There are at least 15 known assembly factors which are necessary for the assembly of Complex I. These assembly factors are only temporarily associated with either a single Complex I subunit or with a larger number of subunits during the formation of different modules. The assembly factors are dissociated once the final holoenzyme is assembled (Sanchez-Caballero et al. 2016; Wirth et al. 2016). Additionally, assembly factors have also been linked to the biogenesis of co-factors including Fe-S clusters (Guerrero-Castillo et al. 2017; Sanchez-Caballero et al. 2016).

3.1.1.1. Determining the structure of Complex I

In recent years, much progress has been made in elucidating the complete structure and allocation of each of the subunits of Complex I. The L shaped structure of the complex was first determined in bacteria using EM (Friedrich and Bottcher 2004). Following this, X-ray crystallography studies allowed for further structural details to be revealed using the enzymes from the bacterium *Thermus thermophilus* (Baradaran et al. 2013; Efremov et al. 2010; Sazanov and Hinchliffe 2006) and the fungus *Yarrowia lipolytica* (Hunte et al. 2010; Zickermann et al. 2015). More recently, a number of studies have used the advancements made in single particle Cryo-EM with direct electron detectors, to identify higher resolution atomic structures of the entire mammalian Complex I. The study by Vinothkumar et al. (2014), produced a 5 Å resolution structure of the enzyme from bovine (*Bos taurus*) heart, which resolved the structures of the core subunits containing Fe-S clusters and 60 transmembrane helices, as well as identifying 18 supernumerary transmembrane helices. This study also modelled 14 of the 30 supernumerary subunits. This was followed by the near completed atomic structure of Complex I derived from *Ovis aries* (Ovine) at a 3.9 Å resolution (Fiedorczuk et al. 2016). Through combining Cryo-EM with cross-linking and mass spectrometry experiments, the study was able to resolve all 14 core and 30 supernumerary mitochondrial subunits. In unison, Zhu et al. (2016) published a 4.2 Å resolution Cryo-EM model for bovine Complex I where the study located and modelled all 45 subunits, thus providing the first structure of the entire mammalian complex. However, in addition to this, a 3.3 Å resolution structure of Complex I from mouse heart mitochondria was resolved in the active state (Agip et al. 2018) – as shown in **Figure 3.1**.

3.1.1.2. Functional modules of Complex I

The L-shaped structure of Complex I consists of two fragments; a hydrophilic peripheral arm which extends into the matrix of the mitochondria and a hydrophobic arm which is embedded in the IMM (Grigorieff 1998; Vinothkumar et al. 2014; Zickermann et al. 2015). This structure can be further divided into three functional modules. There are two modules within the peripheral arm. The first is the N module at the tip of the peripheral arm which binds and oxidizes NADH and therefore provides electrons to the Fe-S clusters. Within this module, the core subunits NDUFV1, NDUFV2 and NDUFS1 alongside FMN are responsible for the oxidation of NADH. The second is the Q module which acts as a connector of both the peripheral and membrane arm and the site at which the electrons are transferred to ubiquinone, leading to the subsequent reduction to ubiquinol. The core subunits NDUFS2, NDUSF3, NDUFV7 and NDUFV8 are located within the Q module. A pocket between

NDUFS7 and NDUFS8 is the proposed site for ubiquinone binding and reduction – referred to as the Q site (Angerer et al. 2012). Collectively, the peripheral arm contains all the of the redox factors necessary for the movement of electrons through the complex.

The membrane arm contains the third module known as the P module which catalyses proton transfer from the matrix to the IMS. This module is often referred to as two parts; the proximal P module (P_P) or distal P module (P_D) (Brandt 2006; Hunte et al. 2010). The seven mtDNA encoded core subunits are found in the P module. A long lateral helix identified in the ND5 subunit bridges the P_P and P_D together. ND1 contains a quinone binding site (Lazarou et al. 2009) and ND2, ND4 and ND5 are known as anti-porter like subunits with discontinuous helices (Zhu et al. 2016; Zickermann et al. 2015). The P module harbours 78 transmembrane helices with a central axis of polar residues that propagates from the Q site to the anti-porter like subunits and is proposed to be important for the translocation of protons across from the matrix, through the channels within ND2, ND4 and ND5 and into the IMS (Baradaran et al. 2013; Fiedorczuk et al. 2016). The proton translocation events in the membrane arm is believed to be due to conformational changes linked to the redox reaction of ubiquinone (Brandt 2006; Fiedorczuk et al. 2016; Sazanov 2015).

Figure 3.1 highlights the functional subunits of Complex I and **Figure 3.2** shows the subunits composition.

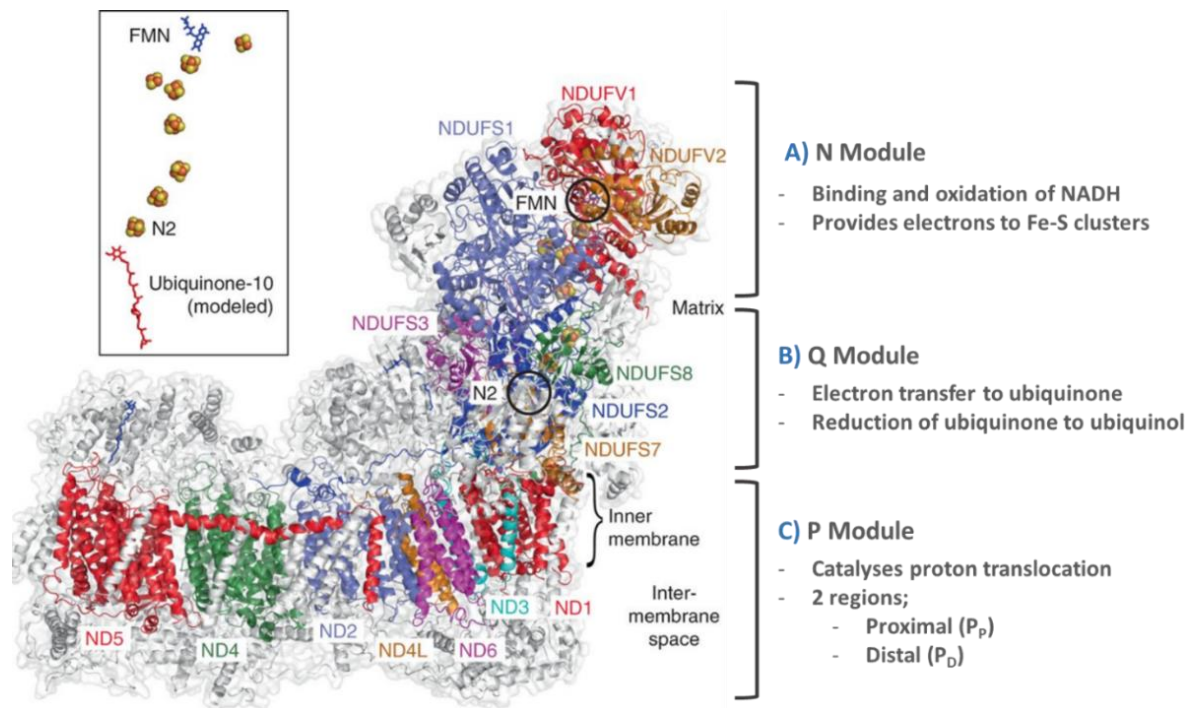


Figure 3.1: A 3.3 Å resolution modular structure of mouse heart Complex I.

The peripheral matrix arm and membrane arm of Complex I forms an L-shape. The complex is composed of three functional regions containing all 14 core subunits – located on the matrix peripheral arm is the (A) N module which has a role of binding and oxidising NADH and contains the three nuclear encoded core subunits – NDUFVI, NDUFV2 and NDUFS1 and (B) Q module which modulates electron transport to ubiquinone and contains four nuclear encoded core subunits – NDUFS3, NDUFS2, NDUFS7 and NDUFS8. Located on the membrane arm is the (C) The P module which translocate protons into the intermembrane space and contains all the mitochondrial DNA encoded subunits of complex I -ND1 – ND6 and ND4L. Figure has been adapted from (Agip et al. 2018).

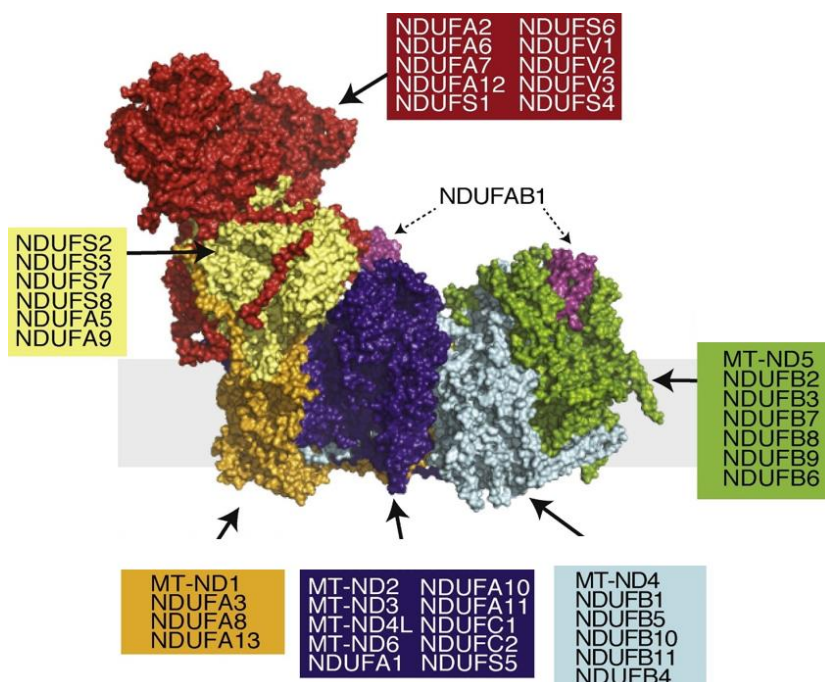


Figure 3.2: Subunit composition of Complex I.

Bovine structure of Complex I highlighting all Complex I core and accessory subunits.

Figure has been adapted from (Formosa et al. 2018).

3.1.2. Complex I assembly

An exhaustive amount of research has been completed in order to progress the understanding of the Complex I assembly process. Studies have employed several model systems to study the assembly process in various organisms including cultured fibroblasts from patients who have pathogenic mutations on Complex I subunits or assembly factors to identify assembly intermediates (Cardol et al. 2004; Lazarou et al. 2009; McKenzie and Ryan 2010; Vogel et al. 2007; Weidner et al. 1993). However, the use of patient cell lines in experiments are sometimes hindered by the fact that the mutated cells lines may lead to improper subassemblies to be formed which are often then degraded (Sanchez-Caballero et al. 2016). More recent experimental approaches include the addition and release of mitochondrial translational inhibitor chloramphenicol and complexome profiling (Guerrero-Castillo et al. 2017), as well as gene editing tools such as TALENS and CRISPR/Cas9 gene (Stroud et al. 2016).

The assembly of Complex I has been shown to be a complicated multistep process. All proposed models follow the same sequence of steps leading to the formation of the complete holoenzyme (Antonicka et al. 2003; Lazarou et al. 2007; McKenzie and Ryan 2010; Vogel et al. 2007). The latest model is described as a “modular assembly model”, whereby five main subassembly intermediates are formed separately, forming higher molecular mass intermediates which assemble together to create the final holoenzyme (Guerrero-Castillo et al, 2016). These intermediates are termed; Q/P_P-a (Q module and the proximal end of the P module, a = first part of this assembly process), P_P-b (proximal end of P module, b = second part of this assembly process), P_D-a (distal part of P module, a= first part of this assembly process), P_D-b (distal part of P module, b = second part of this assembly process) and N. Each of these intermediates have been labelled in **Figure 3.3** (adapted from (Guerrero-Castillo et al. 2017).

Formation of the Q Module: the Q module is first to be assembled (Zhu et al., 2016; Guerrero-Castillo et al., 2017) and is composed of; NDUFS2 and NDUFS3 (core subunits), NDUFA5 and NDUFS7 and NDUFS8 (contain Fe-S subunits). This assembly process is undertaken with the cooperation of the assembly factors NDUFAF3 and NDUFAF4.

Formation of the P Module: the next assembly process is the formation of the Q/P_P-a intermediate which starts with the insertion of ND1 into the P_P-a module with the cooperation from the assembly factor TIMMDC1. The Q/P_P-a intermediate is completed with the insertions of NDUFA3, NDUFA8 and NDUFA13 subunits followed by NDUFA1 and NDUFA9 with assistance of the assembly factor NDUFAF2. Following this process, the

formation of the Pp-b/P_D-a intermediate is formed as two separate modules. The first module is the Pp-b in which ND2, NDUFC1 and NDUFC2 are assembled with the association of the NDUFAF1, ECSIT, ACAD9 and NDUCOA1 assembly factors. ND3 chaperoned by the assembly factor TMEM126B is inserted into the module followed by ND6 and ND4-L, completing the formation of this module. The assembly of the P_D-a module starts with the insertion of subunits NDFUB5, NDUFB6, NDUFB10 and NDUFB11. The assembly factor FOXRED1 then modulates the insertion of ND4 and NDUFB1. This is followed by NDUFB4, NDUFA10 and NDUFS5 which completes the formation of the Pp-b/P_D-a higher intermediate. The P_D-b module is the next to be formed which is the combined assembly of ND5 alongside the subunits NDUFB8, NDUFB7, NDUFB9, NDUFB2, NDUFB3 and NDUFAB1. This module then combines with the previous assembled modules to form the 1.5MDa Q/P intermediate (Guerrero-Castillo et al. 2017; Leman et al. 2015; McKenzie and Ryan 2010).

Formation of the N Module: the final stage of this process is the assembly of the N module which includes the joining of NDUFV1 and NDUFV2 (both of which are core subunits and flavoproteins) with NDUFS1 (a Fe-S containing subunit) and NDUFA2 (Guerrero-Castillo et al. 2017; Leman et al. 2015; McKenzie and Ryan 2010).

Formation of fully assembled Complex I: the completed N module, alongside the following last subunits which include NDUFA11, NDUFV3, NDUFA12, NDUFS4, NDUFS6, NDUFA6, NDUFB1 and NDUFA7, attach to Q/P intermediate. All remaining assembly factors dissociate from the structure leading to the formation of the mature 1MDa Complex I holoenzyme (Guerrero-Castillo et al. 2017; Leman et al. 2015; McKenzie and Ryan 2010)

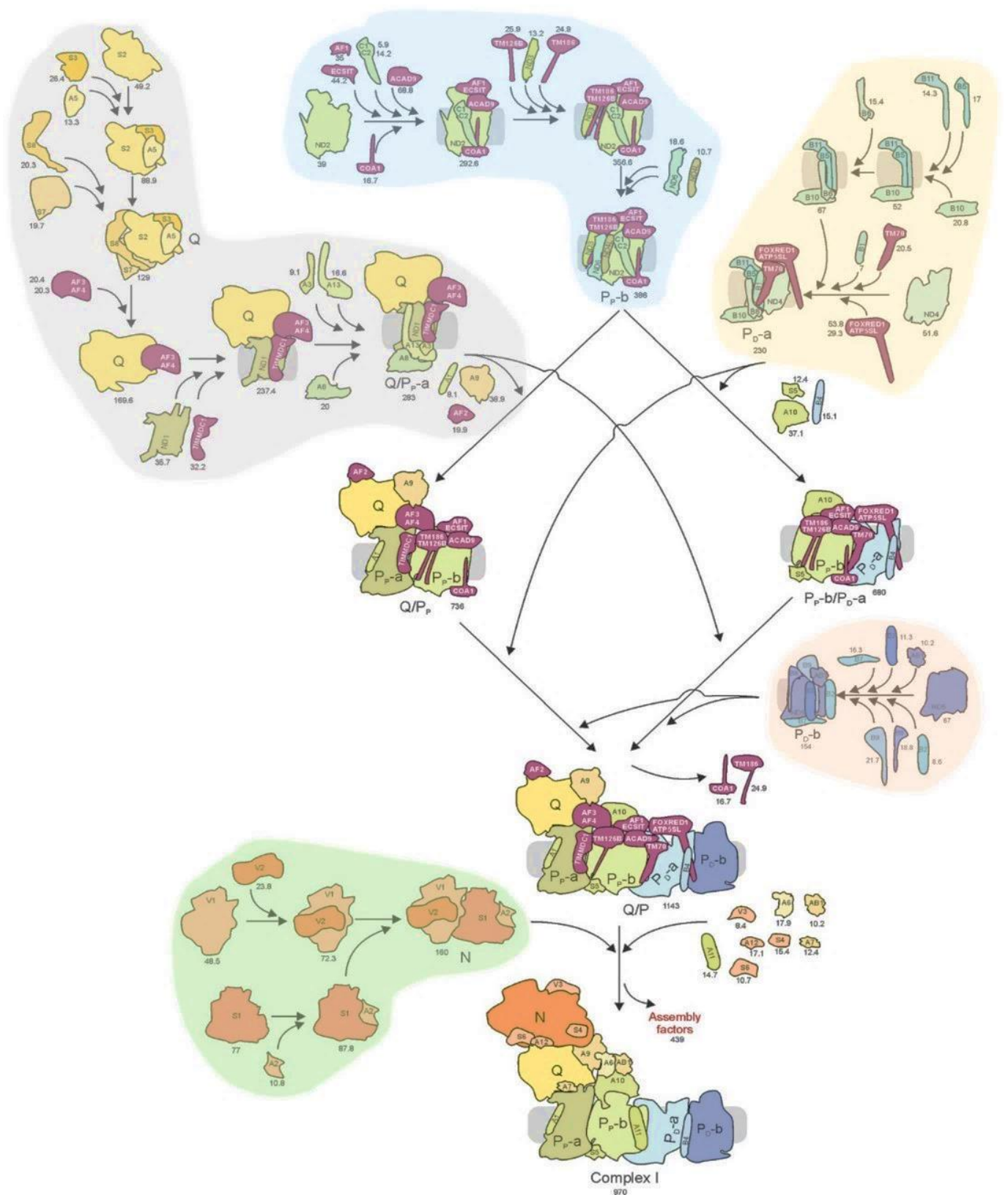


Figure 3.3: A comprehensive model of Complex I assembly.

Individual assembly intermediates have been outlined with the names of the intermediates within a red dashed box; Q/P_p-a, P_p-b, P_p-b/P_p-a, P_p-b and N. Figure is adapted from (Guerrero-Castillo et al. 2017).

3.1.3. Isolated Complex I deficiency in the clinical setting

Isolated Complex I deficiency (OMIM #252010) is the most commonly observed biochemical phenotype in mitochondrial disease patients (Kirby et al. 2004a; McFarland et al. 2004), particularly within paediatric cases (Lazarou et al. 2009; Swalwell et al. 2011). It is characterised by the sole impairment of Complex I and exhibits considerable genetic heterogeneity; mutations can potentially affect one of the 38 nuclear-encoded subunits, 7 mtDNA-encoded subunits or at least 15 Complex I assembly factors (Formosa et al. 2018; Guerrero-Castillo et al. 2017).

3.1.3.1. Pathogenic mutations associated with Complex I deficiency

The first reports of pathogenic mutations causing isolated Complex I deficiency were identified within mtDNA-encoded genes in 1988, specifically in *Mt-ND4* (m.11778G>A point mutation causing an arginine 340 to histidine (R340H) substitution) and large deletions of the mtDNA (Holt et al. 1988; Wallace et al. 1988). To date, pathogenic variants have been reported in all 7 mtDNA- encoded core structural subunits (ND1- 6 and ND4L), 21 of the nuclear-encoded subunits and 12 assembly factors (reviewed in references (Alston et al. 2017; Craven et al. 2017; Ghezzi and Zeviani 2018)). **Table 3.1** highlights the first reported pathogenic mutation associated with each of the subunits and assembly factors. The majority of these mutations are associated with a reduction in Complex I assembly and/or Complex I activity. However there are reports of mutations where only the catalytic activity of the complex has been affected, for example p.Asp446Asn *NDUFS2* (Ngu et al. 2012) and *MT-ND5* m.13514A>G (p.Asp393Asn) (Bugiani et al. 2004; Lebon et al. 2003).

Swalwell et al. (2011), indicated that 25-30% of patient's harbour defects involving mtDNA genes and therefore the remaining 70% of cases are caused by nuclear gene variants (Haack et al. 2012). As expected, Complex I deficiency resulting from defects on nuclear-encoded subunits have an autosomal recessive inheritance pattern whereas defects on any of the seven mtDNA-encoded subunits result in maternal inheritance. However, X-linked inheritance has been observed in patients harbouring mutations in the nuclear encoded genes *NDUFA1* (Fernandez-Moreira et al. 2007) and *NDUFB11* (van Rahden et al. 2015). Additionally, sporadic cases of Complex I deficiency have been reported in cases affected by mtDNA defects (Swalwell et al. 2011).

Table 3.1: List of Complex I subunits and assembly factors and first report of pathogenic mutations associated with each

Subunit	Core/Assembly	Report of first pathogenic mutation
<i>Mitochondrial-encoded subunits</i>		
MTND1	Core	(Kirby et al. 2004a)
MTND2	Core	(Ugalde et al. 2007)
MTND3	Core	(Crimi et al. 2004) (McFarland et al. 2004)
MTND4	Core	(Singh et al. 1989)
MTND4-L	Core	Brown et al., 1995
MTND5	Core	(Santorelli et al. 1997)
MTND6	Core	(Jun et al. 1994)
<i>Nuclear-encoded subunits</i>		
NDUFS1	Core	(Bénil et al. 2001)
NDUFS2	Accessory	(Loeffen et al. 2001)
NDUFS3	Core	(Benit et al. 2004)
NDUFS4	Accessory	(Budde et al. 2000)
NDUFS5	Accessory	n/a
NDUFS6	Accessory	(Kirby et al. 2004b)
NDUFS7	Core	(Triepels et al. 1999)
NDUFS8	Core	(Loeffen et al. 1998)
NDUFA1	Accessory	(Fernandez-Moreira et al. 2007)
NDUFA2	Accessory	(Hoefs et al. 2008)
NDUFA3	Accessory	n/a
NDUFA5	Accessory	n/a
NDUFA6	Accessory	(Alston et al. 2018)
NDUFA7	Accessory	n/a
NDUFA8	Accessory	(Triepels et al. 1998)
NDUFA9	Accessory	(van den Bosch et al. 2012)
NDUFA10	Accessory	(Hoefs et al. 2011)
NDUFA11	Accessory	(Berger et al. 2008)
NDUFA12	Accessory	(Ostergaard et al. 2011)
NDUFA13	Accessory	(Angebault et al. 2015)
NDUFAB1	Accessory	n/a
NDUFV1	Core	(Schuelke et al. 1999)
NDUFV2	Core	(Benit et al. 2003)
NDUFV3	Accessory	n/a
NDUFB1	Accessory	n/a
NDUFB2	Accessory	n/a
NDUFB3	Accessory	(Calvo et al. 2012; Haack et al. 2012)
NDUFB4	Accessory	n/a
NDUFB5	Accessory	n/a
NDUFB6	Accessory	n/a
NDUFB7	Accessory	n/a
NDUFB8	Accessory	(Piekutowska-Abramczuk et al. 2018)
NDUFB9	Accessory	(Haack et al. 2012)
NDUFB10	Accessory	n/a
NDUFB11	Accessory	(van Rahden et al. 2015)
NDUFC1	Accessory	n/a
NDUFC2	Accessory	n/a
<i>Nuclear-encoded assembly factors</i>		
NDUFAF1	n/a	(Dunning et al. 2007)
NDUFAF2	n/a	(Ogilvie et al. 2005)

NDUFAF3	n/a	(Saada et al. 2009)
NDUFAF4	n/a	(Saada et al. 2009)
NDUFAF5	n/a	(Sugiana et al. 2008)
NDUFAF6	n/a	(Pagliarini et al. 2008)
NDUFAF7	n/a	(Wang et al. 2017)
ACAD9	n/a	(Haack et al. 2010)
FOXRED1	n/a	(Calvo et al. 2010)
TIMMDC1	n/a	(Kremer et al. 2017)
TMEM126B	n/a	(Alston et al. 2016)
NUBPL	n/a	(Calvo et al. 2010)

3.1.3.2. Clinical symptoms associated with Complex I deficiency

Further to this wide genetic heterogeneity, Complex I deficiency exhibits a considerable clinical heterogeneity. The spectrum of symptoms ranges from severe presentations including Leigh Syndrome (LS) and fatal infantile lactic acidosis (FILA) in early childhood through to LHON and exercise-induced muscle weakness, which develop during young adult life.

LS is the most common clinical presentation among children associated with isolated Complex I deficiency (Fassone and Rahman 2012; Koene et al. 2012). Presenting as an early onset disorder, the mean age of onset is between 3 to 12 months of age with the median age of death shown to be 2.4 years of age (Sofou et al. 2014). LS is defined as being a severe progressive neurodegenerative disorder in which the most common neuro-radiological features of these infants is bilateral symmetrical lesions in the striatum and brainstem. Thus, affected infants usually show a global developmental delay and failure to thrive (Loeffen et al. 2000). Other symptoms include optic atrophy, dysphagia, cranial nerve palsies and muscle weakness. LS is associated with more than 75 genes encoded by either the nuclear DNA or the mtDNA (Lake et al. 2016; Sofou et al. 2018). Of this number of genes, at least 23 encode for Complex I proteins; *MTND1*, *MTND2*, *MTND3*, *MTND4*, *MTND5*, *MTND6*, *NSUFS4*, *NDUFS8*, *NDUFS7*, *NDUFV1*, *NDUFV2*, *NDUFS1*, *NDUFS3*, *NDUFS2*, *NDUFA1*, *NDUFA2*, *NDUFA9*, *NDUFA10*, *NDUFA12*, *NDUFAF2*, *NDUFAF5*, *NDUFAF6* and *FOXRED1* (Lake et al. 2016).

LHON, an adult onset disorder, is defined by the degeneration of the retinal ganglion cells resulting in acute loss of vision. The age of onset ranges from 15 to 30 years of age, with males being affected five times more than females (Yu-Wai-Man et al. 2009). The cause of LHON in the European population is generally associated with mutations on mtDNA-encoded core subunits of Complex I. The most common mutations, associated with more than 95% of LHON cases, are; m.3460G>A within the *MTND1* gene (Howell et al. 1991), m.11778G>A

within the *MTND4* gene (Wallace et al. 1988) and m.14484T>C within the *MTND6* gene (Mackey and Howell 1992).

Other phenotypes associated with Complex I deficiency are leukoencephalopathy (Bjorkman et al. 2015) and neonatal cardiomyopathy and encephalopathy (Bugiani et al. 2004; Collet et al. 2016a). The latter phenotype has been found to be associated with mutations in *NDUFS2* (Loeffen et al. 2001), *NDUSF4* (Petruzzella et al. 2001), *NDUFA2* (Hoefs et al. 2008), *NDUFAF1* (Fassone et al. 2011) and *ACAD9* (Collet et al. 2016b; Dewulf et al. 2016). Lactic acidosis is also common in paediatric Complex I deficient patients and examples of reported associations include *NDUFS6* (Spiegel et al. 2009), *NDUFAF5* (Sugiana et al. 2008), *NDUFB3* (Calvo et al. 2012; Haack et al. 2012) and *NDUFAF3* (Saada et al. 2009).

There are currently a total of 15 known Complex I assembly factors of which 12 have known pathogenic mutations associated with them (reviewed in Ghezzi and Zeviani (2018)). These known mutations are listed in **Table 3.1**.

3.1.4. Limitations in the current diagnostic setting for Complex I deficiency

The diagnosis of mitochondrial diseases requires a multidisciplinary approach, owing to factors such as the wide genetic heterogeneity, vast clinical spectrum which often overlaps with other neurological disorders and heteroplasmy in cases where mtDNA is affected. The process of diagnosis starts with a detailed clinical examination from specialist clinician(s) and often followed by histological and immunohistochemical studies, enzymatic analysis of the OXPHOS complexes and the genetic analysis of either, or both, the nDNA and mtDNA. The order in which the diagnosis workup is undertaken is dependent on a number of aspects including how well the phenotype- genotype correlates during clinical examination and whether this simplifies the molecular genetic analysis through targeted candidate genes and also the availability of tissue from the patient.

This section of the chapter will focus upon the diagnosis process for isolated Complex I deficiency, which is the most frequently observed biochemical manifestation of an OXPHOS defect within a paediatric setting (Swalwell et al. 2011). While the current diagnosis process is highly efficient, particularly with the development of molecular studies, there are clear limitations in the algorithms for the detection of Complex I deficiency – these aspects will be described below when compared to the advantages of the quadruple immunofluorescence assay in a diagnostic setting.

3.1.4.1. The Molecular Genetics first approach

With the growing knowledge of mitochondrial and nuclear genes responsible for Complex I deficiency, as well as a progress in the recognition of phenotype - genotype correlations, the current diagnostic procedure has shifted towards the “genetic first approach” because of the advances being made with NGS. The targeted gene panels including a custom Ampliseq capture array targeting 49 Complex I genes, WES or WGS are now being commonly used to search for potential genetic diagnoses, with new disease genes constantly being identified (Alston et al. 2016; Haack et al. 2010; Hartmannova et al. 2016; Lieber et al. 2013; Plutino et al. 2018). Clinical features as detailed by the physician can guide the molecular genetic testing for example, a young adult man presenting with visual decline will prompt screening of the mtDNA for the three commonly associated LHON mutations as previously detailed. Furthermore, patients showing symptoms typified of LS would prompt analysis of the following genes; *MTND1*, *MTND2*, *MTND3*, *MTND4*, *MTND5*, *MTND6*, *NSUFS4*, *NDUFS8*, *NDUFS7*, *NDUFV1*, *NDUFV2*, *NDUFS1*, *NDUFS3*, *NDUFS2*, *NDUFA1*, *NDUFA2*, *NDUFA9*, *NDUFA10*, *NDUFA12*, *NDUFAF2*, *NDUFAF5*, *NDUFAF6* and *FOXRED1* (Lake et al. 2016).

3.1.4.2. The use of muscle biopsy for histopathological and biochemical analyses

Despite the advances in the molecular genetic testing associated with isolated Complex I deficiency, skeletal muscle biopsy still plays an essential role in the diagnostic algorithm. Biopsies are most often taken from patients in order to facilitate an appropriate molecular genetic testing to elucidate the underlying genetic cause or to gain an understanding into the effect of the genetic mutation on the respiratory chain complexes in the tissue.

The investigation of the muscle section includes both histopathological and biochemical algorithms, as previously detailed in section 1.8.1, **Chapter 1**. Histopathological analyses include modified Gomori Trichrome (assessing RRF), COX/SDH and more recently, the NBTx assay (Engel and Cunningham 1963; Old and Johnson 1989; Ross 2011; Sciacco et al. 1994; Simard et al. 2018). Although these histochemical investigations are successful in determining RRF and COX-deficient fibres in other mitochondrial diseases, one major limitation when considering patients with isolated Complex I deficiency is that there is no determination of Complex I status in the tissue. Consequently, in such patients, fibres will appear as normal as both Complex II and Complex IV activities will be intact.

In *vitro* spectrophotometric biochemical assays measuring the enzyme activity of each respiratory chain complex in muscle is also commonly undertaken in the diagnosis process. The use of muscle is preferred in comparison to fibroblasts which often show normal findings

despite a respiratory chain defect being present (Horvath et al. 2006; Spinazzola et al. 2006). However most diagnostic laboratories request at least 50mg of muscle tissue in order to reliably measure enzyme activities, which represents a considerable proportion of the total amount of patient material available, particularly in children. Importantly, the drawbacks concerning the diagnosis of Complex I deficiency using the biochemical assay include the fact that the assays for Complex I are known to have both low sensitivity and low specificity. This is believed to be due to the poor solubility of co-enzyme-Q analogues and reaction mixture turbidity. A study by Janssen et al. (2007a), developed an assay to measure Complex I activity in muscle and fibroblast samples which was designed to avoid non-specific NADH oxidation as the electrons produced in these reactions are not accepted by decylubiquinone, resulting in high rotenone sensitivity. Another limitation concerning Complex I deficiency is that the biochemical assay is known to only measure the redox activity of the peripheral arm of Complex I (containing the N-module and Q- module). Therefore, patients with mutations residing in the membrane arm (P-module) - where only the proton pumping ability is affected rather than electron transport - may show a 'normal' enzyme profile following biochemical assessment despite an underlying Complex I defect, although this may reflect the level of mtDNA heteroplasmy in muscle tissue (threshold for biochemical deficiency not reached) (Fassone and Rahman 2012). An example of this would be patients with defects in the *MTND5* gene, particularly those with the *MT-ND5* m.13514A>G (p.Asp393Asn) variant (Bugiani et al. 2004; Corona et al. 2001; Lebon et al. 2003). One last limitation to consider is that the assay may fail to detect subtle deficiencies as a small percentage of respiratory chain deficient cells may not be detectable by enzyme measurements on tissue homogenates.

However, alternative functional biochemical assays such as the assessment of Complex I assembly in muscle homogenates using BN-PAGE are helpful in determining the effects of known or unknown genetic variants on the assembly. Additionally, western blots help with assessing the steady state levels of subunits of Complex I, clarifying the impact the genetic mutation may have on the subunit.

3.1.4.3. The Quadruple immunofluorescence assay and Complex I deficiency

As described in **Chapter 1** and **Chapter 2**, Rocha and colleagues developed the quadruple immunofluorescence assay and validated the technique using skeletal muscle cryosections from patients with various pathogenic variants (Rocha et al. 2015).

Taking into account the limitations described in the current diagnostic tools, predominantly with the histological algorithms, this assay can help overcome the issues regarding isolated Complex I deficient cases. The key advantage of the assay is the direct assessment of

Complex I through the immunodetection of NDUFB8, alongside the assessment of Complex IV (monoclonal antibody labelling COX-1) and mitochondrial mass (porin). Additionally, the assay requires a substantially smaller amount of skeletal muscle tissue - the use of a single 10µm transversely-orientated muscle section is sufficient enough to provide an objective and reliable quantitative method for the assessment of Complex I and Complex IV protein abundance relative to the mitochondrial mass in individual muscle fibres. This is particularly beneficial when material received for the patient is too small of an amount to undergo conventional biochemical assay assessment. Lastly, unlike COX/SDH, an automated quantification method allows for a greater sensitivity in the detection of deficiency.

3.2. Aims

The quadruple immunofluorescence technique has since been applied routinely in a diagnostic setting at the Wellcome Centre for Mitochondrial Research at Newcastle University.

However, given the vast clinical and genetic heterogeneity associated with Complex I deficiency, there has been no study undertaken on how effectively and accurately this assay is able to detect Complex I deficiency in this group of patients. Moreover, accessing how well the findings from applying the assay correlates to the known literature will also be important to identify.

Therefore, this study aims to assess and validate the use of the quadruple immunofluorescence assay in detecting Complex I deficiency in a diagnostic setting. The study will aim to assess Complex I status in skeletal muscle biopsies from 25 patients with proven pathogenic variants in proteins leading to a biochemical defect of isolated Complex I activity, including nuclear-encoded Complex I structural subunits, Complex I assembly factors, or one of the 7 mtDNA-encoded structural subunits.

3.3. Methods

3.3.1. Tissue samples and patient cohort

Twenty-five skeletal muscle biopsies (quadriceps muscle) of patients -both paediatric (<16 years of age) and adult (≥ 16 years of age), who have been investigated for mitochondrial disease and shown to have genetically-confirmed pathogenic variants attributed to isolated Complex I deficiency were included in this study (see **Table 3.2** for detailed information). Moreover, **Table 3.3** highlights the genes affected in the cohort and their associated function and insertion into the assembly of the complex.

Measurements of the enzymatic activities of respiratory chain complexes were undertaken at one of two accredited Mitochondrial Diagnostic laboratories, the NHS Highly Specialised Services located within the Wellcome Centre for Mitochondrial Research at Newcastle University or the Neurometabolic Laboratory at University College London Hospitals (UCLH). Muscle biopsy referral, enzyme measurements and genetic studies were all undertaken as part of the diagnostic work-up of these patients for suspected mitochondrial disease.

All samples were obtained and used with informed consent. This study was approved and performed under the ethical guidelines issued by the Newcastle and North Tyneside Local Research Ethics Committees (reference 09/H0906/75) and complied with the Declaration of Helsinki. Control muscle was obtained from patients who were undergoing anterior cruciate ligament (ACL) operations and demonstrated to have normal respiratory enzyme activities.

Table 3.2: Clinical, biochemical and molecular genetic characteristics of the patient cohort with isolated Complex I deficiency

Patient	Gender	Adult/ Paediatric	Clinical Presentation	Gene	Genetic Defect	Residual Complex I activity	Hom Het (%)
<i>Nuclear- encoded Complex I subunits</i>							
P1 ^a	F	Paediatric	IUGR and oligohydramnios, FTT, mild hypertrophic cardiomyopathy	<i>NDUFB3</i>	Homozygous c.64T>C, pTrp22Arg	33%	n.a.
P2 ^b	F	Paediatric	IUGR. Acute life-threatening event, age 20 days, required intubation. Hypertrophic cardiomyopathy	<i>NDUFB3</i>	Homozygous c.64T>C, pTrp22Arg	32%	n.a.
P3 ^c	F	Paediatric	Oligohydramnios. IUGR. Poor feeding at birth. MRI brain and echocardiogram normal. Age-appropriate skills. Family history of previous neonatal death	<i>NDUFB3</i>	Homozygous c.64T>C, pTrp22Arg	35%	n.a.
P4	F	Paediatric	Leigh syndrome	<i>NDUFS4</i>	Compound heterozygous c.99-1G>A + c.416_417delC, p.(Glu139Alafs*50)	39%	n.a.
P5	F	Paediatric	Consanguineous, first cousin parents; Leigh-like syndrome; elevated lactates	<i>NDUFS4</i>	Homozygous exon 3 and 4 deletion	37%	n.a.
P6	M	Paediatric	Infantile-onset mitochondrial disease; marked lactic acidosis	<i>NDUFS6</i>	Homozygous c.316_319delGAAA, p.(Glu106Glnfs*41)	5%	n.a.
P7	F	Paediatric	Leigh syndrome	<i>NDUFS2</i>	Homozygous c.998G>A, p.(Arg333Gln)	42%	n.a.
P8	F	Paediatric	Leigh-like syndrome; elevated serum lactates	<i>NDUFS3</i>	Homozygous c.642_644delTGA, p.(Asp214del)	26%	n.a.
<i>Nuclear- encoded Complex I assembly factors</i>							

P9	F	Paediatric	Leigh-like syndrome; elevated lactates	<i>NDUFAF6</i>	Compound heterozygous c.805C>T, p.(His269Tyr) and c.581-7A>G	26%	n.a.
P10	F	Paediatric	Lethal infantile mitochondrial disease presentation; presented day 1 with persistent lactic acidosis; died at 9 weeks	<i>NDUFAF6</i>	Homozygous c.659C>A, p.(Thr220Lys)	45%	n.a.
P11	F	Paediatric	Presented at 8 months; developmental regression, rotatory nystagmus bilaterally; elevated blood and CSF lactate; extensive basal ganglia and brainstem changes on MRI	<i>NDUFAF5</i>	Compound heterozygous c.826C>T, p.(Arg276*) and c.848C>T, p.(Ala283Val)	44%	n.a.
P12	M	Paediatric	Myoclonic seizures, developmental delay	<i>FOXRED1</i>	Compound heterozygous c.612_615dup, p.(Ala206Serfs*15) and c.1261G>A, p.Val421Met	31%	n.a.
P13	M	Paediatric	Hypertrophic cardiomyopathy at birth; severe metabolic acidosis (18-30 mmol/L); died at 2 days of age	<i>ACAD9</i>	Compound heterozygous c.868G>A, p.(Gly290Arg) and c.976G>C, p.(Ala326Pro)	13%	n.a.
P14	M	Adult	Exercise intolerance, muscle cramps, elevated serum lactate	<i>ACAD9</i>	Compound heterozygous c.1150G>A, p.(Val384Met) and c.1168G>A, p.(Ala390Thr)	13%	n.a.
P15 ^d	M	Adult	Exercise intolerance, unable to perform sustained aerobic exercise; normal strength; normal ECG and echocardiogram; normal resting lactate, normal CK	<i>TMEM126B</i>	Homozygous c.635G>T, p.(Gly212Val)	36%	n.a.

Mitochondrial DNA- encoded Complex I subunits

P16 ^e	F	Adult	Exercise intolerance, persistent lactic acidemia	<i>MTND1</i>	m.3356T>C, p.(Met17Thr)	3%	92%
P17	M	Paediatric	LS	<i>MTND3</i>	m.10158T>C, p.(Ser34Pro)	44%	90%
P18	M	Paediatric	LS	<i>MTND3</i>	m.10197G>A, p.(Ala47Thr)	n.d.	93%
P19	M	Paediatric	LS	<i>MTND5</i>	m.13514A>G, p.(Asp393Gly)	27%	66%
P20 ^f	F	Paediatric	Chronic renal failure, myopathy and persistent lactic acidosis	<i>MTND5</i>	m.12425delA, p.(Asn30Thrfs*7)	16%	85%

P21	F	Paediatric	Bilateral ptosis, ophthalmoplegia, pyramidal tract signs, elevated blood and CSF lactates	<i>MTND5</i>	m.13094T>C, p.(Val253Ala)	59%	58%
P22	M	Adult	Mitochondrial myopathy, elevated lactates	<i>MTND5</i>	m.13513G>A, p.(Asp393Asn)	39%	60%
P23	M	Paediatric	LS	<i>MTND5</i>	m.13513G>A, p.(Asp393Asn)	38%	77%
P24	F	Adult	Elevated CK, muscle pain and fatigue, myopathy	<i>MTND5</i>	m.13513G>A, p.(Asp393Asn)	100%	45%
P25	M	Paediatric	Failure to thrive, myopathy, increased brainstem signal on MRI, lactic acidosis	<i>MTND5</i>	M.13513G>A, p.(Asp393Asn)	100%	63%

*Residual Complex I activities, normalised to the activity of the matrix marker enzyme citrate synthase, are expressed as a percentage of mean control values. Residual Complex I activity and homogenate heteroplasmy level measured in muscle unless stated otherwise.

Key: Hom het, homogenate heteroplasmy; IUGR, intrauterine growth restriction; FTT, failure to thrive; ECG, electrocardiogram; CK, creatinine kinase; LS, Leigh syndrome; ^{a,b,c,d,e} published patients: ^aP1 = Patient 3 in Alston *et al* (2016) JMG, ^b P2 = Patient 2 in Alston *et al* (2016) JMG, ^c P3 = Patient 6 in Alston *et al* (2016) JMG, ^d P15 = Patient S1 in Alston *et al* (2016) AJHG, ^eP16 = Patient 1 in Gorman *et al* (2015) Clinical Science, ^f P20 = Patient published in Alston *et al* (2010) Neuromuscular disorders, F; Female, M; Male, n.a.; not applicable, n.d.; not determined

Table 3.3: Genes affected in the cohort of confirmed Isolated Complex I deficiency patients; their known/postulated function and assembly intermediate

Gene	Nuclear or mtDNA	Function	Assembly
<i>NDUFB3</i>	Nuclear	Accessory subunit with no role in catalytic function of CI	PD-a intermediate
<i>NDUFS4</i>	Nuclear	Accessory subunit with no role in catalytic function of CI	N module
<i>NDUFS6</i>	Nuclear	Accessory subunit with no role in catalytic function of CI	N module
<i>NDUFS2</i>	Nuclear	Core subunit involved with catalytic function of CI	Q module
<i>NDUFS3</i>	Nuclear	Core subunit of CI involved with catalytic function of CI	Q module
<i>NDUFAF6</i>	Nuclear	Assembly factor involved in the assembly of CI at early stages	Q/Pp-a intermediate
<i>NDUFAF5</i>	Nuclear	Assembly factor involved in the assembly of CI at early stages	Q/Pp-a intermediate
<i>FOXRED1</i>	Nuclear	Assembly factor involved in the assembly of CI at mid-late stage	P _D -a intermediate
<i>ACAD9</i>	Nuclear	Assembly factor involved in the assembly of CI at early -mid stage	P _P -b intermediate
<i>TMEM126B</i>	Nuclear	Assembly factor involved in the assembly of CI at mid-late stage	P _D -a intermediate
<i>MT-ND1</i>	mtDNA	Core subunit involved in electron transfer to ubiquinone	Q/Pp-a intermediate
<i>MT-ND3</i>	mtDNA	Core subunit involved in electron transfer to ubiquinone and proton translocation	P _D -a intermediate
<i>MT-ND5</i>	mtDNA	Core subunit involved in electron transfer to ubiquinone and proton translocation	P _D -b intermediate

3.3.2. Quadruple Immunofluorescence

The quadruple immunofluorescence assay was undertaken on 10µm sections of each patient (n=25) and control (n=5), as described in section 2.5.8.1 in **Chapter 2**. Briefly, sections were incubated with the primary antibodies (**Table 3.4**) overnight at 4°C followed by three wash steps for 10 minutes each. This was followed by incubation with secondary antibodies for 2 hours in 4°C and a further incubation step with streptavidin conjugated with Alexa 647 for 2 hours at 4°C (**Table 3.4**). Sections were then mounted using ProLong gold antifade reagent. NPC sections were processed alongside the OXHPOS sections (**Figure 3.4**). Where stated, this assay was also applied using the antibody targeting NDUFS3 in place of NDUFB8.

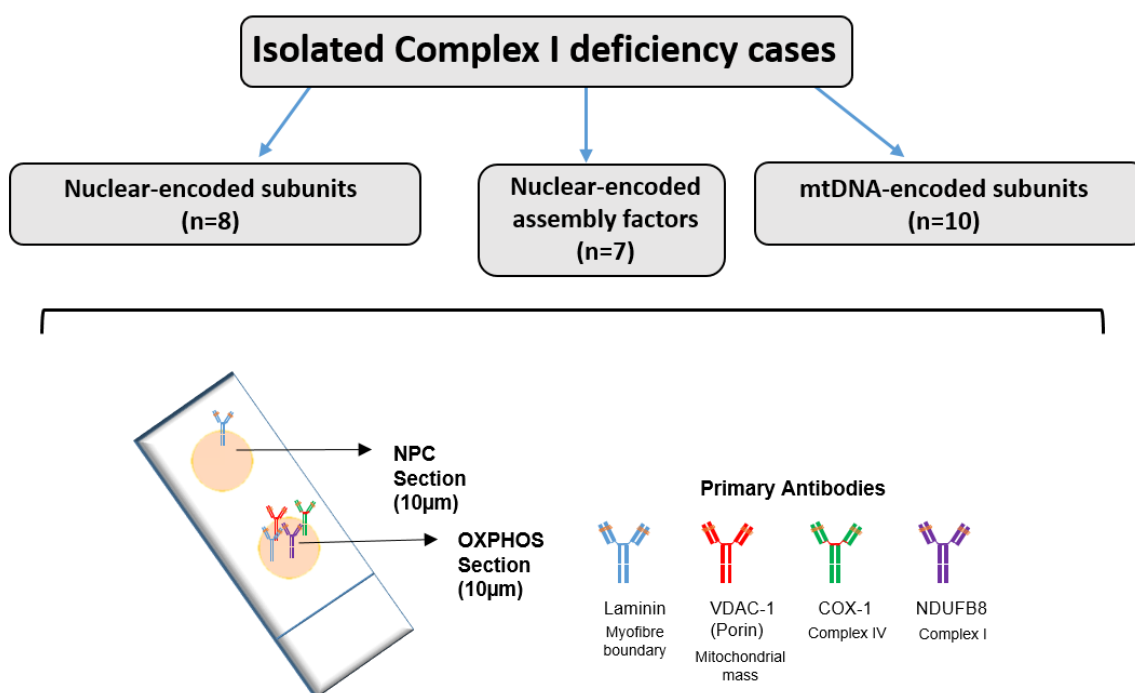


Figure 3.4: A schematic diagram highlighting the study design and the quadruple immunofluorescence protocol.

A total of 25 patients were assessed using the assay which detects the immunoreactivity of complex I, complex IV and porin.

Table 3.4: Primary and secondary antibodies used for immunofluorescence

Antibody	Target	Supplier	Catalogue	Dilution
Primary Antibodies				
Mouse IgG1 NDUFB8	Subunit of Complex I	Abcam	Ab110242	1:100
Mouse IgG2a MTCO1	Subunit of Complex IIV	Abcam	Ab14705	1:100
Mouse IgG2b VDAC (Porin)	Voltage gated anion on outer membrane of mitochondria	Abcam	Ab14734	1:100
Polyclonal Rabbit IgG Laminin α -1	Protein of the extracellular matrix	Sigma Aldrich	L9393	1:50
Secondary Antibodies				
Anti-mouse IgG2a Alexa fluor 488nm	n/a	Life technologies	A21141	1:200
Anti-mouse IgG2b Alexa fluor 546nm	n/a	Life technologies	A21143	1:200
Anti-mouse IgG1 Biotin	n/a	Life technologies	A10519	1:200
Anti-rabbit IgG Alexa fluor 750nm	n/a	Life technologies	S31556	1:100
Antibodies tested				
Mouse IgG1 NDUF3	Subunit of Complex I	Abcam	Ab110240	1:100
Polyclonal Rabbit ND1	Subunit of Complex I	Gifted by Prof. A. Lombres	n/a	1:100

3.3.3. Image Acquisition

As outlined in section 2.5.9 in **Chapter 2**, tiled fluorescent images were captured at x20 magnification using the Zen 2011 (blue edition) software and Zeiss Axio imager MI microscope, equipped with a motorised stage, an AxioCam digital camera and filter cubes detecting wavelengths at 488nm, 546nm, 647nm and 750nm. Exposure times were set for each channel to avoid over saturation – the same exposure times were then maintained across all cases and controls.

3.3.4. Statistical Analysis

3.3.4.1. Densitometry measurements

Fluorescent images were analysed using the Quadruple Immuno Analyser analysis software (coded for by MatLab 2015a), as described in detail in section 2.5.10.1 in **Chapter 2**. The laminin immunofluorescence (750 channel) was used to detect fibres automatically. Any unwanted surfaces including those over background, fibres with poor morphology or folded regions of the section were removed. The surfaces allowed for the measurement of mean intensity/optical density (OD) of 488 (COX-1), 546 (Porin) and 647 (NDUFB8) in each individual fibre. The same procedure was repeated for each NPC in order to determine the levels of non-specific binding.

3.3.4.2. Data Analysis

The Microsoft Excel fibres containing the mean ODs for each case, were merged and uploaded onto the Mitochondrial Immunofluorescence Analysis online tool (<http://research.ncl.ac.uk/mitoresearch/>), as fully described in **Chapter 2**, section 2.5.10.2. The analysis determined the Z scores for porin, COX-1 and NDUFB8 for each fibre analysed based on their expected levels, which were derived using data obtained from control muscle sections. Fibres were classified, based on the SD limits, into groups of NDUFB8 and COX-1 levels; >-3 = normal, -3 to -4.5 = intermediate positive, -4.5 to -6 = intermediate negative and <-6 = deficient/negative. Fibres were also classified into levels of porin according to Z scores (Z-score: "very low" (porin_Z $< -3SD$), "low" (porin_Z between $-3SD$ and $-2SD$), "normal" (porin_Z between $-2SD$ and $+2SD$), "high" (porin_Z between $+2SD$ and $+3SD$) and "very high" (porin_Z above $+3SD$)) (Rocha et al., 2015).

The mitochondrial respiratory chain profiles were produced using Prism 5 (GraphPad Software Inc).

3.3.5. Blue Native–Polyacrylamide Gel Electrophoresis (BN-PAGE)

Mitochondrial fractions from both controls and patient muscle were prepared for BN-PAGE as previously described in detail in **Chapter 2, section 2.5.11**. The protein concentration of samples was determined using the Pierce BCA protein assay kit and absorption spectrophotometry measured at 562nm. A minimum of 150ug of muscle mitochondria extracts were loaded on a native 4-16% BisTris gel (Life technologies) and electrophoretically separated in first dimension according to the NOVEX NativePAGE™ Bis-Tris Gel system instructions (2 hours, 250 volts). Proteins were transferred onto a polyvinylidene fluoride (PVDF) membrane (Immobilon-P, Millipore Corporation) through wet transfer. Thereafter, the membrane was fixed in 8% acetic acid, washed and blocked with 5% milk for 1 hour at room temperature. Membrane was then subjected to standard immunoblotting analysis of OXPHOS complexes using primary and horseradish peroxidase conjugated secondary antibodies against NDUFB8 (980 kDa CI holoenzyme) and SDHA (140 kDa).

3.4. Results

A total of 25 skeletal muscle biopsies taken from patients with genetically confirmed pathogenic variants either shown or predicted to cause isolated Complex I deficiency (P1-P25), were used to validate a recently-developed quadruple immunofluorescence assay within a diagnostic setting. The clinical, biochemical and molecular genetic characteristics of this patient cohort are shown in **Table 3.2**. The fibres in all muscle sections were classified according to Z scores – where any fibres with a Z score under -3SD were classified as deficient (Rocha et al., 2015). The quadruple immunofluorescence assay results in this chapter (particularly the NDUFB8 immunoreactivity) are presented as a percentage of fibres deficient in Complex I – calculated by totalling the percentage of fibres classified as negative, intermediate negative and intermediate positive fibres (**Table 3.5**). These findings were then subsequently correlated with the diagnostic biochemical findings which are presented as residual Complex I activity (**Table 3.2**).

3.4.1. Group 1- Nuclear-encoded Complex I structural subunits

All eight patients in Group 1 (P1-P8) harbouring pathogenic variants in a nuclear-encoded Complex I structural subunits (core or accessory), showed varying levels of decreased NDUFB8 immunoreactivity (representing a decrease in NDUFB8 protein abundance/expression) when compared to non-disease control muscle (**Figure 3.5**). Further analysis revealed that the proportion of Complex I-deficient fibres ranged between 39% and 99% across this group of patients whilst 0% for all patients for Complex IV.

The mitochondrial respiratory chain profiles (**Figure 3.6**), show the NDUFB8 and COX-1 protein abundance in conjunction with mitochondrial mass (porin) in individual muscle fibres as represented by each individual point. The graphs highlight that most of the fibres analysed were outside of the normal range for NDUFB8 (Z-score between -3SD to 3SD) – causing a shift in their distribution on the plot to the left of the graph - despite the normal levels of Complex IV in virtually all fibres assessed (n=131 to 13422 fibres analysed in total in cases; this number is dependent on the size of muscle section). These findings were in agreement with the respiratory chain biochemical findings, where a decrease in residual Complex I activity was observed (**Table 3.2**).

Table 3.5: Percentage of Complex I- deficient fibres detected with the quadruple immunofluorescence assay

Patient ID	Complex I (NDUFB8) Levels (%)					Complex IV (COX-1) Levels (%)					Total n =
	Pos	Int (+)	Int (-)	Neg	% Deficiency	Pos	Int (+)	Int (-)	Neg	% Deficiency	
<i>Nuclear-encoded Complex I structural subunits</i>											
P1	20.20	39.68	31.22	8.90	79%	100	0	0	0	0%	4372
P2	7.16	7.51	9.12	76.21	93%	100	0	0	0	0%	559
P3	61.29	31.33	6.96	0.42	39%	100	0	0	0	0%	13422
P4	19.3	10.95	26.04	61.08	98%	100	0	0	0	0%	5964
P5	11.06	33.78	40.81	14.65	89%	100	0	0	0	0%	4683
P6	21.25	48.86	27.27	2.61	79%	100	0	0	0	0%	880
P7	1.33	11.62	31.68	55.37	99%	100	0	0	0	0%	5337
P8	4.54	17.04	33.06	45.36	96%	100	0	0	0	0%	7175
<i>Nuclear-encoded Complex I assembly factors</i>											
P9	1.5	5.18	12.25	81.23	99%	100	0	0	0	0%	9504
P10	3.68	13.95	32.27	50.10	96%	100	0	0	0	0%	5355
P11	73.9	19.23	6.50	0.37	26%	100	0	0	0	0%	7352
P12	3.57	8.26	11.42	76.76	96%	100	0	0	0	0%	1708
P13	0	0	0	100	100%	100	0	0	0	0%	2684
P14	0	0	0	100	100%	100	0	0	0	0%	239
P15	0	0	0	100	100%	100	0	0	0	0%	131
<i>mtDNA-encoded Complex I structural subunits</i>											
P16	8.48	0.86	0.72	89.94	92%	100	0	0	0	0%	696
P17	9.74	41.66	37.28	11.31	90%	100	0	0	0	0%	5842
P18	100	0	0	0	0%	100	0	0	0	0%	7302
P19	100	0	0	0	0%	100	0	0	0	0%	2427
P20	0	0	0	100	100%	100	0	0	0	0%	3795
P21	100	0	0	0	0%	100	0	0	0	0%	1311
P22	100	0	0	0	0%	100	0	0	0	0%	3341
P23	100	0	0	0	0%	100	0	0	0	0%	2730
P24	100	0	0	0	0%	100	0	0	0	0%	675
P25	100	0	0	0	0%	100	0	0	0	0%	785

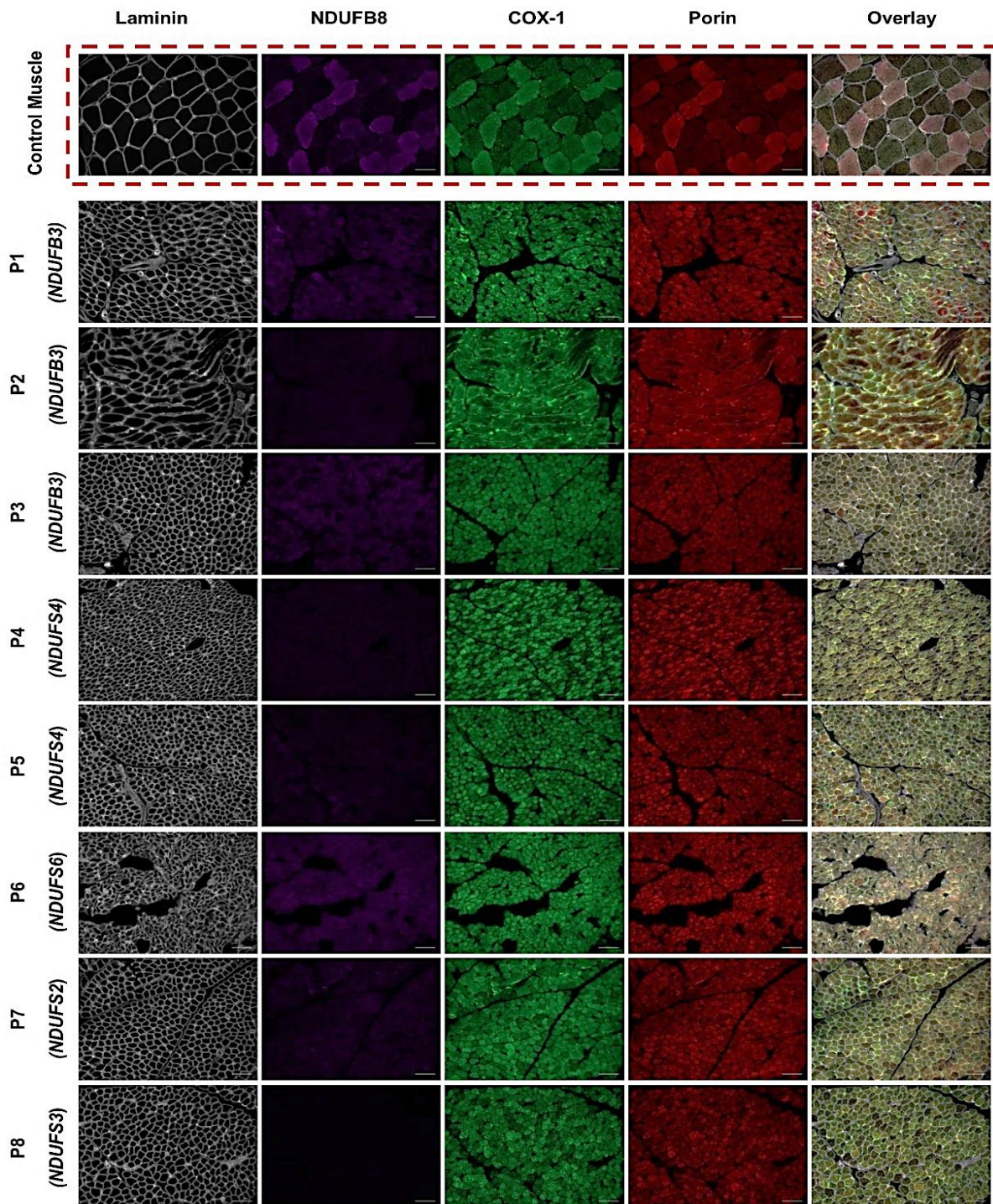


Figure 3.5: Images of Complex I, IV and porin expression in skeletal muscle sections from patients with isolated Complex I deficiency caused by defects on nuclear-encoded Complex I subunits using the immunofluorescence assay.

Fluorescent detection was used to visualise NDUFB8—purple (Complex I), COX-1—green (Complex IV), porin—red (mitochondrial mass) and lamininin—white (fibre boundary marker). Control muscle (highlighted by the red box) shows normal signals for NDUFB8, COX-1 and porin. However, a marked decreased in NDUFB8 signal is seen in all patients (P1-P8) compared to the COX-1 and porin staining. Exposure times were maintained throughout all cases. Images taken at x20 magnification. Scale bars measure 50 μ m.

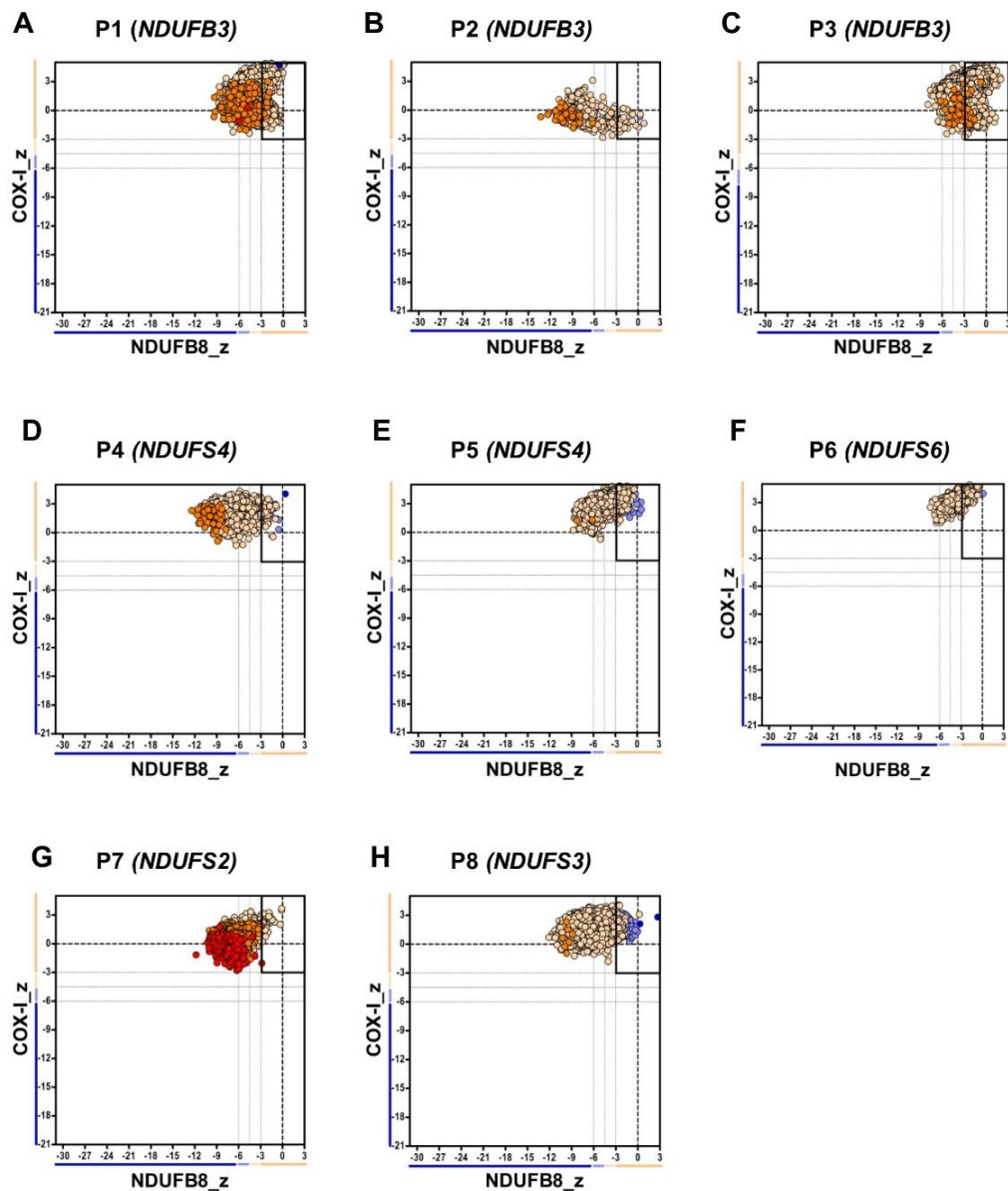


Figure 3.6: Mitochondrial respiratory chain expression profile linking Complex I, Complex IV and porin levels in patients with isolated Complex I deficiency caused by defects in nuclear-encoded Complex I subunits.

Graphs show complex I and complex IV expression profile from (A) Normal adult control and patients with (B – D) homozygous *c.64T>C, p.Trp22Arg* *NDUFB3* variant, P1 - n= 4372 fibres analysed, P2 – n= 559, P3 – n= 13422 (E) compound heterozygous *NDUFS4* variant, P4, n = 5964 (F) Homozygous exon 3 and 4 deletion in *NDUFS4*, P5, n = 4683 (G) homozygous *NDUFS6* variant , P6, n = 880 (H) Homozygous *NDUFS2* variant , P7, n = 5337 (I) Homozygous *NDUFS3* variant , P8, n =7154. Each dot represents a single muscle fibre, colour co-ordinated according to its mitochondrial mass: very low – blue, Low - light blue, Normal – beige, High – orange, Very high -red. Black dashed lines represent the SD limits for the classification of the fibres. Lines adjacent to X and Y axis represent the levels of *NDUFB8* and *COX-1*: beige: normal (<-3), light beige: intermediate (+) (-3 to -4.5), light blue: intermediate (-) (-4.5 to -6) and blue: deficient (> -6). Bold dashed lines indicate the mean expression level of normal fibres.

3.4.2. Group 2- Nuclear-encoded Complex I assembly factors

Similar to patients in Group 1, all seven patients in Group 2 (P9 to P15) who harbour pathogenic variants in nuclear-encoded assembly factors, displayed a severe loss of NDUFB8 immunoreactivity (**Figure 3.7**). With the exception of P11, further quantification showed that the percentage of Complex I- deficient fibres was >96%, highlighting the severe loss of NDUFB8. Specifically, the assay detected a complete loss of NDUFB8 immunoreactivity (100% Complex I -deficient fibres) in patients P13, P14 and P15, all of whom had pathogenic variants in either the *ACAD9* or *TMEM126B* genes; these encode Complex I assembly factors involved in the biogenesis of the proximal part of the P module (P_P). Only P11, who has compound heterozygous pathogenic variants in the *NDUFAF5* gene, encoding a Complex I assembly factor involved in the early step of the biogenesis of the holoenzyme, maintained a relatively mild level of NDUFB8 (26% Complex I -deficient fibres). As previously observed in patients from Group 1, the mitochondrial respiratory chain profiles from patients in Group 2 (**Figure 3.8**) showed a “shifting to the left”, but to a greater extent. Again, the findings determined from quadruple immunofluorescence assay correlated with the available biochemical results which show a more severe decrease in residual Complex I activity in muscle (**Table 3.2**).

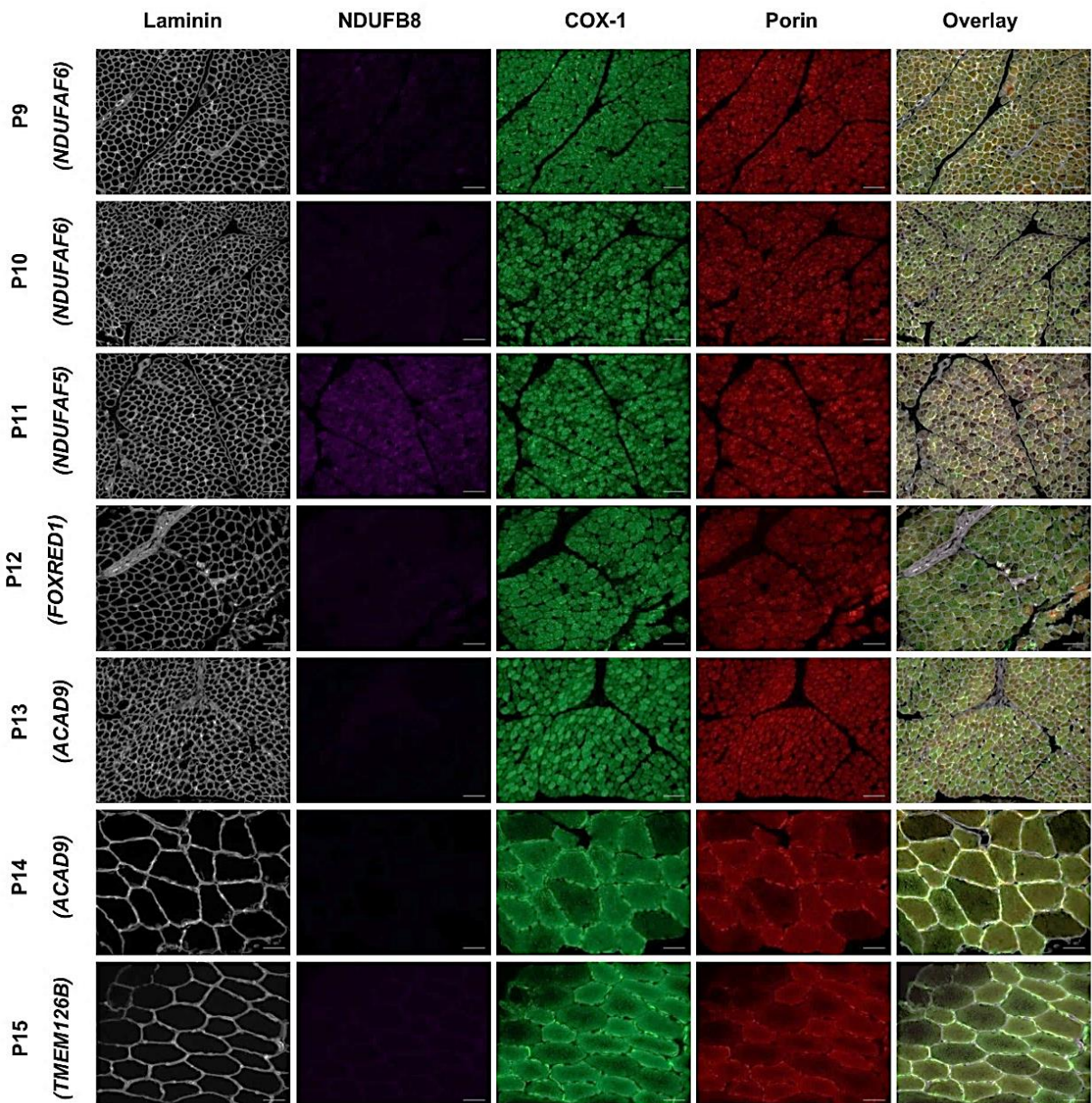


Figure 3.7: Images of Complex I, IV and porin expression in skeletal muscle sections from patients with isolated Complex I deficiency caused by defects on nuclear-encoded Complex I assembly factors using the immunofluorescence assay.

Fluorescent detection was used to visualise NDUFB8—purple (Complex I), COX-1—green (Complex IV), porin—red (mitochondrial mass) and laminin—white (fibre boundary marker). A marked decrease in NDUFB8 signal is seen in all patients (P9-P15) compared to the COX-1 and porin staining. Exposure times were maintained throughout all cases. Images taken at x20 magnification. Scale bars measure 50µm.

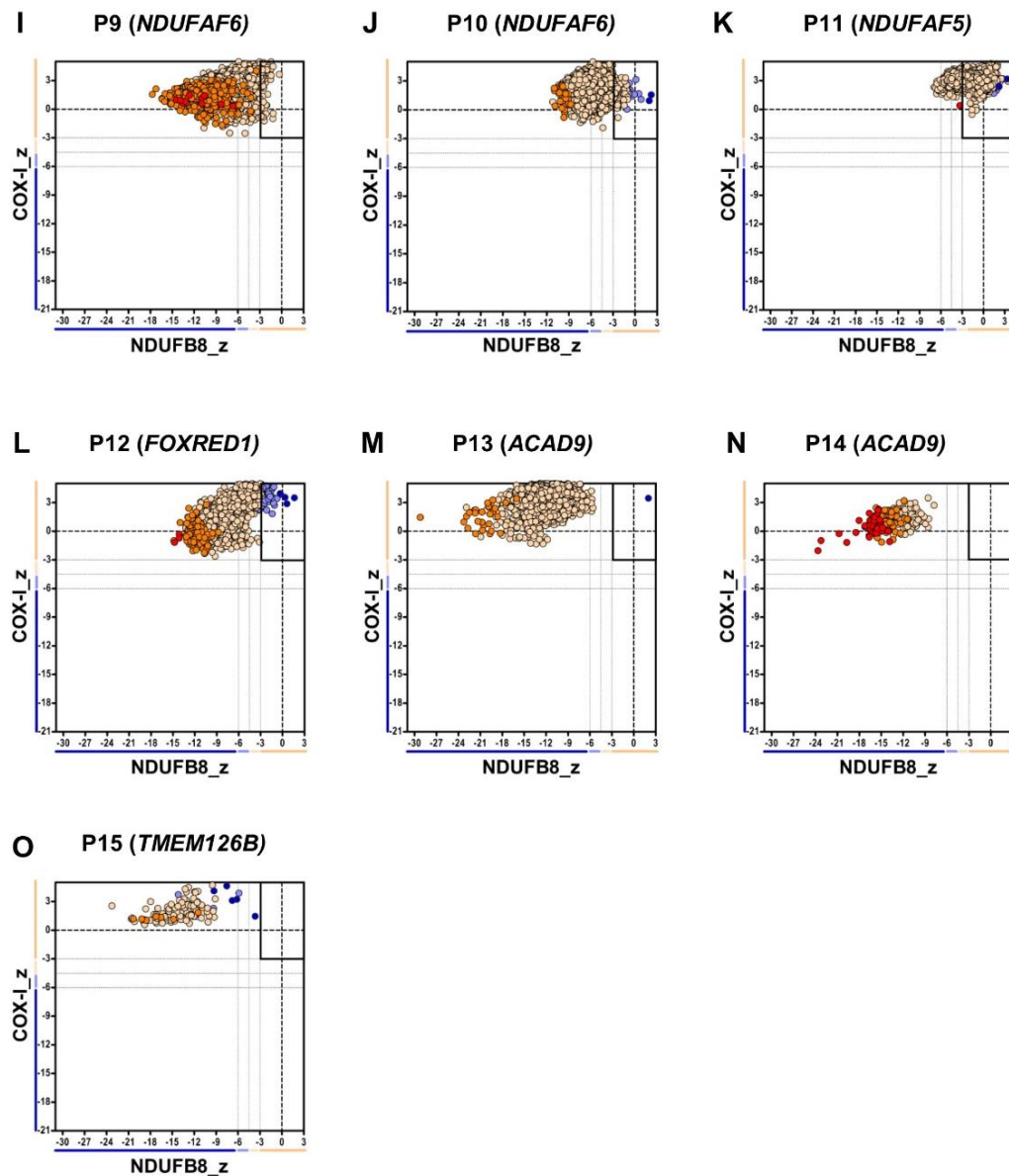


Figure 3.8: Mitochondrial respiratory chain expression profile linking Complex I, Complex IV and porin levels in patients with isolated Complex I deficiency caused by defects in nuclear-encoded Complex I assembly factors.

Graphs show complex I and complex IV expression profile from patients with (A) Compound heterozygous *NDUFAF6* variant, P9, $n = 9501$ (B) Homozygous *NDUFAF6* variant, P10, $n = 5355$ (C) Compound heterozygous *NDUFAF5* variant, P11, $n = 7352$ (D) Compound heterozygous *FOXRED1* variant, P12, $n = 1702$ (E-F) Compound heterozygous *ACAD9* variant, (E = P13, $n = 2684$, F = P14, $n = 239$) (G) Homozygous *TMEM126B* variant, P15, $n = 131$. Each dot represents a single muscle fibre, colour co-ordinated according to its mitochondrial mass: very low – blue, Low - light blue, Normal – beige, High – orange, Very high -red. Black dashed lines represent the SD limits for the classification of the fibres. Lines adjacent to X and Y axis represent the levels of *NDUF8* and *COX-1*: beige: normal (< -3), light beige: intermediate (+) (-3 to -4.5), light blue: intermediate (-) (-4.5 to -6) and blue: deficient (> -6). Bold dashed lines indicate the mean expression level of normal fibres.

3.4.3. Assay showed variable results in patients with mutations in mtDNA-encoded Complex I subunits (Group 3)

The ten patients in Group 3 (P16-P25) who harbour mutations in mtDNA genes encoding core structural subunits of Complex I, showed more heterogeneous results in contrast to both Group 1 and Group 2 patients. The quadruple immunofluorescence assay detected 100% Complex I-deficient fibres, representing a complete loss of NDUFB8 immunoreactivity, in three previously-reported patients with high levels of pathogenic mtDNA variants in muscle; P16 who has a m.3356T>C, p.(Met17Thr) *MTND1* variant, P17 who harbours a m.10158T>C, p.(Ser34Pro) *MTND3* variant and P20 who harbours a m.12425delA *MTND5* frameshift mutation (**Figure 3.9**). As expected, the mitochondrial respiratory chain profiles for these three patients were all shifted to the left, consistent with the loss of NDUFB8 immunoreactivity associated with preserved COX-I immunoreactivity (**Figure 3.11**).

The remaining seven patients (P18, P19, P21, P22, P23, P24 and P25) showed NDUFB8 immunoreactivity similar to control muscle (**Figure 3.10**). The mitochondrial respiratory chain profiles demonstrated normal respiratory chain expression as all fibres fell within the normal range (with Z_scores between -3SD and 3SD) (**Figure 3.11**). Of these 7 patients, P22 to P25 all harbour a common pathogenic m.13513G>A, p.(Asp393Asn) *MTND5* variant, P19 harbours a m.13514A>G, p.(Asp393Gly) variant, P21 harbours a m.13094T>C, p.(Val253Ala) variant whilst P18 has high levels of a m.10197G>A, p. Ala393Thr *MTND3* variant. Detection of normal levels of immunoreactive NDUFB8 subunit in these patients could be due to these variants only affecting the catalytic function of Complex I rather than the assembly.

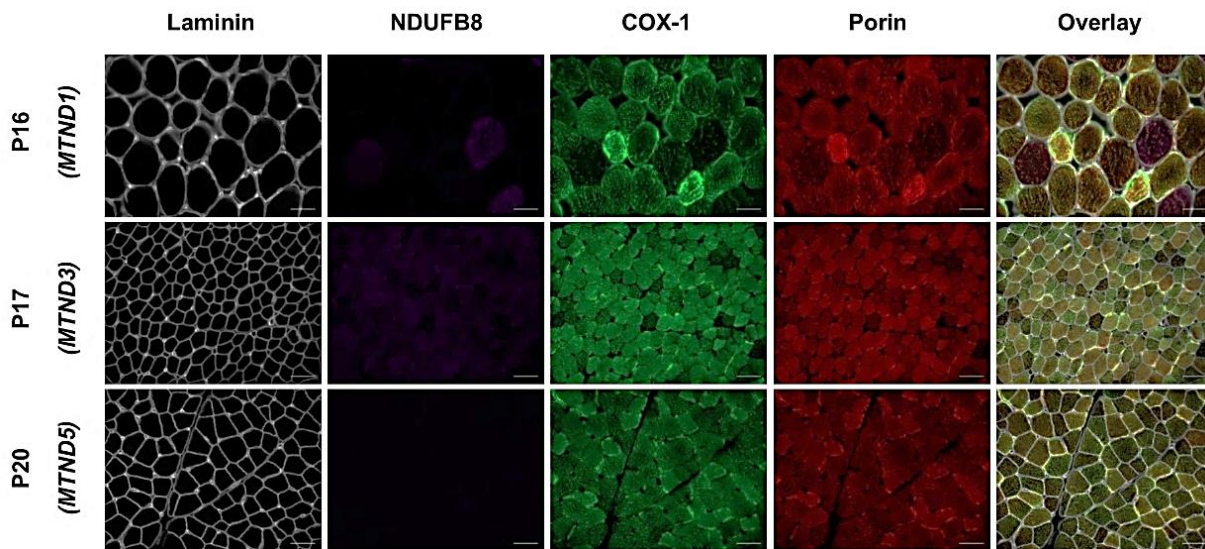


Figure 3.9: Images of Complex I, IV and porin expression in skeletal muscle sections from patients with isolated Complex I deficiency caused by defects on mtDNA-encoded CI subunits using the immunofluorescence assay.

Fluorescent detection was used to visualise NDUFB8—purple (Complex I), COX-1—green (Complex IV), porin—red (mitochondrial mass) and laminin—white (fibre boundary marker). A marked decrease in NDUFB8 immunoreactivity is seen in 3 of the 10 assessed patients in group 3; patients P16, P17 and P20 compared to the COX-1 and porin staining. Exposure times were maintained throughout all cases. Images taken at x20 magnification. Scale bars measure 50 μ m.

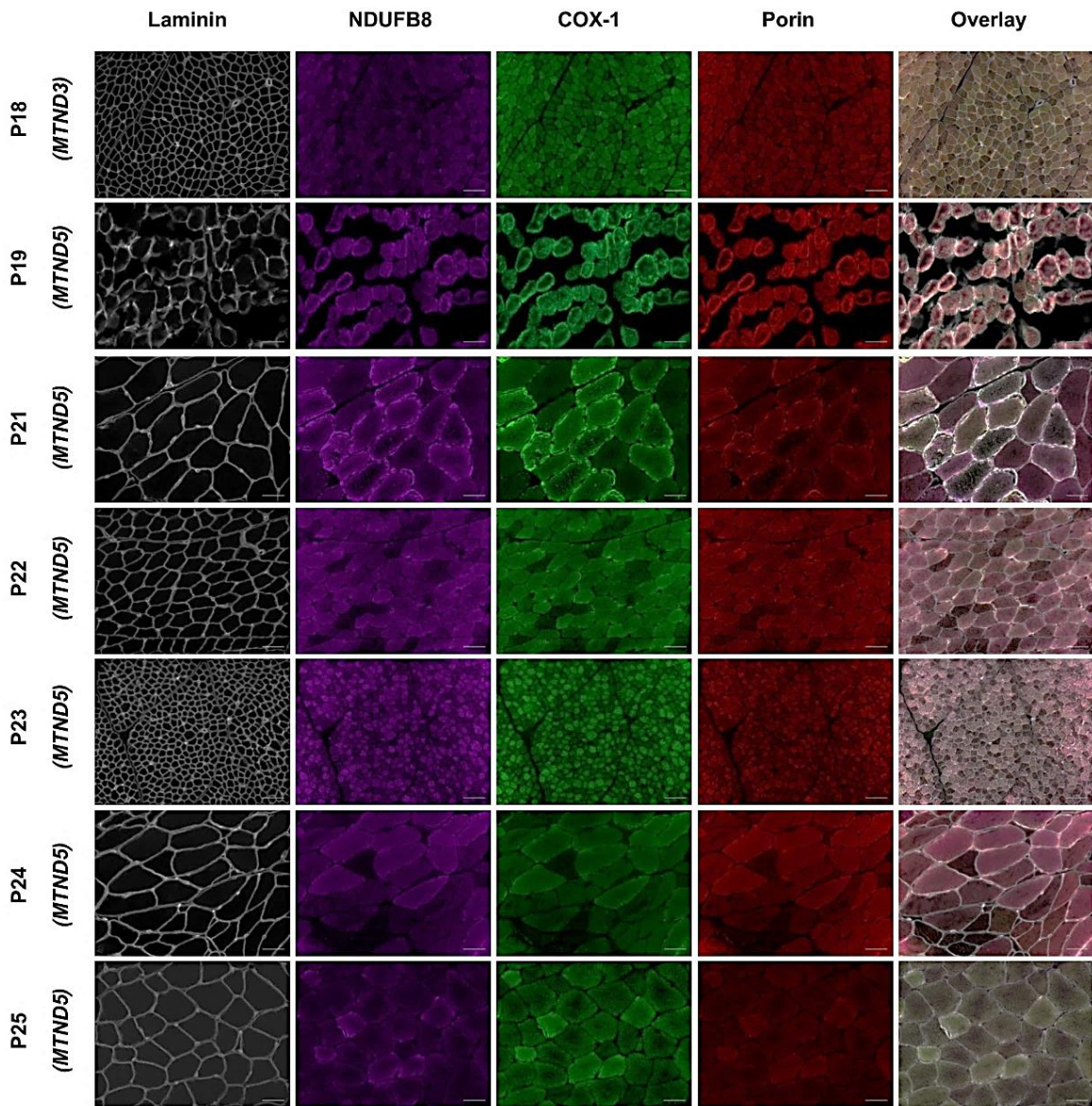


Figure 3.10: Images of Complex I, IV and porin expression in skeletal muscle sections from patients with isolated Complex I deficiency caused by defects on mtDNA-encoded Complex I subunits using the immunofluorescence assay.

Fluorescent detection was used to visualise NDUFB8—purple (Complex I), COX-1—green (Complex IV), porin—red (mitochondrial mass) and laminin—white (fibre boundary marker). In all patients, normal levels of NDUFB8 immunoreactivity is seen. Exposure times were maintained throughout all cases. Images taken at x20 magnification. Scale bars measure 50µm.

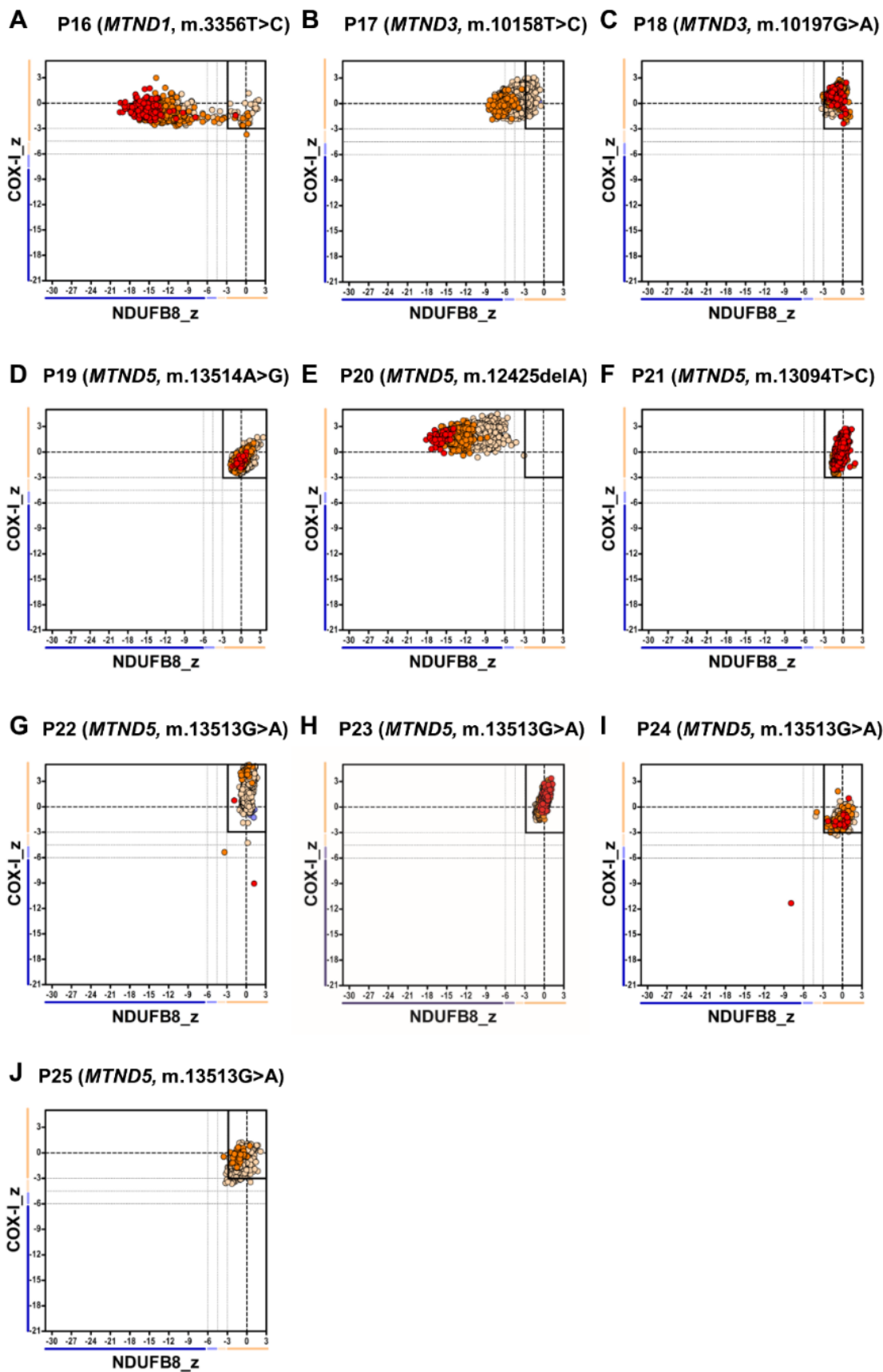


Figure 3.11: Mitochondrial respiratory chain expression profile linking complex I (NDUFB8), complex IV and porin levels in patients with isolated Complex I deficiency caused by defects in mtDNA-encoded Complex I subunits.

Graphs show Complex I and Complex IV expression profile from patients with (A) m.3356T>C MTND1 variant, P16, n=696 (B) m.10158T>C MTND3 variant, P17, n = 5842 (C) m.10197G>A MTND3 variant, P18, n=3341 (D) m.13514A>G MTND5 variant, P19, n = 2427 (E) m.12425delA MTND5 variant, P20, n = 3795 (F) m.13094T>C MTND5 variant, P21, n=1311 (G) m.13513G>A MTND5 variant, P22, n = 3341 (H) m.13513G>A MTND5 variant, P23, n=2730 (I) m.13513G>A MTND5 variant, P24, n =675 (J) m.13513G>A MTND5 variant, P25, n = 785. Each dot represents a single muscle fibre, colour co-ordinated according to its mitochondrial mass: very low – blue, Low - light blue, Normal – beige, High – orange, very high -red. Black dashed lines represent the SD limits for the classification of the fibres. Lines adjacent to X and Y axis represent the levels of NDUFB8 and COX-1: beige: normal (<-3), light beige: intermediate (+) (-3 to -4.5), light blue: intermediate (-) (-4.5 to -6) and blue: deficient (> -6). Bold dashed lines indicate the mean expression level of normal fibres.

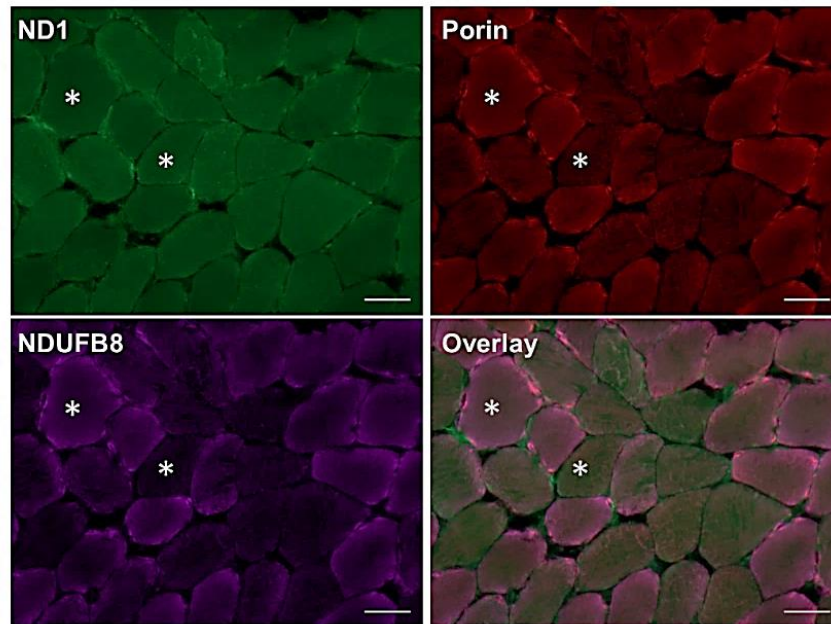
3.4.4. Patients with mutations in mtDNA-encoded CI subunits and normal NDUFB8 profile also display normal NDUFS3 levels

Most interestingly, since the interrogation of NDUFB8 immunoreactivity failed to detect Complex I deficiency in 7 of the 10 patients in Group 3, it was further investigated whether any deficiency could be detected using alternative antibodies against Complex I. The two antibodies tested were targeting the nuclear-encoded core subunit NDUFS3 (a commercially available antibody – Abcam: Ab110240) and the mtDNA encoded core subunit ND1 – both of which are integrated during the early stages of the Complex I assembly. The primary rabbit polyclonal antibody labelling ND1 was gifted by Professor Anne Lombes (as reported in Barthélémy et al., 2001).

To optimise the two antibodies, the quadruple immunofluorescence assay (though not including antibody to label COX-1), was performed on 10µm skeletal muscle sections from a control and P6 (NDUFS6, Homozygous c.316_319delGAAA, p.(Glu106Glnfs*41) (a representative case of isolated Complex I deficiency). The staining was performed using ND1 alongside NDUFB8 and porin. The application of the antibody at a dilution of 1:100 (the same dilution as other mitochondrial antibodies) showed non-specific binding to fibres in the control muscle in comparison to both NDUFB8 and porin levels. The observation of muscle sections needs to take into account the different muscle fibre types and so different staining patterns will be seen indicatively. In fibres where porin staining intensity is low, it signifies a

Type II fibre whilst higher staining intensity will be signifying a Type I fibre (as highlighted on the control tissue with an asterisk (*) in **Figure 3.12(A)**). The staining intensity of NDUFB8 was comparable in both fibre types to the porin, but there is no correlation of ND1 intensity to either hence the inference that there is non-specific binding. In the patient muscle section, ND1 failed to detect Complex I deficiency in fibres that showed loss of NDUFB8 immunoreactivity and intact porin (indicated with asterisk (*) in **Figure 3.12(B)**). This lack of detection alongside the non-specific binding rendered ND1 as an impractical choice of antibody to include into the quadruple immunofluorescence assay as a way of detecting Complex I deficiency.

A) Control case



B) Isolated CI- deficiency case

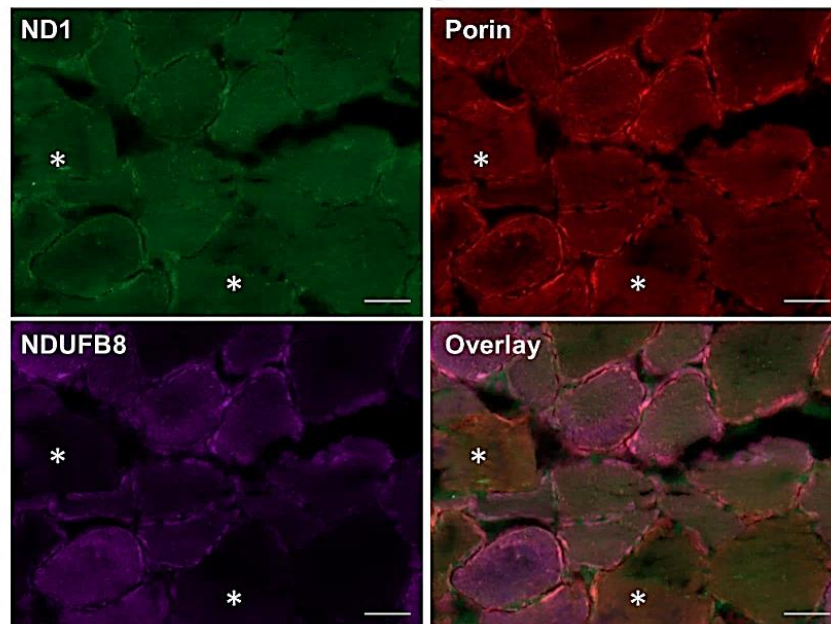
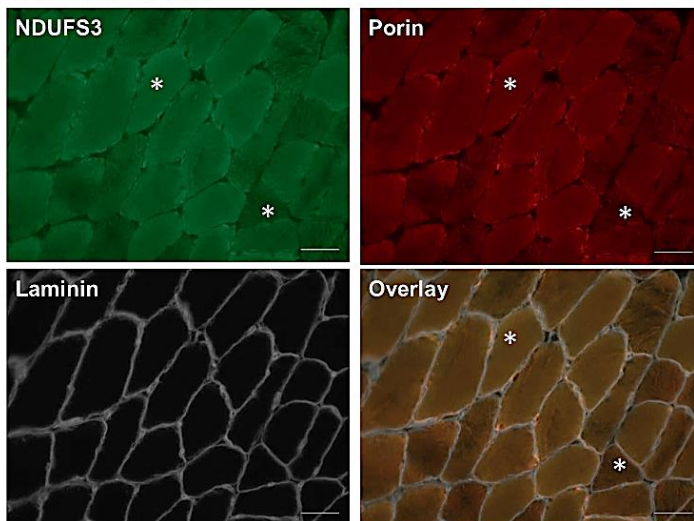


Figure 3.12: Immunofluorescent images of Complex I targeted with ND1 and NDUFB8 alongside porin expression in skeletal muscle sections from A) control case and B) an isolated Complex I deficiency case – P6 (NDUFS6, Homozygous c.316_319delGAAA, p.(Glu106Glnfs*41).

Fluorescent detection was used to visualise ND1— green (Complex I), NDUFB8 – Complex I (purple) and porin—red (mitochondrial mass) and laminin—white (fibre boundary marker). In control case (A), ND1 immunoreactivity is seen to non-specifically bind to the tissue section. No correlation with porin is seen whilst NDUFB8 correlates with porin. In patient case (B), the antibody labelling ND1 failed to detect deficient fibres where NDUFB8 immunoreactivity is decreased compared to porin. Asterisks * = mark fibres given as examples of this. Images taken at x20 magnification. Scale bars measure 50µm.

The antibody targeting NDUFS3 was also investigated in the same patient case and control, alongside porin and laminin. The isotype of NDUFS3 was the same as NDUF8 (IgG1) hence why it could not be included in this experiment. The control muscle section showed correlation of NDUFS3 with porin levels indicating that the antibody was specifically binding to the muscle fibres (as indicated with an asterisks (*) in **Figure 3.13(A)**). In the patient case, NDUFS3 immunoreactivity was decreased in fibres in comparison to the porin levels (Figure 3.13b), showing that the commercially available antibody was able to detect Complex I deficiency in muscle fibres.

A) Control case



B) Isolated CI- deficiency case

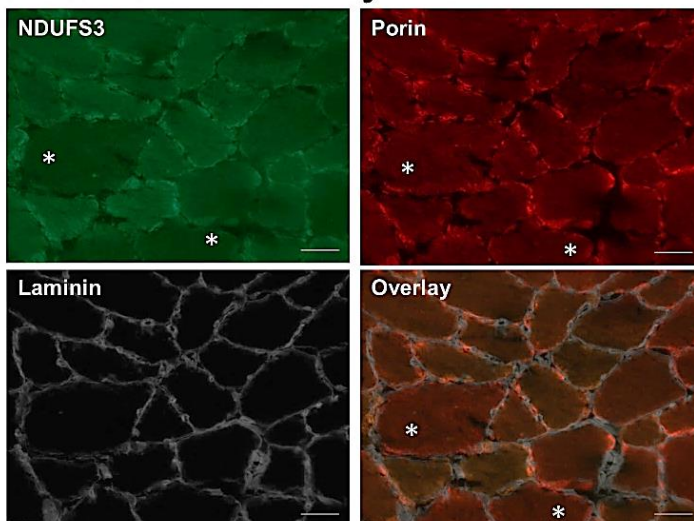


Figure 3.13: Immunofluorescent images of Complex I targeted with NDUFS3 and porin expression in skeletal muscle sections from A) control case and B) an isolated Complex I deficiency case.

*Fluorescent detection was used to visualise NDUFS3— green (Complex I), porin—red (mitochondrial mass) and laminin—white (fibre boundary marker). In control case (A), NDUFS3 immunoreactivity is seen to be equivalent to porin expression. In patient case (B), NDUFS3 immunoreactivity is decreased in fibres compared to porin. * = Asterisks mark fibres given as examples of this. Images taken at x20 magnification. Scale bars measure 50µm.*

To investigate this finding further, the complete quadruple immunofluorescence assay was performed on sections from P18, P19, P20, P21, P23, P4 and P25 using antibodies against NDUFS3, porin, COX-I and laminin (**Figure 3.14**). As shown in **Figure 3.15**, the mitochondrial respiratory chain profile for P20 shows a shift of fibres to the left whilst for all the remaining patients, fibres were shown to be in the normal range – in line with findings from the assessment with the NDUF8 antibody. This provides further clarification that NDUFS3 was capable of reproducing the same findings, but also that the initial results with NDUF8 were accurate.

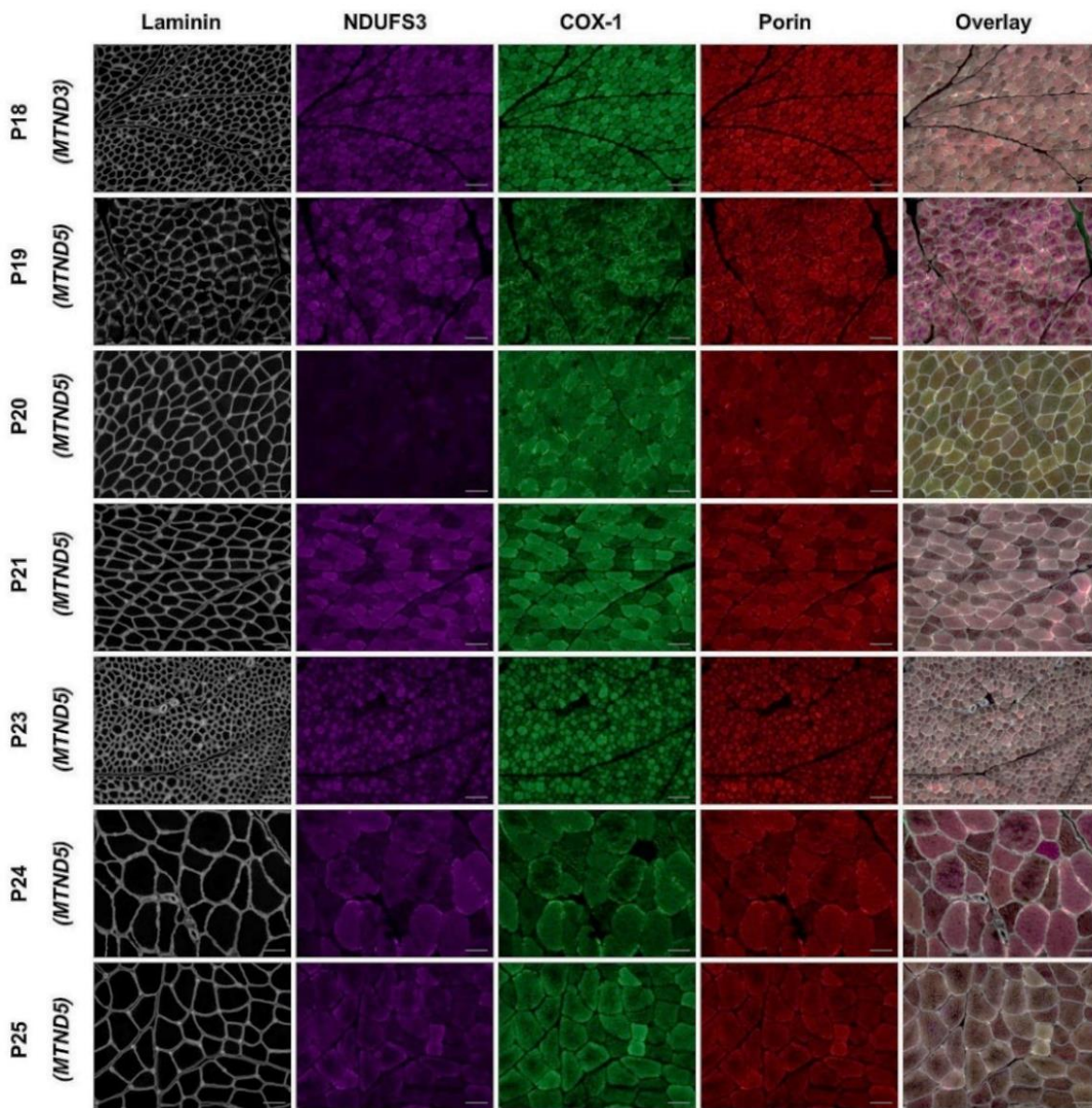


Figure 3.14: Images of Complex I, IV and porin expression in skeletal muscle sections from patients with isolated Complex I deficiency caused by defects on mtDNA-encoded Complex I subunits using the immunofluorescence assay.

Fluorescent detection was used to visualise NDUFS3—purple (Complex I), COX-1—green (Complex IV), porin—red (mitochondrial mass) and laminin—white (fibre boundary marker). Patient P20 was used a positive control and a marked decrease in NDUFS3 immunoreactivity is seen. Whilst in the remaining patients, normal levels of NDUFS3 signal is expressed. Exposure times were maintained throughout all cases. Images taken at x20 magnification. Scale bars measure 50µm.

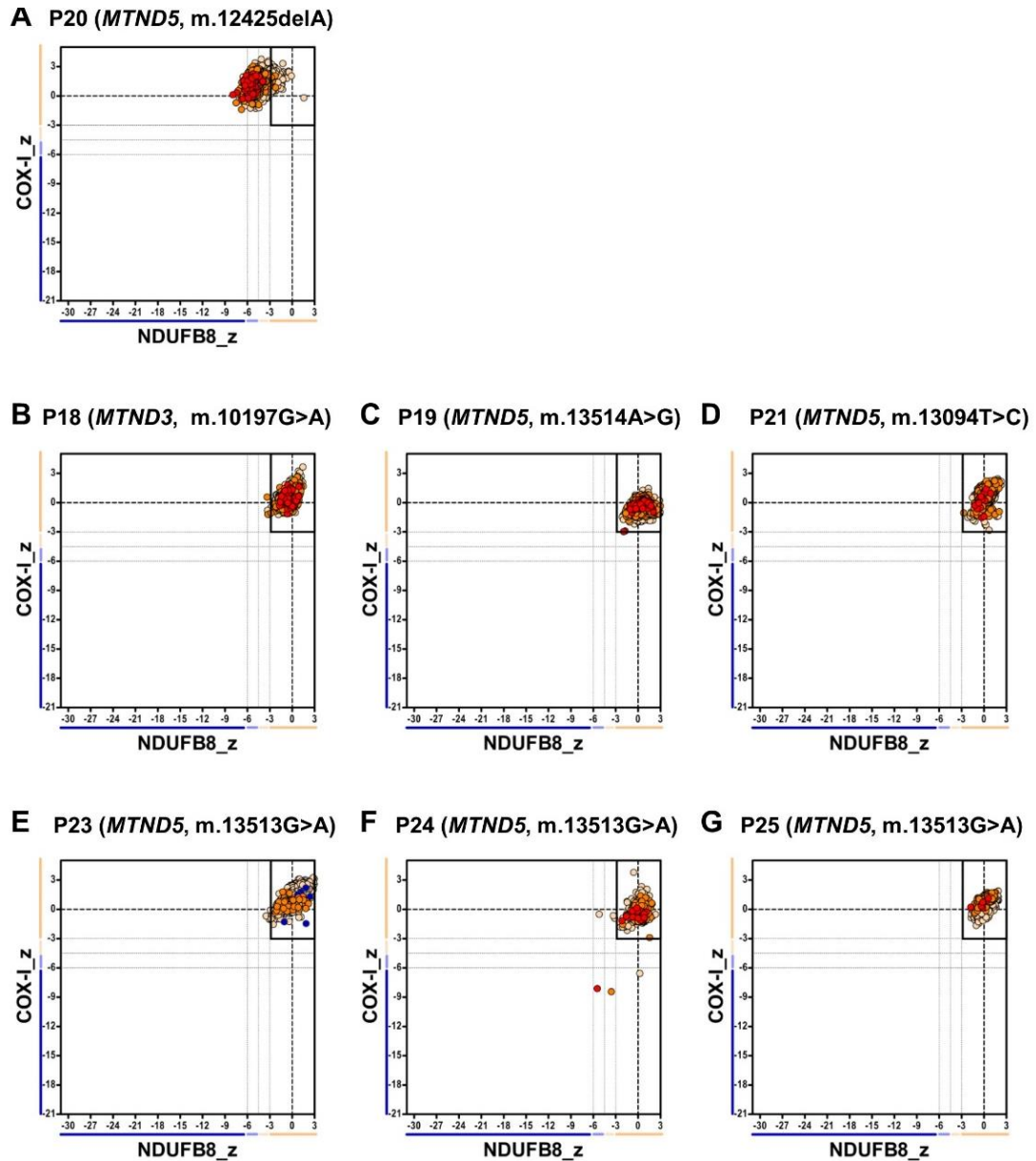


Figure 3.15: Mitochondrial respiratory chain expression profile linking complex I (NDUFS3), complex IV and porin levels in patients with Isolated complex I deficiency caused by defects in mtDNA-encoded Complex I subunits.

Graphs show complex I and complex IV expression profile from patients with (A) m.12425delA *MTND5* variant, P20, n = 5536 (B) m.10197G>A *MTND3* variant, P18, n=6645 (C) m.13514A>G *MTND5* variant, P19, n = 2730 (D) m.13094T>C *MTND5* variant, P21, n=3979 (E) m.13513G>A *MTND5* variant, P23, n=10009 (F) m.13513G>A *MTND5* variant, P24, n =575 (G) m.13513G>A *MTND5* variant, P25, n = 1168. Each dot represents a single muscle fibre, colour co-ordinated according to its mitochondrial mass: very low – blue, Low - light blue, Normal – beige, High – orange, very high -red. Black dashed lines represent the SD limits for the classification of the fibres. Lines adjacent to X and Y axis represent the levels of NDUFB8 and COX-1: beige: normal (<-3), light beige: intermediate (+) (-3 to -4.5), light blue: intermediate (-) (-4.5 to -6) and blue: deficient (> -6). Bold dashed lines indicate the mean expression level of normal fibres.

3.4.5. BN-PAGE assessing the steady-state levels of assembled Complex I

To further interrogate the quadruple immunofluorescent assay results observed in the subset of patients displaying normal NDUFB8 and NDUFS3 immunoreactivity, BN-PAGE analysis was performed to assess the steady-state levels of fully assembled Complex I (980 kDa) where muscle was available for patients (P18, P19, P21, P22, P23 and P25). P17 was also included as a positive control in this analysis given that the assay had shown decreased levels of NDUFB8 immunoreactivity. The samples prepared for BN-PAGE analysis retain OXPHOS complexes in their structural and active form, permitting the investigation of any effects on the assembly of the holoenzyme or catalytic activity. However, as the measured residual Complex I activity had previously been undertaken spectrophotometrically, only the levels of fully assembled Complex I were assessed.

The analysis of muscle mitochondrial fractions by BN-PAGE revealed a decrease in steady-state levels of fully-assembled Complex I in P17, P18, P23 and, P24 (**Figure 3.16**) when compared to controls, indicating that the mutations harboured by these patients affect levels of fully assembled Complex I. As Complex II activity is normal in these patients, the SDHA subunit was labelled (detected by immunoreactivity against the SDHA subunit) and the steady-state levels of assembled Complex II was used as a loading control. By contrast, patients P19, P21 and P22 showed normal levels of fully assembled Complex I, which falls in line with the findings from the assay, therefore likely indicating that these mutations affect the activity of the complex rather than the assembly.

The level of Complex I was also normal in P25, correlating with the findings from the quadruple immunofluorescence assay (**Figure 3.16**). Furthermore, the residual, biochemical Complex I activity measured spectrophotometrically was also 100%, indicating that the m.13513G>A, p.(Asp393Asn) variant in this case has no major effect on the activity or assembly of Complex I, despite the relatively high level of mtDNA heteroplasmy and severe clinical phenotypes (**Table 3.2**).

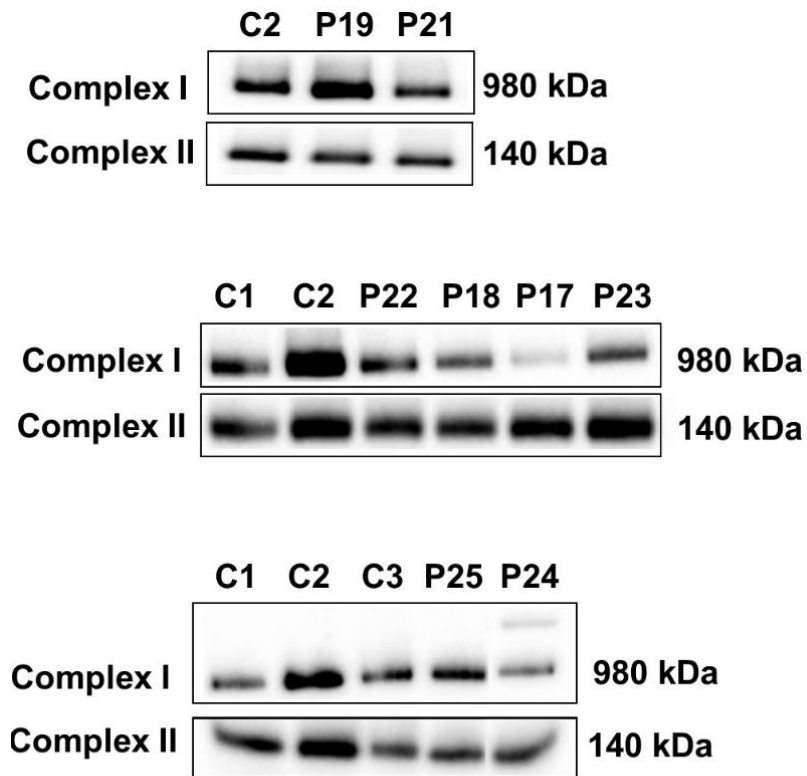


Figure 3.16: Analysis of Complex I assembly by BN-PAGE.

Complex I assembly profiles were analysed using one BN-PAGE (4-16% gradient). Analysis showed a decrease in fully assembled Complex I in patients P17, P18, P23 and P24, whilst normal assembly is seen in patients P19, P21, P22 and P25. Complex II was used as a loading control. Both OXPHOS complexes were detected by immunoblotting using subunit specific antibodies – NDUFB8 (Complex I) and SDHA (Complex II). No assembly intermediates were visualised in these patient samples however an additional band was observed for P24, above 980kDa which is indicative of supercomplex as mass is bigger than that of Complex I.

Considering these findings from the BN-PAGE assessment, **Table 3.6** summarises all the experimental data collected for these patients which will then be discussed in the following section.

Table 3.6: A summary of all experimental data for the cohort of patients with isolated Complex I deficiency

Patient ID	Complex I deficiency (%) quadruple immunofluorescence assay	Complex IV deficiency (%) quadruple immunofluorescence assay	BN-PAGE (steady-state levels of Complex I)	Residual Complex I activity in skeletal muscle (%)*	Homogenate heteroplasmy (%)*
Nuclear-encoded Complex I structural subunits					
P01 ^a	79	0	Decreased	33	n.d
P02 ^b	93	0	Decreased	32	n.d
P03 ^c	39	0	Decreased	35	n.d
P04	98	0	n.d	39	n.d
P05	89	0	n.d	37	n.d
P06	79	0	n.d	5	n.d
P07	99	0	n.d	42	n.d
P08	96	0	n.d	26	n.d
Nuclear-encoded Complex I assembly factors					
P09	99	0	n.d	26	n.d
P10	96	0	n.d	45	n.d
P11	26	0	n.d	44	n.d
P12	96	0	n.d	31	n.d
P13	100	0	n.d	13	n.d
P14	100	0	n.d	13	n.d
P15 ^d	100	0	Complete absence	36	n.d
mtDNA-encoded Complex I structural subunits					
P16 ^e	92	0	Decreased	3	92
P17	90	0	Decreased	44	90
P18	0	0	Decreased	n.d	93
				(100% in fibroblasts)	
P19	0	0	Normal	27	66
P20 ^f	100	0	n.d	16	85
P21	0	0	Normal	59	58
P22	0	0	Normal	39	60
P23	0	0	Decreased	38	77
P24	0	0	Decreased	100	45
P25	0	0	Normal	100	63

*All homogenate heteroplasmy as measured in skeletal muscle section and the biochemical data relating to Complex I enzymatic activity in muscle was provided by the NHS Highly Specialised Service for Rare Mitochondrial Disorders laboratory team

P1^a = Patient 3 in Alston et al. (2016), JMG; P2^b = Patient 2 in Alston et al. (2016), JMG; P3^c = Patient 6 in Alston et al. (2016), JMG; P15^d = patient S1 in Alston et al (2016), AJHG; P16^e = Patient 1 in Gorman et al (2015), Clinical Science; P20^f = Patient published in Alston et al (2010) Neuromuscular disorders

n.d = not determined

3.5. Discussion

This study aimed to assess and validate the application of the quadruple immunofluorescent OXPHOS assay to the diagnosis of patients with isolated mitochondrial Complex I deficiency. The quadruple immunofluorescence assay, which detects NDUF8 as a marker of Complex I integrity, was successful in detecting Complex I deficiency in 18 of the 25 patients tested, including all patients with pathogenic variants in nuclear genes encoding Complex I structural subunits and assembly factors (Groups 1 and 2). However, only three of the ten patients harbouring pathogenic mtDNA variants (Group 3) showed a consistent decrease in NDUF8 immunoreactivity and thus protein abundance/expression, later confirmed using a further commercially available antibody against NDUF3, another key component of Complex I. The assay was optimised using a commercially available and widely-used antibody against NDUF8, a subunit which is assembled at the mid/late stage of assembly, alongside the mtDNA-encoded core structural subunit, ND5. Although, it would have been preferable to use an antibody targeting a mtDNA-encoded subunit, such as ND1 (interrogating the early stage of Complex I assembly), there are currently no robust, commercially-available antibodies raised against this or other mtDNA subunits which is important to consider if the assay is to be adopted across diagnostic centres.

Using this assay, Complex I deficiency was successfully detected in patients that harboured mutations in nuclear genes encoding either the accessory, (P1, P2, P3 = NDUF3 subunit of the P-D region of the P-module, P4 and P5 = NDUF4 subunit of the N-module, P6 = NDUF6 subunit of the N-Module, P7 = NDUF2 subunit of the Q-module) or the core subunits (P8 = NDUF3 subunit of the Q-module) of Complex I, in line with the biochemical findings which were obtained spectrophotometrically during the diagnosis of patients. Of interest, it was noted that despite patients P1, P2 and P3 harbouring the same genetic variant (p.Trp22Arg in NDUF3) and similar residual Complex I activities, the quadruple immunofluorescence assay findings showed variable levels of NDUF8 immunoreactivity (P1= 79%, P2 =93% P3 = 39%). However, these findings are consistent with the steady state levels of the NDUF8 subunit of Complex I on both a western and BN-PAGE originally reported by Alston and colleagues (2016), where it was shown that P1 and P2 (P3 and P2 respectively) had decreased protein levels when compared to P3 (P6 in Alston et al. (2016)). Taken together, the collective data highlights the potential of the assay to be a diagnostic tool for such cases and shows that all mutations in Group 1 exerted a similar effect on steady-state levels of fully assembled Complex I as previously documented (Alston et al. 2016; Kirby et al. 2004a; Petruzzella et al. 2001).

Similarly, the assay was able to diagnose all patients with genetic variants in Complex I assembly factors. As expected, mutation of these genes led to a decrease in Complex I assembly and accordingly the assay recorded a marked loss of Complex I immunoreactivity in many of the fibres analysed; a complete loss of NDUFB8 immunoreactivity (100% CI deficient fibres) was noted in P13, P14 (*ACAD9* variants) and P15 (*TMEM126B* variant), consistent with previous reports of severe Complex I deficiency in *ACAD9* and *TMEM126B* mutations (Alston et al. 2016; Haack et al. 2010; Nouws et al. 2010; Nouws et al. 2014). These two assembly factors, alongside with NDUFAF1, ECSIT and TIMMDC1 (illustrated in the assembly process of Complex I in **Figure 3.17**), form the ‘Mitochondrial Complex I assembly’ (MCIA) complex (Heide et al. 2012), which is associated with the assembly of the P_P submodule (that contains the ND2, ND3, ND4-L and ND6 mitochondrial- encoded subunits). Since depletion of *TMEM126B* leads to the accumulation of the Q/P_P-a (Q module-ND1) intermediate, it seems that NDUFB8 is unstable and as such degraded before the complete assembly of the holoenzyme, explaining why a complete loss of NDUFB8 protein is observed in all fibres (Guarani et al. 2015; Heide et al. 2012).

For patients in Group 3 (pathogenic variants in mtDNA-encoded Complex I structural subunits), the assay was able to detect Complex I deficiency in three patients (P16, P17 and P20). The m.12425delA *MTND5* mutation in P20 leads to a truncated form of the ND5 subunit to be translated, which has previously been shown to have a severe impact on Complex I assembly (Alston et al. 2010). This was supported by the quadruple immunofluorescence assay results, where a complete loss of NDUFB8 immunoreactivity (100% Complex I-deficient fibres) was observed. Similarly, P16 harbours a m.3356T>C, p.(Met17Thr) *MTND1* variant at high levels in muscle, which is associated with a severe defect in Complex I assembly (Gorman et al. 2015b), validating the results from the assay (>90% Complex I-deficient fibres). Finally, P17 harbours a m.10158T>C, p. (Ser34Pro) *MTND3* variant, leading to a marked decrease in NDUFB8 immunoreactivity and steady-state levels of fully-assembled Complex I; together these results show that the quadruple immunofluorescence assay confidently detected the deficiency associated with mtDNA variants which have a severe impact upon Complex I assembly.

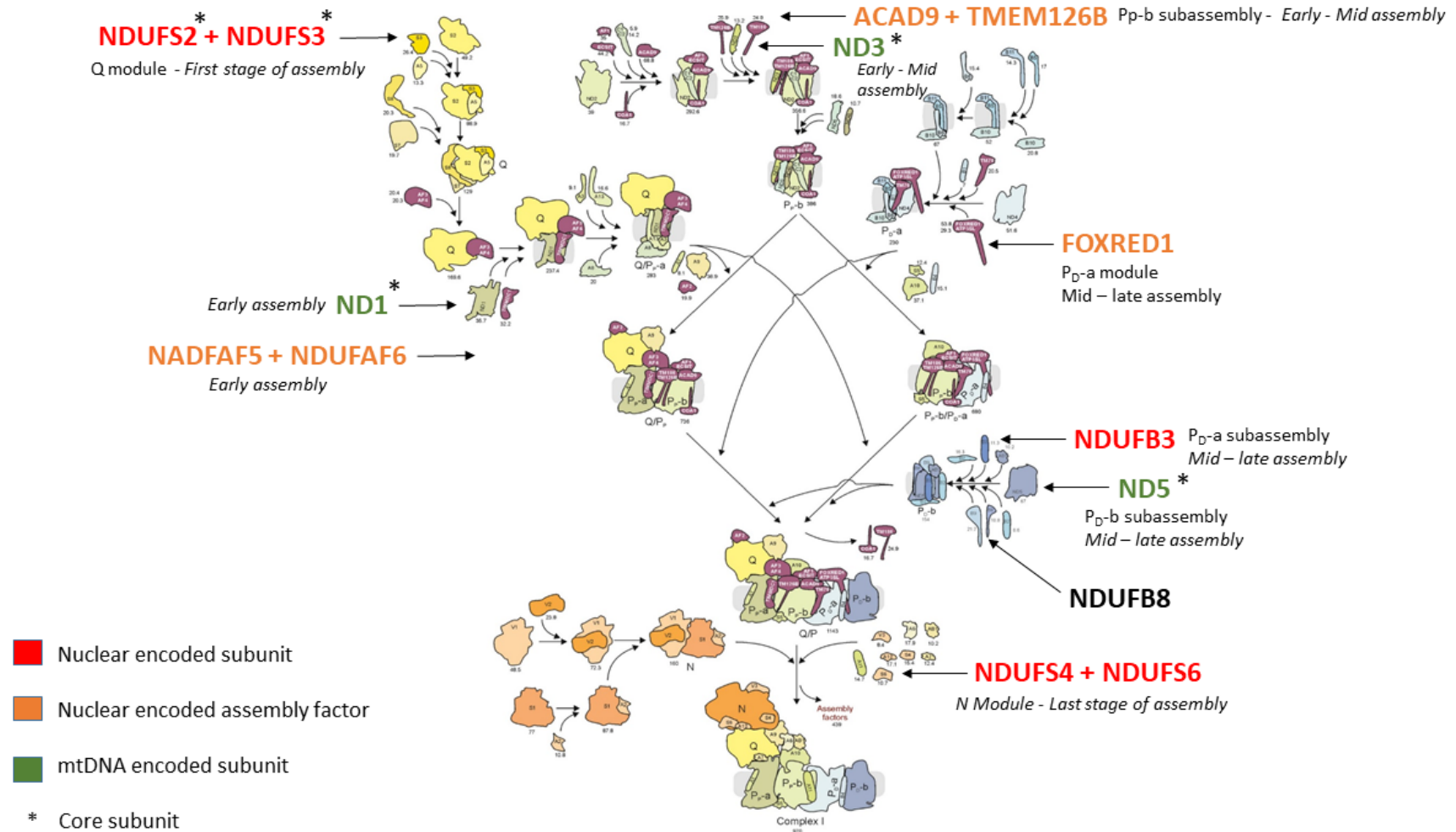


Figure 3.17: The assembly of Complex I with indication of where the subunits affected in the cohort of patients enter the complex.

Indicated under the names of subunit is the modules associated with them and the period of the assembly process. Adapted from Guerrero-Castillo et al., 2017.

The remaining seven patients, where normal NDUFB8 (and, where tested, NDUFS3) immunoreactivity was detected, harbour well-characterised pathogenic variants in either the *MTND5* (P19, P21, P22, P23, P24 and P25) or *MTND3* genes (P18). It has been shown that missense variants in these proteins predominantly affect Complex I redox activity whereas mutations in the *MTND1*, *MTND2* and *MTND6* genes have a more severe impact on complex assembly (Andrews et al. 2013; Kirby et al. 2004a; Lazarou et al. 2009; McFarland et al. 2004; Perales-Clemente et al. 2010; Ugalde et al. 2003). Therefore it can be suspected that in the patients where normal levels of Complex I was detected based on both the assay and BN-PAGE analysis (P19: *MTND5*, m.13514A>G, p.(Asp393Gly); P21: *MTND5*, m.13094T>C, p.(Val253Thr); P22: *MTND5*, m.13513G>A, p.(Asp393Asn)), the mutations are likely to be only affecting the catalytic site of the holoenzyme without disturbing Complex I stability and assembly. In line with this, the m.13514A>G *MTND5* mutation (P19) has been shown to affect the redox activity of Complex I (Bugiani et al. 2004; Corona et al. 2001; Lebon et al. 2003). The change of amino acid at position 393 (which is part of a putative quinone-reactive site of the enzyme), causes a loss of the putative quinone-reactive site, thereby leading to a decline in Complex I activity (Blok et al. 2007; Fisher and Rich 2000), thus validating the findings from the quadruple immunofluorescence assay. Therefore, patients who harbour mtDNA variants which only affect Complex I catalytic activity are likely to show normal mitochondrial respiratory chain profiles as determined by the assay.

Furthermore, many studies have also shown that defects in the *MTND3* and *MTND5* genes display variable biochemical phenotypes; either decreased redox activities as determined by biochemical spectrophotometric assays, decreased levels of fully assembled Complex I or both (Bugiani et al. 2004; Chae et al. 2007; Chol et al. 2003; Corona et al. 2001; Hanna et al. 1998; Kirby et al. 2003; Kirby et al. 2004a; Lebon et al. 2003; Petruzzella et al. 2001; Santorelli et al. 1997; Sarzi et al. 2007; Shanske et al. 2008). This supports the variability found in the results determined by the assay, as the m.13513G>A, p.(Asp393Asn) variant, the most frequently occurring mutation in the *MTND5* gene (Shanske et al. 2008), can manifest differing effects: either a decrease in fully assembled Complex I (P23 and P24) or normal levels of assembled Complex I (P25) (Blok et al. 2007; Bugiani et al. 2004; Chol et al. 2003; Corona et al. 2001; Hanna et al. 1998; Kirby et al. 2003; Petruzzella et al. 2001; Santorelli et al. 1997; Shanske et al. 2008). Somewhat surprisingly, P25 (homogenate m.13513G>A heteroplasmy level of 63% in muscle) also presented with normal redox catalytic activity and Complex I assembly profile, which could likely be due to the confounding factor of heteroplasmy level. While most pathogenic mtDNA variants are proposed to cause a

biochemical defect only when the levels of mutated mtDNA exceeds 80-90% (Mariotti et al. 1994), lower thresholds are reported in patients with Complex I deficiency due to structural subunit mutation (Corona et al. 2001; Kirby et al. 2004a). In the case of P25, it could be possible that the pathogenic threshold in this patient is higher, thereby explaining the absence of a biochemical defect despite the presence of relatively high mutation levels and an associated clinical phenotype. Additionally, it would be important to factor in the age of this patient (a paediatric case), as well as the severity of the clinical phenotype. It could also be suspected that there is a compensatory mechanism which is allowing for the normal assembly and activity of Complex I in this patient.

Finally, normal NDUFB8 immunoreactivity but decreased levels of fully-assembled Complex I was detected in patient P18 harbouring a pathogenic m.10197G>A, p.(Ala47Thr) *MTND3* variant. This has previously been associated with decreased redox catalytic activity and diminished levels of fully assembled Complex I (Chae et al. 2007; Kirby et al. 2004a; Sarzi et al. 2007); although unfortunately due to inadequate amounts of skeletal muscle tissue from this patient, it was not possible to verify if an effect on the activity was also present. The quadruple immunofluorescence data indicates, however, that the subunit must be present as the NDUFB8 level was normal. Interrogating NDUFS3 levels also showed normal results, suggesting that the assay is less likely to identify Complex I defects associated with pathogenic variants causing milder defects in Complex I assembly.

Overall, the assay has been shown to be a beneficial tool for assessing Complex I deficiency, however this is predominantly based on the successful detection of decreased Complex I protein expression in the skeletal muscle sections of patients harbouring pathogenic variants affecting nuclear-encoded subunits and assembly factors. Therefore, the question of “what is the exact role of the quadruple immunofluorescence assay in the diagnostic setting?” arises. As previously emphasised, one of the major advantages of the assay is that the biochemical status of Complex I and Complex IV expression can be deduced from a single 10µm section, which is pertinent in cases where there is a shortage of skeletal muscle tissue from a patient or for paediatric cases where biopsy samples are small in size. However, at a time when the diagnostic process is moving towards the “Genetics first” approach, where and when does this assay fit into this diagnostic approach?

Figure 3.18 highlights a flowchart designating the role of the assay in this current diagnostic pathway. Firstly, in cases where a diagnosis is achieved following the sequencing of either the mtDNA or nuclear DNA-encoded genes (WGS, WES, targeted-panels) after clinical assessment, there is no further requirement of a muscle biopsy; therefore no requirement for

the assay. However, the assay can be used as a way of validating a novel genetic variant to investigate the impact on OXPHOS (determine a biochemical defect). In cases where a diagnosis is not reached via the “Genetic first approach”, this assay can then be used as a diagnostic tool using patient skeletal muscle section to determine a biochemical defect. These findings, potentially alongside other functional assays (spectrophotometric enzymatic assays, BN-PAGE), can then re-direct the screening of the mitochondrial genome or candidate nuclear-encoded genes. As previously stated, in cases where the assay fails to detect deficiency, results from this study would suggest that a direct investigation of the mtDNA needs to be undertaken through NGS, for example patients with point mutations on mtDNA-encoded subunits (particularly *MTND5*) displayed normal expression of Complex I in their skeletal muscle sections. However, time constraints and expense must also be considered which leads to the next question of how necessary and helpful would it be to have all this information for patients? It can be argued that it is helpful given that this study has shown that in some cases, the different algorithms confirm differing impacts of mutations on Complex I, for example, it can be used to identify patients who have Complex I deficiency due to decreased expression or assembly of Complex I as opposed to those who have purely reduced enzymatic activity. Therefore, it can be helpful to have all information, particularly during the functional characterisation of novel genes.

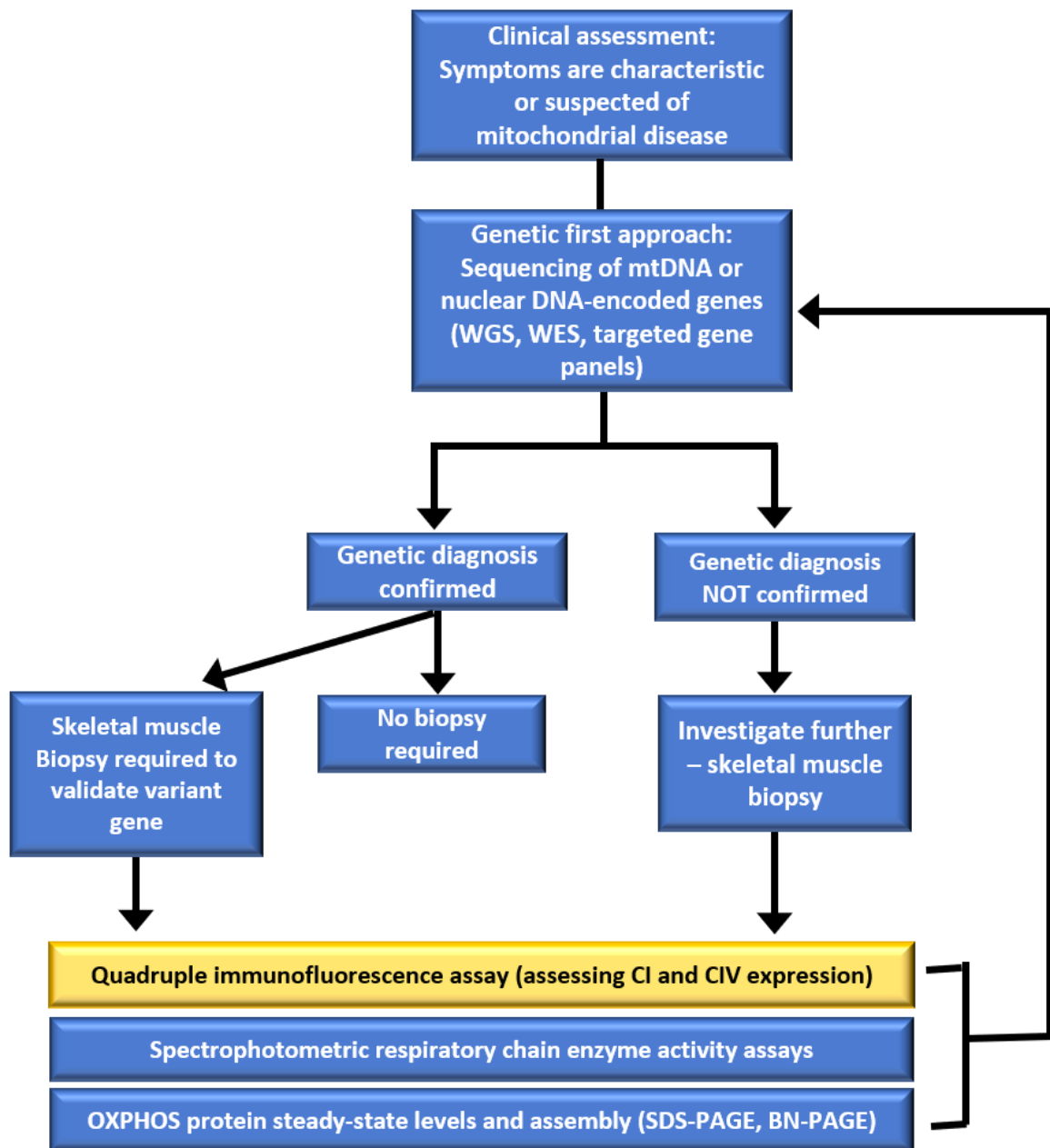


Figure 3.18: A schematic flowchart designating the role of the quadruple immunofluorescence assay in the current diagnostic process for Mitochondrial disease.

The diagnosis of Mitochondrial Disease is being led by the “Genetic first approach” which will lead to either a confirmation of the diagnosis and so no skeletal muscle biopsy will be required. But if the genetic variant is novel or further validation is required, then a biopsy and the quadruple immunofluorescence assay (highlighted by yellow box) on a 10µm section will be helpful to give clarification of an OXPHOS (oxidative phosphorylation) defect, alongside other functional tests (spectrophotometric respiratory chain enzyme assay and BN-PAGE and SDS-PAGE to assess protein steady-state levels and assembled complexes). However, if no diagnosis is reached via the pathway, then the assay can be used a diagnostic tool to investigate the 10µm patient skeletal muscle section further for OXPHOS assessment. Findings from the assay alongside the other functional assays, can then re-direct the screening of mtDNA or nuclear-encoded genes.

3.6. Limitations of this study

Although this study has been able to show the diagnostic properties of the quadruple immunofluorescence assay, a few limitations to this study must be considered.

Firstly, whilst NDUF8 is commercially available and widely used in both research and in the diagnostic setting, a limitation for this study is the absence of antibodies which target mtDNA-encoded subunits of Complex I. Whilst ND1 was tested and seen to have failed in the use of the assay, a commercially available antibody could have provided a helpful tool to interrogate an mtDNA-encoded subunit which is involved at the initial stage of Complex I assembly, similar to NDUF3. A comparison between the two antibodies (NDUF8 and ND1) could have been undertaken to highlight the extent at which the assay is able to detect Complex I deficiency in these cases, particularly within the patients that showed normal levels of both NDUF8 and NDUF3.

Secondly, another limitation to the assay is that it is not cost or time effective and thus could potentially hinder the approach to a certain extent in a diagnostic setting.

Thirdly, another limitation to this study is the use of the adult-derived control tissues to analyse paediatric cases. Ideally, non-disease controls and cases should have been aged-matched in order to ensure that analysis of paediatric cases were based on the expected levels of porin in very small fibres compared to the adult fibres, which are much larger in size. In addition, muscle biopsies taken from these individuals who underwent ACL surgery may not be representative of the area from which biopsies of patients are attained from for diagnostic purposes (quadriceps and TA). However, these limitations could not be accounted for as biopsies attained from non-disease participants who are entirely healthy with no physical injury, is difficult to obtain. Thus, these ACL biopsies were sufficient for these studies (including Chapter 4), further justified by the fact that both histochemical investigations (undertaken by the NHS Highly Specialised Service for Rare Mitochondrial Disorders, located within the Wellcome Centre for Mitochondrial Research at Newcastle University) and immunofluorescent investigations showed normal protein expression of both Complex I and Complex IV, prior to use in studies.

3.7. Conclusion

In conclusion, this study has accessed and validated the use of a quadruple immunofluorescence assay in a diagnostic setting for identifying patients with suspected Complex I deficiency, using a single 10µm transverse skeletal muscle section. Through the application of the assay, it was possible to directly quantify the varying levels of NDUF8

protein abundance at a single cell level, a key advantage of the assay in comparison to current histochemical and histological methodologies. Given the findings attained, this study can provide evidence that this assay has clear diagnostic potential for patients with Complex I deficiency, particularly for those with mutations affecting nuclear-encoded genes, which account for ~75-80% of genetic causes of Complex I deficiency. Whilst the assay is not sufficiently sensitive to identify a biochemical defect associated with some very well-characterised mtDNA variants – or rare catalytic defects affecting either mtDNA-encoded or nuclear-encoded Complex I subunits, it can be emphasised that a combination of the quadruple immunofluorescence assay, in tandem with full mitochondrial genome sequencing and standard biochemical assays, the assay can be used to investigate likely genetic causes of Complex I deficiency in patients with mitochondrial disease (principally pathogenic variants associated with clinical symptoms that may result from mutation of mtDNA-encoded structural Complex I subunits), especially when muscle biopsy sample sizes are small, necessitating the analysis of cryosectioned material.

Therefore, it can be concluded that the assay can contribute to the current available diagnostic tools for studying mitochondrial disease, which are typified by extensive biochemical, genetic and clinical heterogeneity.

Chapter 4: Using the quadruple immunofluorescence assay to determine the OXPHOS biochemical profile of individual skeletal muscle fibres from patients with the m.3243A>G variant.

4.1. Introduction

This chapter will be describing the findings from the second theme of this thesis; understanding the mechanism underlying mitochondrial disease. This section will introduce the background, current proposed pathological mechanisms and clinical features associated with the m.3243A>G pathogenic variant, to underpin the understanding of the aims of this chapter and **Chapter 5**.

4.1.1. The m.3243A>G pathogenic variant

The m.3243A>G variant is the most prevalent pathogenic heteroplasmic point mutation of the mtDNA (Elliott et al. 2008; Gorman et al. 2016; Nesbitt et al. 2013). The mutation is located within the *MT-TLI* gene which encodes mitochondrial tRNA^{Leu(UUR)} (Anderson et al. 1981). A single nucleotide substitution of adenine (A) to guanine (G) occurs at position 3243 within the dihydrouridine loop (D-loop, also known as the DHU loop) of the tRNA^{Leu(UUR)} (**Figure 4.1**) (Goto et al. 1990). The normal function of the tRNA^{Leu(UUR)} gene is the translation of the UUR (R = A or G) leucine codons (UUA or UUG), hence the nomenclature tRNA^{Leu(UUR)} (Kobayashi et al. 1990).

The structure of the mt-tRNA^{Leu(UUR)} is shown in **Figure 4.1**. The tertiary structure of the mt-tRNA consists of four domains; acceptor stem, dihydrouridine (DHU/D loop), anticodon loop and the TΨC (T) loop. These four domains primarily exist as Watson-Crick base pairs which allows for the cloverleaf structure. Mitochondrial tRNAs undergo extensive post-transcriptional maturation and modifications which are essential for the stability and function of their structures. One such modification includes the addition of the CCA sequence (by the CCA-adding enzymes) at the 3' end of the mt-tRNA that represents the site of aminoacylation. This sequence is also important for tRNA positioning in the ribosome and translation termination. The “wobble” base at position U34 is one of the key tRNA positions for modification to occur, particularly the taurinomethyluridine (τm5U) modification (further described in **section 4.1.3**). Other modifications of mt-tRNA^{Leu(UUR)} are also depicted in **Figure 4.1** which include; 1-methyladenosine (m1A), 1-methylguanosine (m1G), 2-methylguanosine (m2G), pseudouridine (Ψ), ribothymidine (T), dihydrouridine (D), and 5-methylcytidine (m5C). These post-transcriptionally modified nucleotides ensure proper stability and function which include base stacking, modulate codon-anticodon binding, allowing rigidity or flexibility in the structure of the mt-tRNA, enhance or restrict codon recognition or to facilitate translocation (D'Souza and Minczuk 2018; Kamble et al. 2017; Kirino et al. 2004; Lorenz et al. 2017).

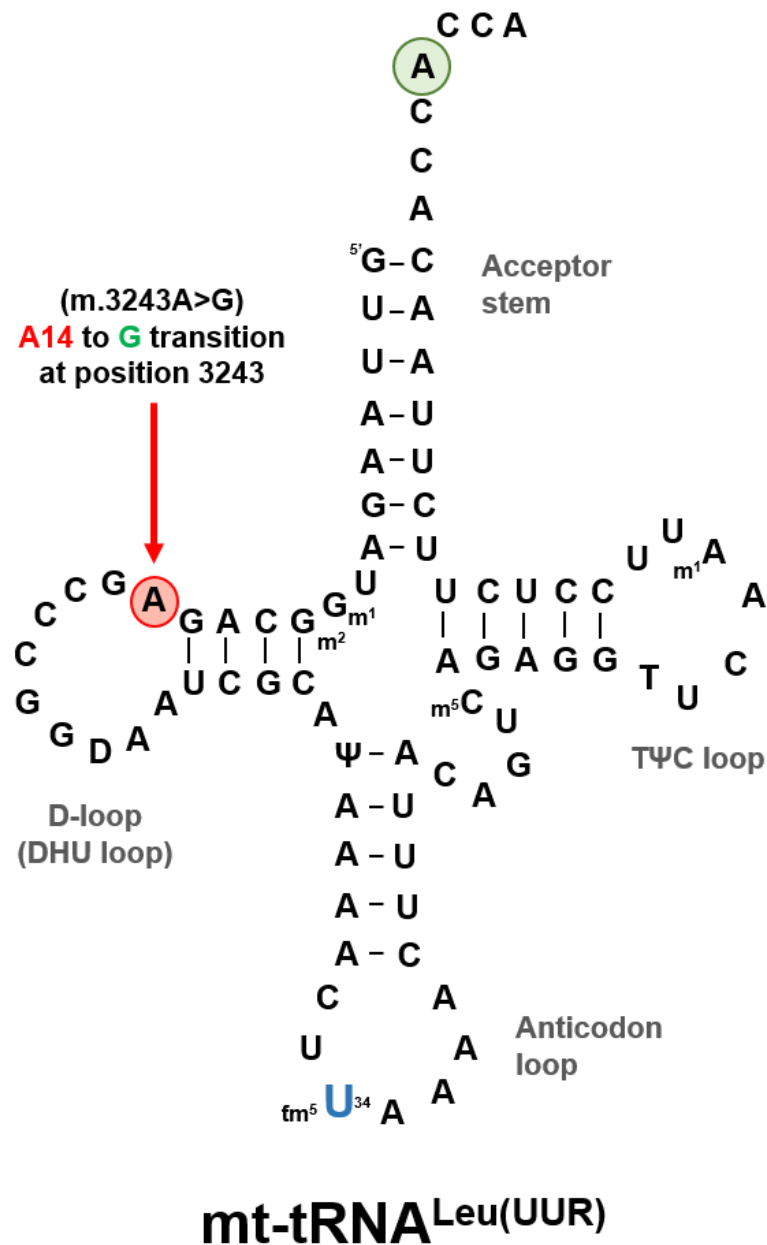


Figure 4.1: A schematic diagram of the cloverleaf secondary structure of mitochondrial tRNA^{Leu} (UUR).

Mitochondrial (mt) tRNA consist of four domains; acceptor stem, dihydrouridine (DHU/D) loop, anticodon loop and the TΨC (T) loop. The A14 nucleotide (encircled in red) of the D-loop/DHU loop is substituted by a guanine residue in the m.3243A>G mutation, as indicated by the arrow. Mitochondrial tRNAs undergo multiple post-transcriptional modifications; the uridine (U in blue) at position 34 (the “wobble” base) is subjected to post-translational modification to become 5-taurinomethyluridine (τm⁵U). Symbol for other modifications; 1-methyladenosine (m¹A), 1-methylguanosine (m¹G), 2-methylguanosine (m²G), pseudouridine (Ψ), ribothymidine (T), dihydrouridine (D), and 5-methylcytidine (m⁵C). The CCA sequence above the discriminator codon (A encircled in green) is the site of aminoacylation and is also added on post-transcriptionally. Adapted from (Wittenhagen and Kelley 2002).

4.1.2. Epidemiology of the mutation

Epidemiological studies have estimated the m.3243A>G mutation prevalence as 7.59-7.8/100,000 in the population of North-East England (Chinnery et al. 2000; Gorman et al. 2015a) and 16.3/100,000 in the population of Northern Finland (Majamaa et al. 1998). The carrier estimate in the population of an Australia cohort was determined to be 236/100,000 in a study undertaken by Manwaring et al. (2007). In the United Kingdom, the MitoCohort consists of 1775 patients (as of October 2019) with mitochondrial disease across all of the sites (Newcastle University, University College London Hospitals and Oxford University Hospitals), of which 455 patients have their genotype recorded as m.3243A>G. More specifically, 292 patients harbouring the mutation are registered with the Newcastle upon Tyne mitochondrial disease clinic.

4.1.3. Mechanisms leading to pathogenicity of the mutation

A plethora of studies have been undertaken to determine the mechanism by which the m.3243A>G mutation causes pathogenicity. These studies have predominantly used *transmitochondrial* cybrid cellular systems; models which are used to study the pathophysiological consequences of a specific mtDNA variant in a control nuclear background. These cell lines are generated by fusing the patient's cytoplasts (enucleated cells that contain mtDNA) with a cell line that lacks mtDNA (rho zero), to produce clones with mixed mitochondrial populations. The use of these cells to study the m.3243A>G mutation allowed for the characterisation of the biochemical phenotypes across different levels of heteroplasmy, as well as investigating the mechanisms. An advantage of this approach is that it provides a uniform nuclear background for studies using cytoplasts made from different individuals, thereby eliminating confounding nuclear variables. However, this is not the case for studies investigating the m.3243A>G mutation (particularly in MELAS) which have used either *transmitochondrial* cybrid cells made from human osteosarcoma derived rho zero cell lines (143B-206) (Chomyn et al. 1992; Chomyn et al. 2000; Janssen et al. 1999; Janssen et al. 2007b; King et al. 1992) or lung carcinoma (A549) (Dunbar et al. 1995). Another is the WS227.546 cell line (Park et al. 2003). Using these different cell lines re-introduces the confounding effects of different nuclear genetic backgrounds, which have been shown to influence the segregation of mutant and wild-type mtDNA, therefore influencing the genotype-phenotype relationship being investigated in these studies. For example, the 143B-206 cell line showed an increase/shift towards higher proportions of mutant mtDNA whilst the A549 cell line showed an increase/shift towards higher proportions of wild-type mtDNA (Dunbar et al. 1995). This will be discussed further in **Chapter 5**. Other studies have used

patient cells (such as myoblasts or lymphoblastoid) and tissue (muscle biopsies) (Borner et al. 2000; Sasarman et al. 2008) but also have the issue of confounding effects of different nuclear genomes.

Whilst the precise mechanism is still under debate, some proposed mechanisms at the molecular level of the mutation have been suggested by these studies and are listed below in **Table 4.1**. Any of the mechanisms described can be debated to be the correct mechanism but it is evident that current findings are either overlapping or conflicting with one another, thus indicating the need for further research. A number of the studies have suggested that the mechanism involves impaired translation of all mitochondrial respiratory chain subunits which consequently results in the decrease in ATP synthesis (Chomyn et al. 1992; Goto et al. 1990; Janssen et al. 1999; King et al. 1992; Koga et al. 1993). This would be an acceptable mechanism as the role of mt-tRNA is to transport amino acids to the ribosomes leading to translation and eventual protein synthesis. However, emphasis has been placed on the taurine modification of the anticodon wobble base theory, particularly within MELAS patients. In normal mt-tRNA^{Leu(UUR)}, uridine at the anticodon wobble position undergoes post translational modification, known as the taurine modification of uridine (5-taurinomethyluridine ($\tau\text{m}^5\text{U}$)). This modification at the wobble position allows for the precise and efficient codon recognition by the tRNA (Yokoyama et al. 1985). However, in the case of the m.3243A>G mutation within *transmitochondrial* cybrid cell lines, this modification does not occur therefore the mutant mt-tRNA^{Leu(UUR)} is deficient of the normal $\tau\text{m}^5\text{U}$ (Suzuki et al. 2002; Yasukawa et al. 2000). This results in impaired protein synthesis either through misreading according to the mitochondrial wobble rule (Watanabe 2010) or a decoding deficiency (Hanada et al. 2001; Takemoto et al. 1995). The study by Kirino et al. (2005) demonstrated that there was a specific correlation between this lack of modification and the clinical features of MELAS, whilst normal modification was described in patient tissue or *transmitochondrial* cell lines harbouring other MT-TL1 mutations associated with non-MELAS phenotypes (m.3242A>G, m.3250T>C and m.3245C>T). This interest in the mechanism had led to investigation into taurine therapy as potential treatment for MELAS patients, however the study concluded that ongoing research will confirm whether or not oral administration of taurine may be an effective therapy (Rikimaru et al. 2012).

However, the change in the L-shaped tertiary structure of the tRNA^{Leu(UUR)} is a likely starting point at which further mechanisms that lead to the pathogenicity of the mutation occur. This is in agreement with Chomyn et al. (2000) who proposed the following; the m.3243A>G mutation causes an alteration to the structure of tRNA^{Leu(UUR)} and a deficiency in the taurine

modification at the wobble position. This results in an unstable molecule (metabolically) and reduction in aminoacylation, causing a decrease in protein synthesis due to reduced association of the mRNA with the ribosomes, which is thought to have an effect on mitochondrial translation factor, such as IF-2_{mt} (Ma and Spremulli 1995). Therefore, after the alteration of the structure, it could be suggested that these mechanisms are all in interplay with one another.

Table 4.1: Proposed mechanisms for the pathogenicity of the *m.3243A>G* mutations and key findings from the studies undertaken

Mechanism and reference	Study findings
Impairment of transcription termination	
Hess et al. (1991)	<ul style="list-style-type: none"> - Mutation caused a decrease in the affinity of mt-TERM (also known as MTERF) to its binding site on the mtDNA which spans between the nucleotides 3229 and 3256 on the region of the <i>MT-TL1</i> gene - Leads to the impairment of transcription termination at the end of the 16S rRNA gene which causes interference in the efficiency and proper synthesis of 16S rRNA
Chomyn et al. (1992)	<ul style="list-style-type: none"> - Mutation causes no change in the rRNA levels in relation to the transcripts from upstream and downstream of the termination site - The mitochondrial protein synthesis rate was decreased
King et al. (1992)	<ul style="list-style-type: none"> - Determined a small but consistent accumulation in the steady state levels of the unprocessed intermediate RNA transcript RNA19 (an intermediate transcript contains the transcripts for 16S rRNA + tRNA^{Leu(URR)} + ND1 genes), in cells with very high levels of the mutation - The mitochondrial protein synthesis rate was decreased - ND1 subunit of Complex I was shown to be slightly altered in mobility on polyacrylamide gel electrophoresis - No significant difference was found in steady state levels of RNA species between controls and mutant cells
Schon et al., 1992	<ul style="list-style-type: none"> - Incorporation of the unprocessed RNA19 into the mitochondrial ribosome renders it functionally defective - Causes eventual protein synthesis defects, likely due to the stalling of translation by the ribosomes
Alterations to the L-shaped tertiary structure	
Wittenhagen and Kelley (2002)	<ul style="list-style-type: none"> - Mutation affects the tertiary structure of tRNA^{Leu(URR)} by inducing abnormal tRNA dimerization of the molecule at the D-stem (self-complementary hexanucleotide (5'GGGCCC;G mutation site) - This attenuates the aminoacylation of the tRNA^{Leu(URR)} thereby leading to a decrease in the biological activity of the tRNA
Taurine modification of the anticodon wobble base	
Yasukawa et al. (2000) Suzuki et al. (2002)	<ul style="list-style-type: none"> - Uridine modification does not occur in <i>trans</i>mitochondrial cybrid cell lines harbouring the mutation

Watanabe (2010)	- Lack of modification results in impaired protein synthesis through misreading according to the mitochondrial wobble rule
Takemoto et al. (1995) Hanada et al. (2001)	- Lack of modification results in decoding deficiency
Kirino et al. (2004)	- <i>Transmitochondrial</i> cells containing constructs of the mt-tRNA ^{Leu(UUR)} molecule lacking the taurine modification ($\tau\text{m}^5\text{U}$ deficiency) showed severe and specific reduction in the UUG decoding, as well as UUA decoding
<i>Decreased steady-levels of tRNA^{Leu(UUR)}</i>	
Janssen et al. (1999)	- Mutation caused a decrease in the steady-state levels of the mt-tRNA ^{Leu(UUR)} molecule which consequently caused a decrease in mitochondrial translation
Chomyn et al. (2000)	- Mutation affected both the steady state levels and aminoacylation efficiency of the molecule, affecting the rate of translation.
<i>Misincorporation of amino acids</i>	
Janssen et al. (2007b)	- <i>Transmitochondrial</i> cells (143B) showed that COX-I and COX-II existed exclusively with the correct amino acid sequence, thus no evidence of misincorporation - Evidence of correct incorporation of leucine occurring at the UUR codons
Sasarman et al. (2008)	- Mutation was found to cause severe combined respiratory chain deficiency in near homoplasmic myoblasts (complete lack of assembly of complexes I, IV and V was observed) - Indicated that amino acids were being misincorporated during protein synthesis in the presence of the mutation - Overall protein synthesis remained close to normal - A loss and gain of function of the tRNA ^{Leu(UUR)} occurring in the presence of the mutation to cause the severe respiratory chain deficiency.
<i>Defects in aminoacylation</i>	
Borner et al. (2000)	- Eight patient samples (seven muscle biopsies and one lymphoblastoid cell line) of which four samples had a decrease in the mutated tRNA ^{Leu(UUR)} in the total tRNA ^{Leu(UUR)} population, indicating that there was a reduction in the expression of the mutated molecule - Reduction in the levels of functional tRNA ^{Leu(UUR)} - Six patients samples showed a reduction in the amount of aminoacylated tRNA ^{Leu(UUR)} - Variability founded in patient samples alluded to involvement of additional factors that are contributing towards the pathogenicity of the mutation
Yasukawa et al. (2000)	- Proposed that the decrease in aminoacylated tRNA ^{Leu(UUR)} was a mechanism by which pathogenicity occurred - A substantial decrease in the steady state levels of the mutated tRNA ^{Leu(UUR)} , likely due to the decreased stability of molecule
Park et al. (2003)	- Mutation caused a 25-fold decrease in the aminoacylation efficiency of tRNA ^{Leu(UUR)} and this combined with the reduction in steady state levels of tRNA ^{Leu(UUR)} led to the reduction in the rates of protein translation in mutant cells - No detection of difference in aminoacylated efficiencies between the wild-type and mutant tRNA ^{Leu(UUR)} transcripts

4.1.4. Clinical phenotypes

The pathogenic m.3243A>G variant is associated with a vast clinical presentation and importantly, with multi-systemic disorders. The mutation was first reported in patients with MELAS and in one patient presenting with CPEO (Goto et al. 1990). MELAS is a severe and progressive multisystem disorder of either child or adult onset, with the vast majority of patients presenting between the ages of two and 40 (El-Hattab et al, 2001). This disorder is defined and diagnosed by the following criteria; stroke like episodes (SLE) before the age of 40, encephalopathy characterised by seizures, dementia or both and finally lactic acidosis with or without the presence of RRFs in skeletal muscle (Hirano et al. 1992). A second clinical diagnostic criteria has also been clarified by Yatsuga and colleagues (2012), whereby the individual can present with at least two symptoms from each of the categories distinguished; Category A (headaches and vomiting, seizures, hemiplegia, cortical blindness, acute focal lesions on neuroimaging) and Category B (high plasma or cerebral spinal fluid (CSF), mitochondrial abnormalities on muscle biopsy, a MELAS-related pathogenic variant) (Yatsuga et al. 2012). The mutation is commonly associated with MELAS, with approximately 80% of affected individuals being m.3243A>G carriers (Goto et al. 1990; Kobayashi et al. 1990). However, this syndrome only accounts for approximately 15% of patients who harbour the m.3243A>G mutation (Nesbitt et al. 2013).

The most common disorder which is associated with the mutation is MIDD (maternally inherited diabetes and deafness) (de Laat et al. 2013; Mancuso et al. 2014; Nesbitt et al. 2013), which was first reported by van den Ouweland et al. (1992). However, both MELAS and MIDD have been shown to have an overlap in clinical phenotypes: it has been reported that 13% of 199 affected members carrying the mutation had a combination of both MIDD and MELAS features (clinically known as MELAS/MIDD) (Gerbitz et al. 1995). Other phenotypes include; MERRF (myoclonus epilepsy with ragged red fibres) (Fabrizi et al. 1996), MELAS/MERRF (Campos et al. 1996), CPEO (Goto et al. 1990; Koga et al. 2000; Mariotti et al. 1995; Moraes et al. 1993b) and Leigh Syndrome (LS) (Koga et al. 2000; Vilarinho et al. 1997).

Many patients present with various other phenotypes that do not fit the criteria of the recognised clinical syndromes. These have been reported as; myopathy (Kärppä et al. 2005), cardiac abnormalities including cardiomyopathy (Anan et al. 1995; Bates et al. 2013; Hollingsworth et al. 2012; Majamaa-Voltti et al. 2002a; Nesbitt et al. 2013), dysphagia (de Laat et al. 2015), gastro intestinal (GI) dysmotility (Kaufmann et al. 2011; Nesbitt et al. 2013), isolated sensorineural hearing loss (Nesbitt et al. 2013), migraine (Ciafaloni et al.

1992; Nesbitt et al. 2013), diabetes mellitus (Kadowaki et al. 1994), renal failure (Damian et al. 1995; Iwasaki et al. 2001; Suzuki et al. 2003), short stature (Moraes et al. 1993a), ataxia (Petruzzella et al. 2004), cognitive impairment (El-Hattab et al. 2015), and depression/psychiatric involvement (Pickett et al. 2018; Verhaak et al. 2016).

A study by Pickett and colleagues (2018) determined the correlation between phenotypes and found that seizures, encephalopathy and SLE (MELAS phenotypes) were all statistically correlated with one another, as well as showing a correlation between hearing impairment and diabetes (MIDD phenotypes). The latter was also found to be statistically significant in the study by Mancuso et al. (2014). Asymptomatic carriers of m.3243A>G mutation have also been reported (Nesbitt et al. 2013).

In terms of mortality in patients harbouring the m.3243A>G mutation, both cardiac and neurological problems have been reported as the most common causes of early death in patients (Nesbitt et al. 2013). Sudden adult death syndrome has also been reported in both symptomatic and asymptomatic patients (Bates et al. 2013; Majamaa-Voltti et al. 2002b; Ng et al. 2016).

4.1.5. Muscle involvement in m.3243A>G patients

As shown above, muscle involvement is common in patients carrying the m.3243A>G variant. Individuals typically present with proximal limb weakness, ptosis and CPEO (Moraes et al. 1993a). Studies have shown the frequency of myopathy in patients to range between 25% (4 of 16 patients) to 61% (22 of 36 patients) (Deschauer et al. 2001; Hammans et al. 1995; Yatsuga et al. 2012). Nesbitt et al. (2013) showed that in the 36 patients who showed a spectrum of phenotypes different to the classical MELAS and MIDD disorders, muscle involvement and CNS were the most common phenotypes observed. Of these patients, 27% presented with proximal myopathy. A population based study undertaken by Kärppä et al. (2005) assessed the spectrum of myopathy in 50 patients harbouring the mutation. Half of the patients were clinically defined as myopathic, presenting as mild or moderate limb weakness defined by clinical observations comprising of patients possessing a waddling gait and symmetrical proximal myopathy. It was previously found that mild limb weakness was commonly observed in affected patients (Hammans et al. 1995). Other myopathic features found in patients included ptosis and CPEO (weakness of the levator muscle and the limitation of eye movements). Further to this study, patients have been found to show a reduction in muscle strength, for example de Laat et al. (2012) reported that 49.9% of patients displayed decreased muscle strength as well 29% of patients manifesting muscle weakness in the hip flexion or shoulder abduction. A further 16% of carriers were shown to have either

mild or moderate proximal muscle weakness. Lastly, exercise intolerance was indicated to be an important subtle sign of m.3243A>G related disease after patients were assessed with either the NMDAS (de Laat et al. 2012) or questionnaires (Kaufmann et al. 2011).

In terms of morphological analysis of muscle biopsies, the presence of RRFs (either COX-positive or deficient as detected by SDH staining) and/or COX-deficient fibres are found in the skeletal muscle sections of patients (Goto et al. 1990; Greaves et al. 2010; Jeppesen et al. 2006; Kärppä et al. 2005; Mimaki et al. 2009). However, in some patients, skeletal muscle may appear normal, particularly in MELAS patients (de Laat et al. 2016; Moraes et al. 1992), even when the Complex I and Complex IV activities were decreased (de Laat et al. 2016). Studies have quantified the proportion of COX-deficient fibres and RRFs in patients and it was shown that the RRFs found in MELAS patients were mostly COX-positive whereas patients with CPEO displayed RRFs that were predominantly COX-deficient (Moraes et al. 1993b; Petruzzella et al. 1994). Additionally, Jeppesen et al. (2006) investigated 51 biopsies of m.3243A>G patients and determined the frequency of abnormal fibres; 25 of 51 had more than 2% RRF and/or COX-deficient fibres, 10 had RRF fibres and COX-deficient fibres, 11 had only RRF fibres and 4 only had COX-deficient fibres. There is currently no literature about the protein expression of Complex I or III in skeletal muscle fibres of patients with m.3243A>G pathogenic variant.

4.1.6. Causes of phenotypic variation

This wide spectrum of clinical phenotypes observed in patients harbouring the m.3243A>G mutation is currently poorly understood. This leads to a complication in the clinical setting when considering the disease burden, with the long term prognosis being very difficult to predict in such patients (Chinnery and Turnbull 1997; Kaufmann et al. 2011; Mancuso et al. 2014). It is generally accepted that the severity of phenotype is correlated to high levels of heteroplasmy (Chinnery and Turnbull 1997; Hammans et al. 1995; Shoffner et al. 1990; Wallace et al. 1988). Although, this relationship is complicated by the variation in heteroplasmy between tissues, for example, muscle is known to harbour high levels of heteroplasmy whilst blood is shown to have less. In addition to this, ongoing research is showing that the phenotypically variability could be explained further by a number of factors, as listed below. The factors which are of interest to this thesis are only listed below but other factors have recently been reviewed in Boggan et al. (2019).

Heteroplasmy

Heteroplasmy has been suggested to be a critical factor contributing to the phenotypic variation observed within patients. The relationship between heteroplasmy level and clinical phenotypes has been extensively studied. Previous studies suggested that patients with high heteroplasmy levels in skeletal muscle presented at an early age with MELAS-like syndrome whilst those with lower heteroplasmy levels presented with less severe phenotypes such as CPEO, myopathy and deafness (Chinnery and Turnbull 1997; Hammans et al. 1995; Kandel et al. 2017; Moraes et al. 1993a; Petruzzella et al. 1994). This correlation between disease severity and phenotypic presentation was further exemplified by Koga et al. (2000) who showed that unrelated patients (n=5) with LS or MELAS had heteroplasmy levels of 92%, 87% and 74% respectively whilst those with CPEO or MIDD had levels of 33% and 5% respectively. In addition, the correlation between heteroplasmy level and specific phenotypic presentation was demonstrated by Jeppesen et al. (2006) where heteroplasmy levels of over 65% in skeletal muscle was correlated to both hearing impairment and diabetes (in 14 of the 51 patients). Furthermore, findings from the study by Pickett et al. (2018) who investigated 238 patients from the MitoCohort, showed that the following phenotypes were significantly associated with higher levels of heteroplasmy; hearing impairment, dystonia-dysarthria, diabetes, SLE, cerebellar ataxia, myopathy, cardiovascular involvement and encephalopathy.

However, the role of heteroplasmy in the phenotypic variation is further complicated by patients who harbour low m.3243A>G heteroplasmy levels but have severe phenotype expressions. For example, a study by Hollingsworth et al. (2012), reported two patients who presented with low m.3243A>G heteroplasmy levels in muscle, yet one patient was asymptomatic (aged 31 and heteroplasmy level of 24%) whilst the second patient presented with a severe MELAS phenotype (aged 46, heteroplasmy level of 26%), highlighting that heteroplasmy levels are a contributing factor towards the phenotypic variation, but does not fully explain it. This is further emphasised by the study undertaken by Grady et al. (2018), where it was shown that age, muscle heteroplasmy level and muscle mtDNA copy number explains only 40% of the variance in disease burden in m.3243A>G-related disease. The main aspect of heteroplasmy and threshold effect will be further discussed in **Chapter 5**.

Mitochondrial DNA copy number

Similarly, to heteroplasmy, mtDNA copy number also impacts the m.3243A>G mutation and therefore the clinical phenotype. Low mtDNA copy number in skeletal muscle of m.3243A>G patients has been associated with disease severity and progression (Grady et al. 2018). When

combining with both homogenate heteroplasmy and age, it was shown that mtDNA copy number accounted for 40% of the phenotypic variation.

The mtDNA copy number differs between cells, particularly in skeletal muscle due to the different fibre types. In patients with mitochondrial disease, a high proportion of wild-type mtDNA can have a compensatory effect against low levels of mutated mtDNA. Therefore, the fact that low mtDNA copy number leads to more severe disease is expected as there is no compensation from the wild-type copy number population. However studies have shown the existence of high levels of wild-type mtDNA copy number in deficient fibres, indicating that this compensatory mechanism was not capable of rescuing the cell phenotype and that high mtDNA copy number does not influence heteroplasmy level (Durham et al. 2007; Moraes et al. 1992; Tokunaga et al. 1994). Additionally, mtDNA copy number in individuals is likely to be influenced by the physical activity, for example a patient who is physically inactive will have low mtDNA copy number in comparison to a patient who is capable of physical activity (Grady et al. 2018).

Biological sex

The first report to show sex as a risk factor for SLE was by Mancuso et al. (2014) who demonstrated a significant prevalence of males in the MELAS phenotype group (33 males out of 51 participants – 67.4%) in comparison to the non-MELAS phenotype group (32 males out of 75 participants – 42.7%). There was no difference seen between the two groups of patients in terms of age of onset, disease duration and levels of m.3243A>G heteroplasmy levels in the three tissues examined (urine, blood and muscle). In addition to this, Pickett et al. (2018) also showed phenotypes in which the effect of sex was significant; males were seen to be a risk factor for ptosis and females for myopathy ($P=2.6 \times 10^{-3}$ and $P=7.9 \times 10^{-3}$ respectively, odds ratio less than 1). Consistent with the findings by Mancuso et al. (2014), this study also observed that males were more affected than females by SLE, however this did not reach significance, possibly due to different ascertainment strategies in the two studies.

Age

Disease caused by the m.3243A>G mutation is progressive, therefore, it is important to consider the age of patients in a clinical setting. It has been shown that higher severity of diabetes, hearing impairment, cerebellar ataxia and neuropathy are strongly associated with age (Pickett et al. 2018).

Nuclear background

The variation of phenotypes in patients could be due to the role of additive nuclear factors. This is supported by a study describing two pairs of monozygotic twins who showed extremely similar clinical courses within each pair; alongside this, the heteroplasmic ratios were also similar between the twins indicating that this may be regulated by nuclear genes (Maeda et al. 2016). The role of nuclear factors was also investigated by Pickett et al. (2018) who demonstrated high to moderate heritability estimates for hearing impairment, psychiatric involvement, cognition, migraine and cerebellar ataxia, thus highlighting a strong indication that the presence of nuclear effects influencing disease phenotype.

4.1.7. Biochemical features associated with the m.3243A>G variant

Mutations in mt-tRNA most likely lead to defects in mitochondrial translation, therefore all mtDNA-encoded OXPHOS complexes (Complex I, III, IV and V) would be affected. However, it is now evident that variable forms of mitochondrial respiratory chain deficiencies have been associated with the m.3243A>G mutation. Both patient skeletal muscles and *transmitochondrial* cybrid cells (either 143B-206 or A549) have shown either combined or isolated deficiencies of Complex I, II and IV (Chomyn et al. 2000; Ciafaloni et al. 1992; Dunbar et al. 1996; Flierl et al. 1997; Janssen et al. 2007a; Jeppesen et al. 2006; Mariotti et al. 1995). However, the dysfunction of Complex I (either loss of enzymatic activity or loss of protein) predominates in m.3243A>G carriers, particularly in MELAS patients (Fornuskova et al. 2008; Goto et al. 1992; Morgan-Hughes et al. 1995). Studies have also shown evidence for this predominance in patient muscle biopsies. Goto and colleagues (1992) showed that 13 of 40 MELAS patients had Complex I deficiency. Further to this, a study by Mariotti et al. (1995) investigated 19 patients of which nine showed decreased Complex I activity. Similar observations were also made by Jeppesen and colleagues (2006) and Morgan-Hughes and colleagues (1995). Additionally, using the quadruple immunofluorescence assay to directly interrogate the NDUF8 subunit of Complex I, Rocha et al. (2015) also highlighted the predominance of Complex I deficiency in five patients through the mitochondrial respiratory chain profile expression plots, indicated by the “left-shift” of individual single fibres as previously shown in **Chapter 3**.

The predominance of Complex I deficiency has been linked to the mechanism/s by which the mutation causes pathogenicity. A severe decrease in the rate of synthesis of both ND6 and ND5 subunits has been observed in *transmitochondrial* cell lines and patient-derived cells (Chomyn et al. 2000; Dunbar et al. 1996; Kirino et al. 2004; Sasarman et al. 2008). This has been attributed to the high UUG codon content in the ND6 polypeptide, thought to be as a

result of taurine modification deficiency which reduces the expression of UUG-dependent proteins (Kirino et al. 2005).

Some of these studies also showed that patients had Complex IV deficiency, mostly in combination with Complex I deficiency (Goto et al. 1992; Mariotti et al. 1995). Again, Rocha et al. (2015) showed Complex IV deficiency in the same four patients. The presence of COX-deficient fibres has been shown to be far less frequent in m.3243A>G carriers than both single, large-scale and multiple mtDNA deletion patients (Zierz et al. 2015).

4.2. Aims

The aims of the work presented in this chapter are two-fold. First, the aim was to characterise the biochemical profile of skeletal muscle sections from patients harbouring the m.3243A>G mutation from the MitoCohort. The study by Rocha et al., (2015) utilised the quadruple immunofluorescence assay to assess only a limited number of patients (n=5). However, it is evident that m.3243A>G patients are heterogeneous in their biochemical profile, therefore this current study utilised the assay in a larger and more comprehensive cohort of patients to capture this heterogeneity and to better characterise the protein expression of Complex I and Complex IV in single muscle fibres.

The second aim was to assess the relationship between the quantitative data from the quadruple immunofluorescence and the clinical data available for each patient.

4.3. Methods

4.3.1. Tissue samples and ethics

Skeletal muscle biopsies (either Tibialis Anterior muscle (TA) or Quadriceps (quads)) from 19 patients who harbour the m.3243A>G mutation were used for this study. The samples were requested from the Newcastle Mitochondrial Research Biobank (Research Ethics Committee reference: 16/NE/0267). Ethical approval and guidelines for the projects were granted by the generic research tissue bank approval for the Newcastle Mitochondrial Research Biobank.

Unless stated in this thesis, the muscle biopsy referrals, clinical, histochemical, molecular genetics and enzymatic investigations were all undertaken as part of the diagnostic work up of these patients for suspected mitochondrial disease at the NHS Highly Specialised Service for Rare Mitochondrial Disorders for adults and children located within the Wellcome Centre for Mitochondrial Research, at Newcastle University.

4.3.2. Clinical information for cohort

Clinical information for the 19 patients included in this study cohort is presented in **Table 4.3**. All clinical information including age (closest to the date at which muscle biopsy taken), clinical presentations, NMDAS scores (closest to the biopsy) and skeletal muscle homogenate m.3243A>G heteroplasmy levels were acquired from the MitoCohort (research ethics committee reference: 13/NE/0326) (section 2.5.3, **Chapter 2**). Both P11 and P19 were not part of the MitoCohort (provided by the Neuromuscular Centre, Institute for exercise and Environmental medicine at the University of Texas, Dallas), therefore there was no NMDAS scores for these patients.

The 17 patients from the MitoCohort were selected from a larger group of patients (58 patients) who had consented for the use of their skeletal muscle tissue in research. The selection of the patients (n=17) were based on homogenate heteroplasmy (high), muscle phenotype (myopathy scored over 2 on NMDAS) and total NMDAS scores (high therefore severe phenotype). This selection process was undertaken to allow for the best chance in capturing deficiencies with the quadruple immunofluorescence assay.

Patient clinical phenotypes, determined using NMDAS scores for individual questions and the thresholds presented by Pickett et al. (2018), are shown in **Table 4.2**. To account for the stochastic nature of traits, such as SLE, the maximum NMDAS score attained by a patient for each phenotype was used.

Patients ranged in age between 25 and 59 years at the time of skeletal muscle biopsy – the mean age being 42.9 years old. There are 12 females and seven males in this patient cohort.

Table 4.2: Clinical and molecular genetic characteristics of the patient cohort harbouring the *m.3243A>G* pathogenic variant on the *MT-TL1* gene

Patient	Gender	Age	Clinical Presentation	Muscle Heteroplasmy (%)*	Total NMDAS	Residual Complex I activity (%)*
P1	M	26	Encephalopathy, GI dysmotility, severe migraine, myopathy, seizures, visual acuity	89	12.4	13%
P2	F	55	Asymptomatic cardiac involvement, severe diabetes, end-stage deafness	84	20.7	n.d
P3	M	49	Mild-ataxia, severe migraines, myopathy	80	20.4	n.d
P4	F	34	Deafness, myopathy, fatigue, mild ataxia, chronic constipation	78	23.2	25%
P5	F	44	Mild-ataxia, symptomatic cardiac involvement, severe diabetes, mild encephalopathy, severe deafness, severe migraine, myopathy, seizures, SLE	78	27.9	n.d
P6	F	25	Mild ataxia, symptomatic cardiac involvement, severely affected cognition, CPEO, moderate encephalopathy, moderate deafness, myopathy, bilateral ptosis, seizures, SLE	77	33.5	n.d
P7	F	48	Mild-ataxia, CPEO, severe migraine, myopathy, bilateral ptosis	74	21.8	n.d
P8	F	57	Mild-ataxia, asymptomatic cardiac involvement, severe diabetes, severe deafness, myopathy	70	26.9	n.d
P9	M	51	Ataxia, symptomatic cardiac involvement, severely affected cognition, severe diabetes, mild encephalopathy, GI dysmotility, severe deafness, myopathy, sensory impairment, bilateral ptosis, seizures	67	45.1	50%

P10	F	18	Severe migraine, myopathy	66	21.5	n.d
P11	F	25	Modest exercise intolerance	64	n/a	n.d
P12	M	32	Mild GI symptoms	63	4.1	n.d
P13	F	59	Moderate deafness	62	9.7	82% (normal)
P14	M	40	Mild-ataxia, severe cardiac involvement, severe cognitive impairment, severe CPEO, severe diabetes, myopathy, sensory impairment, ptosis, SLE	57	26.9	n.d
P15	F	56	Mild-ataxia, asymptomatic cardiac involvement, impaired glucose intolerance, GI dysmotility, moderate deafness, severe migraine, myopathy	55	22.8	n.d
P16	M	52	Mild-ataxia, symptomatic cardiac involvement, CPEO, severe diabetes, moderate deafness, myopathy, motor impairment, ptosis	50	49.7	n.d
P17	M	43	Mild encephalopathy, end-stage deafness, severe migraine	46	14	93%
P18	F	55	Severe ataxia, severe cognitive impairment CPEO, moderate encephalopathy, GI dysmotility, severe deafness, myopathy, seizures	39	49.7	100%
P19	F	47	Exercise intolerance, ptosis	34	n/a	n.d

Age = closest to the biopsy; Total NMDAS = closest to the biopsy; GI = Gastrointestinal; SLE = Stroke-like episodes; CPEO = Chronic progressive external ophthalmoplegia; n/a = not applicable

*All biochemical data relating to Complex I enzymatic activity in muscle was provided by the NHS Highly Specialised Service for Rare Mitochondrial Disorders laboratory team

n.d = not determined

4.3.3. Tissue sectioning, quadruple immunofluorescence and image acquisition

10µm serial transverse skeletal muscle cryosections were collected onto glass slides. Sections were dried at RT for approximately 1 hour and then stored at -80°C. Before undertaking the staining process, slides were taken out of storage and air dried for approximately 1 hour at RT. The quadruple immunofluorescence assay was undertaken on these patient (n=19) and non-disease control (n=5) skeletal muscle cryosections, as outlined in section 2.5.8.1 in **Chapter 2** and **Figure 4.2**. The acquisition of images of the section and the subsequent analysis were undertaken as described in section 2.5.9 and 2.5.10 in **Chapter 2**.

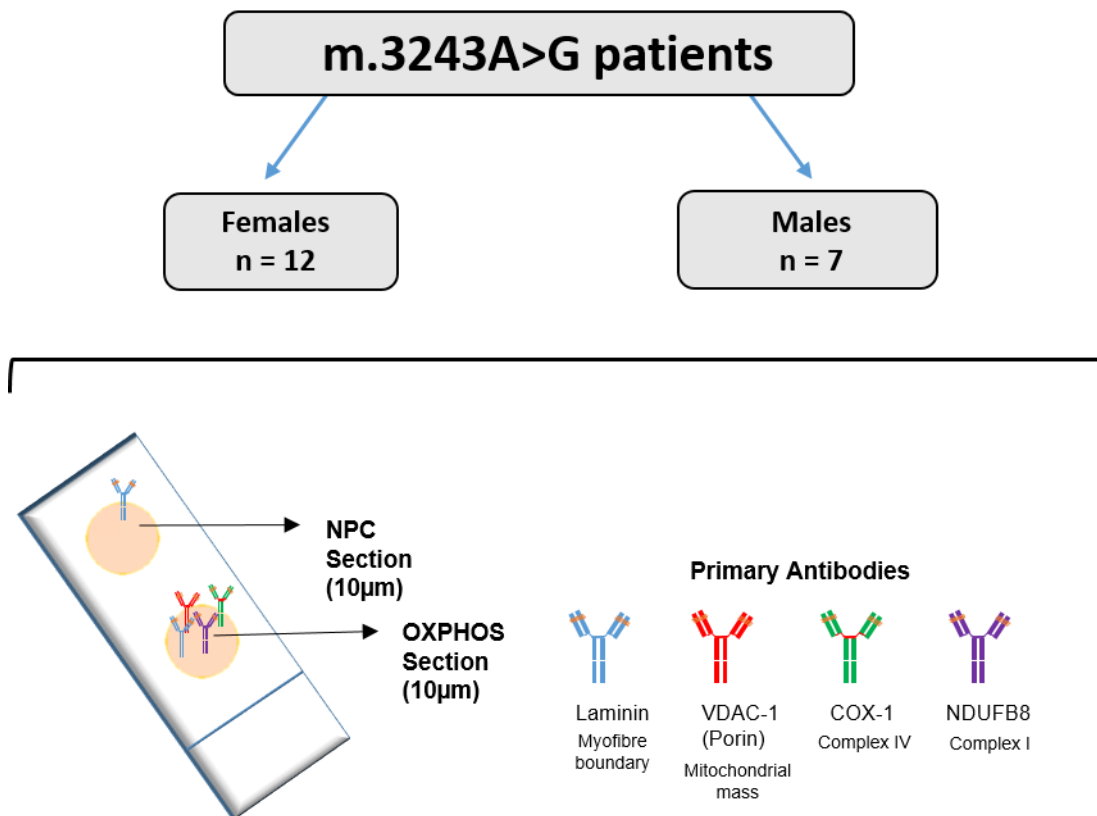


Figure 4.2: A schematic diagram highlighting the study design and quadruple immunofluorescent protocol.

Nineteen patients were assessed using the assay which detects the immunoreactivity of Complex I, Complex IV and porin. NPC = no primary control, OXPHOS = Oxidative phosphorylation

4.3.4. Data and statistical analysis

NMDAS scores obtained closest to the date of the biopsy were used in the overall analysis of the data attained in this chapter. The score for selected phenotypes is listed in **Table 7.1** in **Appendix 2 (Chapter 7)**. As this study is using skeletal muscle, it was important to assess the muscle-related phenotypes myopathy, exercise intolerance, cardiovascular, CPEO and ptosis. Stroke-like-episodes was also included in the analysis, as it is a measure of the severity of the disease. NMDAS thresholds scores as defined by Pickett et al. (2018) were used to determine affection status for binary trait analysis – phenotypes were then expressed as being present or absent.

The statistical analysis in this study was conducted with Microsoft Excel for the quadruple immunofluorescence assay data. Prism 5 (GraphPad Software Inc) was used to generate the mitochondrial respiratory chain profiles. R (version 3.5.2 (2018-12-20)) was used for linear and logistic regression models. The graphs were generated using the ggplot2 (Wickham 2016) package in R.

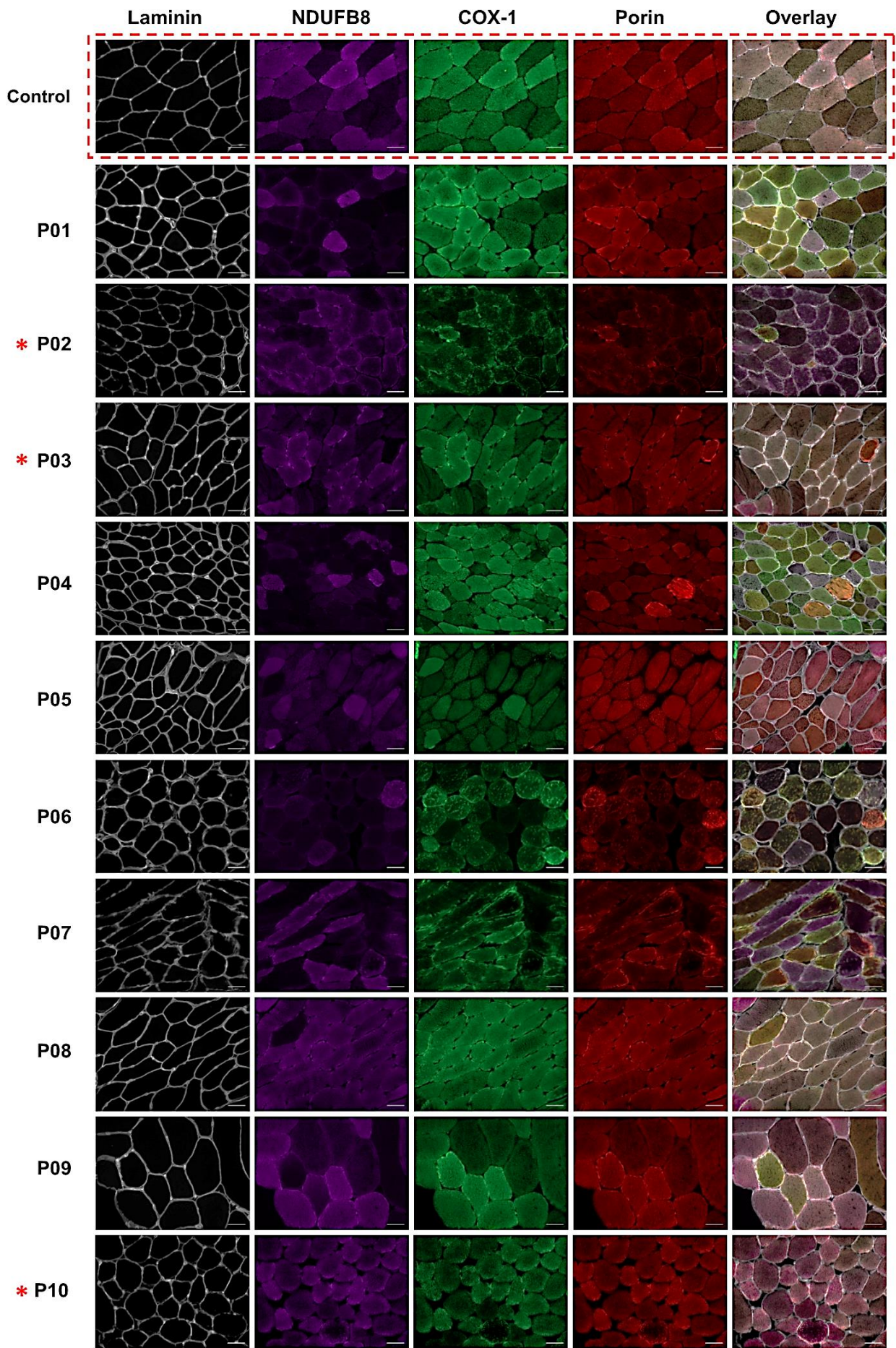
4.4. Results

Nineteen skeletal muscle biopsies taken from patients with the genetically confirmed pathogenic variant of m.3243A>G in the *MT-TL1* gene were assessed using the quadruple immunofluorescence assay. This generated a biochemical profile for each patient by measuring the levels of NDUFB8 (Complex I) and COX-1 (Complex IV) protein abundance in individual muscle fibres of a 10µm skeletal muscle section. The number of muscle fibres analysed per patient ranged from 104 (P09) to 1464 (P11) (see **Table 4.3**).

4.4.1. Immunoreactivity of NDUFB8 and COX-1 in m.3243A>G patients

The fluorescent images obtained from the quadruple immunofluorescence assay showed variable levels of immunoreactivity (therefore protein expression) of NDUFB8 and COX-1 in all patients assessed (**Figure 4.3**). Visual inspection of the x20 images of the muscle sections (a representative area of the whole section), showed decreased expression of NDUFB8 in individual fibres in a number of patients, when compared to the representative non-disease control muscle section. This decrease in Complex I is particularly evident in the tissue sections of patients P01, P04, P05, P06 and P07. The remainder of patients show a decrease in NDUFB8 immunoreactivity in fewer number of fibres, or more of a subtle loss which would require validation through quantification.

In contrast, the immunoreactivity of COX-1 is less apparent visually, although patients P02, P06 and P18 show decreased staining intensity when compared to the control and the other patients. Additionally, in the merged images, patients P03, P06, P07, P11, P16 and P19 display fibres which are visibly red in colour highlighting the immunoreactivity of porin– thus representing a RRF. These RRF could be COX-1 or NDUFB8 deficient or positive.



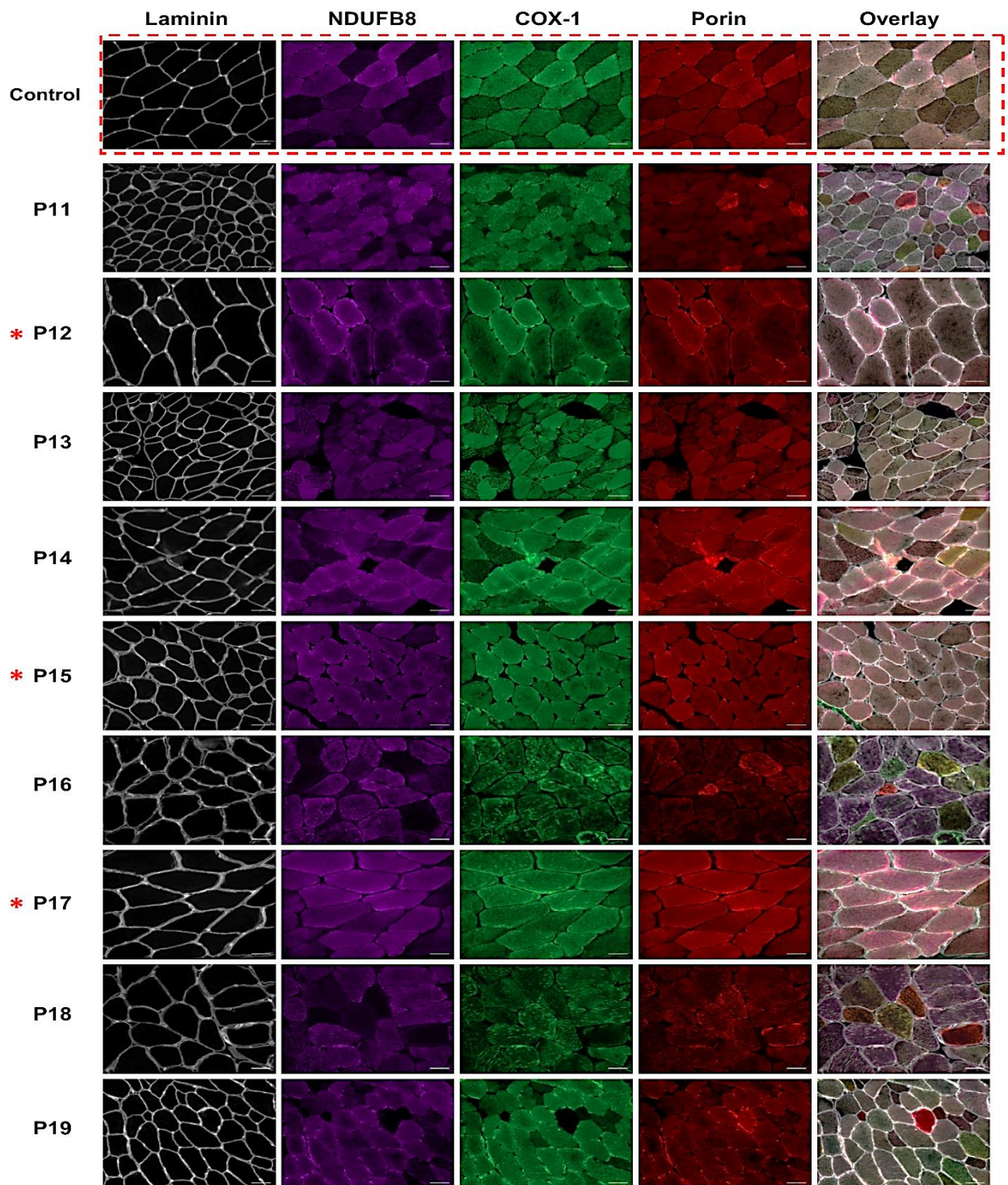


Figure 4.3: Images of Complex I, IV and porin expression in skeletal muscle sections of *m.3243A>G* patients.

Fluorescent detection was used to visualise NDUFB8 (Complex I), —purple COX-1 (Complex IV)—green, porin (mitochondrial mass)—red and laminin (fibre boundary marker)—white. A representative non-diseased control muscle (highlighted by the red box) shows normal immunoreactivity for NDUFB8, COX-1 and porin. Varying immunoreactivity of Complex I and Complex IV was detected in patients (01-P19). Patients marked with red asterisks (*) are those that showed normal immunoreactivity of both Complex I and Complex IV. RRF in merged images show fibres that have no Complex I or Complex IV. Images taken at x20 magnification and scale bars measure at 50µm.

4.4.2. Quantifying the quadruple immunofluorescence assay biochemical findings

The staining intensities of the fluorescent images were analysed, allowing for the quantification of NDUFB8 and COX-1 in single muscle fibres. The quadruple immunofluorescence assay biochemical data are presented as a total percentage of deficient fibres (consistent with **Chapter 3**); fibres which are categorised as intermediate positive, intermediate negative and negative in NDUFB8 and COX-1 protein abundance, based on Z scores (as described in **Chapter 2**, section 2.5.10.2). **Table 4.3** shows the percentage distribution of fibres across each category for NDUFB8 and COX-1.

4.4.2.1. Biochemical findings for control group;

The five non-disease controls (C01, C02, C03, C04 and C05) were analysed; the total percentage of deficiency observed in this group ranged from 0% to 1.35% for Complex I and 0% to 0.62% for Complex IV, across three different experimental batches (see **Table 7.2** in **Appendix 3, Chapter 7**). This demonstrates that there was very little variation between all of the batches which highlights the reproducibility of this assay.

4.4.2.2. Biochemical findings in *m.3243A>G* patient muscle;

In comparison, the findings from the 19 patients showed a greater variation in the percentage of deficient fibres detected. Evaluating the levels of Complex IV (COX-1), it can be seen from **Table 4.3** that the total percentage of Complex IV-deficient fibres ranged from 0% (P10 and P12) to 29.95% (P06). Patients P06 and P18 (11.69%) displayed the greatest proportion of Complex IV-deficient fibres in their skeletal muscle section compared to the other patients. Patients P11 (6.97%) and P13 (4.28%) displayed milder Complex IV deficiency whilst Patients P10 and P12 showed no deficiency. The latter two patients displayed levels that are equivalent to the non-diseased controls. The remainder of the patients showed less than 4% of Complex IV-deficient fibres.

In contrast, Complex I (NDUFB8) levels were more affected in this cohort of patients – the skeletal muscle section of 13 patients displayed Complex I deficiency; P01, P04, P05, P06, P07, P08, P09, P11, P13, P14, P16, P18 and P19. The total percentage of Complex I-deficient fibres ranged from 0% (P10) to 79.45% (P01) (**Table 4.3**).

The skeletal muscle sections of the remaining six patients (P02, P03, P10, P12, P15 and P17), presented with Complex I-deficient fibres ranging from 0% (P10) to 2.20% (P02) – similar to the non-disease control group. Furthermore, in these six muscle sections, the proportion of Complex IV-deficient fibres ranged from 0% (P10 and P12) to 2.77% (P03), highlighting that

these patients showed an absent or a very mild Complex I and Complex IV deficiency in the single muscle fibres analysed – levels similar to the non-disease cases.

Table 4.3: Quantification of Complex I (NDUFB8) and Complex IV (COX-I) deficiency in skeletal muscle fibres from patients with the m.3243A>G point mutation

Patient	Complex I (NDUFB8) Levels (%)					Complex IV (COX-1) Levels (%)					Total n =
	Pos	Int (+)	Int (+)	Neg	% Deficiency	Pos	Int (+)	Int (-)	Neg	% Deficiency	
Group A											
P01	20.55	8.38	12.28	58.78	79.45	97.93	1.84	0.23	0.00	2.07	871
P04	36.39	3.56	7.21	52.84	63.61	96.27	2.88	0.68	0.17	3.73	1179
P05	41.29	39.53	14.15	5.03	58.71	99.30	0.58	0.12	0.00	0.70	855
P06	30.55	15.04	19.21	35.20	69.45	70.05	18.26	9.43	2.27	29.95	838
P07	60.81	9.52	11.36	18.32	39.19	98.72	0.92	0.37	0.00	1.28	546
P08	87.42	4.72	2.52	5.35	12.50	97.80	0.63	1.26	0.31	2.20	318
P09	80.77	3.85	2.88	12.50	19.23	99.04	0.96	0.00	0.00	0.96	104
P11	78.07	2.80	5.19	13.93	21.93	93.03	4.10	2.25	0.61	6.97	1464
P13	91.59	2.70	2.54	3.17	8.41	95.72	2.06	1.51	0.71	4.28	1261
P14	91.00	0.71	1.66	6.64	9.00	98.82	0.47	0.24	0.47	1.18	422
P16	83.62	4.52	3.11	8.76	16.38	96.33	2.54	0.56	0.56	3.67	354
P18	80.13	5.64	5.17	9.06	19.87	88.31	5.56	4.21	1.91	11.69	1258
P19	88.50	2.54	2.30	6.66	11.50	97.58	1.33	0.61	0.48	2.42	826
Group B											
P02	97.80	1.34	0.19	0.67	2.20	99.52	0.29	0.10	0.10	0.48	1047
P03	98.22	0.20	0.99	0.59	1.78	97.23	2.37	0.20	0.20	2.77	506
P10	100.00	0.00	0.00	0.00	0.00	100.00	0.00	0.00	0.00	0.00	501
P12	99.54	0.00	0.00	0.46	0.46	100.00	0.00	0.00	0.00	0.00	431
P15	99.09	0.50	0.30	0.10	0.91	99.80	0.20	0.00	0.00	0.20	991
P17	97.93	0.69	0.00	1.38	2.07	98.28	1.72	0.00	0.00	1.72	290

4.4.3. Two distinct groups of patient muscle biopsies

This difference in the quadruple immunofluorescence data has shown that the patients in this cohort appear to fall into two main groups. Patients were defined as falling into Group A if their muscle biopsies showed decreased levels of Complex I and near normal levels of COX-1 when compared to non-disease controls (except for P06 and P18 who showed larger decrease in COX-1 expression). Patient were then defined as being in Group B if their skeletal muscle section showed none or very low levels of Complex I and Complex IV, similar to the non-disease controls.

Considering the residual Complex I activity (homogenate skeletal muscle), P01, P04 and P09 (Group A) also showed a decrease in enzymatic activity (13%, 25% and 50% respectively). However, P13 and P18 who are also in Group A have normal enzymatic activities (82% and 100%) – indicating that the mutation is affecting the assembly of Complex I and/or Complex IV only. P17 (Group B) also showed normal enzymatic activity (93%).

4.4.4. The mitochondrial respiratory chain expression profiles of m.3243A>G patient skeletal muscle section

As already described in both **Chapters 2** and **3**, a graphical representation of the quadruple immunofluorescence assay biochemical data is given through the mitochondrial respiratory chain expression profiles. **Figure 4.4** shows a representative non-disease control in which all fibres assessed in the muscle section (represented by individual dots) fall within the normal range – all fibres having a Z_score above -3 for both Complex I (NDUFB8_z) and Complex IV (COX_z). Reiterating the findings above, the expression profiles for the skeletal muscle sections of the 13 Group A patients (Patients P01, P04, P05, P06, P07, P08, P09, P11, P13, P14, P16, P18 and P19) show a “left shift” in a group of fibres – indicative of the Complex I-deficient fibres ((Z_scores fall below -3 for NDUFB8_z). In all of these patient sections excluding P09, a “downward shift” is then seen in a small proportion of fibres, highlighting that these fibres fall below -3 Z_score for COX-1_Z and therefore are Complex IV-deficient. The six Group B patient muscle sections (P02, P03, P10, P12, P15 and P17) show profiles that are similar to the non-disease control, in which the vast majority of fibres are within the normal range – as expected following the analysis. Patients P02, P03, P15 and P17 have very few fibres that are deficient for Complex I and Complex IV, however as stated in **Table 4.3**, the proportion of these fibres range between 0.% to 2.20% of total fibres for Complex I and 0% to 2.77% of total fibres for Complex IV. Thus, for example in P15, a total number of 991 fibres were analysed of which nine fibres are deficient for Complex I and two fibres are both Complex I and Complex IV-deficient.

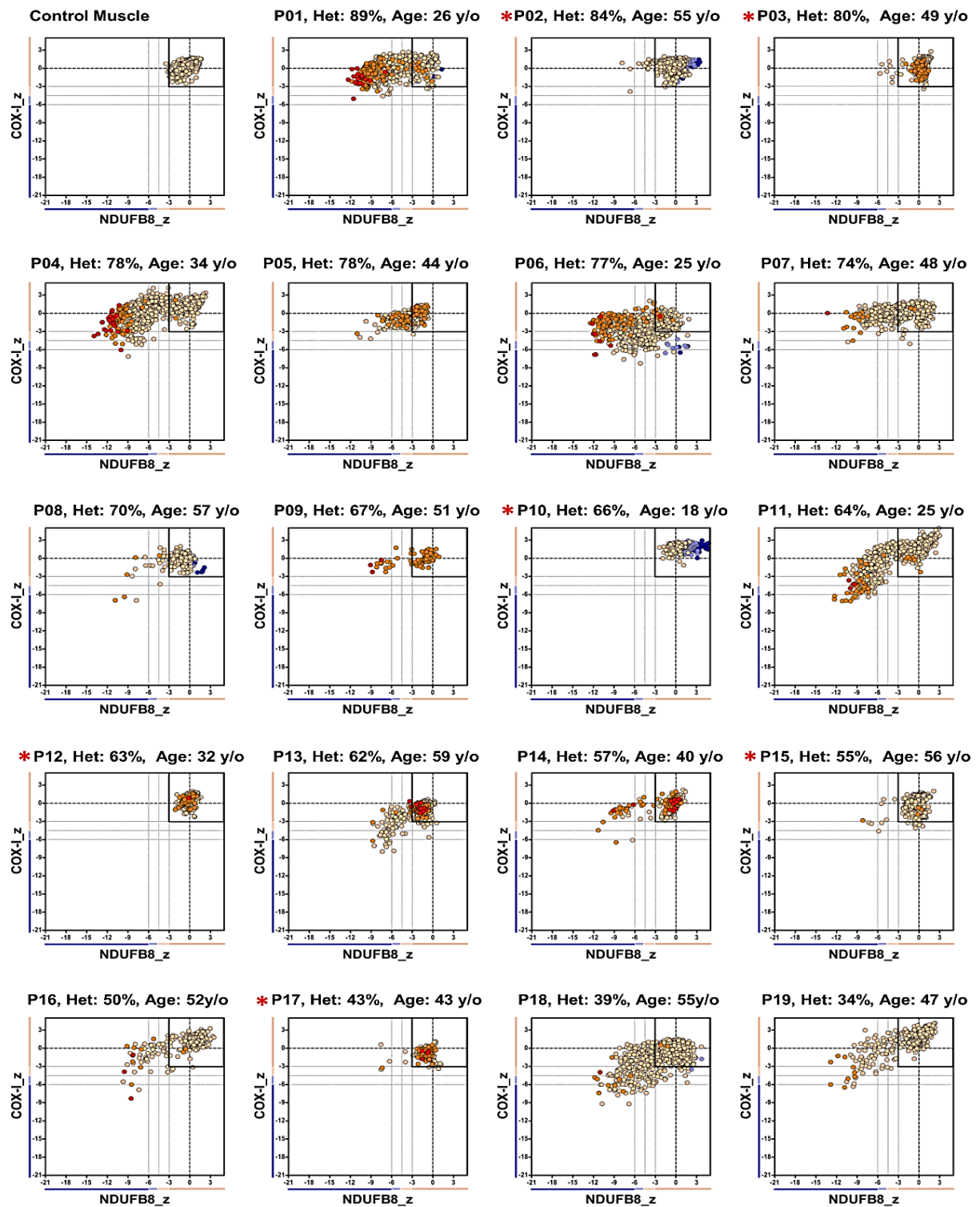


Figure 4.4: Mitochondrial respiratory chain (MRC) expression profile linking Complex I (NDUFB8), Complex IV (COX-I) and porin levels in *m.3243A>G* muscle sections.

Complex I and Complex IV expression profiles from all patients (n=19) and one representative non-disease control (control muscle). Fibres within black box (top left) are normal fibres. Fibres that show a “left shift” are Complex I-deficient. A “downward shift” shows Complex IV deficiency. Patients marked with red asterisk (*) are those in Group B. Porin level colours = Red fibres = very high levels, Orange = high, Beige = normal, Blue = low, Dark blue = very low. Het = skeletal muscle homogenate heteroplasmy. y/o = years old.

4.4.5. Correlating the quadruple immunofluorescence data with the clinical data

Using the data generated from the quantitative quadruple immunofluorescence assay (the Z_scores for individual fibres and the total percentage of deficient fibres for Complex I and IV), it was investigated whether the clinical data are associated with the biochemical status.

Table 4.4 highlights the total deficiency for Complex I and IV, alongside the level of m.3243A>G heteroplasmy in muscle homogenate and age (closest to the date of biopsy).

Table 4.4: Age, homogenate heteroplasmy and total Complex I and Complex IV deficiency in skeletal muscle sections

Patient ID	Age	Muscle homogenate heteroplasmy (%)	Residual Complex I enzymatic activity (%)	Total Complex I Deficiency (%)	Total Complex IV Deficiency (%)	Total fibres
Group A						
P01	26	89	13 (decreased)	79.45	2.07	871
P04	34	78	25 (decreased)	63.61	3.73	1179
P05	44	78	n.d	58.71	0.70	855
P06	25	77	n.d	69.45	29.95	838
P07	48	74	n.d	39.19	1.28	546
P08	57	70	n.d	12.50	2.20	318
P09	51	67	50 (decreased)	19.23	0.96	104
P11	25	64	n.d	21.93	6.97	1464
P13	59	62	82 (normal)	8.41	4.28	1261
P14	40	57	n.d	9.00	1.18	422
P16	52	50	n.d	16.38	3.67	354
P18	55	39	100 (normal)	19.87	11.69	1258
P19	47	34	n.d	11.50	2.42	826
Group B						
P02	55	84	n.d	2.20	0.48	1047
P03	49	80	n.d	1.78	2.77	506
P10	18	66	n.d	0.00	0.00	501
P12	32	63	n.d	0.46	0.00	431
P15	56	55	n.d	0.91	0.20	991
P17	43	46	93 (normal)	2.07	1.72	290

n.d = not determined

4.4.5.1. Biochemical data (Z_scores) vs homogenate m.3243A>G heteroplasmy levels

The relationships between the Z_scores for Complex I and Complex IV in individual fibres of each patient and their homogenate heteroplasmy were investigated using linear mixed effects models (**Figure 4.5**). Complex I Z_scores were significantly positively correlated with the homogenate heteroplasmy of patients (P=0.0260, gradient of slope = -0.0597, SE = 0.0245 and y intercept = 2.1793, SE = 1.6251) – **Figure 4.5(A)**. This shows that as the homogenate heteroplasmy increased, the Z_score value for Complex I decreased. In contrast, the Z_scores for Complex IV were not significantly correlated to the homogenate heteroplasmy (P = 0.3423, gradient of slope = -0.0147, SE = 0.0150, y intercept = 1.0004, SE = 0.9971) – **Figure 4.5(B)**. This was as expected as Complex IV deficiency was far less frequent in this

cohort of patients. Age (closest to biopsy) was not associated with either Complex I or Complex IV Z_scores ($P = 0.2098$ and $P = 0.5541$ respectively), so was not included in the model.

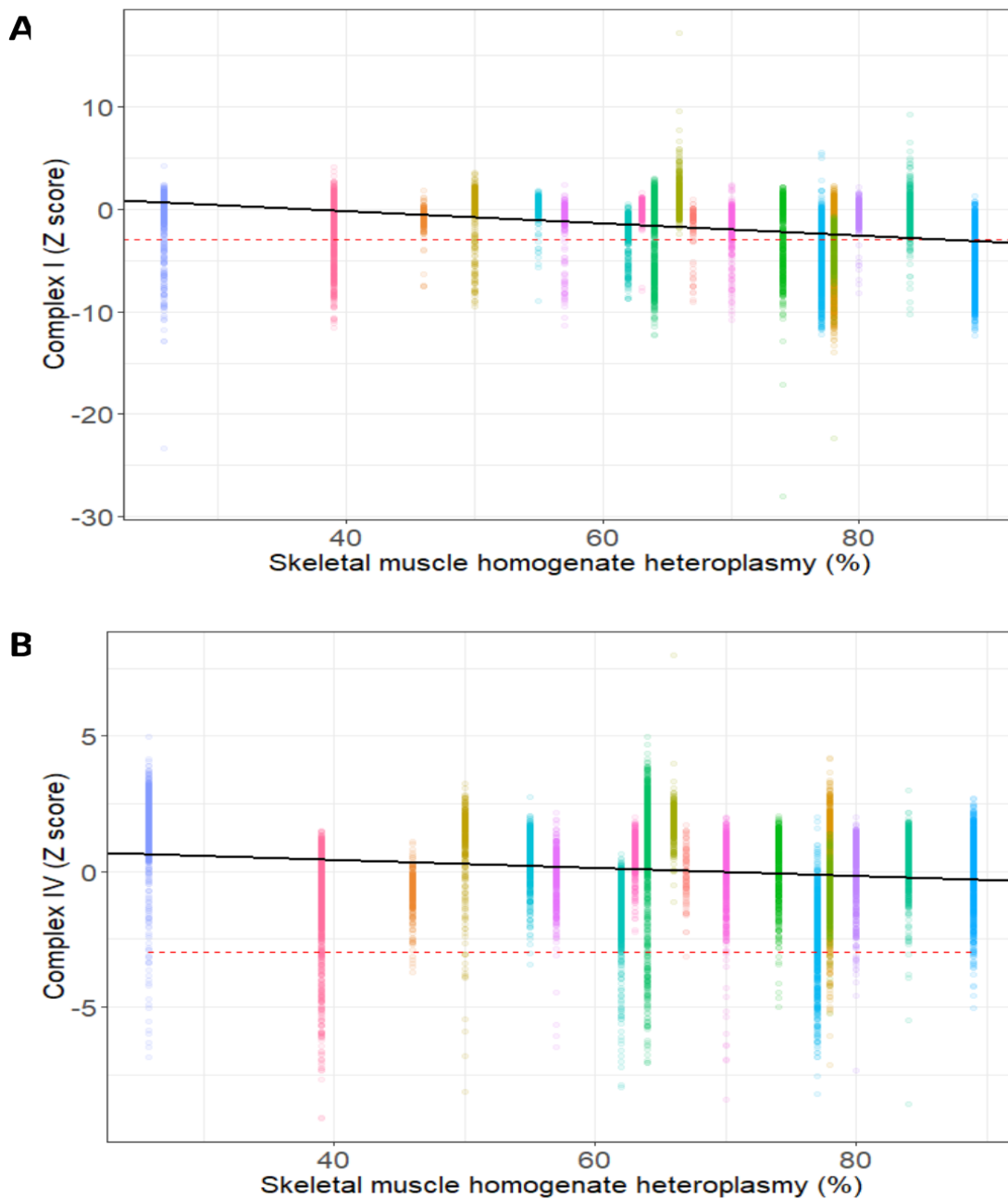


Figure 4.5: Relationship between homogenate heteroplasmy and the Z-scores determined for a) Complex I and b) Complex IV deficiency in individual muscle fibres.

Complex I Z_scores are significantly correlated to homogenate heteroplasmy ($P=0.0260$, gradient of slope = -0.0597 , $SE = 0.0245$ and y intercept = 2.1793 , $SE = 1.6251$), but Complex IV is not ($P = 0.3423$, gradient of slope = -0.0147 , $SE = 0.0150$, y intercept = 1.0004 , $SE = 0.9971$). Patients are represented with different colours and each individual point represents a single fibre. Red dashed line at $y=-3$ is the Z_score deficiency. Solid black lines are the regression lines representing the slope and intercepts of the model.

4.4.5.2. Biochemical deficiency vs homogenate m.3243A>G heteroplasmy levels

Although a significant relationship was detected for Complex I Z_scores and homogenate heteroplasmy, this analysis took into account all fibres; both normal and deficient. So, to explore this further, the relationships between the proportion of Complex I and Complex IV-deficient fibres and homogenate m.3243A>G heteroplasmy were investigated (**Figure 4.6**).

Homogenate heteroplasmy was significantly positively correlated with the proportion of Complex I-deficient fibres ($R^2 = 0.216$, $P = 0.026$, $\beta = 0.869$, $SE=0.356$). However, it is apparent in **Figure 4.6(A)**, that despite the high heteroplasmy levels, a number of patients (P02, P03, P10, P12, P15 and P17) still presented with low proportions of Complex I-deficient fibres (**Table 4.4**). In contrast, homogenate heteroplasmy and the proportion of Complex IV deficiency levels was not significantly correlated ($R^2 = -0.058$, $P = 0.909$, $\beta = 0.012$, $SE=0.109$) – **Figure 4.6(B)**. This was as expected as all patients but P06 and P18 presented with no deficiency or very low levels similar to controls. This is consistent with the findings above with the Z_score data. Furthermore, age (closest to the biopsy) was also not associated with either Complex I or Complex IV deficiency ($P = 0.080$ and $P = 0.266$ respectively), so was not included in the model.

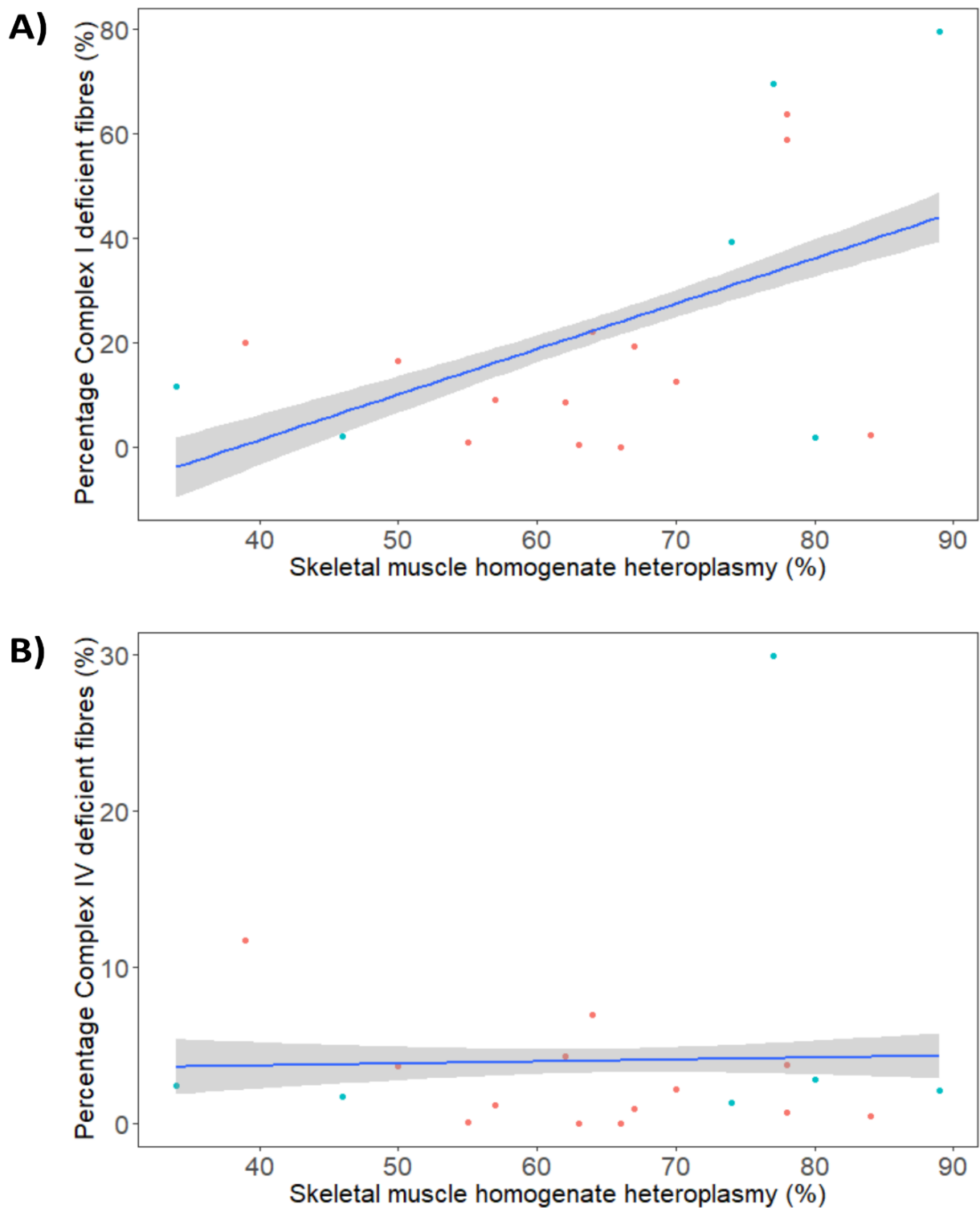


Figure 4.6: Relationship between homogenate heteroplasmy and the percentage of A) Complex I and B) Complex IV deficiency.

A) Homogenate heteroplasmy was significantly positively correlated with the proportion of Complex I-deficient fibres ($R^2 = 0.216$, $P = 0.026$, $\beta = 0.869$, $SE=0.356$) **B)** Homogenate heteroplasmy was not significantly correlated with the proportion of Complex IV- deficient fibres ($R^2 = -0.058$, $P = 0.909$, $\beta = 0.012$, $SE=0.109$) Blue line = linear regression, Grey shading = 95% confidence interval. Each individual patient is coloured according to their groups; red = Group A patients; blue = Group B patients.

4.4.5.3. Correlating the biochemical findings with clinical phenotypes

Next, the relationship between the quadruple immunofluorescence assay data and the phenotypes scored on the NMDAS (closest to the biopsy) for each patient was investigated to determine which category of patients (present or absent for the phenotype according to Pickett et al., 2018) had the highest proportion of Complex I-deficient and Complex IV-deficient fibres. However, it must be noted that due to the small number of patients (n=19), statistical tests could not be undertaken in certain phenotypes (SLE, cardiovascular and exercise intolerance), as a meaningful number of patients did not fall into both “present” and “absence” categories, thus hindering the statistical comparisons.

It was found that patients who presented with myopathy had the highest proportion of Complex I-deficient fibres (**Figure 4.7(A)**). However, statistical significance was not reached (Mann-Whitney U test; $P= 0.497$). **Figure 4.7(B)** shows no difference in the patients between the two categories for Complex IV-deficiency ($P = 1.00$). Again, this is as expected as all but two patients showed low or no levels of Complex IV-deficiency in the cohort. The analysis of the CPEO NMDAS scores with the biochemical deficiency were also analysed and **Figure 4.7(C)** shows that patients who were absent from the phenotype had the highest proportion of Complex I-deficient fibres but this difference was not statistically significant (Mann-Whitney U test; $P= 0.6868$). Likewise, whilst patients who were absent for ptosis had the highest proportion of Complex I-deficient fibres, no significance was reached in this difference between the two categories of patients (Mann-Whitney U test; $P= 0.597$). However, the number of patients per group is likely to be influencing these statistical outcomes as it limits the statistical power to detect an effect. As with myopathy, CPEO and ptosis did not show a statistically significant relationship with Complex IV deficiency.

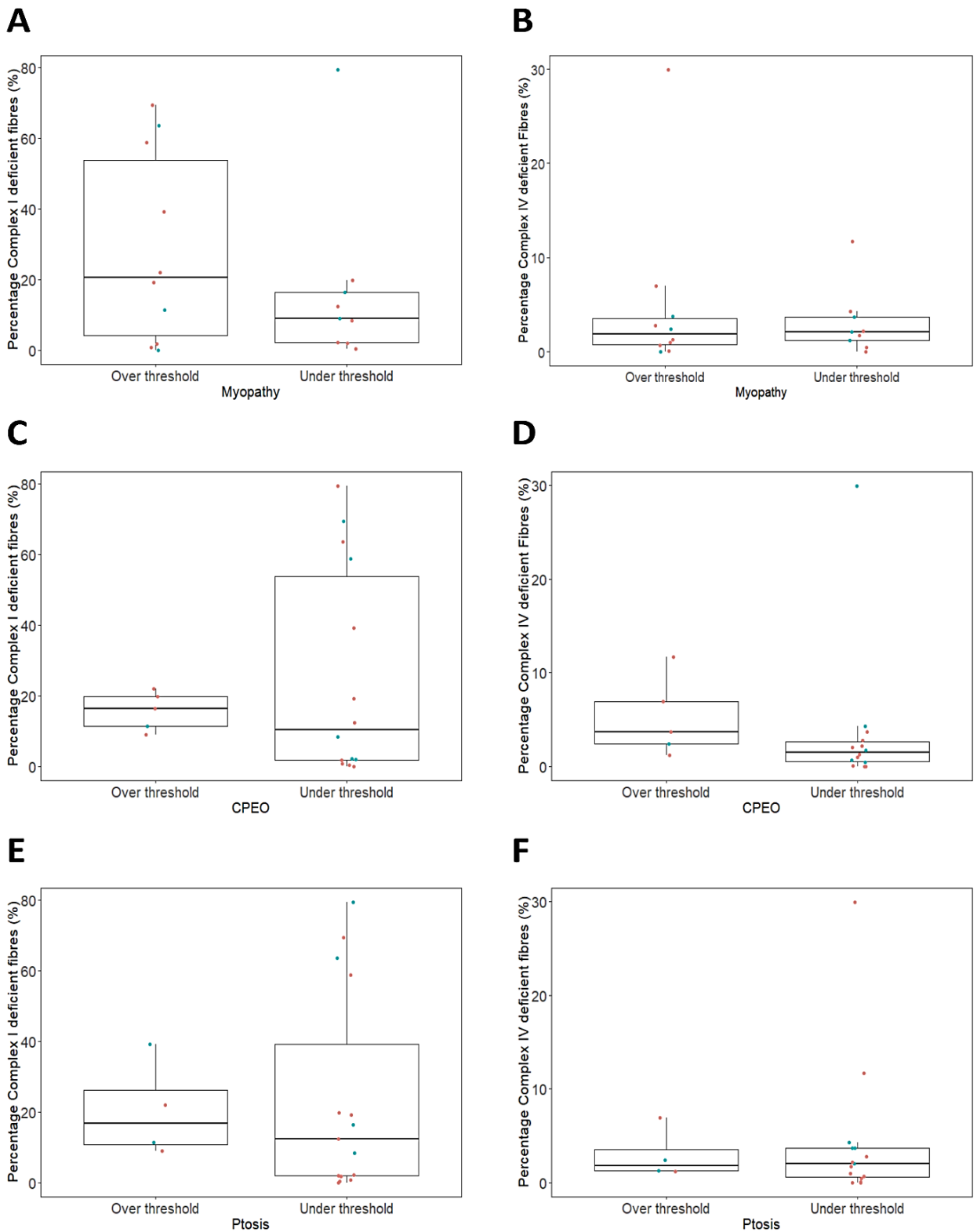


Figure 4.7: Boxplots showing the proportion of Complex I-deficient and Complex IV-deficient fibres (%) within patients who fall below (absent) and above thresholds (present) scores:

For a – b) Myopathy, c-d) CPEO and e – f) Ptosis. Proportion of Complex I-deficient fibres are higher in those with myopathy and lower for those with CPEO and Ptosis. No significance was reached for these differences. The proportion of Complex IV-deficient fibres are similar for both categories of patients. Each individual patient is coloured according to their groups; red = Group A patients; blue = Group B patients.

4.5. Discussion

This study aimed to characterise the biochemical status of skeletal muscle sections of patients harbouring the m.3243A>G mutation, using the quadruple immunofluorescence assay to determine the abundance of Complex I and Complex IV in fibres within a 10µm section. The relationship between the quantitative data (Z_scores for all individual fibres on muscle sections and the proportion of Complex I and Complex IV-deficient fibres) and the clinical data (level of m.3243A>G heteroplasmy level in muscle homogenate, clinical phenotypes and age (both closest to the biopsy) of patient) was also investigated. A total number of 19 patients were included in this study.

4.5.1. The biochemical status of m.3243A>G patients is heterogeneous based on Complex I interrogation

The study by Rocha et al. (2015) first determined the profiles of skeletal muscle sections of four m.3243A>G patients through quantifying the protein abundance of Complex I and Complex IV in single muscle fibres within a 10µm section, using antibodies labelling the subunits NDUF8 and MTCO1. However, this current study has characterised the biochemical profile of these patients in a larger, more comprehensive cohort. The application of the immunofluorescence assay in this cohort has identified that the biochemical status of m.3243A>G patient skeletal muscle sections can be divided into two groups; those with a biochemical deficiency (Group A) and those with normal biochemical status (Group B).

The assay detected both Complex I and Complex IV deficiency in 13 of the 19 patient skeletal muscle sections, however Complex I deficiency predominated. The skeletal muscles from Group A patients displayed Complex I deficiency ranging from 8.41% to 79.45%. Four of these 13 patients also displayed a combined Complex IV deficiency alongside the Complex I deficiency – ranging from 4.28% and 29.95%. These findings add to the existing literature in that Complex I is primarily affected in patients with m.3243A>G (Fornuskova et al. 2008; Goto et al. 1992; Mariotti et al. 1995; Morgan-Hughes et al. 1995). As previously discussed, the predominance of Complex I deficiency is hypothesised to be due to the impact the m.3243A>G mutation has on the synthesis of ND6 and ND5 subunits as a result of the high UUG codon content in the polypeptides (Chomyn et al. 2000; Dunbar et al. 1996; Kirino et al. 2004; Sasarman et al. 2008).

The skeletal muscle section of the remaining six Group B patients displayed profiles showing no biochemical deficiency of Complex I and Complex IV, comparable to the non-disease control group. Again, this is in line with the existing literature; of the 19 patients assessed by Mariotti et al. (1995), seven presented with normal Complex I and Complex IV biochemical

activity as measured by spectrophotometric assays and normalised to citrate synthase. However, this study used homogenate muscle sample and therefore any potential biochemical defect could be lost when globally assessed. For that reason, the use of the quadruple immunofluorescence assay has confirmed the findings of normal skeletal muscle sections at a single cell level, for these patients. Although, investigating a number of serial sections from the remainder of the biopsy of these patients will confirm the current findings.

4.5.2. Complex I deficiency correlates with homogenate heteroplasmy levels

As this assay has generated unique quantitative data, it enabled the exploration of the relationships between the biochemical deficiency of Complex I and Complex IV to the homogenate heteroplasmy recorded for these patients. Previous studies have attempted to correlate the biochemical deficiency observed in m.3243A>G patients to the heteroplasmy levels, but no clear correlations were reported – studies either described a strong inverse correlation between Complex I enzymatic activity and heteroplasmy level in homogenate muscle biopsy (Hollingsworth et al. 2012; Mariotti et al. 1995) or no association of Complex I or Complex IV with heteroplasmy level (Ciafaloni et al. 1992; Jeppesen et al. 2006; Morgan-Hughes et al. 1995). However, this current study has found a significant positive relationship between Complex I-deficiency (protein expression) and homogenate heteroplasmy levels, both when analysing the Z_scores for all fibres analysed with the assay and also with the proportion of Complex I-deficient fibres only. Thus, these findings are consistent with those of Mariotti et al. (1995) and Hollingsworth et al. (2012) who found that Complex I activity decreased in skeletal muscle as the heteroplasmy level increased. This increase in biochemical deficiency observed in patient skeletal muscle sections has also been shown by Jeppesen et al. (2006) who found that the 25 patients (of 51) who displayed COX-deficient fibres and RRFs all had heteroplasmy level above 50% in skeletal muscle.

In contrast, the level of Complex IV deficiency was not correlated to homogenate heteroplasmy in this cohort of patients. This was expected as the patients had very little deficiency in comparison to Complex I. In a larger cohort of patients, the power to detect an association between Complex IV and homogenate heteroplasmy would potentially be greater.

Although increasing age has been associated with an accumulation of COX-deficient fibres in normal human skeletal muscle (Muller-Hocker et al. 1992), this study did not detect an association between age and biochemical deficiency (both Complex I and Complex IV). This could be because the m.3243A>G mutation is masking the effect of ageing, which could be resolved with an increased cohort size. On the other hand, age is not correlated with the

homogenate heteroplasmy of this cohort ($P = 0.2296$), which is consistent with the known literature (de Laat et al. 2012; Kaufmann et al. 2011).

4.5.3. No correlation is observed between the biochemical deficiency and clinical phenotypes

This current study has been able to investigate the relationship between phenotypes and the severity of the biochemical deficiency (the percentage of Complex I and or Complex IV-deficient fibres). Whilst no significant difference was found between the two categories (presence or absence of the phenotype) for myopathy, CPEO and ptosis, those over the threshold for myopathy had, on average, a higher proportion of Complex I-deficient fibres (31.6%). However, three of the six Group B patients (P03, P10 and P15) where no biochemical deficiency was detected, also showed myopathy. Therefore, it is difficult to conclude if the presence of myopathy in patients is linked to Complex I-deficiency in terms of protein expression, or not. This is further highlighted by the fact that only four patients with myopathy show higher Complex I deficiency compared to the other patients, whilst one patient without myopathy showed the highest percentage deficiency. Studies have either shown no or an inverse correlation between myopathy and m.3243A>G heteroplasmy levels, therefore it would be interesting to investigate further if this is similar for myopathy and the biochemical deficiency (Chinnery and Turnbull 1997; Kärppä et al. 2005). By undertaking this assessment in a larger cohort of patients, it would allow for a more robust conclusion to be drawn between the two groups.

4.5.4. What is causing the difference in the biochemical status between patients in Group A and Group B?

The most interesting finding from this study is the difference in the biochemical status between the patients in Group A and the patients in Group B. This has raised important questions; what is causing this difference between the two groups? Could this difference in the biochemical status be driving the wide spectrum of clinical phenotypes observed in m.3243A>G patients?

A few factors, as mentioned in section 4.1.6 of this chapter, can be alluded to why this difference has been observed. Briefly, the age of the patients in both groups could have an impact, however, there was no correlation between age and biochemical deficiency.

Moreover, the mean age of both groups is very similar; (mean = 43.3, SEM = 3.40 in Group A and mean = 42.1, SEM= 6.03 in Group B). In addition to this, there is no statistical difference between the two groups with regards to biological sex (Fisher's exact test; $P=0.617$).

There is a growing interest regarding the role of the nuclear DNA and nuclear factors in mitochondrial disease (Battersby et al. 2003; Hudson et al. 2005; Maeda et al. 2016). *In vitro* work by Dunbar et al. (1995) has shown the impact of nuclear genetic background on the m.3243A>G phenotypic and biochemical expression in different *transmitochondrial* cells. Furthermore, the work by Pickett et al. (2018), has shown a strong indication into the presence of nuclear effects in influencing the disease phenotype in m.3243A>G patients. Therefore, it could be likely that nuclear background is also influencing the biochemical status in these patients and is an aspect that needs to be investigated further.

According to the threshold hypothesis (**section 1.5.1 in Chapter 1**), skeletal muscle fibres become biochemically deficient when mutant mtDNA reaches a specific proportion, in comparison to the wild-type mtDNA. The mosaic pattern observed in histochemical assessments show that different fibres have different levels of heteroplasmy, with some reaching the threshold and becoming deficient. Therefore, the difference in the biochemical status observed between the two groups is a strong indication of a difference in the heteroplasmy level at which the biochemical defect occurs; known as the critical threshold. Thereby, it is possible that fibres from patients in Group A have exceeded the threshold level in order to present with Complex I and (to a lesser extent) Complex IV deficiency, whilst this is not the case for fibres analysed from patients in Group B. These patients may have a higher threshold for deficiency in comparison, therefore the findings from this study poses another important question; is there a difference in the threshold between m.3243A>G patients?

Both groups of patients have overlapping levels of homogenate heteroplasmy; Group A's heteroplasmy levels range from 34% to 89% and Group B ranges from 46% and 84%. Homogenate heteroplasmy is the average level of m.3243A>G mutation across all fibres, both biochemically normal and deficient. Therefore, it is difficult to evaluate the relationship between the m.3243A>G mutation and the biochemical defects occurring within individual cells. As such, a single cell approach examining the heteroplasmy level in individual fibres in these patients could serve as a better approach in examining the relationship between the m.3243A>G mutation and the biochemical defect observed in patients in Group A. It will also allow for the investigation into the levels of m.3243A>G mutation in the biochemically normal fibres of Group B patients. This could then have the potential of deducing threshold for deficiency at an individual basis for these patient muscle sections.

Single cell studies have already shown evidence of this principle. For example, Kärppä et al. (2018) utilised the approach to examine a patient harbouring m.15923A>G in the *MT-TT* gene who presented with a milder phenotype in comparison to previous reports of the mutation.

The patient had a homogenate heteroplasmy level of 33% in skeletal muscle and following single cell analysis, it was found that COX-deficient fibres had an average heteroplasmy level of 92% whilst COX-positive fibres averaged at 43%. The authors concluded that the single cell analysis indicated that high heteroplasmy levels were required to cause a biochemical defect and therefore, a homogenate heteroplasmy level of 33% may not have been sufficient to cause a biochemical defect that would lead to a more severe phenotype – following the classic “higher heteroplasmy levels results in more severe phenotypes”. Studies have shown that the cellular threshold for m.3242A>G is between 80% and 90% (Petruzzella et al. 1994; Shoffner et al. 1990) whilst Miyabayashi et al. (1992) reported a lower threshold at 60%. Similar to the patient described by Kärppä et al. (2018), it can be hypothesised that different individuals have different thresholds. Therefore, perhaps Group B patients have higher threshold and thus have not reached the critical threshold for deficiency in skeletal muscle, which could be exemplified by P02 and P03 who have homogenate heteroplasmy levels of 84% and 80% and so their threshold could be closer to or over 90%, as shown by Shoffner et al. (1990). Whilst, in Group A patients, the thresholds could be as low as the level reported by Miyabayashi et al. (1992). Although, it is important to recognise that three of the six Group B patients presented with myopathy in equal severity to those patients in Group A, according to the NMDAS.

Another recent study by Rocha et al. (2018), utilised the quadruple immunofluorescence assay and a single cell approach to access single, large-scale mtDNA deletions. This approach was particularly valuable in showing that threshold levels differed in patients according to the site of deletions. Therefore, this same approach could be highly advantageous for accessing the difference between the two groups of patients defined in this current study, particularly for assessing heteroplasmy levels in the different populations of fibres and deducing a potential threshold in individual patients. Moreover, using this technique to assess the heteroplasmy levels in individual fibres between the two groups can potentially allow for investigation into the pattern of mutational segregation across the section.

4.6. Limitations of this study

Whilst this study has provided a more comprehensive evaluation of m.3243A>G patients, a number of limitations need to be discussed.

Firstly, although this is currently the only study that has assessed the skeletal muscle of the m.3243A>G patients using the quadruple immunofluorescence assay targeting Complex I and Complex IV, the ability to draw statistically significant conclusions, particularly for the phenotypes and biochemical deficiency, has been limited due to the small number of patients

in the cohort. This is largely due to the heterogeneity on a clinical basis between these patients. In some patients, the use of skeletal muscle to draw these conclusions may not have been sufficient as they could be more neurologically affected in their phenotype.

Secondly, the method by which the patients have been selected for this study is also a limitation. An approach to select patients likely to show deficiency through the assay was undertaken. Extending the application of the assay across the other available biopsies at random would serve a better approach in knowing how representative these findings are. Additionally, a larger cohort will allow a better assessment of the extent of Complex IV deficiency in m.3243A>G patients.

Thirdly, this assay provides an invaluable insight into the expression of Complex I and Complex IV from a single 10µm section, which has huge advantages for the diagnosis algorithm or in terms of tissue availability, but it proves a limitation when accessing the biochemical status of skeletal muscle sections of patients. Work by Elson et al. (2002) showed striking variation in the length of COX-deficient segments across a length of a biopsy in individuals (ranging from 10µm to ≥1.2mm). Hence, biochemical deficiency (Complex I and/or Complex IV-deficiency) may appear at multiple sites along the length of the muscle fibre. Therefore, whilst findings have been insightful, they are/may not be representative of the entire biopsy, or indeed the whole muscle.

Finally, the quadruple immunofluorescence assay has provided data on the protein expression of the complexes, rather than the enzymatic activity. So, although the Group B patients displayed normal expressions of both complexes, the enzymatic activity should be investigated for further confirmation. As discussed in **Chapter 3**, it could be that the m.3243A>G has variable effects on Complex I; either on assembly, enzymatic activity or both. However, this limited information has been provided in **Table 4.2** and **4.4** but requires further investigation.

4.7. Conclusion

In conclusion, by assessing Complex I and Complex IV expression, the biochemical status in the skeletal muscle sections of 19 patients with the m.3243A>G pathogenic variant has been extensively characterised in this study. This work presents the first study in which Complex I protein abundance, at a single cell level, has been assessed in a large cohort of patients, as previous studies have been restricted to the use of sequential COX/SDH, thereby this study has provided a more accurate characterisation of the biochemical profile in these patient skeletal muscles. Using the assay, the following findings have been determined; i) two groups of patients have been identified according to their biochemical status; patients in group A

showing a predominance of Complex I deficiency and patients in Group B who have shown no biochemical defect in their skeletal muscle section, ii) homogenate heteroplasmy is significantly correlated to the extent of Complex I deficiency. Moreover, from these findings, further questions have been raised; i) why is there a difference in the biochemical status between these groups, ii) is the critical threshold different between patients and iii) is this contributing to the phenotypic variation? These questions could potentially be answered using a single cell approach.

Chapter 5: A single cell approach to estimate the heteroplasmic threshold for biochemical deficiency of Complex I in skeletal muscle sections from patients harbouring the m.3243A>G pathogenic variant

5.1. Introduction

In **Chapter 4**, a cohort of 19 patients harbouring the m.3243A>G pathogenic variant was divided into two groups based on the OXPHOS biochemical profile (as determined by the quadruple immunofluorescence assay) of their skeletal muscle biopsy. Muscle biopsies from patients showing a Complex I deficiency were termed as Group A whilst those showing a normal biochemical profile were termed as Group B. These two groups of patients had overlapping homogenate heteroplasmy levels and clinical phenotypes. Thus, this difference in the biochemical status could be due to a difference in the critical m.3243A>G heteroplasmic threshold between these two groups of patients; do patients in Group A have a lower threshold hence a biochemical deficiency in their skeletal muscle? A single cell approach was used for this investigation, combining data from the quadruple immunofluorescence assay and a molecular genetics approach.

Single cell studies investigating threshold levels for the m.3243A>G pathogenic variant:

Estimates of the critical heteroplasmic threshold for the m.3243A>G mutation range from 50 to 90% in the literature. This variability could have arisen because of variation between individuals or because of differences between experimental methods used to detect biochemical deficiency. Here, I consider the available data in the literature which have been obtained in an attempt to determine this critical threshold.

Studies using transmitochondrial cells;

Early studies investigating the threshold of the m.3243A>G variant utilised *transmitochondrial* cybrid cells, harbouring different levels of heteroplasmy. These studies demonstrated that the critical threshold level at which mitochondrial respiratory chain dysfunction was induced was at ~90% (Attardi et al. 1995; Chomyn et al. 1992; Dunbar et al. 1996; Koga et al. 1993; Yoneda et al. 1992). However, as described previously (section 4.13 of **Chapter 4**), findings from studies using these cybrid cells need to be interpreted carefully. One difficulty with these observations is that *transmitochondrial* cell lines are cancerous (human osteosarcoma (143B-206) or lung carcinoma (A549)) and therefore do not accurately represent the *in vivo* conditions of most tissues in patients. Another reason to be cautious is that these studies have utilised different *transmitochondrial* cell lines which have different nuclear genetic backgrounds. It became evident that the confounding effects of difference in the nuclear backgrounds influenced the segregation of mutant and wild-type mtDNA present in these cells and therefore influenced the genotype-phenotype relationship being investigated. For example, Dunbar et al. (1995) showed that in the 143B-206 cell line, a

heteroplasmy level of 90% was required to cause a 30% decrease in COX-activity. Whilst, for the A549 cell line, a lower threshold of 55% resulted in a 50% reduction in COX-activity measured using biochemical enzymatic assay.

Studies using patient fibroblast cells;

Alternatively, a number of studies have utilised fibroblasts from patients to study the effect of high levels of the m.3243A>G variant. A study by Miyabayashi et al. (1992), cloned cells from fibroblasts of a MELAS patient and found that the activity of Complex I, as measured by NADH-cytochrome *c* reductase (NCR), decreased when heteroplasmy levels of the mutation increased to more than 60%. In contrast to this, Yokota et al. (2015), also used single cell derived clonal fibroblasts from two MELAS patients and found that the threshold for deficiency was at 90%, consistent with the findings observed in 143B-206 *transmitochondrial* cell lines.

Studies using single muscle fibres;

A multitude of studies have used the single cell approach through isolating skeletal muscle fibres from affected patients. By using COX/SDH staining to identify the biochemical defect, these studies isolated RRFs, COX-positive and COX-deficient fibres, and the m.3243A>G heteroplasmy levels were determined in each. Some examples of these studies include the study by Tokunaga et al. (1994) who used single muscle fibres from three MELAS patients to show that the heteroplasmy levels were significantly higher in RRFs ($88.1 \pm 5.5\%$) than non-RRFs ($63.32\% \pm 21.6\%$). Petruzzella et al. (1994) isolated fibres from PEO and MELAS patients and showed that normal fibres had heteroplasmy levels of $56 \pm 21\%$, COX-positive RRF fibres had high levels ($90 \pm 6\%$) and an almost complete segregation of the mutation in COX-deficient RRF ($95 \pm 3\%$). Similarly, Ozawa et al. (1998) investigated single fibres from five patients harbouring the mutation and RRFs had higher levels of heteroplasmy (average of 89.8%) compared to non-RRF (average of 42.4%). Further to this, Kärppä et al. (2005) analysed fibres taken from 10 patients (a total of 251 biochemically normal fibres, 8 COX-deficient fibres, 19 COX-positive RRF fibres and 13 COX-deficient RRF) and also showed that COX-deficient fibres had a mean heteroplasmy level of 90% (ranging between 81 to 97%) and normal fibres had a mean of 50% (ranging from 3 to 92%). In line with the findings shown through the A549 cell line (Dunbar et al. 1995), Jeppesen et al. (2006) suggested 50% as the threshold for m.3243A>G in skeletal muscle whereby 25 out of 51 individuals who had heteroplasmy level above 50% showed abnormal histological findings on skeletal muscle biopsies.

These findings highlight the lack of consensus from these studies. Moreover, these studies have used single muscle fibres that have been isolated based on observations derived from the study of COX-deficient fibres. It is well known that in fact, Complex I is predominantly affected in these patients, further highlighted in the findings from **Chapter 4** for this current cohort of patients. Therefore, a more precise approach to deduce the threshold level in these patients would be to investigate the heteroplasmy levels within Complex I positive and deficient fibres – the threshold for Complex I deficiency may differ to that for Complex IV. This has been alluded to by Dunbar et al. (1996) who showed that a decrease in oxygen consumption with pyruvate (Complex I substrate) occurred in *transmitochondrial* cells (A549) harbouring between 60-90% m.3243A>G heteroplasmy level, whilst only cells with over 95% heteroplasmy levels also showed Complex III and Complex IV deficiencies.

5.2. Aims

The first aim of this study was to characterise the distribution and relationship of m.3243A>G heteroplasmy level in both biochemically normal fibres and those deficient (in Complex I and Complex IV) from both Group A and Group B patient skeletal muscle sections.

Following this, a second aim was to estimate a critical heteroplasmy threshold for Complex I deficiency in individual patients and to ascertain whether there is a difference in threshold between different patients.

5.3. Methods

5.3.1. Selecting patients for the single cell study

Ten of the 13 skeletal muscle sections of Group A patients (P01, P04, P05, P06, P07, P11, P13, P15, P18 and P19) were selected based on the size of the biopsy that would allow for sufficient number of fibres to be isolated for the single cell study. The remaining three Group A patients were not used due to either insufficient number of fibres (for example P09; n= 104 fibres) or folding of skeletal muscle sections which would interfere with matching fibres (see section 5.3.5). Three of the six skeletal muscle sections of Group B patients were selected at random.

5.3.2. Single muscle fibre workflow

The workflow for this single cell study is shown in **Figure 5.1**. The individual methods undertaken are also listed below.

5.3.3. Tissue sectioning for fibre typing

Serial transverse skeletal muscle cryosections were collected as shown in **Figure 5.1**; a 10 μ m section, which was used for the quadruple immunofluorescence assay (**Chapter 4** and denoted by A in **Figure 5.1**) and a 20 μ m section which was used for fibre typing immunofluorescence (denoted by B). Sections were dried at RT for approximately 1 hour and then stored at -80°C until use.

5.3.4. Fibre Typing

Fibre types in the skeletal muscle sections were determined following an immunofluorescence protocol outlined in section 2.5.8.2 of **Chapter 2**. Following this, the skeletal muscle sections were imaged (see section 2.5.9, **Chapter 2**) and then stored at 20°C until laser microdissection.

5.3.5. Matching fibres to OXHOS defect and fibre type:

Muscle fibres in the 20 μ m fibre type section were manually matched to the 10 μ m OXPPOS section, so that each muscle fibre now had information on their OXPPOS status and their fibre type. An example is shown in **Figure 5.2**. This was undertaken for 11 of the 13 muscle sections.

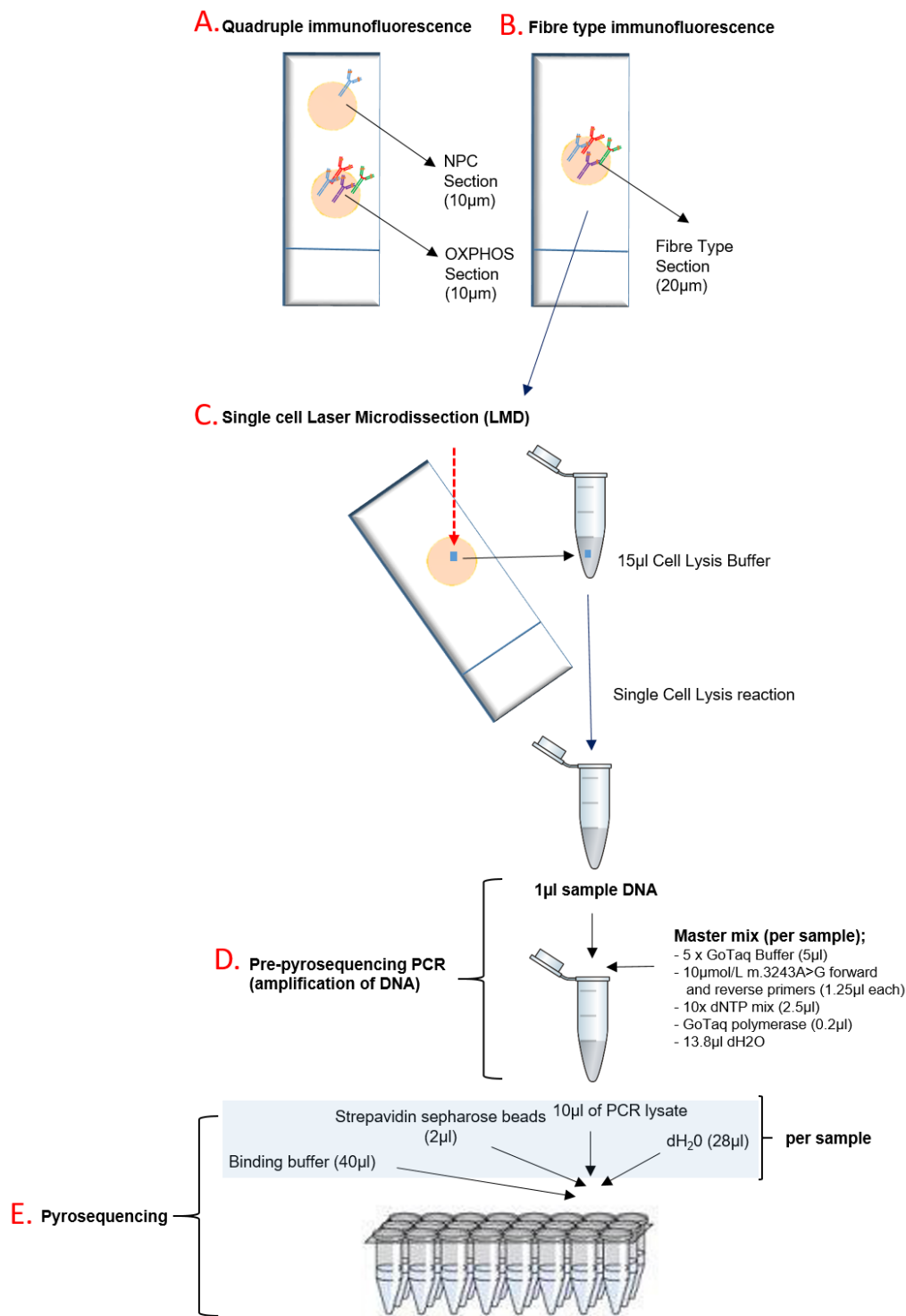


Figure 5.1: A schematic diagram of the single cell study experimental workflow.

A) the quadruple immunofluorescence assay was undertaken on two 10µm sections (NPC and OXPPOS) followed by B) the fibre type immunofluorescence on a 20µm serial section C) fibres (a single fibre represented by the blue square) from this muscle section were isolated using laser microdissection, into 15µl cell lysis buffer. Fibres underwent single cell lysis reaction followed by D) PCR to amplify the DNA and E) molecular genetics investigation through quantitative pyrosequencing to determine the m.3243A>G heteroplasmy levels in each single muscle fibre. OXPPOS = oxidative phosphorylation.

5.3.6. Section preparation for single muscle fibre isolation

The 20µm sections stained for fibre typing were left to soak in PBS at 4°C overnight which allowed for coverslips to be easily removed. The slides were dehydrated in an ethanol gradient – 70% for 10 minutes, 95% for 10 minutes, 100% for 10 minutes and a further 10 minutes in 100% ethanol. Sections were stored in -20°C for later use for laser microdissection.

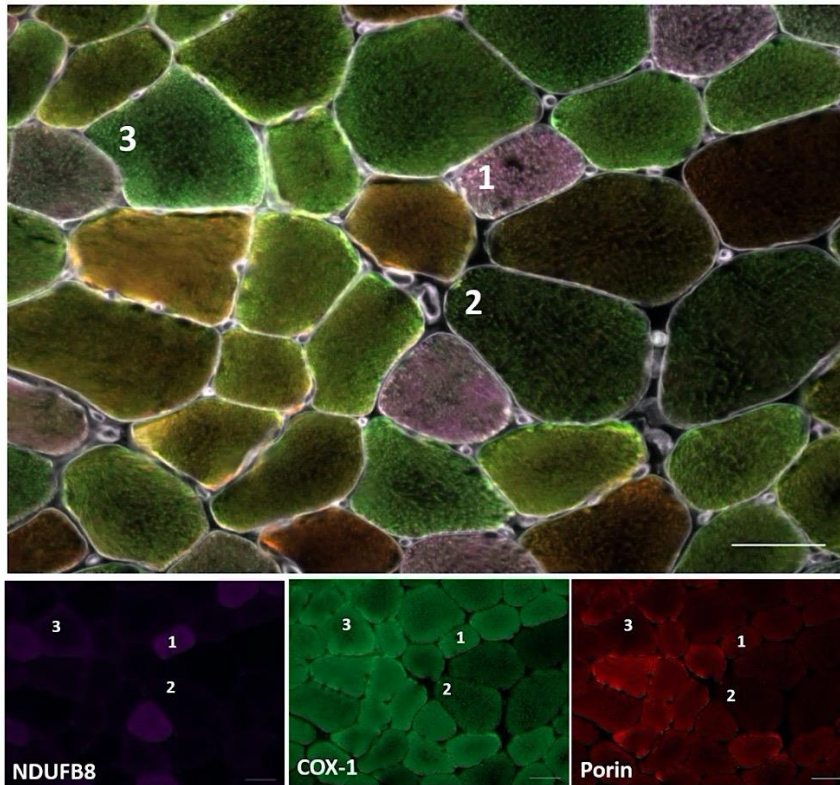
5.3.7. Isolation of single muscle fibres

Single cell laser microdissection on the selected fibres was undertaken as described in detail in section 2.5.12 of **Chapter 2** and depicted in **Figure 5.1** (labelled C.). The single cell lysates were stored at -20°C until quantitative pyrosequencing was undertaken.

5.3.8. Assessing the m.3243A>G heteroplasmy levels in single muscle fibres with quantitative pyrosequencing

PCR was used to amplify a fragment of 210bp length of mtDNA, spanning the targeted mutation site (described in section 2.5.13 of **Chapter 2**) as depicted in **Figure 5.1** (labelled D). Thereafter, the m.3243A>G heteroplasmy level of each single muscle fibre was assessed by quantitative pyrosequencing, performed using the Pyromark Q24 platform, Qiagen (**Figure 5.1**, labelled E). This, alongside the interpretation of the sequencing using the Pyromark Q24 software, is described in detail in section 2.5.13.7 of **Chapter 2**. Three mutation-positive controls with known levels of m.3243A>G heteroplasmy (18%, 48% and 72%) and one blank (no template) control were included within each experimental run. According to validated criteria set by the accredited NHS Highly Specialised Diagnostic Laboratory at the Wellcome Centre for Mitochondrial Research, Newcastle University, a $\pm 3\%$ of the expected heteroplasmy level of the controls was accepted and used to authenticate the experimental run.

A. Quadruple immunofluorescence assay



B. Fibre type immunofluorescence

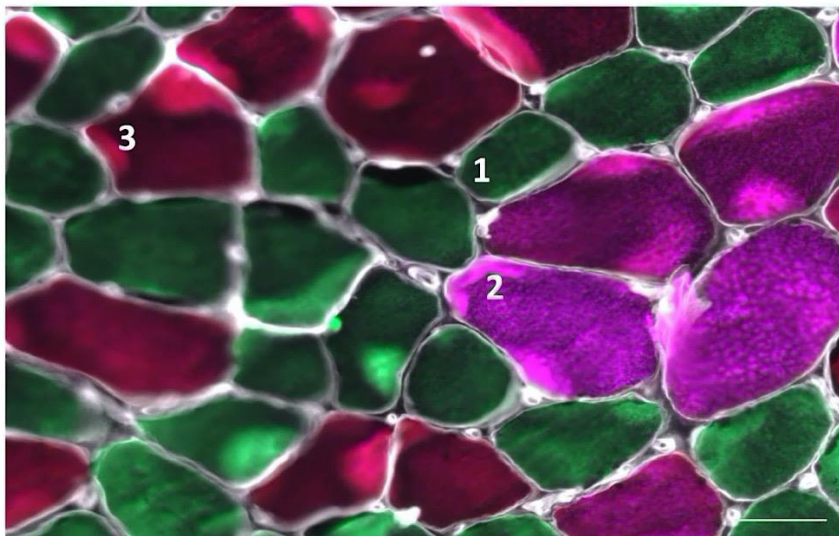


Figure 5.2: Matching OXHPOS status and fibre type.

A) Quadruple immunofluorescence assay and B) Fibre type fluorescence staining showing 3 fibres as examples. Fibre 1 = OXPHOS status (panel A); normal for Complex I (NDUFB8, purple), normal for Complex IV (COX-1, green) and fibre type (panel B) = fibre type I (Mouse BA-F8-s (IgG2b) labelling myosin heavy chain (MHC) slow type I, green). Fibre 2 = OXPHOS status (panel A); deficient for Complex I, normal for Complex IV, and fibre type (panel B) = fibre type IIx (Mouse SC-71-s (IgG1 labelling MHC type II, purple). Fibre 3 = OXPHOS status (panel A); deficient for Complex I, normal Complex IV and fibre type (panel B) = fibre type IIa (6H1-s (IgM) labelling MHC type IIx, red). The myofibre boundaries of single muscle fibres are marked with laminin (white).

5.3.9. Selection of single muscle fibres for single cell study

The method for selecting muscle fibres was based on the protocol outlined by Rocha et al. (2018). Briefly, muscle fibres were first categorised by their OXHOS status based on their level of deficiency in Complexes I and IV, as determined by their Z_scores. As shown in **Chapter 4**, the skeletal muscle sections of patients observed in this study predominantly showed four groups of fibres based on OXPHOS status, as depicted by the mitochondrial respiratory chain profiles in **Figure 5.3**, however some cases showed five groups of fibres. This study aimed to determine a threshold for biochemical deficiency, specifically for Complex I, which according to the quadruple immunofluorescence occurred between Group 1 fibres (normal for both complexes) and Group 2 (these fibres are classified as intermediate positive and negative for Complex I) and therefore, more fibres were selected from these two groups. In addition, biochemically normal fibres were expected to have a wider distribution of heteroplasmy level based on previous findings using COX/SDH, therefore it was important to capture this to enable the threshold to be determined. Although these fibres were first categorised according to their OXPHOS status and their fibre type, fibres were selected at random for analysis from these resulting groups.

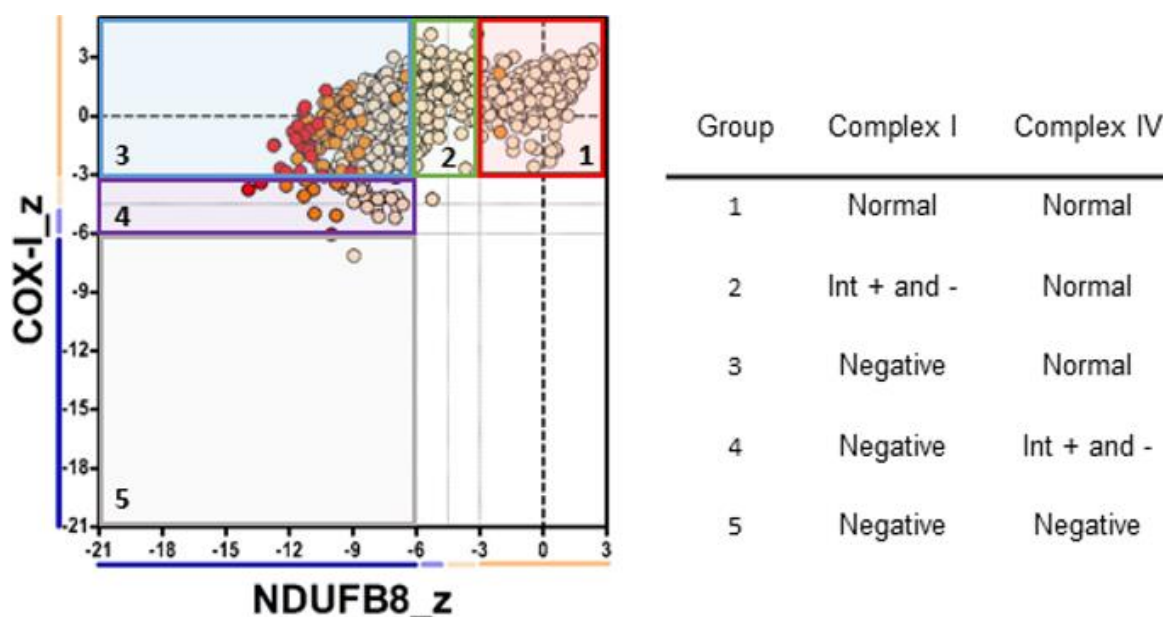


Figure 5.3: The OXPHOS status groups seen in *m.3243A>G* patient mitochondrial respiratory chain profiles.

Skeletal muscle section of patients predominantly showed four groups of fibres according to the mitochondrial respiratory chain profiles showing the Z_score categories of respiratory chain defects. This is shown by the coloured boxes and described in adjacent table; red = Group 1, green = Group 2, blue = Group 3, purple = Group 4 and grey = Group 5. Fibres were coloured according to porin levels; red = very high, orange = high, beige = normal, blue = low, dark blue = very low.

Table 5.1 summarises the target number of fibres to be selected for analysis per fibre type in each OXPHOS group. Each patient’s biopsy section presented differently in the number of fibres per group and the fibre type composition, thus where possible, the maximum number of fibres were taken from the outlined selection process (n=10). Due to low numbers present in the patient skeletal muscle sections, both Type IIa and Type IIx were grouped as Type II fibres. Where fibres were found to be fluorescently labelled for both Type IIa and Type IIx, they were accounted for as the third fibre type group (Type IIa/Type IIx). Examples of this occurrence include P06 and P13.

Table 5.1: The number of fibres targeted for selection per OXPHOS status and fibre type

OXPHOS status					
Fibre Type	Group 1	Group 2	Group 3	Group 4	Group 5
I	20	20	10	10	10
II (IIa +IIx)	20	20	10	10	10
IIa/IIx	20	20	10	10	10
Total:	210 fibres per patient				

Table 5.2: Overall number of fibres actually sampled per case per group of OXPHOS status in each patient and the final number included in the molecular genetics investigation

Patient	Group 1	Group 2	Group 3	Group 4	Group 5	Total sampled	Total after pyrosequencing
Group A patients							
P01	37	39	20	10	-	106	106
P04	40	37	40	10	2	129	116
P05	40	51	11	2	-	104	120
P06	65	37	13	13	-	128	128
P07	40	35	25	2	-	102	89
P11	26	17	21	21	3	88	77
P13	65	23	5	11	-	104	89
P16	80	23	13	11	5	132	106
P18	40	35	19	20	17	131	115
P19	20	15	18	12	-	65	55
Group B patients							
P02	105	-	-	-	-	105	105
P10	107	-	-	-	-	107	107
P15	108	-	-	-	-	108	108

Following **Table 5.2**, **Figure 5.4** shows examples of cases (P04 and P10) where the fibres actually sampled from the skeletal muscle sections are highlighted (remainder of the 11 patients are shown in **Appendix 4 (Figure 7.1, Chapter 7)**). As previously mentioned, fibres sampled from the three Group B patients (P02, P10 and P15) were all selected at complete random, as all fibres were classified as biochemically normal for Complex I and Complex IV.

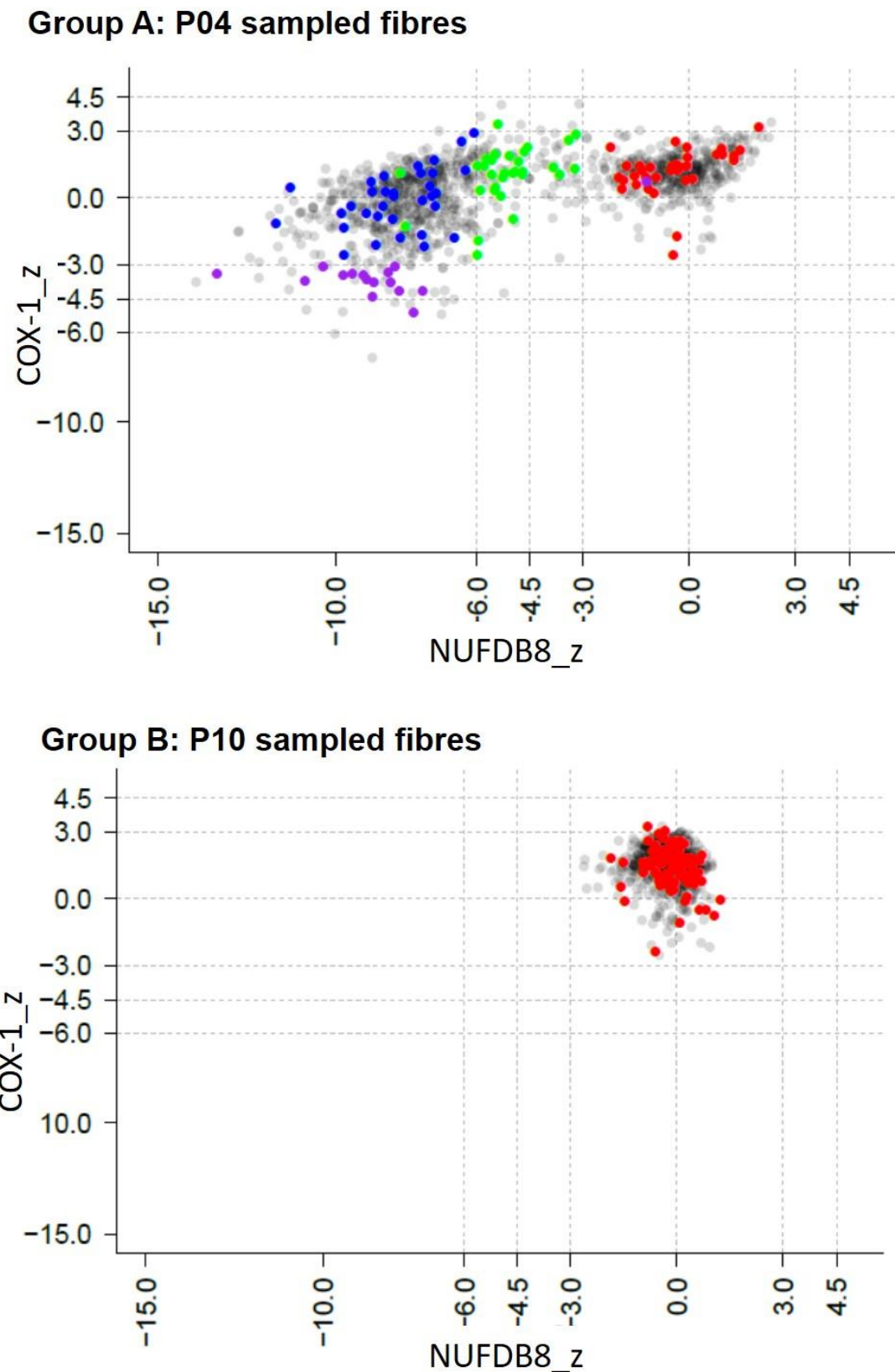


Figure 5.4: Mitochondrial respiratory chain profiles highlighting sampled fibres.
 Examples of sampled fibres from **a)** from P04 (patient in Group A) and **b)** P10 (Group B patient).
 Coloured dots represent the fibres sampled and correspond to each OXHOS group; Group 1 = red,
 Group 2 = green, Group 3 = dark blue, Group 4 = purple, Group 5 = orange.

5.3.10. Analysis

Statistical analysis and graphs were produced in R version 3.5.2 (2018-12-20) using the following R packages; plyr (Wickham 2011), ggplot2 (Wickham 2016), matrixStats (Bengtsson 2017), ggforce (Pedersen, 2018), data.table (Dowle and Srinivasan 2017), fitdistrplus (Delignette-Muller and Dutang 2015) and gmp (Lucas et al. 2019).

5.3.10.1. LOESS profiles

The LOESS non-parametric model allows for an unbiased curve to be fitted to the data points, whereby it allows for the data to drive shape of the relationship (in this instance the relationship between heteroplasmy and biochemical deficiency as measured by z-score).

The LOESS regression curve was fitted to the dataset of each patient using the LOESS function (`loess`) in R (R Core Team, 2018) as schematically depicted in **Figure 5.5a**. The estimates of the threshold were determined by the highest heteroplasmy level at which the curve intercepted the -3 Z_score deficiency cut off, as defined by Rocha et al. (2015).

To capture uncertainty about the threshold estimate, the dataset was bootstrapped (a statistical test that relies on random sampling of data from each patient's muscle section, with replacement) 10,000 times (**Figure 5.5b**). Essentially, this test allowed for 10,000 LOESS fits to occur and for 10,000 corresponding threshold estimates to be made. These bootstrapped estimates were also used to calculate the mean and 95% confidence intervals of the Z_score distribution across the full range of achievable heteroplasmy levels (0-100%). This final bootstrapped data (the mean) and the original dataset were plotted onto one LOESS profile for each patient. In addition, the heteroplasmy level at which the upper and lower 95% confidence intervals intercepted the $y = -3$ Z_score deficiency cut off were also plotted (**Figure 5.5c**).

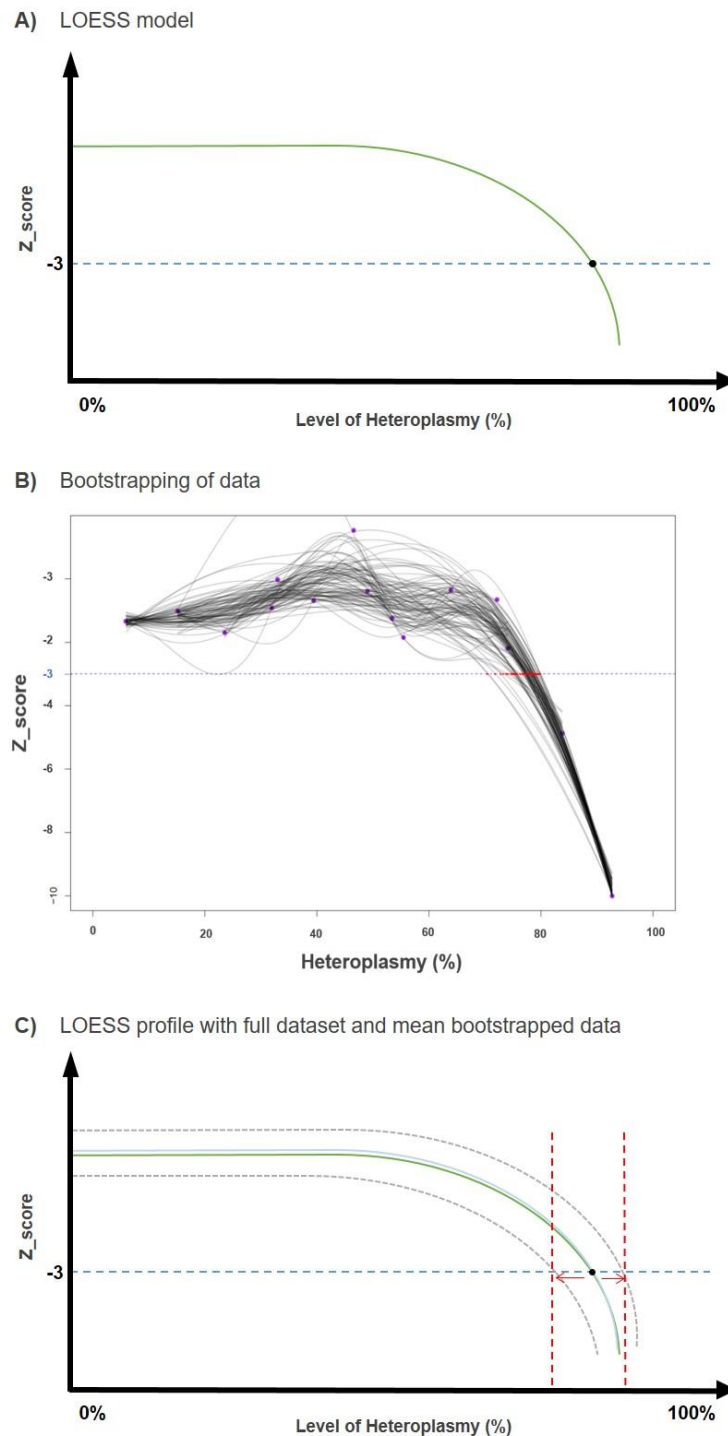


Figure 5.5: A schematic diagram of the LOESS regression and bootstrapping.

A) LOESS model was fitted to the original data (green curve) and the estimate of threshold (black dot) was defined as the intercept between the curve and a Z-score of -3 – cut off for biochemical deficiency (dark blue dashed line at $y=-3$). B) bootstrapping of this data (example of 100 times); red dots = threshold estimates through bootstrapping, purple dots = examples of original data points and C) final LOESS profile with both original dataset (green curve) and the mean of final bootstrapped data (light blue). Grey dashed line = 95% confidence intervals of bootstrapped data, vertical red dashed line = heteroplasmy level at which the upper and lower 95% confidence intervals intercept -3 Z_score cut off.

5.3.10.2. Hierarchical clustering

To investigate an alternative method of fibre classification, unsupervised hierarchical clustering (Ward J 1963) of fibres into at most two populations, was carried out using the `hclust` function in R (R Core Team, 2018). This statistical method was coded by Dr Conor Lawless.

This classification method used the optical density data (protein expression level of each target in each single fibre) generated from the quadruple immunofluorescence assay. Fibres in each individual patient were classified based on the log transformed data of porin (VDAC) and Complex I (NDUFB8) expression. By classifying fibres as either biochemically normal or deficient based solely on each patient's Complex I – porin profile, it allowed the data to be clustered largely independent of the non-disease control data, in that the patient's own fibres were used to identify two populations of fibres; biochemically normal and deficient. After segregating fibres into two populations by clustering, the population most similar to that of the control data was classified as “normal” while the remaining cluster was classified as “deficient”.

Two-dimensional scatter (2D) plots, known as 2Dmito plots, were generated showing the biochemically normal fibres (blue) and the biochemically deficient fibres (red) after Complex I optical density values were log transformed and plotted against the log transformed porin values. This is schematically shown in **Figure 5.6**.

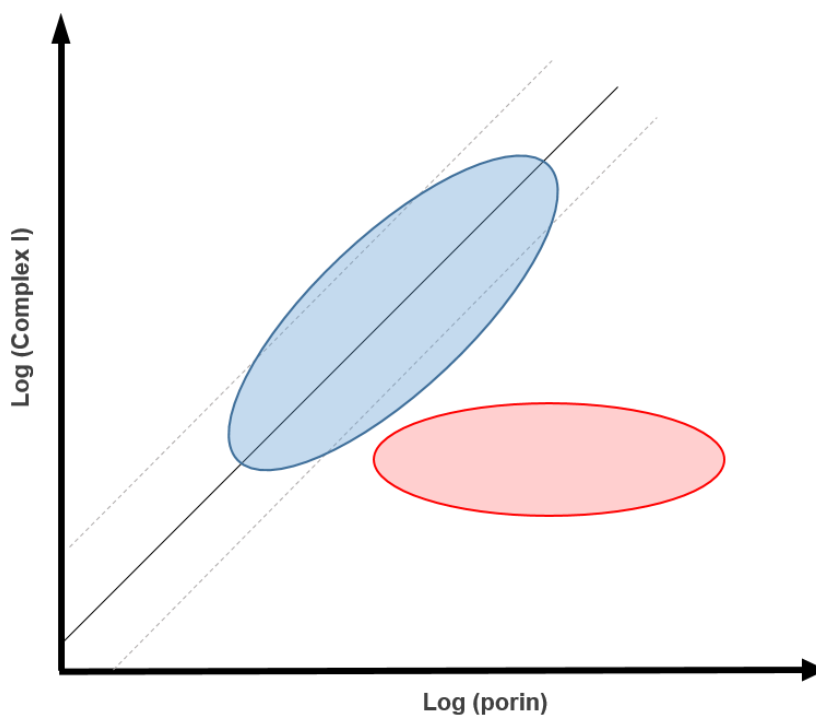


Figure 5.6: Schematic illustration of two-dimensional scatter plot (2Dmito plot) after hierarchical clustering for fibre classification.

Blue shows the cluster of biochemically normal fibres and red shows the biochemically deficient cluster. The solid grey line indicates a regression fitted to the non-disease control data, with a 95% confidence interval shown with dotted grey lines for comparison.

5.3.10.3. Kernel density estimate plots

Data from the sampled fibres (classified as biochemically normal fibres or deficient, according to the hierarchical clustering) from all patients were bootstrapped (n=10,000) and kernel density estimate models were fitted to each replicate, using the density function in R (R Core Team, 2018). The heteroplasmy level at which the mutation load distribution for the biochemically normal fibres intersected with the distribution for the deficient fibres was defined as the threshold, as depicted in **Figure 5.7**. Bootstrapping the estimates in this way allowed the uncertainty in the estimated thresholds to be measured. This aspect of the work was also coded by Dr Conor Lawless.

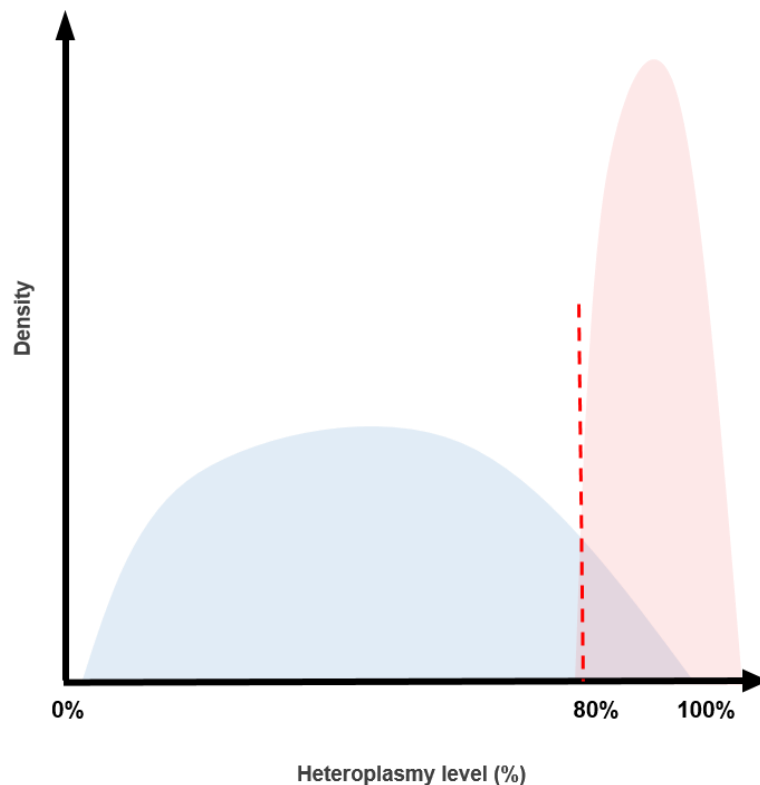


Figure 5.7: Schematic illustration of kernel density estimate.

The distributions of both the biochemically normal fibres (blue) and deficient fibres (red) were determined using kernel density estimates. The red vertical dashed line represents the heteroplasmy level at which the distribution of both intersect and this is the threshold estimate.

5.4. Results

A total of 1,483 single fibres were isolated and analysed through quantitative pyrosequencing during this study, across the 13 patient muscle sections. These findings were used alongside the quantitative data from the quadruple immunofluorescence assay that was initially attained in **Chapter 4**.

5.4.1. Optimisation of the single cell study

5.4.1.1. *Investigating the sampling method for single cell study*

The ideal method for sampling fibres for this study would have been complete random sampling from the skeletal muscle sections of patients from Group A, without knowing the OXPPOS groups. However, this project aimed to analyse and characterise the distribution in heteroplasmy levels in both the normal and deficient fibres from as many patient skeletal muscle sections, within a specific time frame. The aim thereafter was to deduce an estimated threshold and compare these between the different patients. Therefore, the selection strategy was based on that described by Rocha et al. (2018). This method allowed for sampling and characterisation of both normal and deficient fibres and it was ideal for the timeframe of the project.

To emphasise this further, **Table 5.3** highlights the number of fibres that would need to be sampled at complete random to achieve (at a probability of >0.5) the current number of deficient fibres already shown in **Table 5.2** of section 5.3.9. For example, P13 had a total of 1261 fibres analysed with the quadruple immunofluorescence assay, of which 75 fibres were below $-3 Z_score$ and therefore deficient. A total of 89 fibres were selected for pyrosequencing of which 17 were the deficient fibres. In order to achieve this same number through complete random sampling, 279 fibres would need to be sampled. It is evident from the table that those patients (P11, P13, P18 and P19) who presented with much lower number of deficient fibres compared to normal in their skeletal muscle, would require sampling over 250 fibres at random to achieve the current number of deficient fibres analysed. Therefore, given the aim of the study, to look at variability in threshold between individuals, the current sampling method was chosen.

Table 5.3: Random sampling compared to current sampling method

Patient	Total fibres analysed	Number of fibres deficient in total	Number of fibres sampled for pyrosequencing using sampling method from Rocha et al., 2018	Number of deficient fibres in sample	Random sampling: number of fibres required to get same number of deficient fibres
P01	871	597	106	47	68
P04	1179	710	114	66	109
P06	838	723	128	112	133
P07	546	247	89	52	131
P11	1464	295	77	53	261
P13	1261	75	89	17	279
P18	1258	387	115	76	331
P19	826	87	55	33	310

5.4.1: Optimisation and validation of the pyrosequencing approach for the single cell study:

Given the high number of single fibres per patient (ranging between 65 and 132 fibres in the 13 patients), a cost and time effective approach was required for this study. Therefore, the reproducibility of pyrosequencing was investigated in 44 fibres (combining fibres from P01, P04, P11 and P19) to assess if one pyrosequencing assay per fibre was reliable. This was achieved with three different experiments; experiments 1 and 2 which assessed the variability of the pyrosequencing using the same PCR amplicons and experiment 3, which assessed the variability of the whole assay (new experimental set up). The variability between experiments 1 and 2 were compared as well as 1 and 2 with experiment 3. Following set criteria, a $\pm 3\%$ range (equivalent to a range of 6%) was used to determine a heteroplasmy readout. The heteroplasmy level measurements per fibre (technical replicates) are shown in **Figure 5.8** and are further summarised in **Appendix 5, Table 7.3 (Chapter 7)**. Overall, the total range observed across all of the experiments for individual fibres were within 6% of each other, apart from fibre 925 (total range of 9%). This is also reflected by the SD for each of the fibres which is within 3%. In addition, experiment 3 showed more variability in heteroplasmy levels compared to heteroplasmy levels determined in experiment 1 and 2, highlighting that as expected, variabilities are likely to occur from a new experimental set up (**Chapter 7, Appendix 5, Table 7.3**).

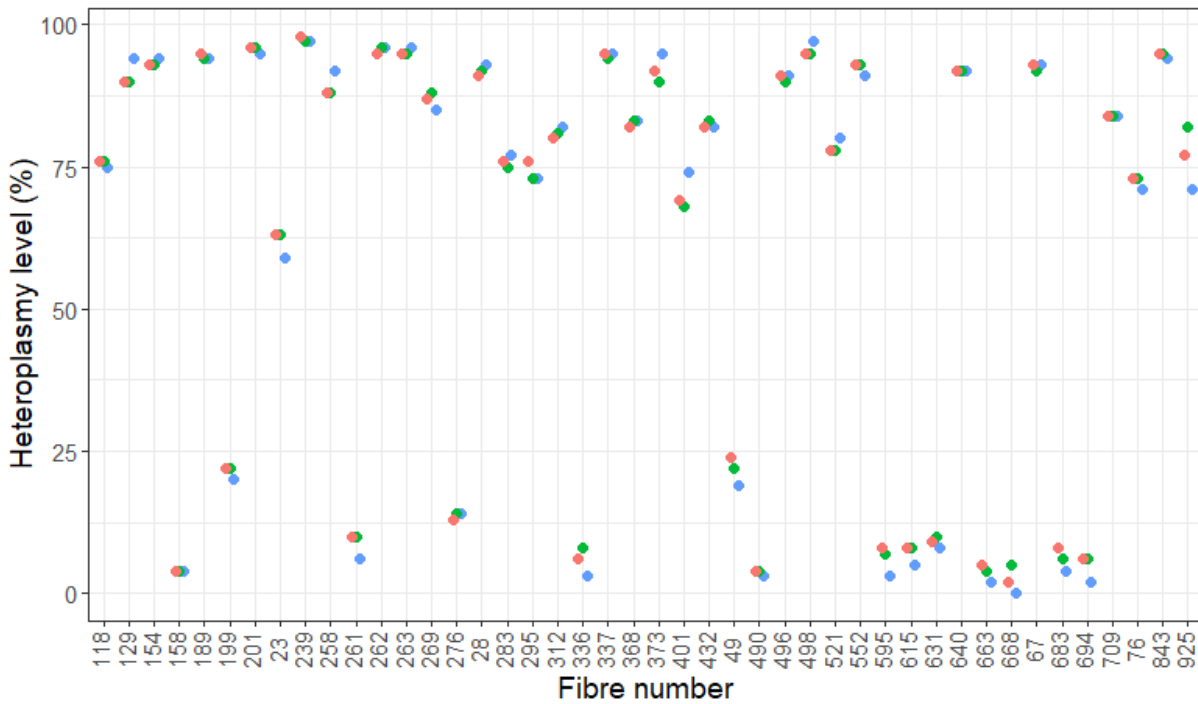


Figure 5.8: Heteroplasmy levels in fibres accessing inter and intra variability of pyrosequencing. The heteroplasmy levels of 44 fibres, taken from P01, P04, P11 and P19, were assessed from the same PCR amplicons (Experiment 1 (red) and 2 (green)) and from a new experimental set up (Experiment 3 (blue)). All fibre triplicates, apart from fibre 925, fell within a range of 6%. SD was within 3%.

Three controls of known heteroplasmy levels were also included in every pyrosequencing experiment undertaken for this study (n=89); 18% (control 1), 48% (control 2) and 72% (control 3). The spread of the heteroplasmy levels determined for each of these controls in all experiments is shown in **Figure 5.9**. The mean of the overall data for each control is within $\pm 3\%$ of the expected heteroplasmy levels. The SD for all controls are between 1% and 1.4%. Control 1 shows the biggest range in the data (14% to 23%), however, as seen in **Figure 5.9** this wide range is due to only a few experimental runs (n=6). In these instances, the read outs for the other two controls were also checked and results were accepted on the basis the heteroplasmy levels of these controls were as expected, as well as the negative control showing no sequence read out. Therefore, from these findings it can be concluded that one measurement per sample was sufficient.

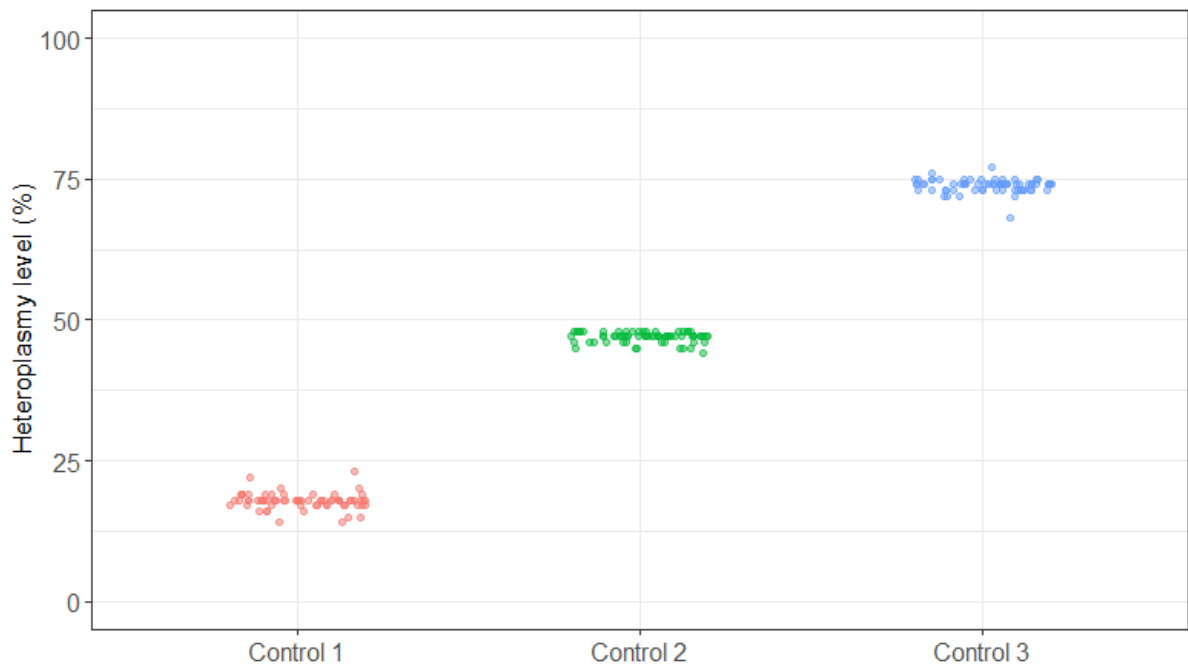


Figure 5.9: Distribution of heteroplasmy levels in the three controls in all pyrosequencing experiments.

The controls all show a tight distribution in the range. The summary data is as follows; total range in Control 1 = 14-23%, Control 2 = 44-48% and Control 3 = 72-77%. The mean of the controls are 18.0%, 46.9% and 73.7% and SDs; 1.4%, 1.0% and 1.2% respectively.

5.4.2. Heteroplasmy level and respiratory chain deficiency

Heteroplasmy level of the m.3243A>G variant was determined by pyrosequencing in all sampled fibres from the 13 patient skeletal muscle sections. The range of the m.3243A>G heteroplasmy levels detected in individual fibres per OXPHOS group for each patient is highlighted in **Table 5.4**. This distribution of the data is shown in the boxplots in **Figure 5.10**.

5.4.2.1. m.3243A>G heteroplasmy levels increase in deficient fibres

In all patients from Group A, apart from P05 and P19, Group 1 fibres (biochemically normal) show a broad distribution in the heteroplasmy levels determined, collectively ranging from 3% to 98%. In comparison, the distributions of heteroplasmy levels in fibres sampled from Groups 2 to 4 and 5, were higher and had a narrower range. Therefore, fibres with respiratory chain deficiency tend to have higher heteroplasmy levels. Although **Table 5.4** highlights that a number of fibres in Groups 2, 3 and 4 (and 5) have low heteroplasmy levels, **Figure 5.10** shows that this is only representative of a very small number of fibres, whilst the majority of fibres in these groups show consistently high heteroplasmy levels.

The Group 1 fibres sampled from Group B patient skeletal muscle sections showed an overall range in heteroplasmy level between 14% and 97% (**Table 5.4**). However, the vast majority of the fibres analysed were clustered within a narrow range of heteroplasmy levels (**Figure 5.11**) – contrasting with the larger range observed in the normal fibres from patients in Group A. This narrow range is also seen in the fibres sampled from P05, which despite showing deficiency and an increase in heteroplasmy level per OXPHOS group, had a range of 58-88% heteroplasmy levels in normal fibres.

The fibres sampled from P19 showed a different distribution in the heteroplasmy levels. The heteroplasmy levels in Group 1 fibres ranged from 3% to 84%, however of the 20 fibres analysed in this group, 16 fibres were shown to have heteroplasmy levels ranging from 3% to 22%. Therefore, in comparison to the other patients, P19 Group 1 fibres presented with lower levels of heteroplasmy. An increase of heteroplasmy level was observed in fibres within Groups 2, 3 and 4, however as shown in **Figure 5.10**, there are a number of fibres with much lower heteroplasmy levels within these groups. The boxplot highlights that there are seemingly two groups of fibres, fibres with very high levels of heteroplasmy and fibres with very low levels of heteroplasmy, irrespective of the biochemical deficiency. These findings could be alluding to this patient harbouring another mtDNA mutation (point mutation or possibly a mtDNA deletion) which could be influencing the heteroplasmy levels determined in the single fibres from the patients skeletal muscle section, particularly the normal fibres that show low levels of m.3243A>G heteroplasmy.

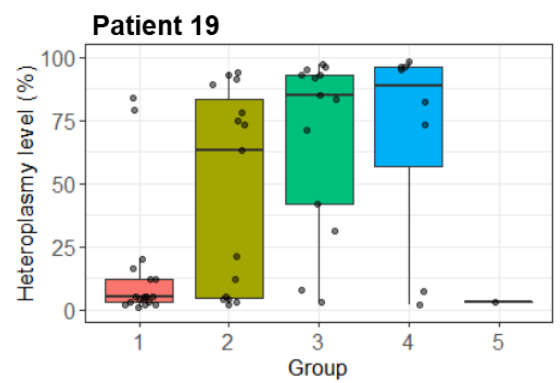
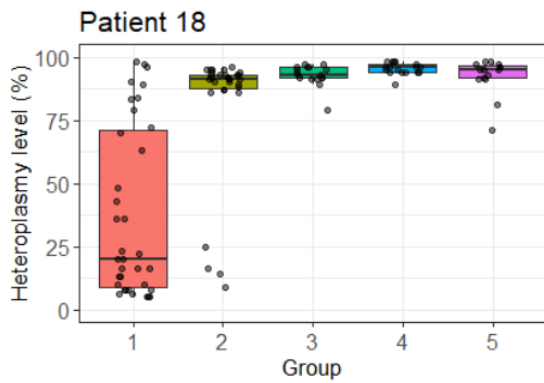
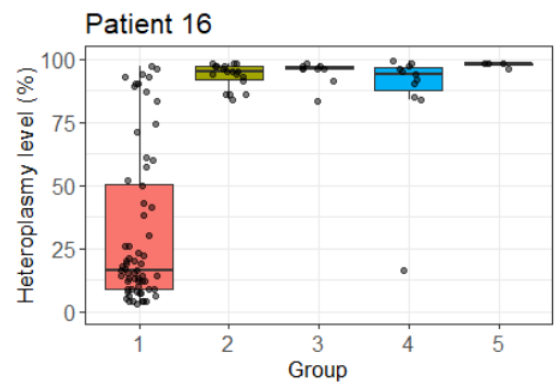
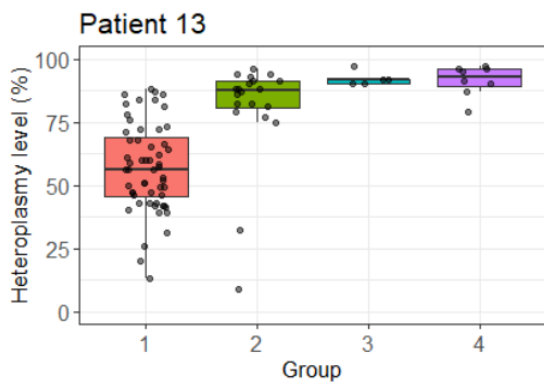
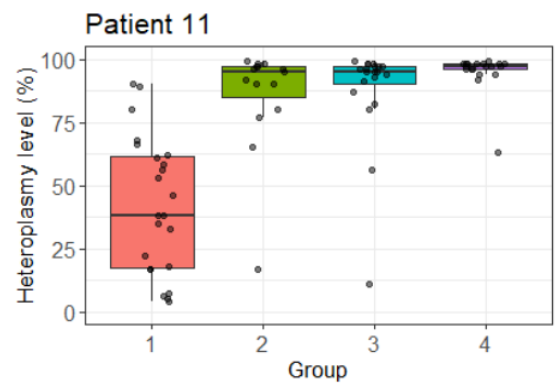
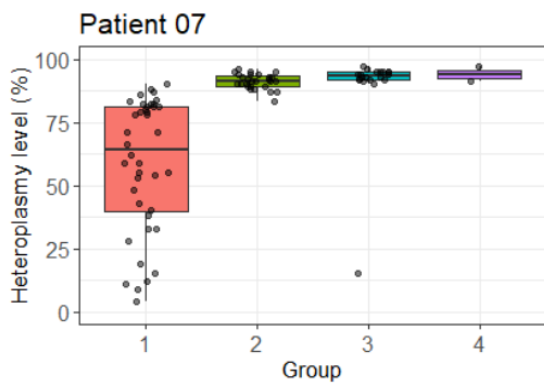
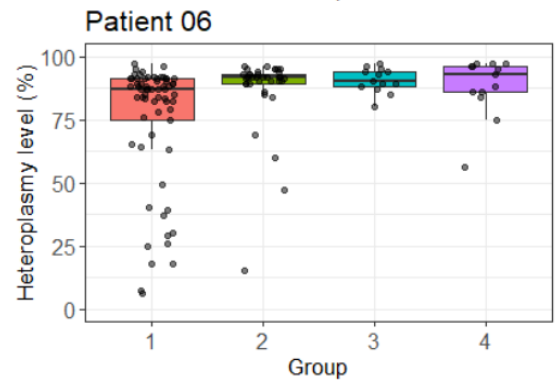
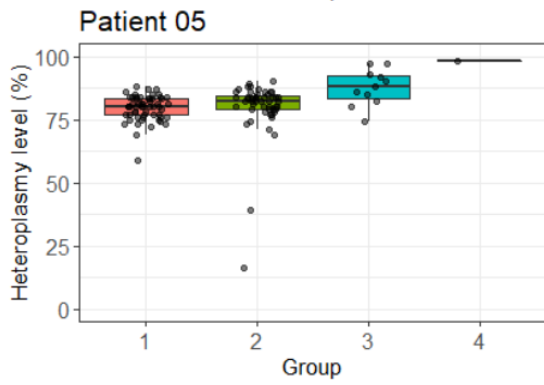
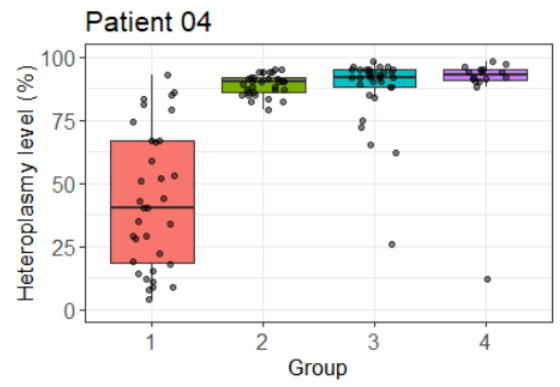
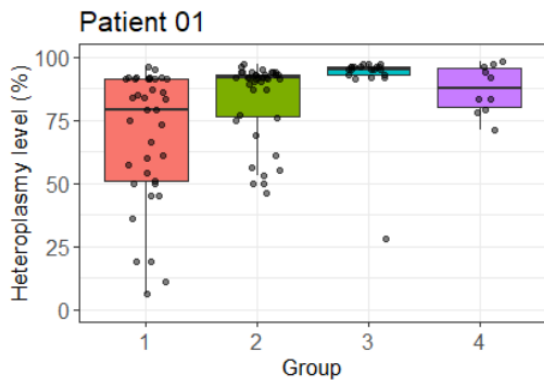


Figure 5.10: Distribution of single fibre heteroplasmy levels in each OXPHOS group observed in patients in Group A.

Fibres from all Patients in Group A, apart from P05 and P19, show a broad distribution in heteroplasmy level in fibres in Group 1. Heteroplasmy level increases and narrows in range from Group 2 to 5. P05 shows a narrow range in heteroplasmy level in all groups. P19 shows fibres with both low and high levels of heteroplasmy in all groups. Each individual dot represents a single muscle fibre. OXPHOS groups = Group 1= normal Complex I and Complex IV; Group 2 = Intermediate positive and negative for Complex I, normal Complex IV; Group 3; Negative for Complex I and normal Complex IV; Group 4; Negative for Complex I, intermediate positive and negative for Complex IV; Group 5 = Negative Complex I and Complex IV.

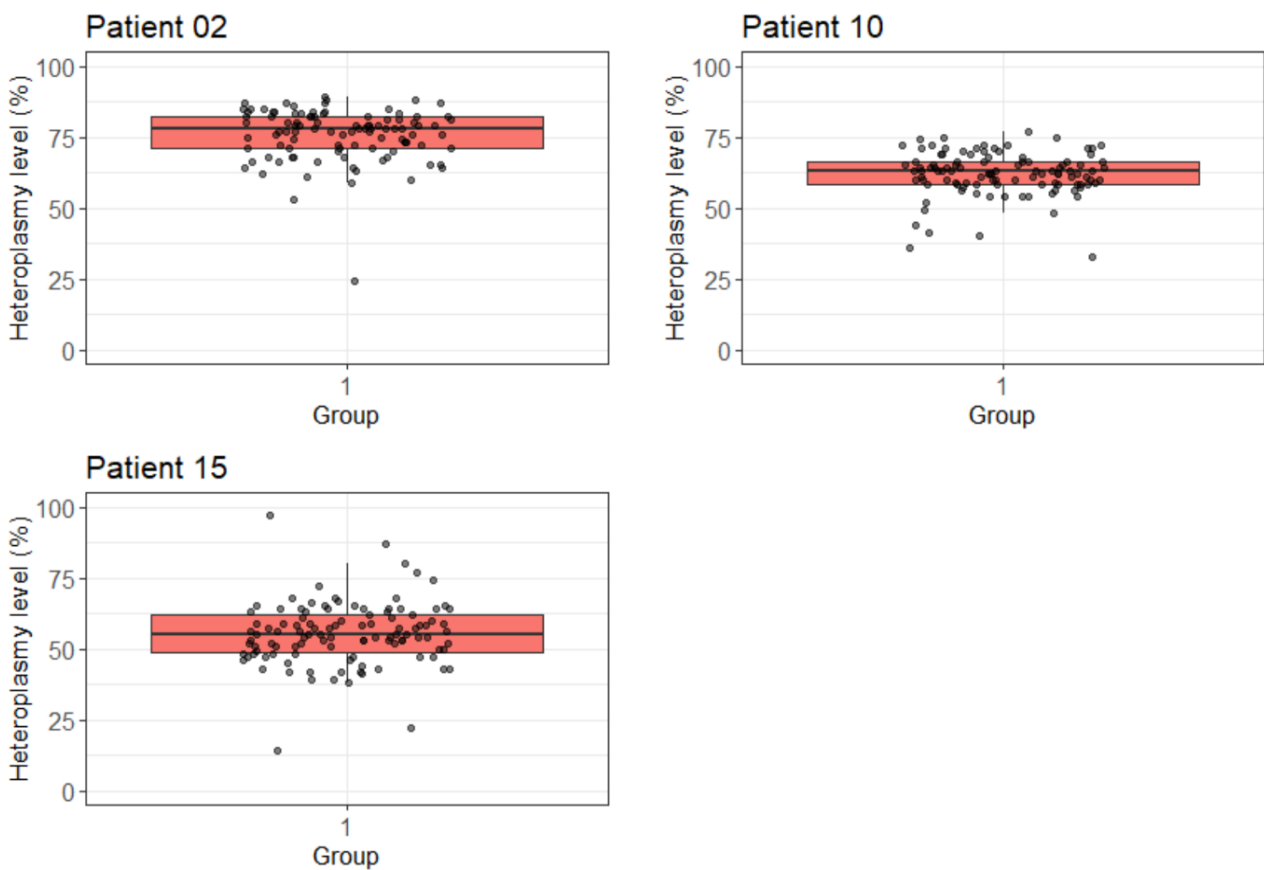


Figure 5.11: Distribution of single fibre heteroplasmy levels from Group B patient muscle sections. Heteroplasmy levels in Group 1 fibres sampled from patients in Group B are within a narrow range for each patient (P02, P10; P15) in comparison to the broad distribution observed in Group I fibres sampled from patients in Group A. Each individual dot represents a single muscle fibre. Heteroplasmy levels for the group 1 fibres are within a narrow range for each patient. Group = OXPHOS Groups 1.

Table 5.4: The range of heteroplasmy level determined in single fibres per OXPHOS group from all patient skeletal muscle sections

Heteroplasmy levels per OXPHOS status group (%)													
Patients	Group 1		Group 2		Group 3		Group 4		Group 5		Median	Mean	Homogenate heteroplasmy level (%)
	Lowest	Highest											
Group A													
P01	6	96	46	97	91	97	71	98	-	-	94	88	89
P04	4	93	79	95	26	98	88	98	-	-	88	75	78
P05	59	88	16	90	74	98	98		-	-	82	81	78
P06	6	97	15	96	87	97	95	97	-	-	89	81	77
P07	19	81	83	96	15	97	91	97	-	-	88	76	74
P11	4	90	17	99	11	99	63	99	-	-	93	76	64
P13	13	88	9	96	90	97	79	97	-	-	69	67	62
P16	3	97	84	98	83	98	16	99	96	98	61	55	50
P18	5	98	9	96	79	97	89	98	71	98	91	73	39
P19	3	84	4	97	4	96	4	97	-	-	66	49	34
Group B													
P02	24	89	-	-	-	-	-	-	-	-	78	76	84
P10	33	77	-	-	-	-	-	-	-	-	63	61	66
P15	14	97	-	-	-	-	-	-	-	-	55	55	55

5.4.2.2. The relationship between single cell m.3243A>G heteroplasmy levels and homogenate heteroplasmy levels

The homogenate heteroplasmy levels previously measured for each patient is presented in **Table 5.4**. In 11 of the 13 patients, the mean and median heteroplasmy levels of the sampled muscle fibres were similar to their homogenate levels – which would be expected and indicative of the fact that the sampling strategy is representative of the whole section. However, the single cell work allows an insight into the distribution of heteroplasmy level in individual fibres, particularly for Group 1 fibres. Only P18 and P19 single muscle fibres had higher mean and median when compared to the homogenate heteroplasmy levels of 39% and 35% respectively.

5.4.2.3. Investigating the difference in porin levels between the two patient groups

The quadruple immunofluorescence assay used porin as a marker for mitochondrial mass which can be indicative of mitochondrial biogenesis. The difference between the log(Porin) levels in patients from Group A and Group B was investigated using a linear mixed effects model to establish if this could be influencing the biochemical differences between fibres in the muscle sections from the two groups of patients (**Figure 5.12**). Fibres from patients in Group B (P02, P05, P10 and P15) were shown to have lower levels of log(Porin) compared to fibres from patients in Group A, however this was a small difference and not significant (coefficient = -0.035, SE = 0.031, P= 0.3000). Therefore, these data show that porin levels are not causing the difference in the biochemical status between the muscle fibres from these two groups of patients.

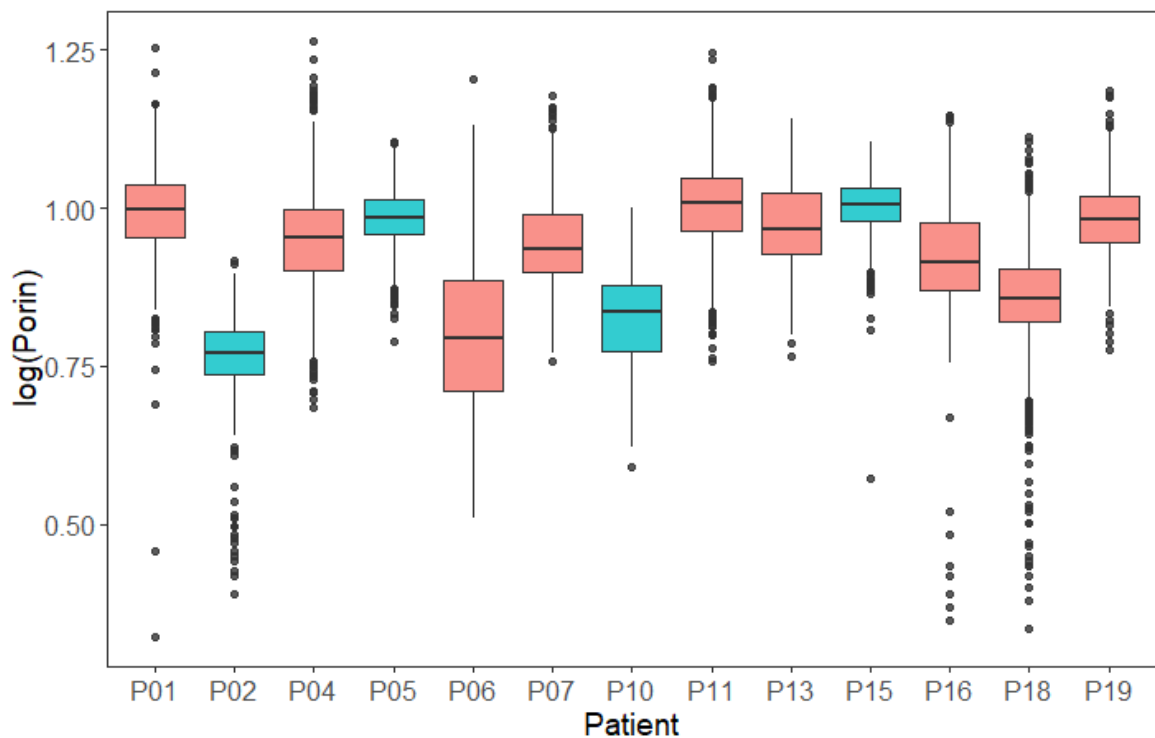


Figure 5.12: Boxplot showing $\log(\text{Porin})$ levels in muscle fibres from each patient muscle section. Variable levels of $\log(\text{Porin})$ are seen between muscle fibres from patient sections but fibres sampled from patients in Group B (blue) were shown to have lower levels of porin in comparison to fibres sampled from patients in Group A (red), although this difference was not significant ($SE = 0.031$, $P = 0.3000$). Individual dots = single muscle fibres that are outliers.

5.4.2.4. Muscle fibre types and $m.3243A>G$ heteroplasmy levels

The sampling of fibres for single cell analysis was representative of the different muscle fibre types found in skeletal muscle sections. Of the 13 patient muscle sections, 11 sections had fibre type data matched with the OXPHOS status (see section 5.3.5). The difference in $m.3243A>G$ heteroplasmy level was investigated between these two fibre types (Type I and Type II (consisted of Type IIa and IIx) fibres) using a linear mixed-effects model. There was a significant difference in heteroplasmy levels between the two types; Type II fibres had higher heteroplasmy levels than Type I, by 6% ($SE = 1.600$, $P = 0.0002$).

However, of the 11 patients that had fibre type data collected from their skeletal muscle section, only three had significantly higher median heteroplasmy levels in Type II fibres than Type I; P11, P13 and P16 ($P=0.053$, $P= 0.001$ and $P= 0.005$ respectively), following a Wilcoxon rank sum test. This is shown in **Figure 5.13** and also summarised in **Table 5.5**. Moreover, it can be seen that in some patients' skeletal muscle section (P06, P07, P15 and P18), Type I fibres (red) had a higher median heteroplasmy level than Type II, though not

significantly. This highlights the variability in these findings and indicates that the significant difference overall (as detailed above) is likely to be due to the influence of data from a small number of patient sections.

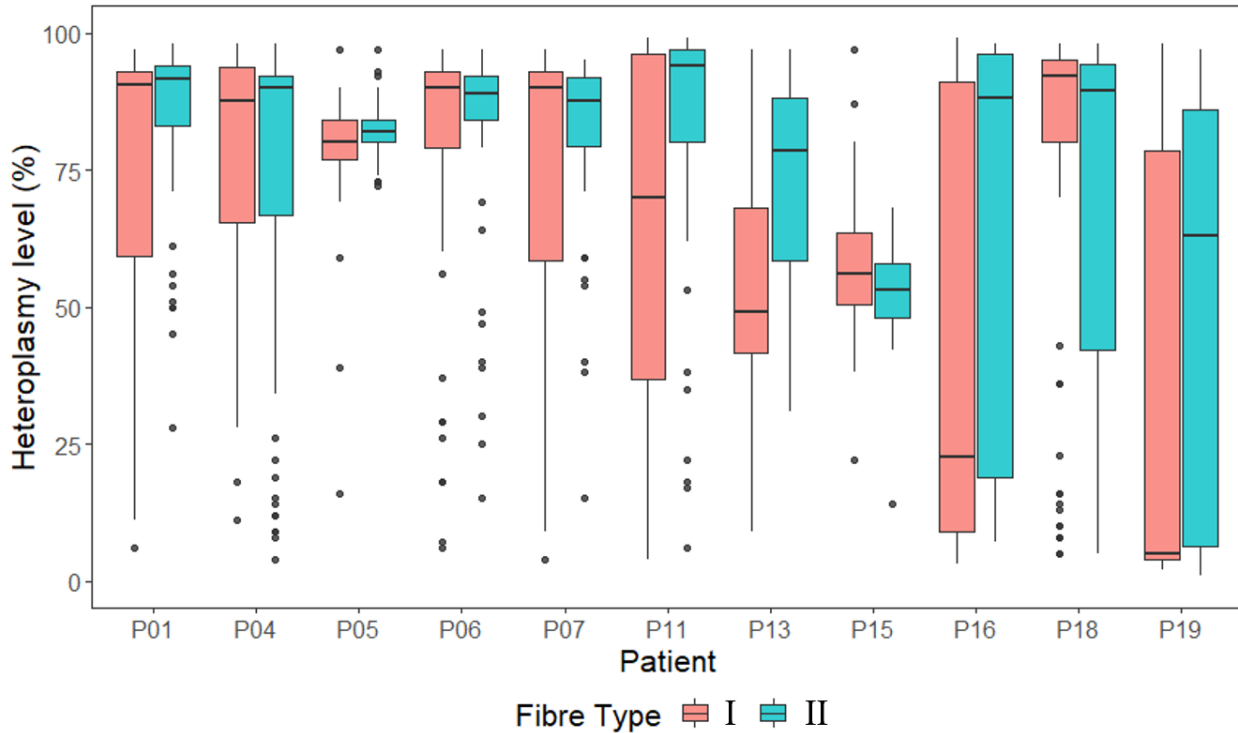


Figure 5.13: Boxplot of *m.3243A>G* heteroplasmy level in Type I and Type II muscle fibres.
A comparison of heteroplasmy levels in Type I (red) and Type II (blue) fibres per patient muscle section. The overlaid boxplot shows the median heteroplasmy level (black horizontal line in box) is higher in Type II fibres in muscle sections of patients P01, P04, P05, P11, P13, P16 and P19 but only significantly different in P11 ($P= 0.053$), P13 ($P= 0.001$) and P16 ($P= 0.005$), as determined by a Wilcoxon test. Median heteroplasmy level is higher in Type I fibres than Type II fibres in patients P06, P07, P15 and P18 but not significantly. Individual dots = single muscle fibres that are outliers.

Table 5.5: Median, W and P-value showing differences in m.3243A>G heteroplasmy levels between the different muscle fibre types

Patient	Fibre type	Minimum	Lower quartile	Median	Mean	Upper quartile	Maximum	W	P-value
P01	I	6.00	59.25	90.50	75.06	93.00	97.00	1155	0.132
	II	28.00	83.00	91.50	84.52	94.00	98.00		
P04	I	11.00	65.50	87.50	77.07	93.75	98.00	1689.5	0.700
	II	4.00	66.75	90.00	72.45	92.00	98.00		
P05	I	16.00	77.00	80.00	78.56	84.00	97.00	1466	0.059
	II	72.00	80.00	82.00	82.13	84.00	97.00		
P06	I	6.00	79.00	90.00	79.73	93.00	97.00	2194.5	0.697
	II	15.00	84.00	89.00	82.63	92.00	97.00		
P07	I	4.00	58.50	90.00	73.43	93.00	97.00	1018.5	0.684
	II	15.00	79.25	87.50	79.87	91.75	95.00		
P11	I	4.00	36.75	70.00	64.18	96.25	99.00	503.5	0.053
	II	6.00	80.00	94.00	82.00	97.00	99.00		
P13	I	9.00	41.50	49.00	54.15	68.00	97.00	477.5	0.001
	II	31.00	58.50	78.50	72.92	88.00	97.00		
P15	I	22.00	50.50	56.00	56.47	63.50	97.00	1384	0.098
	II	14.00	48.00	53.00	52.00	58.00	68.00		
P16	I	3.00	9.00	22.50	44.15	91.00	99.00	952	0.005
	II	7.00	19.00	88.00	65.07	96.00	98.00		
P18	I	5.00	80.00	92.00	76.49	95.00	98.00	353.5	0.350
	II	5.00	45.25	89.50	70.48	94.25	98.00		
P19	I	2.00	4.00	5.00	34.87	78.50	98.00	1939.5	0.202
	II	1.00	6.25	63.00	48.72	86.00	97.00		

5.4.3. Estimating the biochemical threshold for Complex I in the skeletal muscle of m.3243A>G patients

In order to determine a biochemical threshold for Complex I deficiency (the predominant biochemical deficiency observed) in these patient muscle sections, various statistical methods were considered. Although the statistical details are not within the scope of this thesis, they are important to discuss in order to understand the final estimation of the threshold per patient.

5.4.3.1. LOESS profiles using single fibre Z-scores and heteroplasmy level data

Firstly, the NDUFB8_z values from each sampled single fibre were plotted against their associated heteroplasmy level. The LOESS non-parametric model (described previously in section 5.3.10.1) was fitted to the data (red curve in **Figure 5.12**). The mean and 95% confidence intervals of the bootstrapped model are also plotted (black curve in **Figure 5.12**). From this, estimates of the heteroplasmic threshold (where the mean bootstrapped curve intercepted the -3 Z_score deficiency cut off) were determined alongside both the lower and upper 95% confidence intervals (dark blue vertical lines). The heteroplasmy levels at which both the lower and upper 95% confidence intervals intercepted the $y = -3$ cut off was also plotted and determined. These are summarised in **Table 5.6**.

The LOESS profiles of P01, P05, P07 and P19 are exemplified in **Figure 5.14**. As it can be seen in all four profiles, both the red and black curves are either identical or very similar in their fit along the x-axis. The LOESS profile for P07 (**Figure 5.12a**) shows an estimation in the heteroplasmic threshold for biochemical deficiency at of 87.2%, which is supported by a narrow upper and lower 95% confidence intervals (86.0% and 88.4% respectively) due to the good spread in the data attained from this patient's skeletal muscle section.

However, this was not the case for the sections from P01, P05 or P19 (**Figure 5.14**) or the remaining six patients in Group A (see **Appendix 6** in **Chapter 7**, **Figure 7.2**). The curves (red and black) in P01 LOESS profile intercepted the -3 Z_score cut off twice, leading to inaccuracy in the estimation of threshold (mean at 88.8%) (**Figure 5.12b**). The 95% confidence intervals are also wide due to the uneven spread of data and the lower and upper intervals intercept -3 cut off at heteroplasmy levels of 18.9% and 91.1% respectively. P05 LOESS profile shows the dominant effect of one data point on the LOESS model and calculation of only the heteroplasmy level at which the upper confidence interval intercepts the -3 Z_score (82.9%) whilst the lower confidence interval did not intercept the cut off and so no heteroplasmy level for this was determined. Interestingly, the profile for P05 further highlights the narrow range in heteroplasmy levels. The profile for P19 shows that due to the

uneven spread of data between low and high heteroplasmy levels in both deficient and normal fibres, the curve intercepted the -3 Z_score cut off at a lower heteroplasmy level (19.7%) and similarly to P05, only the upper confidence interval intercepted the -3 cut-off (77.7), whilst the lower confidence interval was below the -3 cut-off and therefore no heteroplasmy level value determined.

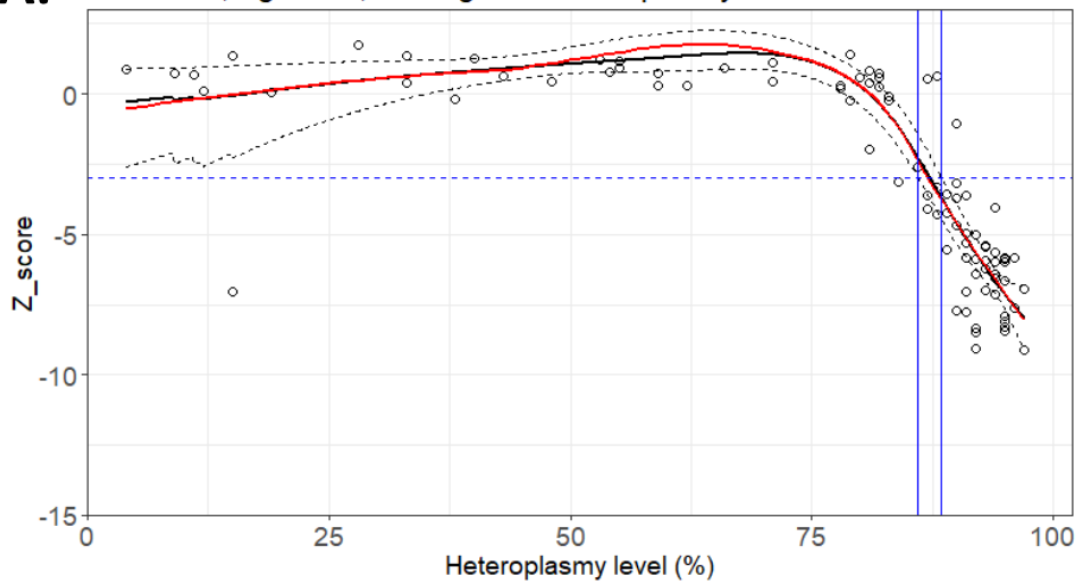
The threshold estimates deduced using this statistical method for patients in Group A are presented in **Table 5.6**. The 95% confidence intervals of the threshold estimates were wide for most of the patients; P01, P04, P05, P06, P11, P18 and P19, highlighting the high uncertainty of the threshold estimates for these patients

Table 5.6: Threshold estimates and upper and lower confidence intervals for selected patients using LOESS model fitted to the bootstrapped data

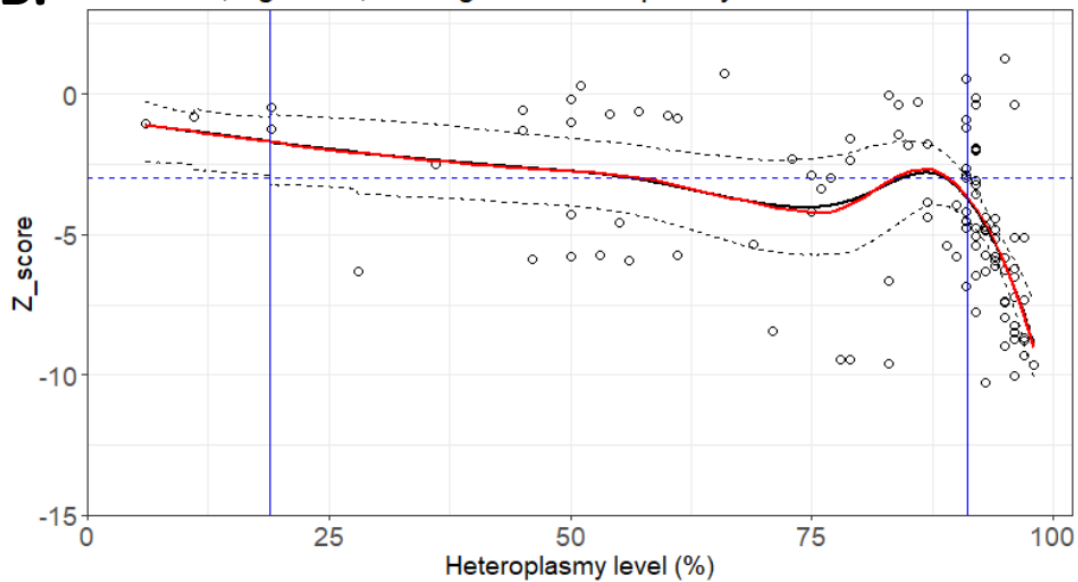
Patient	Mean	Lower confidence interval	Upper confidence interval
P01	88.8	18.9	91.1
P04	74.5	47.2	82.3
P05	78.2	0.00	82.9
P06	83.9	36.5	91.8
P07	87.2	86.0	88.4
P11	68.3	45.1	85.8
P13	80.1	75.0	83.4
P16	84.7	76.6	89
P18	75.3	35.8	85.3
P19	19.7	0.00	77.7

Overall, the LOESS profiles for these patients highlight the heterogeneity of the data and the disadvantages of this statistical method in determining the critical heteroplasmic threshold for Complex I deficiency. The most important disadvantage is the reliance on the use of Z_scores and the arbitrary -3 Z_score cut-off that defines the biochemical deficiency, which are all dependent upon on the data obtained from the non-diseased control group.

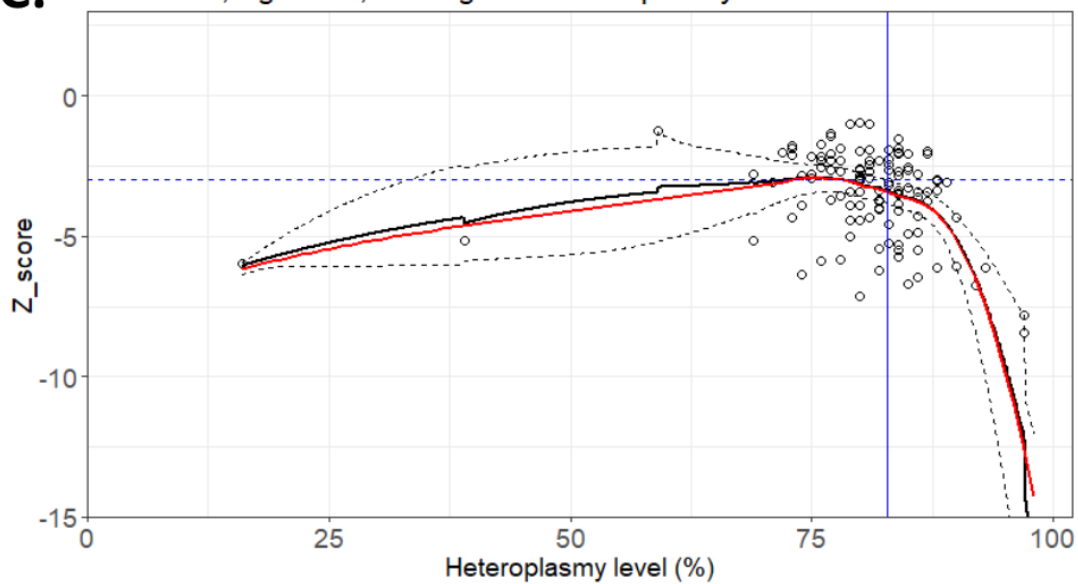
A. Patient 07, Age = 48, Homogenate heteroplasmy level = 74%



B. Patient 01, Age = 26, Homogenate heteroplasmy level = 89%



C. Patient 05, Age = 44, Homogenate heteroplasmy level = 78%



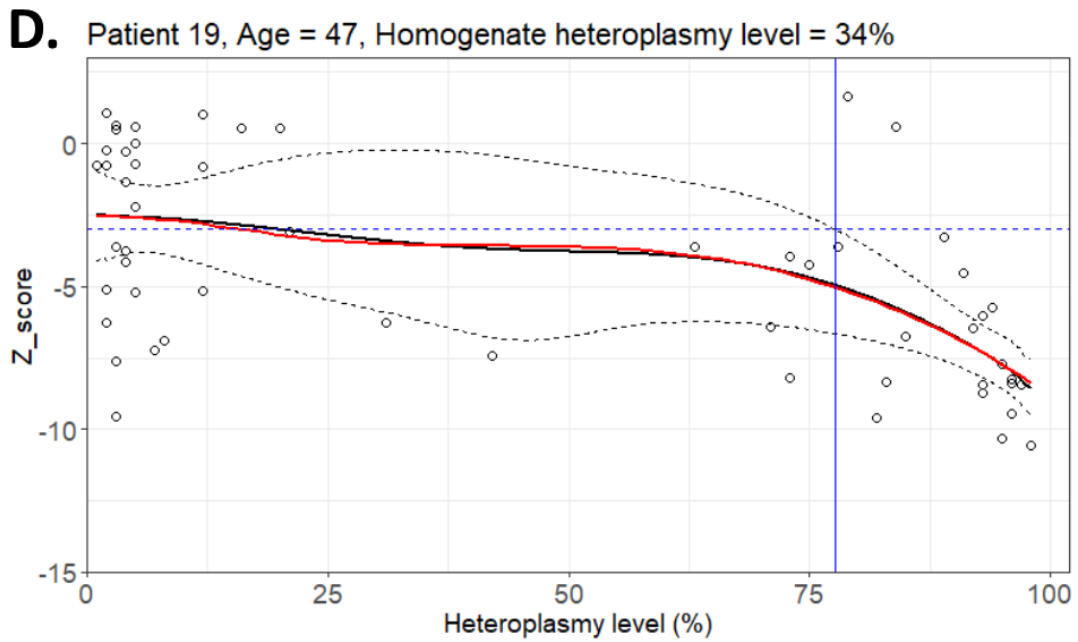


Figure 5.14: LOESS profiles showing the Z_score and heteroplasmy level distribution of single fibres and the estimated heteroplasmic threshold for deficiency.

Profiles are representative of fibres from skeletal muscle sections of patients in Group A and estimated threshold defined at point at which models curves cross the deficiency cut off at Z_score of -3 ($y=-3$). **A)** P07 shows a good spread of data across the heteroplasmy levels and narrow confidence intervals around the estimated threshold where curves intercept the $y=3$. **B)** P01 curve crosses $y=-3$ twice and wide confidence intervals and heteroplasmy levels at which these intercept the $y= -3$, **C)** P05 profile shows the influence of one data point (representing one fibre) on the shape of the curve and no intercept of the lower confidence interval at $y=-3$ and **D)** P19 shows wide confidence intervals around spread of the data and no intercept of lower confidence interval at $y= -3$. Each white dot represents a single fibre. The blue dashed line ($y=-3$) is the Z_score deficiency cut off. The black curve represents the model fitted to the mean of the bootstrapped data and the red curve represents the model fitted to the original data. The dotted black line around the curves = 95% confidence intervals of bootstrapped estimate. Solid dark blue lines represent the heteroplasmy levels at which the confidence intervals for the model cross the threshold Z_score of -3.

5.4.3.2. Control-free classifications using hierarchical clustering:

The analysis of the data with the LOESS model made it apparent that using the Z_scores, particularly the -3 Z_score cut off to determine the heteroplasmic threshold level for biochemical deficiency, was not a stringent way to investigate the heterogeneous dataset to achieve the aim of this project. Taking this into account and the fact that Z_score classification of fibres is based on the non-disease control group (not representative of the diseased group), a control-free classification of fibres was investigated. Thus, there was no reliance on Z_score measures for biochemical deficiency (only requiring the available protein expression (immunoreactivity) data) and therefore no direct reliance on the non-disease control groups. As described and depicted in **Figure 5.6** in section 5.3.10.2, unsupervised hierarchical clustering was applied to the optical density values (the raw expression values) attained from the assay, to provide a control-free classification of the fibres, based on the patient's own population of fibres. The classification of fibres was solely based on the Complex I/porin expression profile. The data could be split into two branches/clusters (V-shaped data) representing two different populations of fibres; biochemically normal (branch 1) and biochemically deficient fibres (branch 2) based on Complex I. Fibres were classified as deficient only when the frequency of this population was >5% of the total number of fibres analysed.

The 2Dmito plots of log Complex I expression level against log porin for P04 (Group A patient) and P10 (Group B patient) is shown in **Figure 5.15**, as examples. The colouring of the fibres in panel B and D of **Figure 5.15** (Complex IV panels) is based on Complex I clustering - the red fibres within the Complex IV plot are those fibres that are deficient for Complex I. The plot of P04 shows a definitive splitting (branching – V-shaped) of the fibre populations into two different clusters – blue cluster representing the biochemically normal fibres and red cluster representing the biochemically deficient fibres. The red cluster of fibres show a decrease in Complex I expression in relation to the porin level (**Figure 5.15a**). This definitive split in the Complex I data is also seen in the following Group A patients; P01, P07, P11, P13, P16, P18 and P19 (plots shown in **Appendix 7 (Figure 7.3)**). As expected, the Complex IV data in these patients showed no splitting in the data, but rather all being within one cluster, representing fibres with normal CIV expression. To provide the confirmation that the biochemically normal fibres were similar to what is seen in the non-disease controls, the regression line which was fitted to the control data and the 95% confidence intervals (shown by the grey lines) was also plotted onto the 2Dmito plots.

As represented by the 2Dmito plot of P10 in **Figure 5.15c**, fibres from Group B patients (P02, P10 and P15), also showed no splitting in their data (only one cluster present from the clustering method) and therefore only showed fibres that are biochemically normal. This was expected, as previously demonstrated with the Z_score analysis of the data. The majority of these fibres fall within the 95% confidence intervals of the non-disease control data, showing that although this classification is independent from these controls, both are still comparable. The 2Dmito plots for the following patient sections are shown in **Appendix 7 (Appendix Figure 7.3, Chapter 7)**; P01, P07, P11, P13, P16, P18 (Group A) and P02 and P15 from Group B.

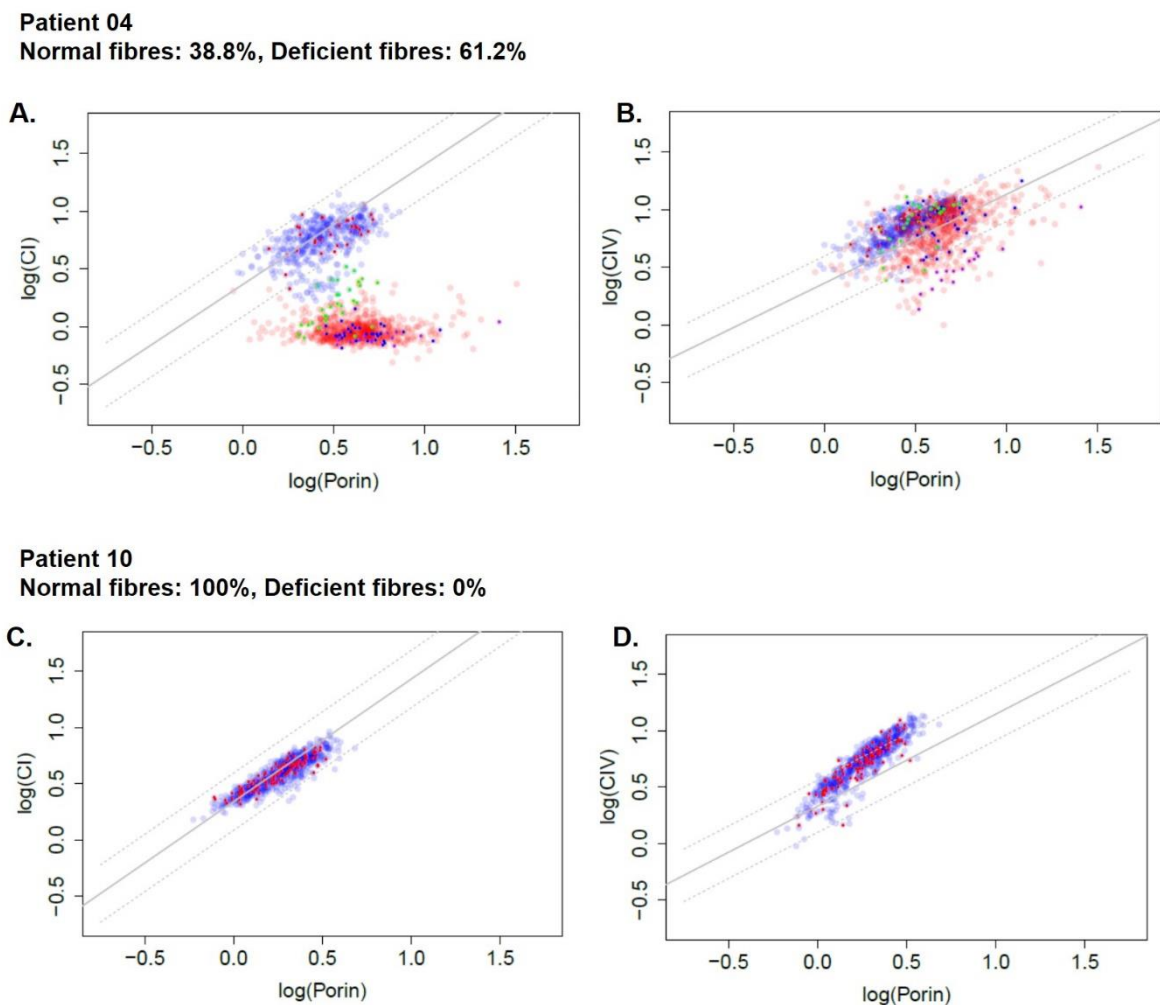


Figure 5.15: Two-dimensional scatterplots (2Dmito plots) comparing Complex I protein expression with mitochondrial mass.

(A – B) P04 and (C-D) P10. A) Complex I (CI) data in P04 shows clustering of fibres into two branches after hierarchical clustering; blue = biochemically normal fibres and red = biochemically deficient fibres for Complex I which is indicated by the decrease in Complex I in relation to log of

porin). **B)** Complex IV data in P04 shows only one cluster, therefore, no deficient fibres for Complex IV (CIV). Red fibres are indicative of Complex I deficient fibres in that cluster. **C)** P10 data also shows only one cluster in the data for either Complex I or **D)** Complex IV therefore all fibres are biochemically normal (blue). Sampled fibres have been colour co-ordinated according to the original Z_score classification; red = Group 1 fibres, green = Group 2 fibres, blue = Group 3 fibres, purple = Group 4 fibres. Grey solid and dashed line showing the regression line fitted to the control data and the 95% confidence intervals, for comparison.

Although the clustering was achievable for the majority of patients, as listed above, it was less convincing for P06. This is shown through the 2Dmito plot of P06 where the data appeared to have split into two populations of fibres (V-shape) as shown through the blue and red coloured fibres. However, deficient fibres are shown to have levels of Complex I that are comparable to the levels that would be expected of the non-disease controls (indicated by the 95% confidence interval) (**Figure 5.14**, panel C). Therefore, this shows that the clustering has not successfully identified between the biochemically normal fibres and the deficient.

Intriguingly, P05 was shown to have a Complex I- deficient mitochondrial respiratory chain profile from the Z_score analysis (58.71% Complex I- deficient fibres) (panel E of **Figure 5.16**). However, hierarchical clustering classified all of the fibres as normal for Complex I on the 2Dmito plot (panel A and B in **Figure 5.16**) as the shape of the data does not show two clear populations, but rather a shift down in relation to the control regression. This highlights how the difference in the classification methods can cause discrepancy in the proportion of fibres classified as normal or deficient. This comparison between the two classification methods is shown in **Table 5.7**. In all cases, aside from P05 and P06, the proportion of total Complex I deficient fibres are very similar with both methods.

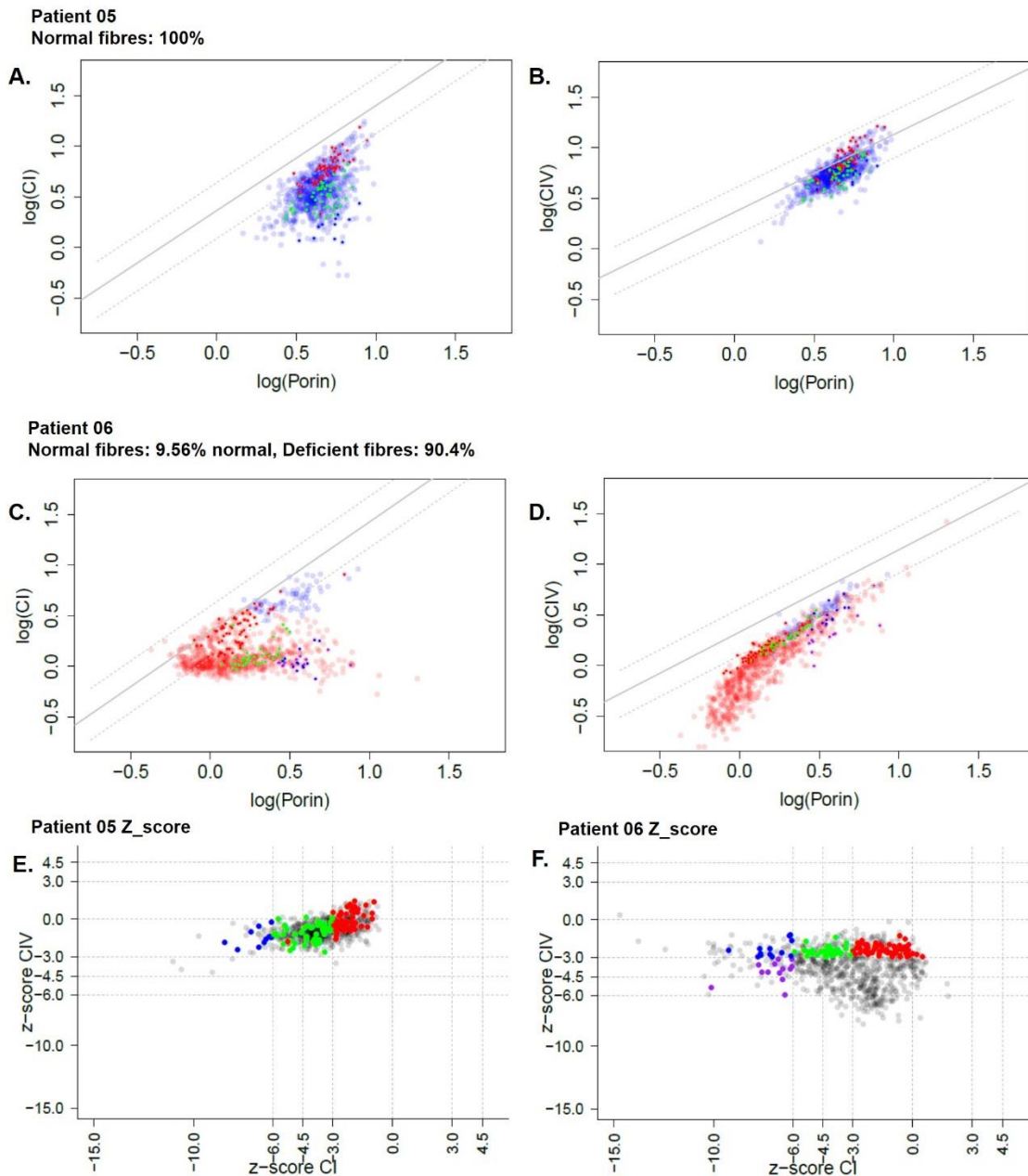


Figure 5.16: 2Dmito plots and mitochondrial respiratory chain profiles representing the data for P05 and P06.

A) In comparison to the mitochondrial profile for P05 (shown in E), hierarchical clustering classified all fibres as biochemically normal for Complex I and B) Complex IV. Only one cluster was identified in the data but there is a shift downwards from the control regression (in grey). C) P06 data shows two clusters (V-shape) however clustering has failed to identify the biochemically normal fibres which are in line with the control regression. Fibres have been classified as deficient for Complex I. F) Complex IV data shows a shift down from the control regression. Blue fibres in A, B, C and D = biochemically normal fibres, red fibres = deficient fibres. Coloured dots are representative of Z_score classification of fibres into OXPHOS groups = red = Group 1 fibres, green = Group 2 fibres, blue = Group 3 fibres, purple = Group 4 fibres. Regression line fitted to the control data and the 95% confidence intervals, for comparison.

Both methods of fibre classification showed similarities and differences in regard to the level of Complex I deficiency determined. The small differences in the results between the two methods can be explained by the fact that hierarchical clustering only determines either biochemically normal or deficient fibres. Therefore, the fibres that were initially classified as intermediate positive or negative through the Z_score analysis, were now classified as normal or deficient. This is exemplified by the previous 2Dmito plots (**Figure 5.13**) where the sampled fibres were coloured according to their stated OXPHOS groups, (as defined by the Z_score) and highlighting P04 as an example, it can be seen that the intermediate positive fibres (highlighted green) were classified as normal or deficient. Despite this, both methods of fibre classification were comparable for 11 of the 13 patients, showing that hierarchical clustering detected expected levels of Complex I deficiency in these patients, but most importantly, without reliance on the non-disease control data (**Table 5.7**).

Furthermore, whilst the sampled fibres were selected based on Z_score classifications into the different OXPHOS groups, the 2Dmito plots show that these sampled fibres (as coloured by their representative OXPHOS group) provide a good spread of sampling when placed into the context of the hierarchical clustering method.

Table 5.7: Differences in the proportion of fibres (%) classified as Complex I and Complex IV deficient through Z_scores classification and Complex I deficient with hierarchical clustering

Patient	Proportion of deficient fibres (%)		
	Hierarchical clustering based on Complex I/Porin expression levels	Z_score - Complex I	Z_score - Complex IV
Group A patients			
P01	69.3	79.45	2.07
P04	61.2	63.61	3.73
P05	0	58.71	0.70
P06	90.4	69.45	29.95
P07	36.2	39.19	1.28
P11	21.9	21.93	6.97
P13	6.9	8.41	4.28
P16	15.5	16.38	3.67
P18	22.3	19.87	11.69
P19	10.5	11.50	2.42
Group B Patients			
P02	0	2.20	0.48
P10	0	0.00	0.00
P15	0	0.91	0.20

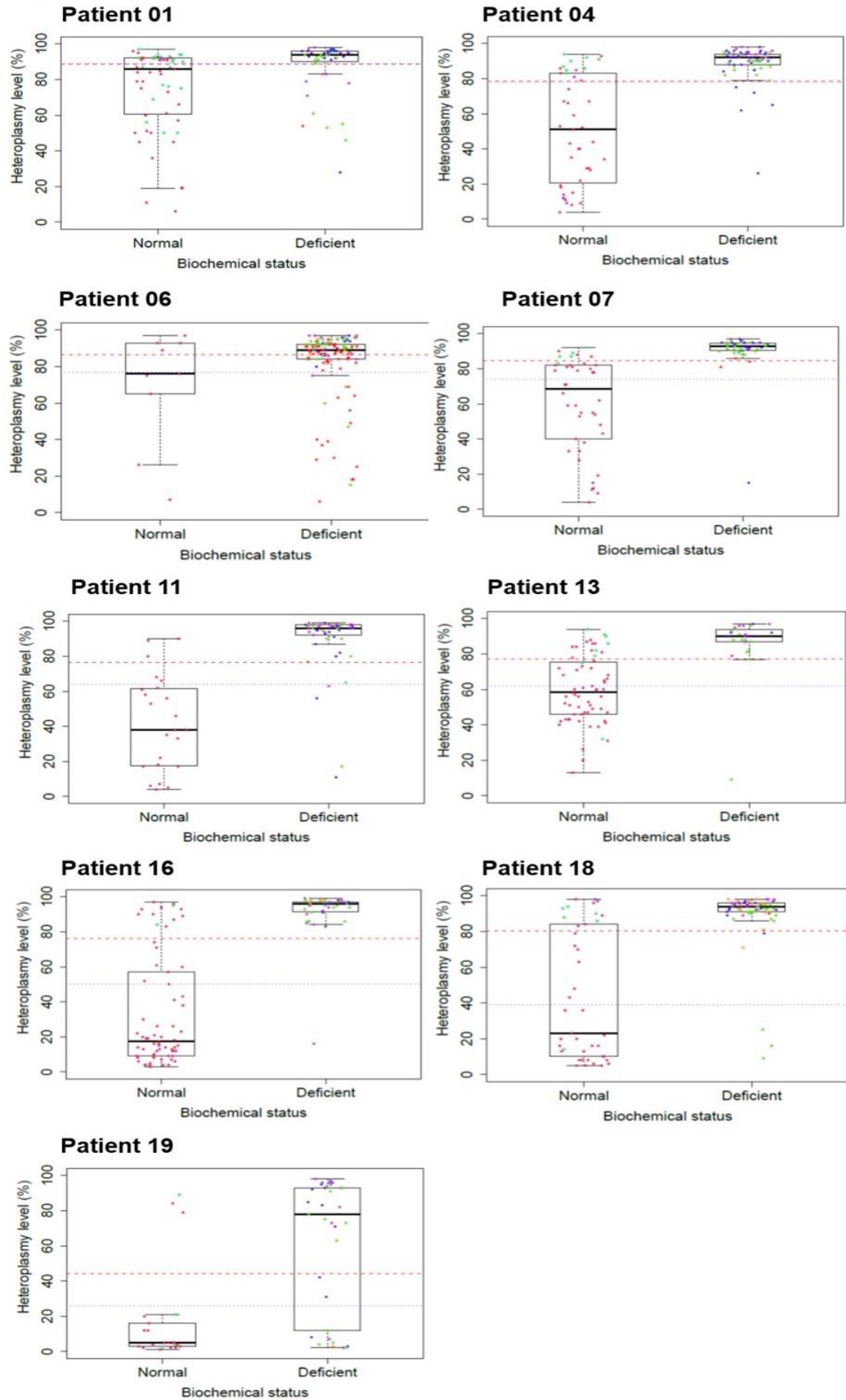
5.4.3.3. The heteroplasmy levels in the biochemically normal and deficient fibres

As shown previously through the Z_score analysis, the sampled biochemically normal fibres (as now classified by the hierarchical clustering) of the following patients in Group A; P01, P04, P07, P11, P13, P16 and P18, have a broad distribution in the heteroplasmy levels whilst the sampled deficient fibres have high heteroplasmy levels within a narrower distribution (**Figure 5.17**). Although, P01 and P11 both have a number of fibres that are deficient but showing lower levels of heteroplasmy.

However, both P06 and P19 do not follow this pattern. Instead, the deficient fibres show a wider spread in the heteroplasmy levels compared to the normal fibres. This further confirms that the hierarchical clustering method was not successful in identifying the difference between the biochemically normal or deficient fibres for P06 data. Conversely, the data for P19 were as expected, and as previously highlighted by the Z_score analysis, – the uneven spread of the data showed normal fibres with low levels of heteroplasmy whilst the deficient fibres showed both low and high levels of heteroplasmy.

Additionally, as already stated, fibres sampled from P05 skeletal muscle section showed the same pattern as the fibres sampled from patients P02, P10 and P15 (**Figure 5.15**), whereby normal fibres harboured heteroplasmy levels within a narrower range compared to the patients in Group A. In this instance, P05 was classed as Group B based on hierarchical clustering (100% biochemically normal fibres).

A)



B)

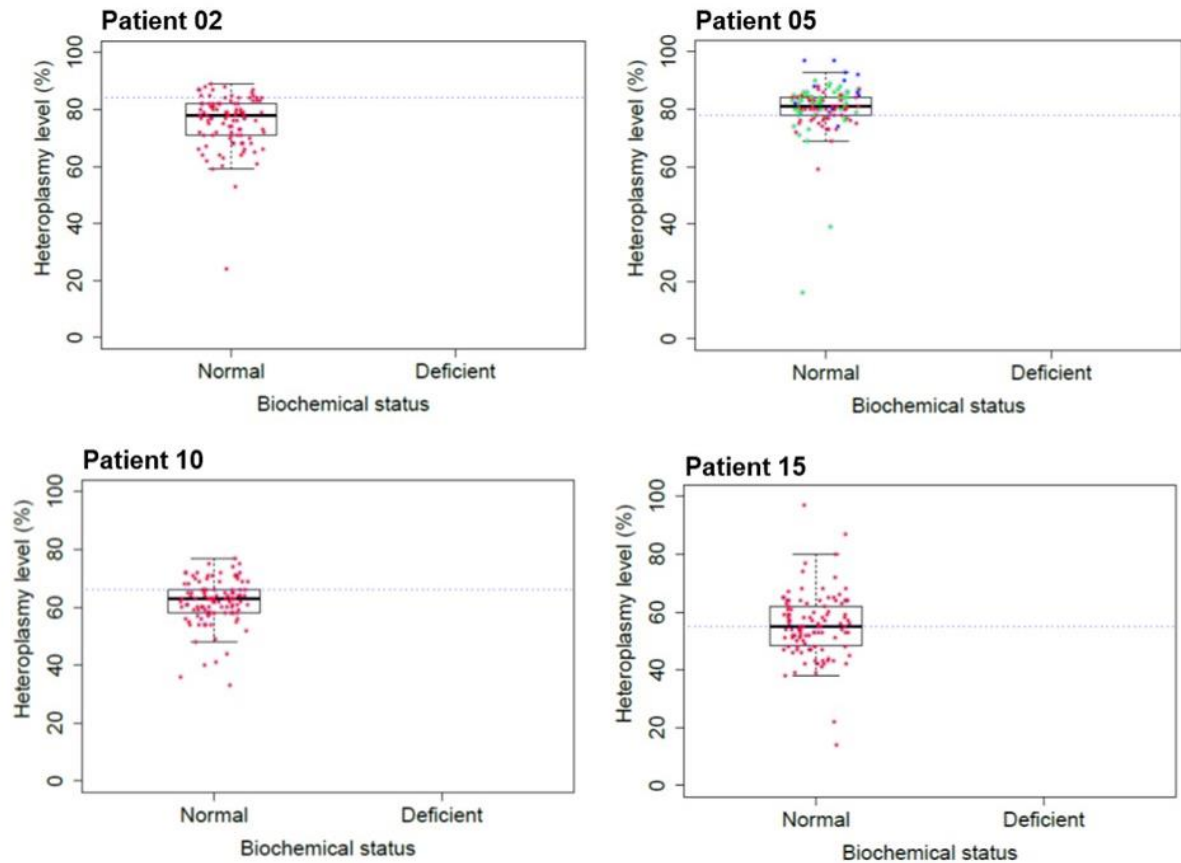


Figure 5.17: Boxplot distribution of heteroplasmy levels in biochemically normal and deficient fibres from patients in Group A and B.

A) In all patients in Group A, apart from P06 and P19, the biochemically normal fibres show a broad distribution in heteroplasmy levels whilst deficient fibres show a narrow distribution of high heteroplasmy levels. P06 and P19 show the contrasting distribution; normal fibres show narrow range and deficient fibres show a broad distribution in heteroplasmy level. B) Single fibres sampled from all patients in Group B show a narrow distribution in heteroplasmy levels. Each single dot is representative of a single fibre. Blue dashed line = homogenate heteroplasmy level of each patient. Red dashed line = point at which two kernel densities intersect to determine the threshold estimate. Dots (fibres) have been coloured according to Z_score classification of fibres into OXPHOS groups; red = Group 1 fibres, green = Group 2 fibres, blue = Group 3 fibres, purple = Group 4 fibres.

5.4.3.4. Kernel density estimate for threshold levels

Kernel density distributions were fitted to the heteroplasmy data from both the normal and deficient groups of sampled fibres. The heteroplasmic threshold estimate for each patient was then defined as the point at which these two distributions intersected, as indicated by the red dashed line in **Figure 5.17**. These data were bootstrapped (n=10,000) to produce a range of threshold estimates for each patient. The heteroplasmic threshold estimate and the distribution in the uncertainty of this estimate as determined by bootstrapping is shown for each patient in **Figure 5.18**. This uncertainty is shown by the overlay of the boxplots as well as the R summary data from the kernel density estimate, shown in **Table 5.8**.

The median threshold estimates (as shown by the middle black line within the overlaid boxplots) is seen to differ between patients (**Figure 5.18**), with P01 showing the highest estimate in comparison to the other eight patients in Group A. Moreover, **Figure 5.18** also highlights the multimodal distribution that is present in the data for two patients, P06 and P19; the distribution of the data is either bimodal (P06) or trimodal (P19) in comparison to the other seven patients in Group A. As previously stated, the distribution for P06 highlights that the clustering has failed to accurately classify fibres, therefore the threshold estimate for P06 is not accurate. The trimodal distribution seen for P19 also further highlights the uneven spread in the heteroplasmy levels determined in the single muscle fibres for this section. Therefore, the median estimates for these two patients could not be assumed to be entirely accurate in this instance and so were not included in further analysis. Similarly, to the LOESS model, P07 shows a narrow variance (minimum; 79.50, mean; 84.34 and maximum; 86.90) whilst the remainder of the now six patients in Group A show bigger variances.

Group B patients show no data points as they only harbour biochemical normal fibres, therefore no heteroplasmic threshold was estimated.

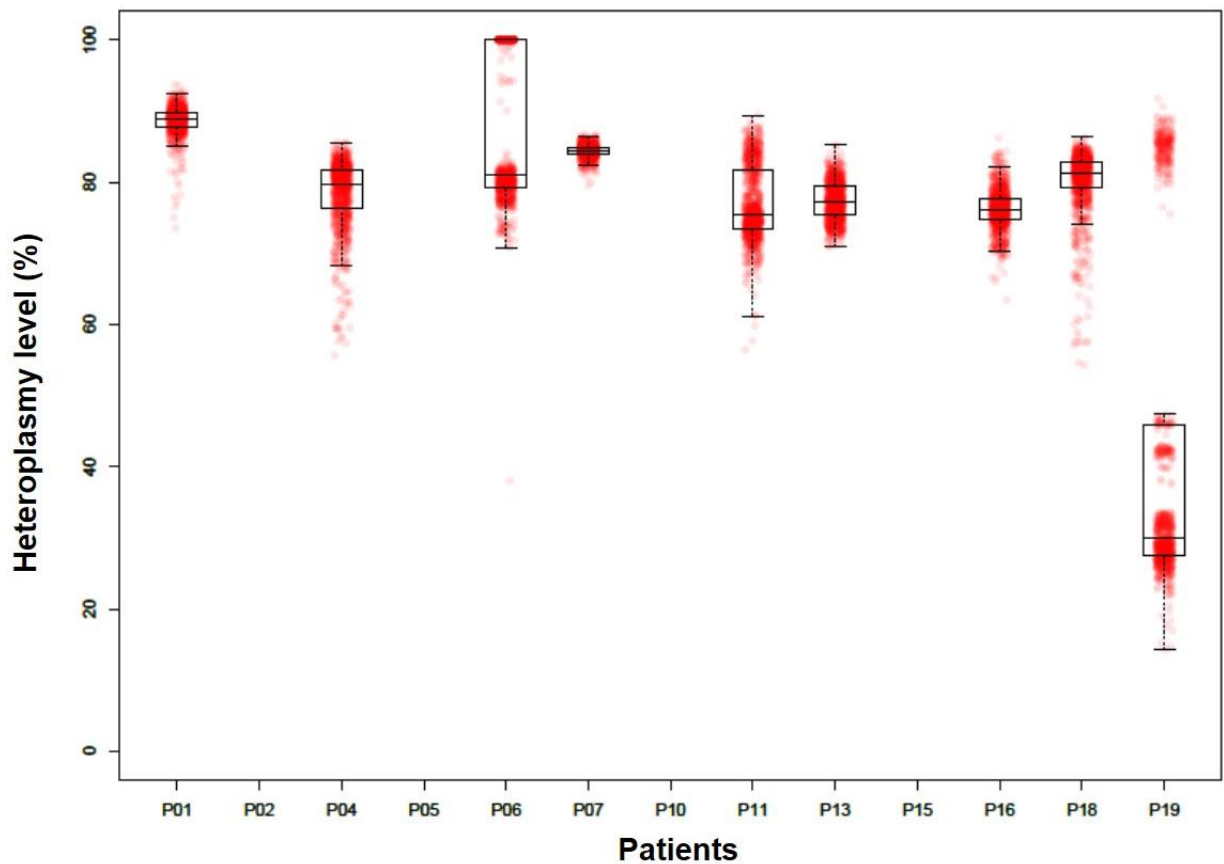


Figure 5.18: Kernel density estimate plot showing heteroplasmic threshold estimates of Complex I deficiency in all patients.

Each single red dot is a threshold estimate from one bootstrapped sample (undertaken 10,000 times). The middle black solid line of overlaid box plot indicates the median threshold estimates for each patient. P01 shows the highest median threshold estimate. P06 and P19 have multimodal distributions; P06 = bimodal, P19 = trimodal. Patients in Group B (P02, P05, P10 and P15) show no threshold estimates as all fibres in skeletal muscle sections were classified as being biochemically normal.

Table 5.8: Summary data for heteroplasmic threshold estimates (%) as plotted on kernel density estimate plot (Figure 5.18)

Summary						
Patient	Minimum	1 st Quartile	Median	Mean	3 rd Quartile	Maximum
P01	73.50	87.80	88.80	88.63	89.70	93.70
P04	55.60	76.30	79.70	78.36	81.70	85.60
P07	79.50	83.90	84.40	84.34	84.90	86.70
P11	56.40	73.30	75.40	76.9	81.70	89.90
P13	70.90	75.40	77.25	77.33	79.40	85.20
P16	63.40	74.70	76.20	76.18	77.70	86.20
P18	54.30	79.30	81.30	80.14	82.30	86.30

The median threshold estimates for the seven Group A patients (P01, P04, P07, P11, P13, P16 and P18), range from 75.40% (P11) to 88.80% (P01) (**Table 5.8**).

5.4.3.5: Patients show significant differences in estimated heteroplasmic thresholds

Following this analysis, it was important to determine if these median threshold estimates were significantly different between these individual patients. To obtain a probability-based estimate of the differences between the median estimate thresholds of these patients' muscle sections (P01, P04, P07, P11, P13, P16 and P18), bootstrapping was undertaken on the threshold estimates. Briefly, 1,000 bootstrapped estimates were taken from P01 and 1,000 bootstrapped estimates from P04. This generated 10^6 pairwise comparisons between the two sets of estimates. For example, the proportion of times that the estimated threshold for P01 (row P01) was greater than that of P04 (column P04) was calculated – this proportion is the probability that the threshold for P01 is greater than that for P04. A probability > 0.95 was deemed to be a significant difference (equivalent to $P < 0.05$). These values are highlighted by blue in **Table 5.9** (top half of table). The corresponding magnitude of the difference (%) in heteroplasmy thresholds are highlighted in red (bottom half of **Table 5.9**).

Table 5.9: Probability-based estimates of the difference in threshold between the seven patients in Group A. The top half shows probability estimates and the bottom half shows the corresponding magnitude of the difference (%).

		Probabilities						
		P01	P04	P07	P11	P13	P16	P18
Difference in threshold (%)	P01		0.992	0.972	0.988	0.996	0.997	0.989
	P04	9.4		0.029	0.604	0.642	0.715	0.348
	P07	4.4	-4.8		0.883	0.995	0.996	0.923
	P11	12.8	2.3	2.2		0.425	0.486	0.305
	P13	11.3	2.0	7.0	-1.3		0.607	0.206
	P16	12.5	3.0	8.1	-0.2	1.0		0.055
	P18	7.6	-1.6	3.0	-4.9	-3.8	-4.9	

Interestingly, significant differences in the threshold estimates were found between patients harbouring the m.3243A>G pathogenic variant in this study. The median threshold estimate of P01 is significantly higher than that for the six Group A patients (P04, P07, P11, P13, P16 and P18) – the difference in heteroplasmy levels ranging between 4.4% (P07) and 12.8% (P11) (**Table 5.7**). Additionally, the median threshold estimate of P07 is significantly higher than P13 (by 7%) and P16 (by 8%).

Overall, these findings have shown that not only do these patient skeletal muscle sections differ in their biochemical status in terms of Complex I expression (thus level of deficiency), but (significant) differences in the median heteroplasmic threshold between patient muscle sections have also been determined. Patient 01 has the highest heteroplasmic threshold, requiring heteroplasmy levels to exceed 88.80% in order for a respiratory chain defect to occur (in this instance, defect in Complex I) whilst P11 required a lower level of heteroplasmy (75.40%) to lead to a biochemical defect. These differences in the heteroplasmic threshold could therefore be a potential mechanism that drives a wide phenotypic spectrum in these patients.

Given that differences in threshold occur between patients from Group A, it could be proposed that patients from Group B also have varying thresholds. Whilst it was hypothesised that patients in Group A have a lower critical threshold, hence a biochemical deficiency in their skeletal muscle section, this may not be the case. For example, a patient from Group B

could have a threshold lower than that of one from Group A but, due to the narrow distribution of heteroplasmy levels in individual fibres, this threshold may not have been exceeded and so a biochemical deficiency does not occur. As already discussed in section 5.1, this could be linked to nuclear background. Thus, not only does this suggest that differences in heteroplasmic thresholds could influence phenotypic differences, but also that there may be differences between individuals in the underlying mechanisms that modulate heteroplasmy levels.

5.5. Discussion

The heteroplasmic m.3243A>G *MT-TL1* gene variant is well known for causing clinical heterogeneity. Taking forward the findings from the quadruple immunofluorescence assay in **Chapter 4**, this study used a single cell approach to investigate the distribution of heteroplasmy levels in both biochemically normal and deficient fibres. Thereafter, the approach was used to determine an estimate of the heteroplasmic threshold beyond which biochemical deficiency is apparent for Complex I in the skeletal muscle cryosections of 13 patients harbouring the m.3243A>G mutation (a subset of the original 19 from **Chapter 4**). Skeletal muscle sections from 10 of these 13 patients presented with profiles representing a biochemical deficiency (dominated by Complex I) and three showed normal biochemical profiles. A total of 1,483 single muscle fibres from patient muscle sections were isolated by laser microdissection and molecular genetic analysis was undertaken through pyrosequencing to determine the m.3243A>G heteroplasmy levels in each individual fibre.

5.5.1. Increased m.3243A>G heteroplasmy levels in deficient fibres

Single muscle fibres from all Group A patients, aside from P19 (and P06 if based on hierarchical clustering), showed an obvious increase in the m.3243A>G heteroplasmy levels from biochemically normal fibres (Group 1 according to *Z*_score analysis) to the deficient fibres (Group 2 to Group 4/5), demonstrating that respiratory chain function becomes increasingly impaired as heteroplasmy level increases. This finding is consistent with previous single cell studies, where it is already well established in literature that fibres deficient in Complex IV (COX-deficient fibres), have higher heteroplasmy levels (Kärppä et al. 2005; Moraes et al. 1992; Petruzzella et al. 1994; Tokunaga et al. 1994).

However, it is shown in **Chapter 4**, as well as in the literature (Kirino et al. 2005), that Complex I is the predominating biochemical deficiency observed with the m.3243A>G mutation. Therefore, by using the quadruple immunofluorescence assay, this current study has had the advantage of analysing fibres based on both Complex I and Complex IV protein expression; allowing for the identification of fibres that were normal or deficient in Complex I, normal or deficient in Complex IV and normal or deficient for both. Therefore, I was able to sample fibres from a wider range of OXPHOS deficiency in comparison to the studies that had used sequential COX/SDH.

The range of heteroplasmy levels observed in the normal fibres from Group A patients (ranging from 3% to 98%) is also in line with the findings from previous single cell studies (Kärppä et al. 2005; Moraes et al. 1992; Petruzzella et al. 1994; Tokunaga et al. 1994). For

example, Kärppä et al. (2005) showed the range of heteroplasmy to be 3% to 92% in 251 normal fibres, based on normal COX-activity as determined by sequential COX/SDH histochemistry.

The only exception to this observation is P19. It was shown that there was an increase in the heteroplasmy level between Group 1 and Group 3 fibres, however there were many fibres that were biochemically deficient yet harboured very low levels of m.3243A>G heteroplasmy. A total of 55 fibres were analysed from this patient's section; increasing this number could provide a clearer picture of the distribution of fibre heteroplasmy. However, it is also likely that this difference in heteroplasmy distribution in comparison to the other patients in Group A could be due to an additional underlying mutation, alongside the m.3243A>G mutation. Essentially, could the biochemical deficiency observed in the sampled fibres from P19 be due to another point mutation or an mtDNA rearrangement? In order to investigate this, the Newcastle Highly Specialised Mitochondrial Diagnostic Laboratory undertook long-range PCR screening of this patient's DNA sample to assess the presence of large-scale mtDNA rearrangements, confirming that this was not the case (results not presented in this thesis). In fact, this patient was confirmed again as having 34% m.3243A>G heteroplasmy in a homogenate skeletal muscle DNA sample. Screening the patient's full mitochondrial genome sequence could potentially identify an additional point mutation contributing to the phenotype, but this must be rather unlikely.

5.5.2. Type II fibres harbour higher levels of m.3243A>G heteroplasmy levels

The selection of fibres for single cell analysis included the representation of different muscle fibre types; Type I and Type II fibres which was a combination of both Type IIa and IIx. Overall, Type II fibres harboured higher levels of heteroplasmy in comparison to Type I fibres, by 6%. This is in line with previous finding by Rocha et al. (2018). However, this was only representative of three of the 11 patients who were shown to have significant difference between the median heteroplasmy level in Type I and Type II fibres, whilst the remaining patients showed no consistent or significant differences between the two fibre types. Therefore, this study has provided further evidence that there is no consistent relationship observed between muscle fibre types and heteroplasmy level (Rocha et al. 2018).

5.5.3. Difference in tissue segregation of the m.3243A>G mutation between patients in Group A and Group B;

Unlike previous single cell studies which examined fibres from patient skeletal muscle sections that harboured both COX-positive and COX-deficient fibres, this current study has also investigated muscle sections from patients who presented with normal protein expression

of Complex I and Complex IV (biochemically normal) in their skeletal muscle sections. This was undertaken to assess if there were any differences in the distribution in the heteroplasmy level that could help distinguish why patients in Group B showed no biochemical deficiency, compared to patients in Group A.

Interestingly, a difference was observed between the two groups of patients. The heteroplasmy levels determined in the normal fibres sampled from skeletal muscle sections of patients from Group B, were clustered within a narrow range, unlike the broad distribution observed in the normal fibres from patients in Group A. This indicates that the broad distribution in heteroplasmy levels may be linked to the presence of deficient fibres whilst the narrow distribution is linked to patients with no deficiency in their skeletal muscle. To the best of knowledge, this has not yet been reported in the literature.

The most obvious explanation for the difference between these two groups of normal fibres is that fibres from patients in Group B have not yet reached the critical threshold for biochemical deficiency. However, what is causing these fibres to stay within a certain range of heteroplasmy levels without exceeding that threshold? A number of aspects can be considered, though these are predominantly based on studies undertaken on *transmitochondrial* cell lines or mitotic cells such as colonic crypts.

Could this difference in distribution be due to the difference in nuclear genetic background?

These two patterns of heteroplasmy levels have been reported in *transmitochondrial* cell lines – either stable (within a range) (Lehtinen et al. 2000; Shoubridge 1995) or shifts towards either low or high levels of heteroplasmy (Dunbar et al. 1995). This shift in heteroplasmy and segregation was owed to the difference in nuclear background of the cells (Dunbar et al. 1995; Raap et al. 2012; Shoubridge 1995). Although it was also recognised that the differences in experimental procedures in such studies could also be accountable for these differing outcomes, for example the number of passages undertaken and the length of time that the cells were cultured (Bentlage and Attardi 1996; Shoubridge 1995). Nonetheless, the change in heteroplasmy levels in post-mitotic cells is due to the continuous recycling of mtDNA molecules in a process called relaxed replication (Stewart and Chinnery 2015) and like the *transmitochondrial* cell lines, heteroplasmy level within a given cell is thought to be able to increase, decrease or remain stable over time. Again, it is thought to be influenced by nuclear genes. Thus, a likely hypothesis for this difference in heteroplasmy distribution is that the patients in Group B have different nuclear background to those in Group A. As previously

discussed in **Chapter 4**, studies have shown strong indication towards the role of the nuclear DNA and nuclear factors in mitochondrial disease (Battersby et al. 2003; Hudson et al. 2005; Maeda et al. 2016; Pickett et al. 2018).

Could this difference in distribution be due to clonal expansion?

Another aspect that can be considered in understanding these findings is clonal expansion; the process by which the proportion of the mutated mtDNA (caused by either a point mutation or deletions), increases and eventually exceeds the critical threshold that is required to induce a biochemical deficiency. The mechanism that drives mtDNA molecules to undergo clonal expansion is of longstanding interest in research with current mechanisms that have been suggested including random genetic drift (Baines et al. 2014; Elson et al. 2002; Greaves et al. 2014) and preferential selection of mutant mtDNA due to increased biogenesis in the perinuclear region of the skeletal muscle section (Vincent et al. 2018).

It could be postulated that the mutant mtDNA in the fibres of patients in Group A have clonally expanded to high levels and exceeded the threshold to then consequently cause the Complex I (and Complex IV) deficiency that has been observed in the skeletal muscle sections. In addition to this, the broad distribution of heteroplasmy levels observed in these normal fibres includes the many fibres that harbour very low levels of heteroplasmy in comparison to the overall homogenate level. This is potentially a result of random segregation (distribution) of mutant mtDNA molecules into skeletal muscle progenitor cells during embryogenesis, which results in a broad distribution of heteroplasmy levels in the resulting skeletal muscle fibres. Clonal expansion, potentially in response to exceeding threshold for deficiency, within individual fibres could then contribute to this spread becoming even broader. In contrast, fibres from Group B patients may not have undergone clonal expansion to the same extent, resulting in narrower ranges of heteroplasmy.

Furthermore, this narrow range could potentially be indicating that the process of segregation during embryogenesis may not be random in these patients as all fibres that have been sampled harbour similar levels of heteroplasmy levels.

Could this difference in distribution be due to mtDNA copy number?

The quadruple immunofluorescence assay allowed for the determination of mitochondrial mass through the immunoreactivity/expression of porin. Interestingly, it was found in this cohort that fibres analysed in the muscle sections from patients in Group B had lower porin

levels than fibres in sections from patients in Group A, but this difference was not significant. The direct measure of mtDNA copy number in these patients would clarify this finding better.

Differences in mtDNA copy number in these single muscle fibres could also account for the differences observed, particularly in those fibres that show very high levels of heteroplasmy yet remain biochemically normal. At a population level, Grady et al. (2018) showed an association between low homogenate skeletal muscle mtDNA copy number and increased disease severity and progression. Therefore, at a single cell level, it could be hypothesised that low copy number also drives the existence of deficient fibres. A recent study by Filograna et al. (2019) demonstrated that mice (carrying the m.5024C>T mutation on the *tRNA^{Ala}* gene (the so called “C5024T” mice)) with an increase in mtDNA copy number (achieved by overexpressing (OE) TFAM in *Tfam^{+OE}* C5024T mice) decreased the frequency of COX-deficient cardiomyocytes compared to mice with low mtDNA copy number (knock out (KO) *Tfam*; *Tfam^{+KO}* C5024T mice) – thereby concluding that an increase in mtDNA copy number was sufficient to decrease the biochemical defect in cells owed to slowing down the process of clonal expansion. This decrease was not observed in the skeletal muscle sections of these mice, however, this may have been influenced by the fact that these mice had very low frequency of COX-deficient fibres. Therefore, normal fibres from patients in Group B may have a higher mtDNA copy number in comparison to the fibres in patients in Group A, therefore potentially decreasing the process of clonal expansion of the m.3243A>G variant to reach the threshold for deficiency and consequently not display a biochemical defect.

Heteroplasmic mutations involving various tRNA genes have been shown to be associated with mtDNA proliferation (Moraes et al. 1992; Shoubridge 1998; Tokunaga et al. 1994) – represented by increased total mtDNA copy number in the classic RRF observed in the skeletal muscle sections of patients (Tokunaga et al. 1994). This proliferation in mtDNA is indicative of a compensatory mechanism which is known as the “maintenance of the wild-type hypothesis” (Chinnery et al. 1999; Durham et al. 2007; Stewart and Chinnery 2015). This theory proposes that in the presence of mutated mtDNA, the mtDNA pool is replicated in the cell as a way of restabilising an adequate level of wild-type mtDNA. However, this also leads to non-selective replication and so an increased amount of mutated mtDNA molecules. The heteroplasmy level would then increase in the post-mitotic tissue with time, potentially leading to respiratory chain deficiency. Alternatively, this theory of proliferation of wild-type mtDNA is not supported by the findings from the study by Durham et al. (2007) who investigated muscle fibres from a patient harbouring the m.3243A>G mutation and showed that COX-deficient fibres had superabundance of wild-type mtDNA which was not sufficient

enough to halt the respiratory chain deficiency. The authors concluded that the pathogenic mechanism of the m.3243A>G mutation involves interference with the function of the wild-type mtDNA or the wild-type mt-tRNA^{Leu(UUR)}, as previously described in **Chapter 4**, section 4.1.3. This is further exemplified by the presence of RRF that are COX-deficient – evidence of the fact that proliferation of mtDNA copy number in these fibres is not capable of compensating for the high levels of heteroplasmy (Petruzzella et al. 1994).

This leads to notion that it could be possible that fibres from different individuals vary in their ability to compensate for the presence of the mutation (Apabhai et al. 2011; Cao et al. 2001; Grady et al. 2018). Thus, it could be suggested that the compensatory mechanism of proliferation has been compromised in fibres from patients in Group A whilst fibres from patients in Group B are able to compensate in the presence of the m.3243A>G mutation, hence show no biochemical defect.

5.5.4. Differences in the estimated heteroplasmic threshold for Complex I deficiency between patients

Using both hierarchical clustering and kernel density estimates, this study was able to determine the estimated critical threshold for biochemical deficiency (Complex I deficiency) in patients harbouring the m.3243A>G pathogenic variant. In line with the literature, the threshold estimates determined for patients were shown to be between 74% and 89%.

This is the first study that has been able to statistically demonstrate significant differences in estimated thresholds between the patients, in particular patient P01 who was shown to have higher thresholds in comparison to the remainder of the six patients. These differences may be biologically meaningful given their magnitude (up to 12.8% difference in heteroplasmy level), particularly in terms of a clinical outlook. It also supports the hypothesis that thresholds are different between individuals, and could be responsible, in part, for the phenotypic variation observed. Therefore, it would be interesting to investigate the association between these differences in threshold levels and the clinical data of these patients. Unfortunately, in this current study, this could not be investigated further due to the small cohort of patients in whom the threshold was determined (n= 7). However, it has paved way for further patients to be investigated in order to determine the exact clinical relevance of these significant differences in threshold levels.

5.6. Limitations of this study

This single cell study is the first study to investigate single muscle fibres from patients with the m.3243A>G mutation, based on Complex I and Complex IV expression. Therefore, a

large number of fibres have been analysed in 13 patients, four of whom had biochemically normal skeletal muscle sections (based on the hierarchical clustering). Although the combination of the quantitative immunofluorescence assay data and molecular genetics (pyrosequencing data) has improved the understanding of genetic and respiratory chain defects, there are some limitations to consider.

The fibre sampling strategy could be biased as fibres were selected from known OXPHOS groups, despite random sampling from within these groups. However, given the time-constraint, it was the better option over random sampling which was also shown to be inadequate for sampling a sufficient number of fibres in some cases without sampling more than 250 fibres. The sampling of fibres was limited by the fibre type groupings, especially as each patient presented differently with their fibre type composition. For example, some sections had more Type I fibres whilst others had more Type IIa/x fibres. Although it was found that heteroplasmy level was 6% higher in Type II fibres than Type I, the linear regression model seemed to be influenced by three patients in particular, whilst in the remaining 8 patients, there was no consistency. Moreover, due to the different levels of deficiency and fibre type composition, each patient had their own individual selection method – dependent on the fibres per OXPHOS group and the number of fibres per fibre type. Random sampling from these OXPHOS groups without taking into account fibre type may have been a better selection method.

Whilst muscle sections from 13 patients have been used in this study, it was only possible to determine the threshold for seven of these. This small group size did not allow for the correlation between these threshold findings and the clinical phenotypes of these patients, which would have been particularly interesting given the phenotypic heterogeneity in the cohort.

The statistical work up allowed for the estimates of thresholds to be determined, however, hierarchical clustering failed to classify fibres in P06 which then could not be compared to the remaining patients after the summary from kernel density plots. This highlights that the classification needs to be refined to ensure it can be applied for all patients, particularly for patients who show a substantial amount of Complex IV deficiency.

This study has utilised fibres sampled from the 20µm fibre type section for pyrosequencing, rather than sampling directly from the 10µm OXPHOS section. Although fibres were matched, it cannot be assumed that the heteroplasmy levels are the same across serial

sections, given that COX-deficiency occurs segmentally across the muscle. However, the fibres did show the expected levels of heteroplasmy according to their OXPHOS group.

Similarly, the threshold estimates for Complex I deficiency, were determined from fibres sampled from one skeletal muscle section. It would be ideal to take a section from further down the biopsy and/or from a different biopsy and repeat the experimental procedure to investigate if similar levels of heteroplasmy are found, as well as how similar the estimated threshold is to the initial finding.

As this current study has only investigated fibres based on protein expression for Complex I and Complex IV, it could be suggested that the activity of the complexes need to be investigated in order to accurately determine the Group B patients as being biochemically normal. However, measuring the activity of complexes at a single cell level is not possible, therefore this would be investigated using homogenate skeletal muscle sample and spectrophotometric assays.

Lastly, due to the time constraint of this project, the assessment of the heteroplasmy levels in the single muscle fibres was only undertaken once, rather than in duplicates or triplicates. However, by investigating a sample of fibres as duplicates from the same experimental run as well as from a new experimental set up, showed that the heteroplasmy levels of most of these fibres fell within a 6% range. In addition, controls of known heteroplasmy level were included in order to validate each pyrosequencing run.

5.7. Conclusion

In conclusion, through using quantitative data from the quadruple immunofluorescence assay combined with laser capture microdissection and pyrosequencing, this study has been able to assess m.3243A>G heteroplasmy levels in fibres deficient in Complex I and Complex IV in muscle sections from patients harbouring the m.3243A>G pathogenic variant. The following findings have been determined; i) based on Complex I and Complex IV expression, fibres have shown an increase in heteroplasmy level with increased biochemical deficiency, ii) biochemically normal fibres from skeletal muscle sections of patients from Group A and Group B show a difference in heteroplasmy distribution; normal fibres from patients in Group A show a wide distribution whilst normal fibres from patients in Group B show a narrow distribution. Furthermore, this study has used stringent statistical methods including using bootstrapping, hierarchical clustering, kernel density estimates, followed by probability paired calculations to show the following findings; i) estimated threshold levels could be determined in seven of the Group A patients and ii) the threshold levels were statistically different

between some of the patients. Overall, this study has been able to demonstrate the difference in threshold for Complex I deficiency in patients with the m.3243A>G mutation. Further research into whether these differences can account for the phenotypic variability in these patients is warranted – this will be discussed further in the final discussion of this thesis (**Chapter 6**).

Chapter 6: Final discussion and future work

6.1. Conclusions

Mitochondrial diseases are caused by pathogenic variants which reside within genes that are either encoded by the nuclear DNA or the mtDNA. Thus, affected individuals present with genetic, clinical and biochemical heterogeneity and for those who are affected by pathogenic mtDNA variants, this is further confounded by heteroplasmy. The studies described in this thesis had the aim of improving the diagnosis of mitochondrial disease and improving the understanding of molecular mechanisms underlying mitochondrial disease and the expression of a biochemical defect. These aims have been achieved with the use of the quadruple immunofluorescence assay which allowed for the assessment of Complex I (NDUFB8), Complex IV (COX-1) and porin (mitochondrial mass) protein expression in individual fibres, within 10µm skeletal muscle sections from patients.

There are several areas in which this thesis has presented novel findings that contribute towards the ongoing advancement in the knowledge and understanding of mitochondrial disease. These key findings are described below.

6.1.1. The quadruple immunofluorescence assay is a beneficial tool in the diagnosis of Complex I deficiency:

Complex I deficiency is the most frequently observed biochemical defect in patients with mitochondrial disease. Prior to the quadruple immunofluorescence assay (Rocha et al. 2015), there were no histochemical tests that interrogated Complex I expression in skeletal muscle in a diagnostic setting. Therefore, following on from work undertaken by Rocha et al. (2015), it was important to validate the assay and its ability to detect Complex I deficiency in a heterogeneous cohort of patients (n= 25) with genetically-proven pathogenic variants within mtDNA or nuclear-encoded genes.

This study demonstrated the clear diagnostic potential of the assay in detecting Complex I deficiency, particularly within patients harbouring pathogenic variants of nuclear-encoded genes (encoding either structural subunits or assembly factors). Moreover, this study also showed that in some cases, the assay cannot detect Complex I deficiency, using antibodies against NDUFB8 and NDUFS3. This is most likely because the mutation is only affecting the enzymatic activity of the complex rather than assembly, or the mutation has variable effects on either the assembly, activity or both. Although, in some instances, the assay was able to give further insight into the effect of the mutation on Complex I, for example, in one patient harbouring the m.13513G>A, p.(Asp393Asn) variant (P25), the protein expression of Complex I was normal as detected with the assay, normal steady state levels of assembled

Complex I were detected (with BN-PAGE) as well as normal residual biochemical Complex I activity. Combining these findings, it could be concluded that this variant may have no effect on the activity or assembly of Complex I in skeletal muscle, despite the relatively high level of mtDNA heteroplasmy and severe clinical phenotypes.

Overall, these findings highlight the key advantage that this assay has introduced to the diagnostic pathway for mitochondrial diseases - Complex I expression can be interrogated in the single fibres of a 10µm skeletal muscle section and provide essential information on the status of the complex; a decrease in the expression (deficiency) or a normal expression. Importantly, these findings add further importance to the multidisciplinary approach required in the diagnosis of mitochondrial diseases, for example the necessity of the spectrophotometric assay to measure the activity of Complex I in cases where protein expression is normal in skeletal muscle sections, as well as BN-PAGE to assess the assembly of Complex I. In addition, these findings show the importance of completing mitochondrial genome sequencing in those patients where the immunofluorescence assay was unable to detect a deficiency.

6.1.2. Skeletal muscle sections of patients harbouring the m.3243A>G pathogenic variant show variable biochemical status based on Complex I expression

The m.3243A>G mutation, located within the *MT-TL1* gene (encoding mitochondrial tRNA^{Leu} (UUR)), is the most prevalent, pathogenic mitochondrial point mutation. It is associated with a broad clinical spectrum, from asymptomatic individuals to patients with MELAS. This is due to a number of factors that include heteroplasmy, age, mtDNA copy number and nuclear factors (Boggan et al. 2019). The study in this thesis focused on the role of heteroplasmy.

Previous studies have used the classic sequential COX/SDH histochemical assessment to investigate skeletal muscle of patients with m.3243A>G variant. However, the downregulation of Complex I is of predominance in these patients (Fornuskova et al. 2008; Goto et al. 1992; Kobayashi et al. 1990; Morgan-Hughes et al. 1995) and so would go undetected using this method. Therefore, in order to provide novel findings to progress the knowledge of the m.3243A>G mutation, the study described in **Chapter 4** used the quadruple immunofluorescence assay to characterise – at a single cell level - the biochemical status (particularly of Complex I) of skeletal muscle fibres from patients harbouring the mutation (n=19).

Firstly, the findings from this study showed that Complex I is indeed the predominant biochemical defect observed in patients, particularly within this current cohort of patients. Only three of the 19 patients showed Complex IV deficiency at a single cell level.

Secondly, the study identified two groups of patients based on Complex I expression in the skeletal muscle biopsies; those patients showing Complex I deficiency were termed as Group A whilst those showing a normal biochemical profile were termed as Group B. Previous studies have shown a decrease in Complex I activity in patient samples, owed to the fact that the m.3243A>G mutation directly impacts both ND6 and ND5 (Chomyn et al. 2000; Dunbar et al. 1996; Kirino et al. 2004; Sasarman et al. 2008). A preliminary study by Rocha et al. (2015) used the quadruple immunofluorescence assay to assess Complex I and Complex IV deficiency in muscle sections from a heterogeneous group of mitochondrial disease patients, including five carriers of m.3243A>G. By interrogating a larger cohort of m.3243A>G carriers, this current study has given insight into the variable levels of Complex I deficiency found in patient skeletal muscle sections, as well as showing that some patients can present with normal levels of Complex I (and Complex IV) expression in single muscle fibres, despite the severe clinical presentations or high homogenate heteroplasmy levels in some cases.

6.1.3. m.3243A>G heteroplasmy distribution differs in biochemically normal fibres between patients in Group A and B

The findings from **Chapter 4** initiated the investigation into why this difference was observed between these two groups of patients. It was hypothesised that the difference in the critical heteroplasmic threshold for deficiency was different between the two groups of patients. Isolation of single muscle fibres from 13 of the 19 patients enabled investigation of the relationship between biochemical deficiency and single fibre m.3243A>G heteroplasmy, as described in **Chapter 5**.

The first novel finding from this study is the difference in the heteroplasmy distribution observed in the biochemically normal fibres sampled from patients in Group A and the normal fibres sampled from the patients in Group B; fibres from Group A patients have a broad distribution in heteroplasmy levels whilst fibres from patients in Group B have a narrower distribution. Therefore, this difference appears to determine the skeletal muscle biopsy biochemical profile, as detected by the quadruple immunofluorescence assay.

6.1.4. Patients showed a difference in their biochemical threshold

The second novel finding in this study is the differences in the critical heteroplasmic threshold for Complex I deficiency between patients (from Group A) and in some instances, this

difference is statistically significant. P01 was shown to have a significantly higher threshold estimate than all patients analysed whilst P07 was shown to have a higher heteroplasmic threshold level than P13 and P16. These findings have paved the way to asking further questions such as; do these differences in threshold cause the phenotypic differences observed in these patients? Do those patients that have a significantly higher threshold level have a less severe phenotype than patients with lower thresholds?

6.2. Future work and potential studies

A discussion of potential future research is described below. These proposed studies would allow for better understanding of these current findings and the understanding of the complexity that is associated with the m.3243A>G pathogenic variant.

Future work after expanding the size of the cohort:

One of the limitations to the study undertaken on the m.3243A>G pathogenic variant is the relatively small cohort size (n=19). Therefore, one crucial next step is to undertake the quadruple immunofluorescence assay in the remaining biopsies of patients with the m.3243A>G mutation. The MitoCohort contains approximately 60 patient muscle biopsies; increasing the number of patients investigated will allow for confirmation of the findings described in **Chapter 4**. Would biopsies from these patients also present with muscle biopsies that are either deficient for Complex I or normal for both Complex I and Complex IV expression, or could some of these patients present with a much a higher degree of Complex IV deficiency compared to those in this current cohort? Thus, increasing the cohort size will allow a further insight into the biochemical status of Complex I and Complex IV in single fibres of patients harbouring the m.3243A>G pathogenic variant. Further to this, once the assay has been performed on the muscle biopsies, family members can be targeted to investigate whether deficient or normal Complex I and Complex IV cluster in families. In this current cohort of patients, there are three family members; P03 is the first cousin of P15; P04 is the sister of P05 and P08 is the first cousin, once removed of P10. The protein expression of Complex I and Complex IV is normal in both P03 and P15 skeletal muscle sections. However, the skeletal muscle section of P08 had Complex I-deficient fibres whilst P10 displayed normal expression of both OXPHOS complexes. According to the Z_score analysis, P05 displayed deficiency which would be in line with the findings for P04, however the hierarchical clustering defined P05 as all normal fibres. This could potentially be indicative of the role of nuclear genetic factors shared between family members hence some evidence of familial

clustering. However, this could be by chance and therefore, to investigate this relationship further, a larger sample size would be needed.

Increasing the cohort size would also provide more statistical power to detect a relationship between the phenotypes observed in these individuals (as scored by the NMDAS) and the level of Complex I deficiency (and potentially Complex IV). In addition to this, increasing the number of muscle sections with single fibre data would also help to confirm the findings with regards to critical threshold estimates. Working alongside Dr Conor Lawless, I have only investigated two of many statistical models that can be used to interrogate these single cell findings in the given time length of this project. Whilst the hierarchical clustering was an effective alternative approach to Z_score analysis, future work will include working with other statistical models, one being the Gaussian clustering method, to allow for an informed decision on how to best approach such heterogeneous data attained from these patients.

The inclusion of more patients would also allow the correlation of phenotypes with threshold estimates to answer the question: does the difference in threshold level for deficiency of Complex I account for the phenotypic variation observed in these patients? By correlating these estimates with NMDAS data (total and scores for individual phenotypes), it would allow an insight into how these differences (particularly the significant differences) can impact these patients in a clinical setting,

Investigating mtDNA copy number, signalling pathways and nuclear factors alongside the heteroplasmy levels

Mitochondrial DNA copy number was not investigated in this study as the main aim was to determine the heteroplasmic threshold differences in this cohort of patients. In light of the findings from this study, particularly the difference in heteroplasmy distribution in biochemically normal fibres between two groups of patients, determining the mtDNA copy number in the single muscle fibres is another essential molecular genetic investigation that should be undertaken. By determining copy number; total and wild-type mtDNA copy number, the interplay between these, heteroplasmy levels and biochemical deficiency can be investigated.

One suggestion for potential research that could be linked to mtDNA copy number, is to investigate the difference between the biochemically normal fibres (in Group A patients) that show very high levels of heteroplasmy (for example 98% as shown in this current study) and the deficient fibres with same or similar heteroplasmy levels (also in Group A patients). This could then lead to the research question of “what mechanism is allowing these normal fibres

tolerate high heteroplasmy levels without reaching threshold to cause a respiratory chain deficiency?" This latter question could then be linked to the investigation into why there is a difference in distribution of heteroplasmy levels between the normal fibres sampled from patients in Group A and the normal fibres sampled from patients in Group B. Why have some patients' fibres reached high heteroplasmy levels and exceeded the critical threshold for deficiency, whilst other patients' fibres have maintained a narrow range of heteroplasmy levels and have not yet reached the threshold?

A recent development with Imaging Mass Cytometry (IMC) at the Wellcome Centre for Mitochondria Research could potentially be used to investigate these research questions. IMC is a single cell 'omics' technique that combines time of flight mass cytometry (CyTOF) and immunohistochemistry with a high resolution ablation system (Giesen et al. 2014). It utilises rare earth metals as reporters on antibodies instead of fluorophores and therefore allows for the labelling of up to 40 different proteins on a single tissue section, for example the muscle or the brain. Antibodies targeting a number of proteins in various signalling pathways are currently being investigated and optimised at the Centre, including TFAM and PGC1- α (implicated in mitochondrial biogenesis) which could be linked to mtDNA copy number and helpful in investigating potential compensatory mechanisms within individual fibres of m.3242A>G patients. IMC would also allow for assessment of brain tissue (post-mortem) of a subset of these patients to decipher if similar findings of respiratory chain defects are observed in this tissue. In addition to this, the inclusion of antibodies targeting mtDNA-encoded subunits of the respiratory chain enzymes (for example, ND1 and ND4 for Complex I, CYTB for Complex III and also ATP6 and ATP8 for Complex V), alongside the antibodies that target nuclear-encoded subunits, would expand our understanding of the biochemical deficiency in these patients' muscle fibres. This could also prove beneficial at a diagnostic level when looking to expand the panel of antibodies to interrogate the mitochondrial respiratory chain.

Additionally, an investigation similar to that described by Vincent et al. (2018) could be undertaken on muscle sections from patients with m.3243A>G pathogenic variant. They investigated the presence of focal regions of respiratory chain deficiency in the perinuclear region of the cell/fibre in skeletal muscle sections of patient with mtDNA deletions. From this, Vincent and colleagues were able to propose a model to explain clonal expansion by showing that these focal regions showed local elevations of both mitochondrial mass and mtDNA copy number and therefore were associated with a local increase in mitochondrial biogenesis and unfolded protein response signalling pathways. A similar investigation could

potentially give insight into clonal expansion of the mutation in single fibres of patients with m.3243A>G. Furthermore, investigating whether deficient focal regions exist in muscle fibres of patients who presented with biochemically normal muscle sections could help determine whether these truly are biochemically normal fibres or if clonal expansion of a foci is to occur in muscle fibres of this subset of patients.

Finally, this work has further highlighted the importance of understanding the effect of nuclear background on the biochemical and clinical heterogeneity observed in patients harbouring the m.3243A>G pathogenic variant. This further encourages studies that are currently underway, for example, those using whole genome sequencing (WGS) and genetic linkage and association to identify nuclear variation influencing phenotypic differences and the segregation and modulation of heteroplasmy levels in these patients (Boggan et al. 2019).

Therefore, whilst this current study has investigated heteroplasmy and determined differences in the critical thresholds between individual patients, it has also highlighted that indeed, multiple factors contribute to the complexity of the m.3243A>G pathogenic variant and mitochondrial disease in general.

6.3. Final conclusion

In conclusion, the studies detailed in this thesis have utilised the quadruple immunofluorescence assay to contribute towards the current diagnostic process of mitochondrial disease and also to improve the understanding of the pathogenesis of the m.3243A>G variant. In addition, this work has also highlighted a number of important research questions, which together with these current findings, will hopefully contribute towards the ongoing research aiming to advance the understanding of the different mechanisms underlying the disease pathology of mitochondrial disease, particularly those associated with the m.3243A>G mutation.

Chapter 7: Appendices

Appendix 1: Newcastle Adult Mitochondrial Disease scale (NMDAS) questionnaire which is used to assess mitochondrial disease severity and progression in the Newcastle Mitochondrial disease cohort.

THE NEWCASTLE
MITOCHONDRIAL DISEASE ADULT SCALE
(NMDAS)

Name: _____

Date of birth: _____

Age at assessment: _____

Date of assessment: _____

Checklist – please tick off when completed.

- **Height:**

- **FVC - 1st attempt**

- **FVC - 2nd attempt** **% Predicted** _____

- **FVC - 3rd attempt**

Raw Score		Scaled Score	Centile
<input type="checkbox"/>	SF-12v2 self completion questionnaire	_____	_____
<input type="checkbox"/>	WTAR reading test (1 minute)	_____	_____
<input type="checkbox"/>	Symbol Search (2 minutes)	_____	_____
<input type="checkbox"/>	Speed of comprehension test (2 minutes)	_____	_____

Disease score (sections I-III) _____

SF-12v2 Quality of Life score (section IV) _____

Section I- Current Function

Rate function over the preceding **4 week period, according to patient and/or caregiver** interview only. The clinician's subjective judgement of functional ability should **not** be taken into account.

1. **Vision** with usual glasses or contact lenses

0. Normal.
1. No functional impairment but aware of worsened acuities.
2. Mild - difficulty with small print or text on television.
3. Moderate - difficulty outside the home (e.g. bus numbers, road signs or shopping).
4. Severe - difficulty recognising faces.
5. Unable to navigate without help (e.g. carer, dog, cane).

2. **Hearing** with or without hearing aid

0. Normal.
1. No communication problems but aware of tinnitus **or** deterioration from prior 'normal' hearing.
2. Mild deafness (e.g. missing words in presence of background noise). **Fully** corrected with hearing aid.
3. Moderate deafness (e.g. regularly requiring repetition). **Not fully** corrected with hearing aid.
4. Severe deafness - poor hearing even with aid (see 3 above).
5. End stage - virtually no hearing despite aid. Relies heavily on non-verbal communication (e.g. lip reading) **or** has cochlear implant.

3. **Speech**

0. Normal.
1. Communication unaffected but patient or others aware of changes in speech patterns or quality.
2. Mild difficulties - usually understood and **rarely** asked to repeat things.
3. Moderate difficulties - poorly understood by strangers and **frequently** asked to repeat things.
4. Severe difficulties - poorly understood by family or friends.
5. Not understood by family or friends. Requires communication aid.

4. **Swallowing**

0. Normal.
1. Mild - sensation of solids 'sticking' (occasional).
2. Sensation of solids 'sticking' (most meals) **or** need to modify diet (e.g. avoidance of steak/salad).
3. Difficulty swallowing solids - affecting meal size or duration. Coughing, choking **or** nasal regurgitation infrequent (1 to 4 times per month) but more than peers.
4. Requires adapted diet - regular coughing, choking, **or** nasal regurgitation (more than once per week).
5. Requiring enteral feeding (e.g. PEG).

5. **Handwriting**

0. Normal.
1. Writing speed unaffected but aware of increasing untidiness.
2. Mild – Has to write slower to maintain tidiness/legibility.
3. Moderate – Handwriting takes at least twice as long **or** resorts to printing (must previously have used joined writing).
4. Severe – Handwriting mostly illegible. Printing very slow and untidy (e.g. 'THE BLACK CAT' takes in excess of 30 seconds).
5. Unable to write. No legible words.

6. Cutting food and handling utensils (irrespective of contributory factors – e.g. weakness, coordination, cognitive function etc. This is also true for questions 7-10)

0. Normal.
1. Slightly slow and/or clumsy but **minimal** effect on meal duration.
2. Slow and/or clumsy with extended meal duration, but no help required.
3. Difficulty cutting up food and inaccuracy of transfer pronounced. Can manage alone but avoids problem foods (egg peas) or carer typically offers minor assistance (e.g. cutting up steak).
4. Unable to cut up food. Can pass food to mouth with great effort or inaccuracy. Resultant intake minimal. Requires major assistance.
5. Needs to be fed.

6. Dressing

0. Normal.
1. Occasional difficulties (e.g. shoe laces, buttons etc.) but no real impact on time or effort taken to dress.
2. Mild – Dressing takes longer and requires more effort than expected at the patient's age. No help required.
3. Moderate - Can dress unaided but takes at least twice as long and is a major effort. Carer typically helps with difficult tasks such as shoe laces or buttons.
4. Severe – Unable to dress without help but some tasks completed unaided.
5. Needs to be dressed.

7. Hygiene

0. Normal.
1. Occasional difficulties only but no real impact on time or effort required.
2. Mild – hygienic care takes longer but quality unaffected.
3. Moderate - bathes and showers alone with difficulty **or** needs bath chair / modifications. Dextrous tasks (e.g. brushing teeth, combing hair) performed poorly.
4. Severe - unable to bathe or shower without help. Major difficulty using toilet alone. Dextrous tasks require help.
5. Dependent upon carers to wash, bathe, and toilet.

8. Exercise Tolerance

0. Normal.
1. Unlimited on flat - symptomatic on inclines or stairs.
2. Able to walk < 1000m on the flat. Restricted on inclines or stairs - rest needed after 1 flight (12 steps).
3. Able to walk < 500m on the flat. Rest needed after 8 steps on stairs.
4. Able to walk < 100m on the flat. Rest needed after 4 steps on stairs.
5. Able to walk < 25m on the flat. Unable to do stairs alone.

9. Gait stability

0. Normal.
1. Normal gait - occasional difficulties on turns, uneven ground, or if required to balance on narrow base.
2. Gait reasonably steady. Aware of impaired balance. **Occasionally** off balance when walking.
3. Unsteady gait. **Always** off balance when walking. **Occasional** falls. Gait steady with support of stick or person.
4. Gait grossly unsteady without support. **High likelihood** of falls. Can only walk short distances (< 10m) without support.
5. Unable to walk without support. Falls on standing.

Section II – System Specific Involvement

Rate function according to patient and/or caregiver interview and consultation with the medical notes. Each inquiry should take into account the situation for the preceding **12 month period** only, unless otherwise stated in the question.

1. Psychiatric

0. None.
1. Mild & transient (e.g. reactive depression) - lasting **less** than 3 months.
2. Mild & persistent (lasting **more** than 3 months) **or** recurrent. Patient has consulted GP.
3. Moderate & warranting specialist treatment (e.g. from a psychiatrist) - e.g. bipolar disorder or depression with vegetative symptoms (insomnia, anorexia, abulia etc.).
4. Severe (e.g. self harm - psychosis etc.).
5. Institutionalised or suicide attempt.

2. Migraine Headaches. During **the last 3 months**, how many days have headaches prevented the patient from functioning normally at school, work, or in the home?

0. No past history.
1. Asymptomatic but past history of migraines.
2. One day per month.
3. Two days per month.
4. Three days per month.
5. Four days per month or more.

3. Seizures

0. No past history.
1. Asymptomatic but past history of epilepsy.
2. Myoclonic or simple partial seizures only.
3. Multiple absence, complex partial, or myoclonic seizures affecting function **or** single generalised seizure.
4. Multiple generalised seizures.
5. Status epilepticus.

4. Stroke-like-episodes (exclude focal deficits felt to be of vascular aetiology)

0. None.
1. Transient focal sensory symptoms only (**less** than 24 hours).
2. Transient focal motor symptoms only (**less** than 24 hours).
3. Single stroke-like episode affecting one hemisphere (**more** than 24 hours).
4. Single stroke-like episode affecting both hemispheres (**more** than 24 hours).
5. Multiple stroke-like episodes (**more** than 24 hours each).

5. Encephalopathic episodes

0. No past history.
1. Asymptomatic **but** past history of encephalopathy.
2. Mild - single episode of personality or behavioural change but retaining orientation in time/place/person.
3. Moderate - single episode of confusion or disorientation in time, place or person.
4. Severe – multiple moderate episodes (as above) **or** emergency hospital admission due to encephalopathy **without** associated seizures or stroke-like episodes.
5. Very severe - in association with seizures, strokes or gross lactic acidemia.

6. Gastro-intestinal symptoms

0. None.
1. Mild constipation only **or** past history of bowel resection for dysmotility.
2. Occasional symptoms of 'irritable bowel' (pain, bloating or diarrhoea) with long spells of normality.
3. Frequent symptoms (as above) most weeks **or** severe constipation with bowels open less than once/week **or** need for daily medications.
4. Dysmotility requiring admission **or** persistent and/or recurrent anorexia/vomiting/weight loss.
5. Surgical procedures **or** resections for gastrointestinal dysmotility.

7. Diabetes mellitus

0. None.
1. Past history of gestational diabetes or transient glucose intolerance related to intercurrent illness.
2. Impaired glucose tolerance (in absence of intercurrent illness).
3. NIDDM (diet).
4. NIDDM (tablets).
5. DM requiring insulin (irrespective of treatment at onset).

8. Respiratory muscle weakness

0. FVC normal ($\geq 85\%$ predicted).
1. FVC $< 85\%$ predicted.
2. FVC $< 75\%$ predicted.
3. FVC $< 65\%$ predicted.
4. FVC $< 55\%$ predicted.
5. FVC $< 45\%$ predicted **or** ventilatory support for over 6 hours per 24 hr period (**not** for OSA alone).

9. Cardiovascular system

0. None.
1. Asymptomatic ECG change.
2. Asymptomatic LVH on echo **or** non-sustained brady/tachyarrhythmia on ECG.
3. Sustained or **symptomatic** arrhythmia, LVH **or** cardiomyopathy. Dilated chambers **or** reduced function on echo. Mobitz II AV block or greater.
4. Requires pacemaker, defibrillator, arrhythmia ablation, **or** LVEF $< 35\%$ on echocardiogram.
5. Symptoms of left ventricular failure **with** clinical and/or x-ray evidence of pulmonary oedema **or** LVEF $< 30\%$ on echocardiogram.

Section III – Current Clinical Assessment

Rate current status according to examination performed at **the time of** assessment

1. Visual acuity with usual glasses, contact lenses or pinhole.

0. CSD \leq **12** (i.e. normal vision - 6/6, 6/6 or better). 1. CSD \leq **18** (e.g. 6/9, 6/9).
2. CSD \leq **36** (e.g. 6/12, 6/24).
3. CSD \leq **60** (e.g. 6/24, 6/36).
4. CSD \leq **96** (e.g. 6/60, 6/36).
5. CSD \geq **120** (e.g. 6/60, 6/60 **or worse**).

2. Ptosis

0. None.
1. Mild ptosis - not obscuring **either** pupil.
2. Unilateral ptosis obscuring $<$ 1/3 of pupil.
3. Bilateral ptosis obscuring $<$ 1/3 **or** unilateral ptosis obscuring $>$ 1/3 of pupil **or** prior unilateral surgery.
4. Bilateral ptosis obscuring $>$ 1/3 of pupils **or** prior bilateral surgery.
5. Bilateral ptosis obscuring $>$ 2/3 of pupils **or** $>$ 1/3 of pupils **despite** prior bilateral surgery.

3. Chronic Progressive External Ophthalmoplegia

0. None.
1. Some restriction of eye movement (any direction). Abduction complete.
2. Abduction of worst eye incomplete.
3. Abduction of worst eye below 60% of normal.
4. Abduction of worst eye below 30% of normal.
5. Abduction of worst eye minimal (flicker).

4. Dysphonia/Dysarthria

0. None.
1. Minimal - noted on examination only.
2. Mild – clear impairment but easily understood.
3. Moderate – some words poorly understood and infrequent repetition needed.
4. Severe – many words poorly understood and frequent repetition needed.
5. Not understood. Requires communication aid.

5. Myopathy

0. Normal.
1. Minimal reduction in hip flexion and/or shoulder abduction **only** (e.g. MRC 4+/5).
2. Mild but clear proximal weakness in hip flexion and shoulder abduction (MRC 4/5). Minimal weakness in elbow flexion and knee extension (MRC 4+/5 - both examined with joint at 90 degrees).
3. Moderate proximal weakness including elbow flexion & knee extension (MRC 4/5 or 4 -/5) **or difficulty** rising from a 90 degree squat.
4. Waddling gait. **Unable** to rise from a 90 degree squat (=a chair) unaided.
5. Wheelchair dependent **primarily** due to proximal weakness.

6. Cerebellar ataxia

0. None.
1. Normal gait but hesitant heel-toe.
2. Gait reasonably steady. Unable to maintain heel-toe walking **or** mild UL dysmetria.
3. Ataxic gait (but walks unaided) **or** UL intention tremor & past-pointing. Unable to walk heel-toe - falls immediately.
4. Severe - gait grossly unsteady without support **or** UL ataxia sufficient to affect feeding.
5. Wheelchair dependent **primarily** due to ataxia **or** UL ataxia **prevents** feeding.

7. Neuropathy

0. None.
1. Subtle sensory symptoms **or** areflexia.
2. Sensory impairment only (e.g. glove & stocking sensory loss).
3. Motor impairment (distal weakness) **or** sensory ataxia.
4. Sensory ataxia **or** motor effects severely limit ambulation.
5. Wheelchair bound **primarily** due to sensory ataxia or neurogenic weakness.

8. Pyramidal Involvement

0. None.
1. Focal or generalised increase in tone or reflexes only.
2. Mild **focal** weakness, sensory loss or fine motor impairment (e.g. cortical hand).
3. Moderate hemiplegia allowing unaided ambulation **or** dense UL monoplegia.
4. Severe hemiplegia allowing ambulation with aids **or** moderate tetraplegia (ambulant).
5. Wheelchair dependent **primarily** due to hemiplegia or tetraplegia.

9. Extrapyrarnidal

0. Normal.
1. Mild and unilateral. Not disabling (H&Y stage 1).
2. Mild and bilateral. Minimal disability. Gait affected (H&Y stage 2).
3. Moderate. Significant slowing of body movements (H&Y stage 3)
4. Severe. Rigidity and bradykinesia. Unable to live alone. Can walk to limited extent (H&Y stage 4).
5. Cannot walk or stand unaided. Requires constant nursing care (H&Y stage 5).

10. Cognition

Patients undergo testing using WTAR, Symbol Search and Speed of Comprehension Test.

0. Combined centiles **100 or more.**
1. Combined centiles **60 - 99**
2. Combined centiles **30 - 59**
3. Combined centiles **15 - 29**
4. Combined centiles **5 - 14**
5. Combined centiles **4 or below.**

Appendix 2:

Table 7.1: NMDAS scores and thresholds for clinical phenotypes assessed in cohort

Patient ID	Total NMDAS	Phenotype	Exercise tolerance	SLE	Cardio	Ptosis	CPEO	Myopathy
		Threshold	4	1	2	2	2	2
P01	12.4		0	0	0	0	0	1
P02	20.7		1	0	0	0	0	1
P03	20.4		3	0	1	0	0	2
P04	23.2		3	0	-	0	0	3
P05	27.9		2	0	0	0	0	2
P06	33.5		3	3		0	0	3
P07	21.8		2	0	0	3	0	2
P08	26.9		2	0	1	1	0	1
P09	45.1		2	0	1	1	0	2
P10	21.5		2	0	0	1	0	2
P11	-		-	-	-	-	-	-
P12	4.1		0	0	0	0	0	0
P13	9.7		0	0	0	0	0	0
P14	26.9		4	0	2	3	2	1
P15	22.8		3	0	0	0	1	2
P16	49.7		4	0	0	0	2	1
P17	14		0	0	-	0	0	0
P18	49.7		4	0	0	0	2	1
P19	-		-	-	-	-	-	-

SLE = Stroke-like episodes; Cardio = cardiovascular; CPEO = Chronic Progressive External Ophthalmoplegia

Appendix 3:

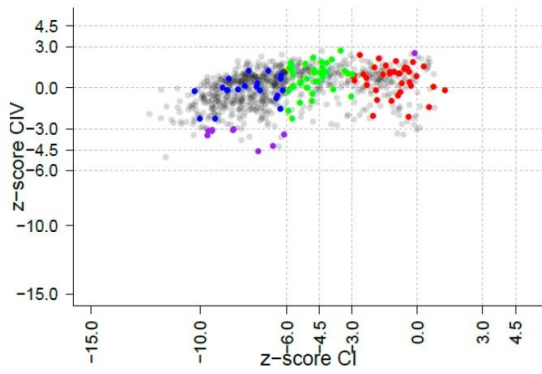
Table 7.2: Quantification of Complex I (NDUFB8) and Complex IV (COX-I) deficiency in skeletal muscle fibres from non-disease controls

Control ID	Complex I (NDUFB8) Levels (%)					Complex IV (COX-1) Levels (%)					Total n =
	Pos	Int (+)	Int (-)	Neg	% Deficiency	Pos	Int (+)	Int (-)	Neg	% Deficiency	
Experiment 1											
C01	99.85	0.15	0.00	0.00	0.15	100.00	0.00	0.00	0.00	0.00	1988
C02	99.91	0.04	0.00	0.04	0.09	99.91	0.04	0.00	0.04	0.09	2295
C03	99.73	0.09	0.09	0.09	0.27	99.91	0.09	0.00	0.00	0.09	1103
C04	100.00	0.00	0.00	0.00	0.00	99.65	0.35	0.00	0.00	0.35	1986
C05	100.00	0.00	0.00	0.00	0.00	99.97	0.03	0.00	0.00	0.03	3401
Experiment 2											
C01	100.00	0.00	0.00	0.00	0.00	99.72	0.28	0.00	0.00	0.28	2174
C02	99.94	0.06	0.00	0.00	0.06	99.88	0.12	0.00	0.00	0.12	1691
C03	99.71	0.19	0.10	0.00	0.29	99.81	0.10	0.10	0.00	0.19	1026
C04	100.00	0.00	0.00	0.00	0.00	98.23	1.72	0.06	0.00	0.00	1084
C05	100.00	0.00	0.00	0.00	0.00	99.72	0.22	0.04	0.00	0.00	2680
Experiment 3											
C01	99.92	0.08	0.00	0.00	0.08	100.00	0.00	0.00	0.00	0.00	1313
C02	98.65	1.28	0.07	0.00	1.35	99.93	0.07	0.00	0.00	0.07	1479
C03	100.00	0.00	0.00	0.00	0.00	99.38	0.62	0.00	0.00	0.62	950
C04	100.00	0.00	0.00	0.00	0.00	99.26	0.75	0.00	0.00	0.75	989
C05	100.00	0.00	0.00	0.00	0.00	100.00	0.00	0.00	0.00	0.00	1558

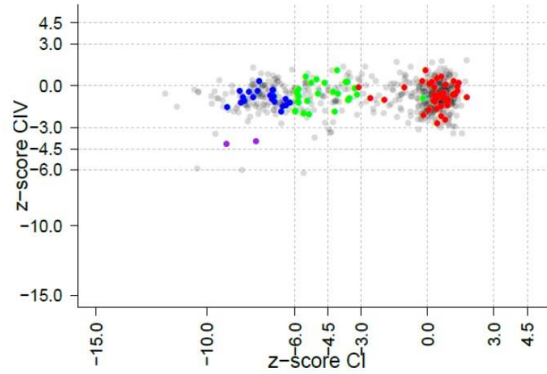
Appendix 4:

Mitochondrial respiratory chain profiles highlighting sampled fibres from all patients.

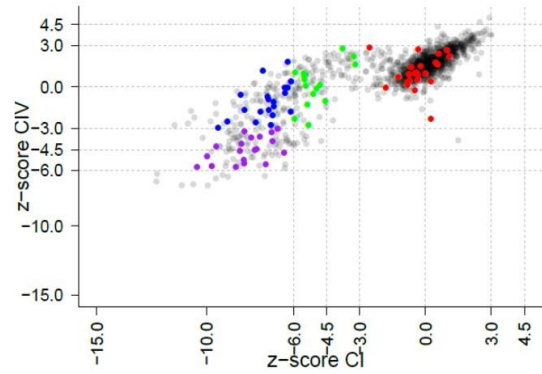
Patient 01 (Group A)



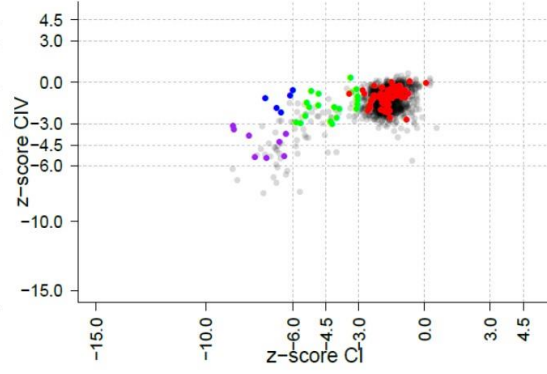
Patient 07 (Group A)



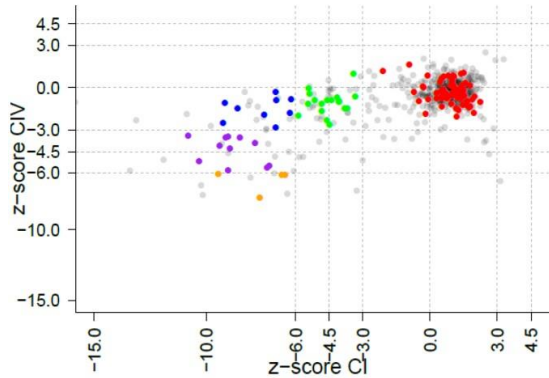
Patient 11 (Group A)



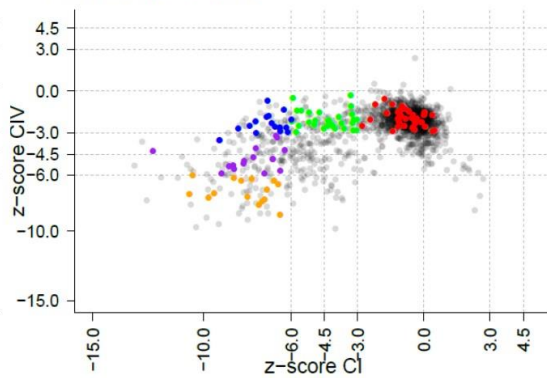
Patient 13 (Group A)



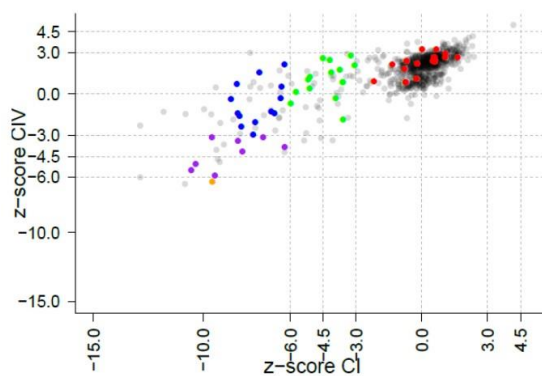
Patient 16 (Group A)



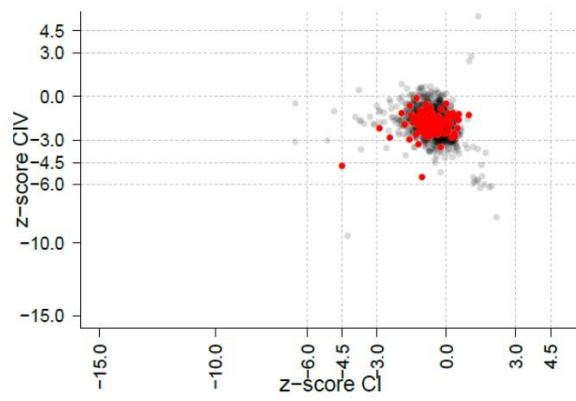
Patient 18 (Group A)



Patient 19 (Group A)



Patient 02 (Group B)



Patient 15 (Group B)

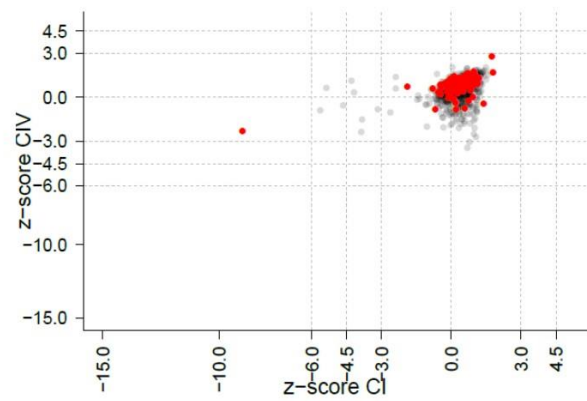


Figure 7.1: Mitochondrial respiratory chain profiles highlighting sampled fibres from all patients.
Coloured dots represent the fibres sampled and correspond to each OXHOS group; Group 1 = red, Group 2 = green, Group 3 = dark blue, Group 4 = purple, Group 5 = orange.

Appendix 5:

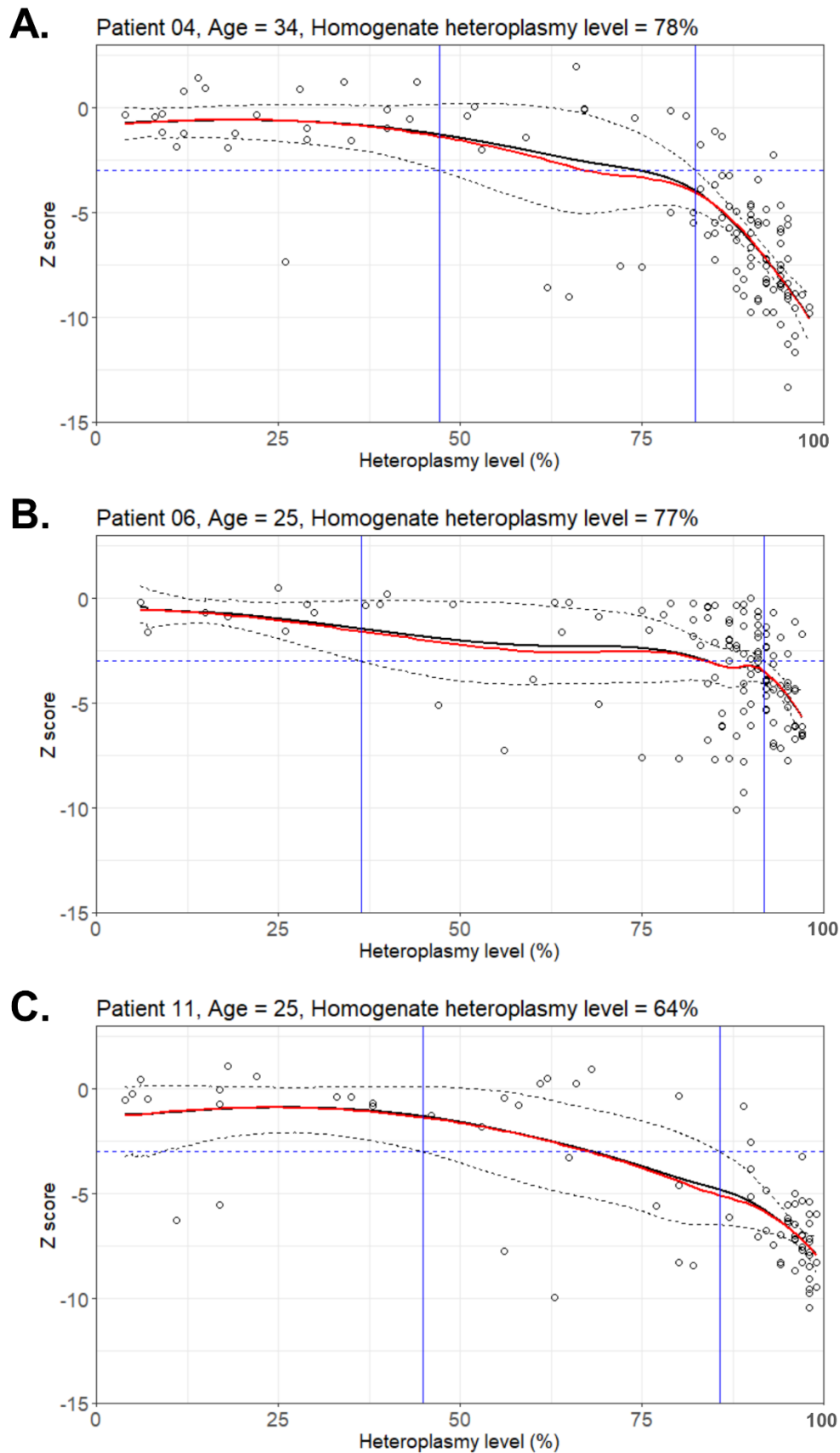
Table 7.3: The m.3243A>G heteroplasmy levels through inter and intra-variability testing of pyrosequencing

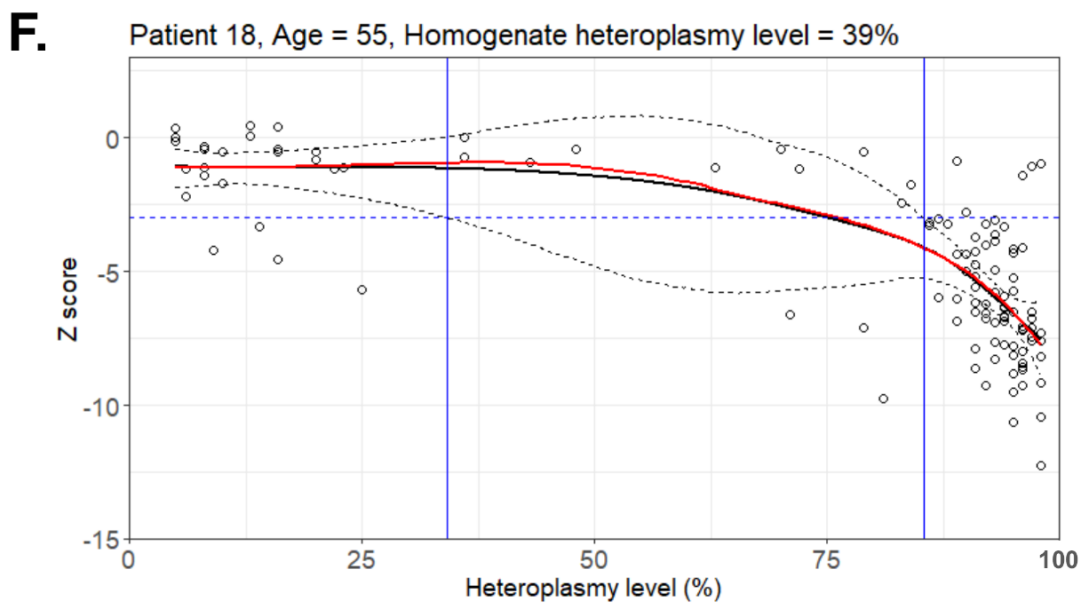
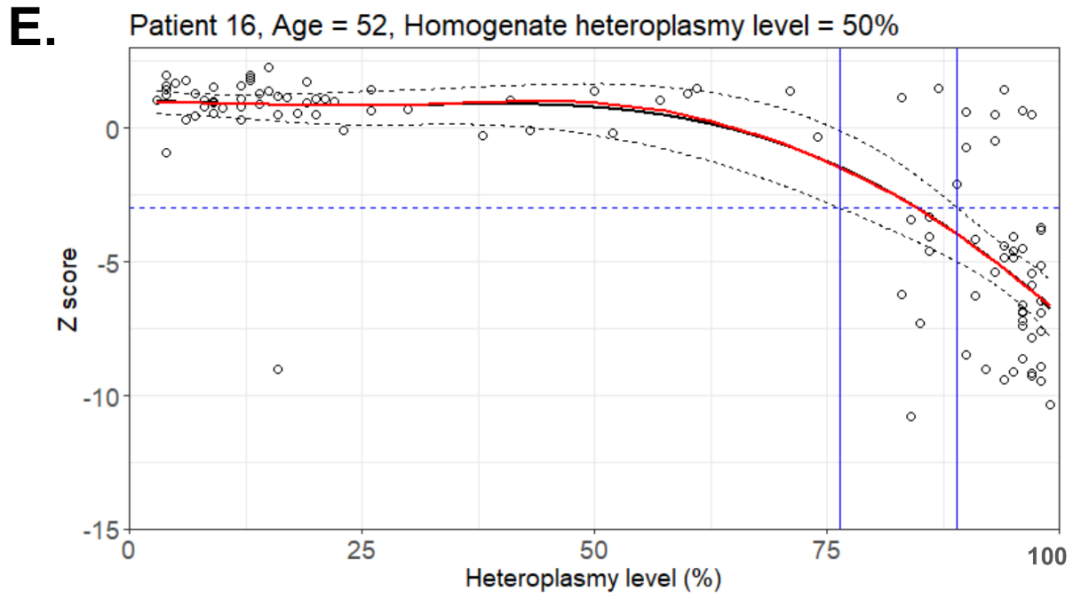
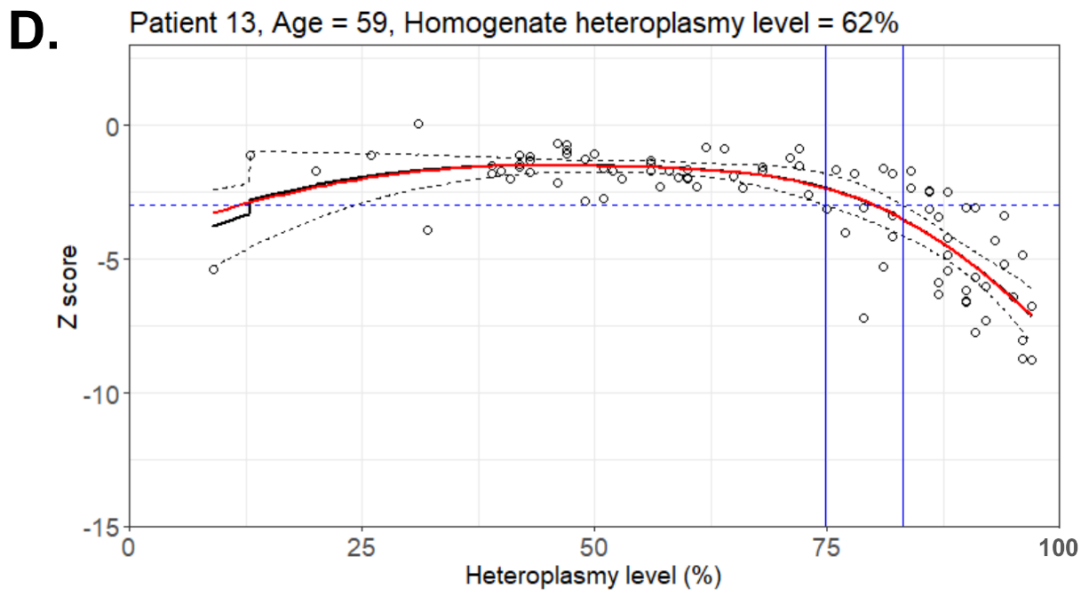
Fibre	Experiment 1	Experiment 2	Experiment 3	Range between Experiment 1 and 2	Total range between all experiments	Mean	Standard deviation (SD)
23	63	63	59	0	4	62	2
28	91	92	93	1	2	92	1
49	24	22	19	2	5	22	3
67	93	92	93	1	1	93	1
76	73	73	71	0	2	72	1
118	76	76	75	0	1	76	1
129	90	90	94	0	4	91	2
154	93	93	94	0	1	93	1
158	4	4	4	0	0	4	0
189	95	94	94	1	1	94	1
199	23	22	21	1	2	22	1
201	96	96	95	0	1	96	1
239	98	97	97	1	1	97	1
258	88	88	92	0	4	89	2
261	10	10	6	0	4	9	2
262	95	96	96	1	1	96	1
263	95	94	96	1	1	95	1
269	86	88	85	2	2	86	2
276	13	14	15	1	2	14	1
283	77	75	76	2	2	76	1
295	76	73	73	3	3	74	2
312	80	82	81	2	2	81	1
336	6	8	3	2	5	6	3
337	95	94	95	1	1	95	1

368	82	83	83	1	1	83	1
373	92	90	95	2	5	92	3
401	69	68	74	1	6	70	3
432	82	83	82	1	1	82	1
490	4	3	3	1	1	3	1
496	91	90	91	1	1	91	1
498	95	95	97	0	2	96	1
521	78	78	80	0	2	79	1
552	93	93	91	0	2	92	1
595	8	7	3	1	5	6	3
615	8	8	5	0	3	7	2
631	9	10	8	1	2	9	1
640	92	92	92	0	0	92	0
663	5	4	2	1	3	4	2
668	2	5	0	3	5	2	3
683	8	6	4	2	4	6	2
694	6	6	2	0	4	5	2
709	84	84	84	0	0	84	0
843	95	95	94	0	1	95	1
925	77	82	71	5	9	77	6

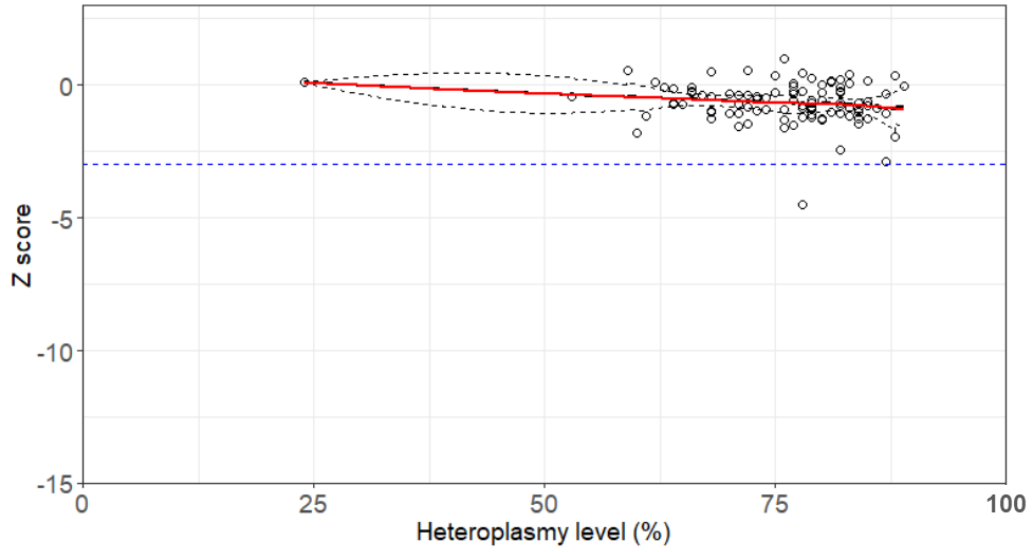
Appendix 6:

LOESS profiles showing the Z_score and heteroplasmy level distribution of single fibres and the estimated heteroplasmic threshold for deficiency

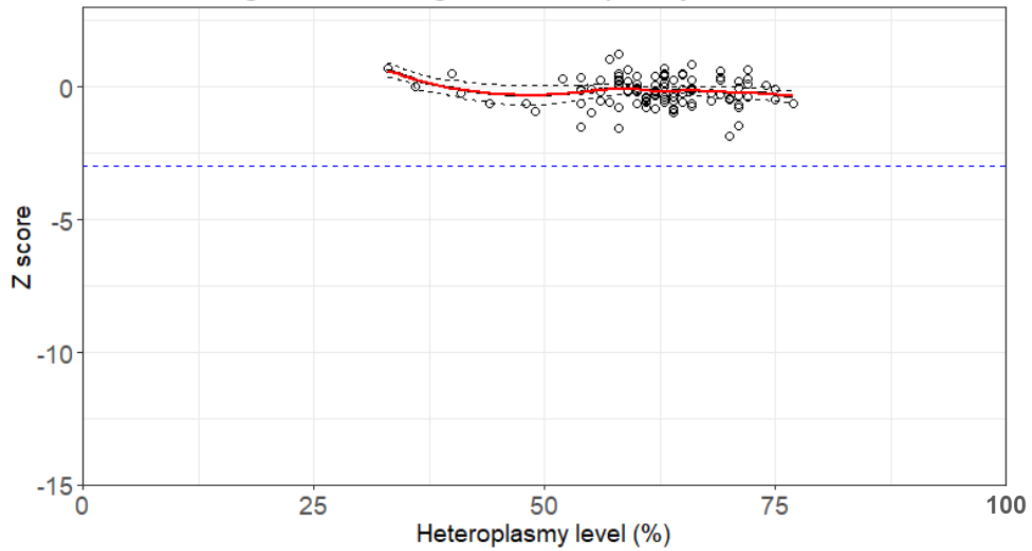




G. Patient 02, Age = 55, Homogenate heteroplasmy level = 84%



H. Patient 10, Age = 18, Homogenate heteroplasmy level = 66%



I. Patient 15, Age = 56, Homogenate heteroplasmy level = 55%

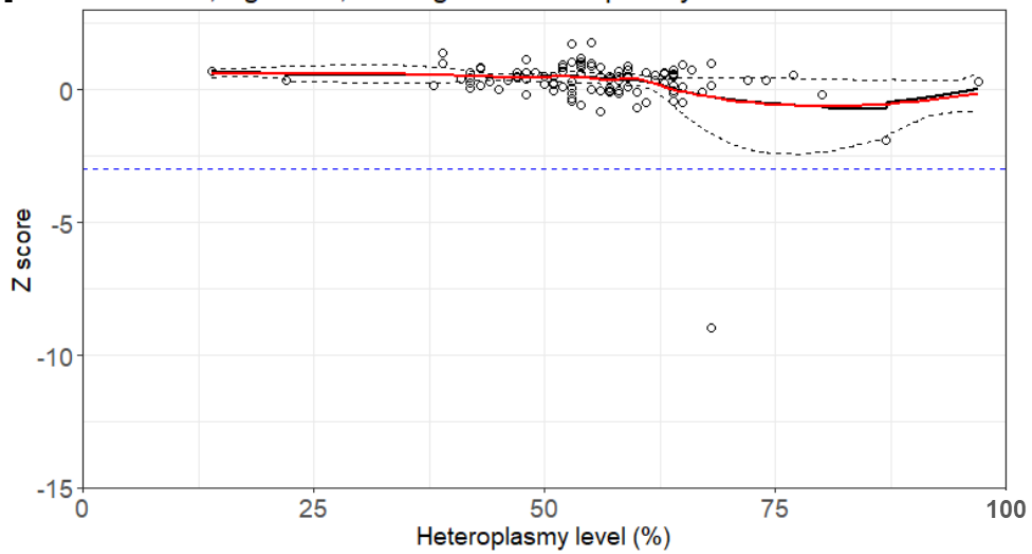


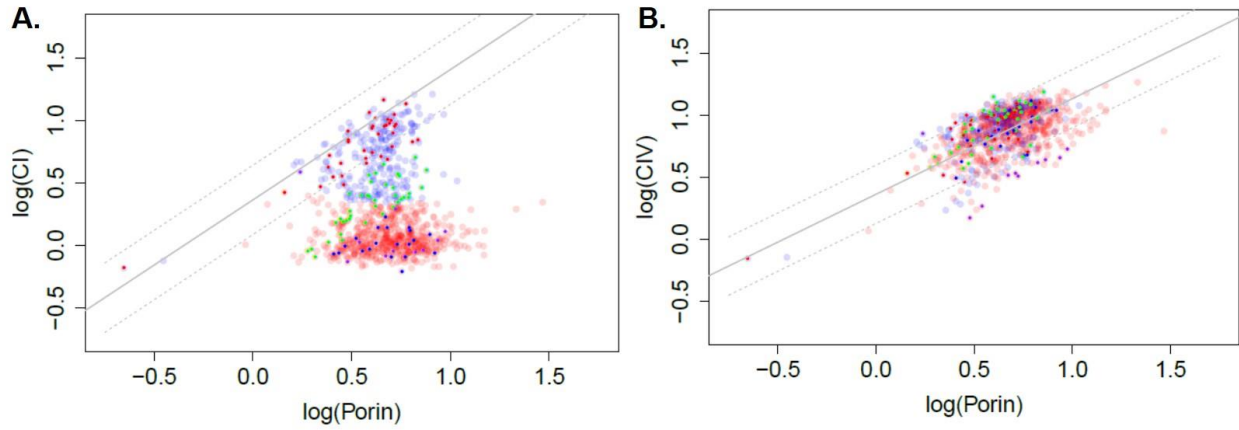
Figure 7.2: LOESS profiles showing the Z_score and heteroplasmy level distribution of single fibres and the estimated heteroplasmic threshold for deficiency.

Profiles are representative of fibres from skeletal muscle sections of patients in Group A (**A, B, C, D, E, F**) and patients in Group B (**G, H, I**) and the estimated threshold defined at the point which model curves cross the deficiency cut off at Z_score of -3 ($y=-3$). Each white dot represents a single fibre. The blue dashed line ($y=-3$) is the Z_score deficiency cut off. The black curve represents the model fitted to the mean of the bootstrapped data and the red curve represents the model fitted to the original data. The dotted black line around the curves = 95% confidence intervals of bootstrapped estimate. Solid dark blue lines represent the heteroplasmy levels at which the confidence intervals for the model cross the threshold Z_score of -3.

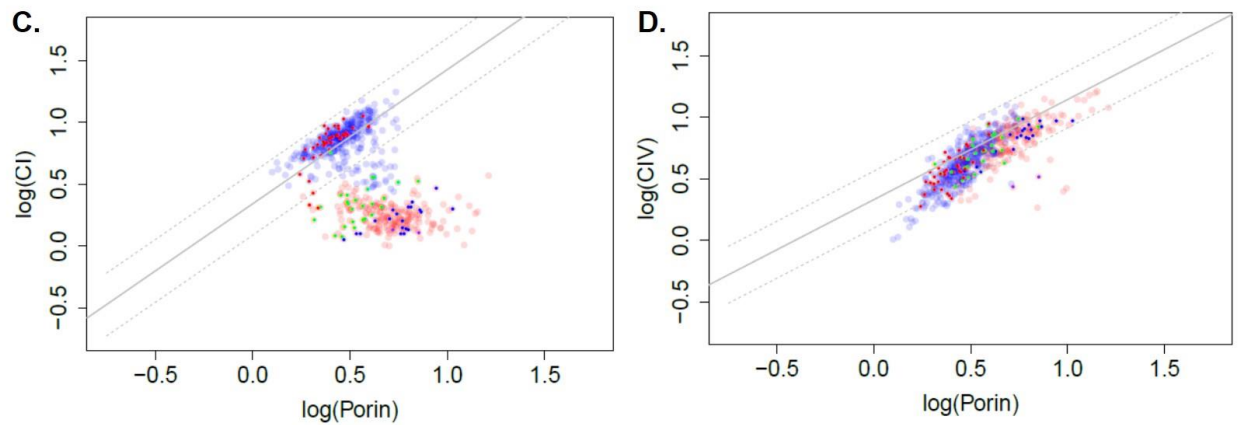
Appendix 7:

Two-dimensional scatterplots (2Dmito plots) comparing Complex I protein expression with mitochondrial mass.

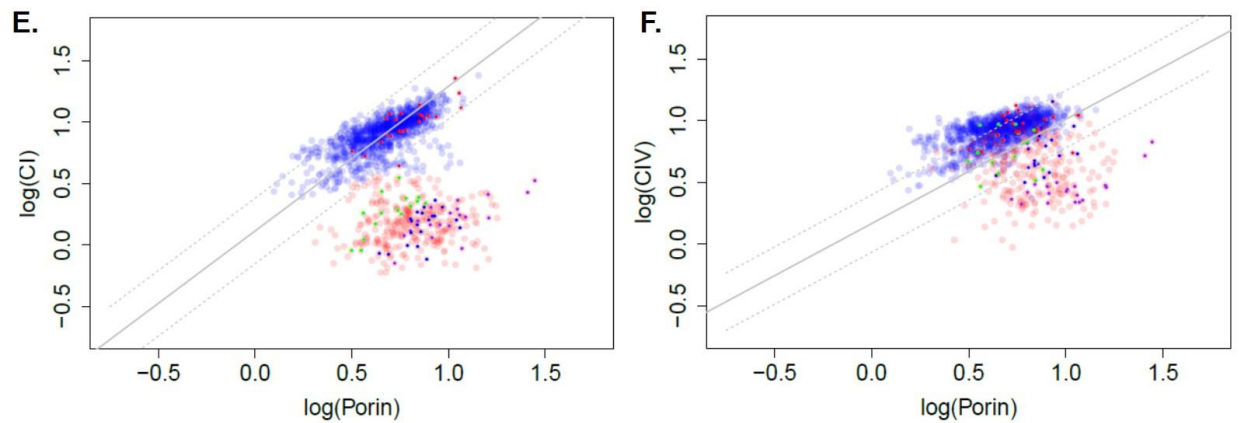
Patient 01
Normal fibres: 30.7%, Deficient fibres: 69.3%



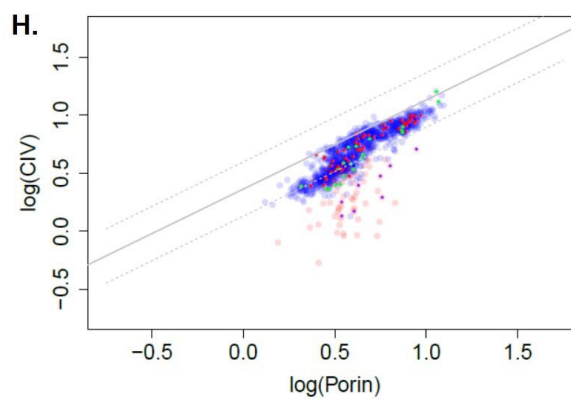
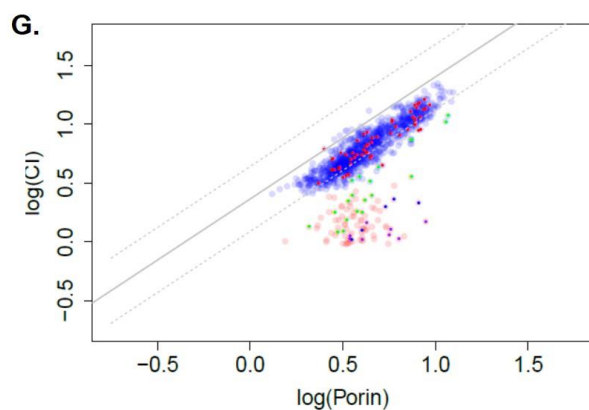
Patient 07
Normal fibres: 63.8%, Deficient fibres: 36.2%



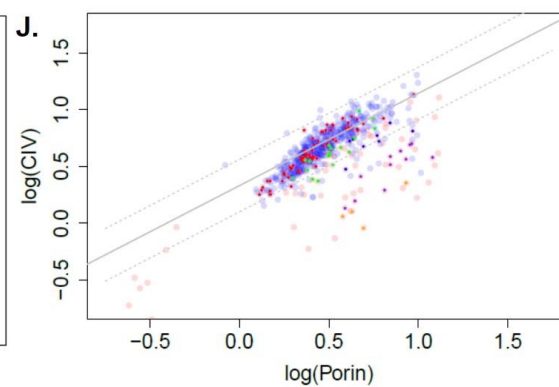
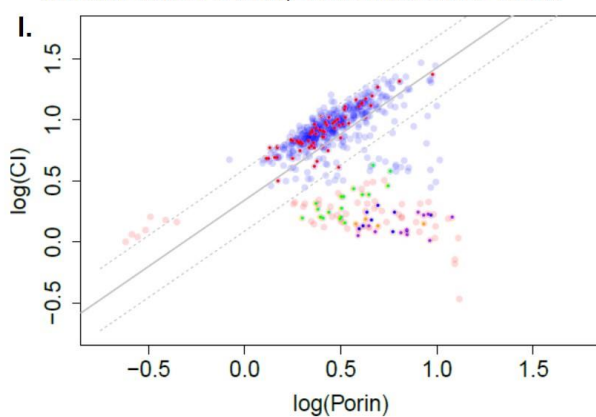
Patient 11
Normal fibres: 78.1%, Deficient fibres: 21.9%



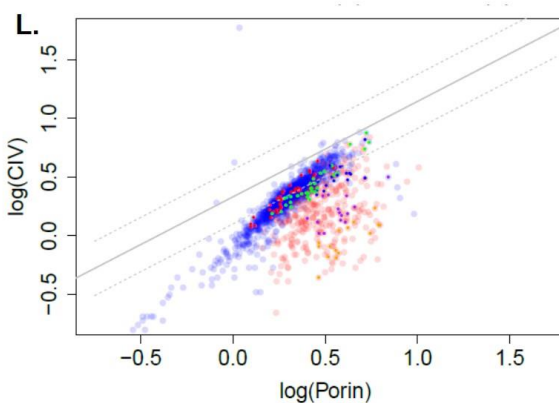
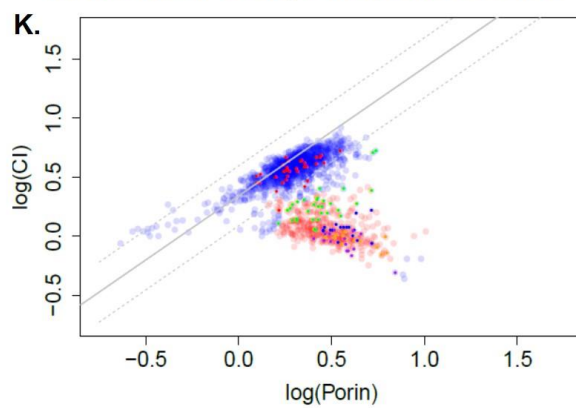
Patient 13 (Group A)
Normal fibres: 93.1%, Deficient fibres: 6.9%



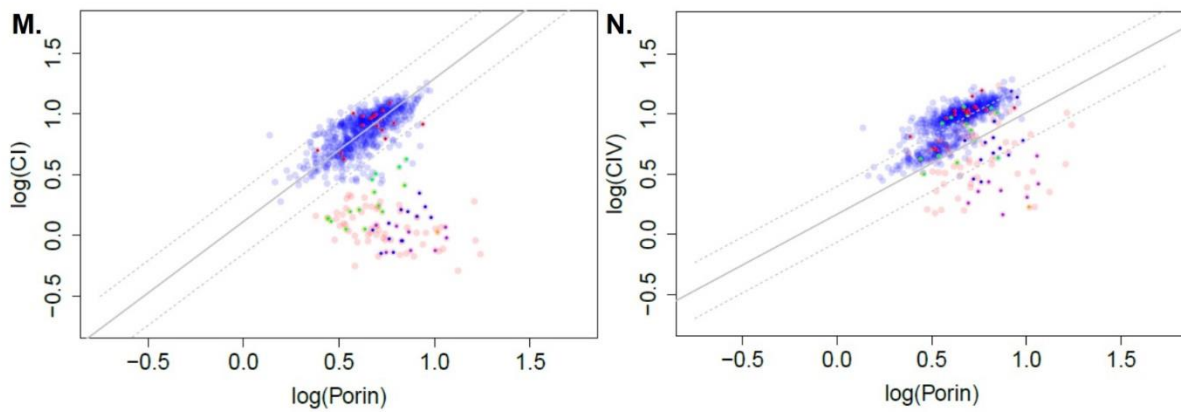
Patient 16 (Group A)
Normal fibres: 84.5%, Deficient fibres: 15.5%



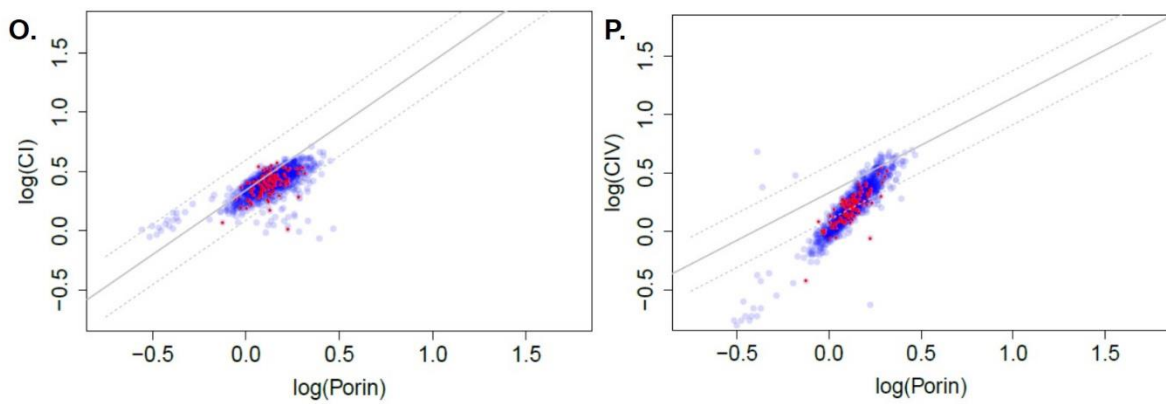
Patient 18 (Group A)
Normal fibres: 77.7%, Deficient fibres: 22.3%



Patient 19 (Group A)
Normal fibres: 89.5%, Deficient fibres: 10.5%



Patient 02 (Group B)
Normal fibres: 100%, Deficient fibres: 0%



Patient 15 (Group B)
Normal fibres: 100%, Deficient fibres: 0%

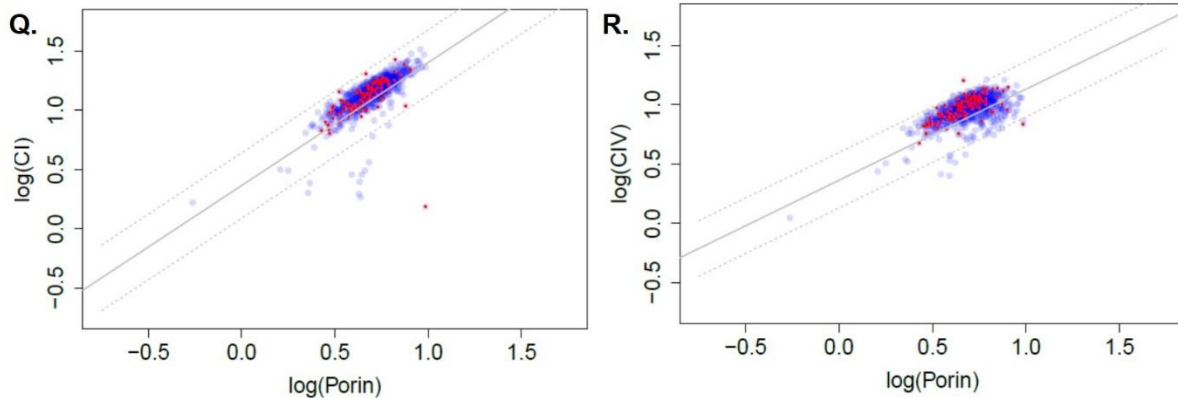


Figure 7.3: Two-dimensional scatterplots (2Dmito plots) comparing Complex I protein expression with mitochondrial mass.

Patients from Group A (A – B) P01, (C-D) P07, (E-F) P11, (G-H) P13, (I-J) P16, (K-L) P18, (M-N) P19 show clustering of fibres into two cluster populations for Complex I after hierarchical clustering; blue = biochemically normal fibres and red = biochemically deficient fibres for Complex I which is indicated by the decrease in Complex I in relation to log of porin). But only on cluster for Complex IV, therefore no deficient fibres for Complex IV. Patients from Group B (O-P) P02 and (Q-R) P15 also

show only one cluster in the data for both Complex I and Complex IV therefore all fibres are biochemically normal (blue). Sampled fibres have been colour co-ordinated according to the original Z_score classification; red = Group 1 fibres, green = Group 2 fibres, blue = Group 3 fibres, purple = Group 4 fibres. Grey solid and dashed line showing the regression line fitted to the control data and the 95% confidence intervals, for comparison.

Chapter 8: References

- Abrahams, J. P., et al. (1994), 'Structure at 2.8 Å resolution of F1-ATPase from bovine heart mitochondria', *Nature*, 370 (6491), 621-8.
- Acin-Perez, R., et al. (2008), 'Respiratory active mitochondrial supercomplexes', *Mol Cell*, 32 (4), 529-39.
- Agip, Ahmed-Noor A., et al. (2018), 'Cryo-EM structures of complex I from mouse heart mitochondria in two biochemically defined states', *Nature structural & molecular biology*, 25 (7), 548-56.
- Ahmed, Syeda T., et al. (2017), 'Using a quantitative quadruple immunofluorescent assay to diagnose isolated mitochondrial Complex I deficiency', *Scientific Reports*, 7 (1), 15676.
- Ajioka, R. S., Phillips, J. D., and Kushner, J. P. (2006), 'Biosynthesis of heme in mammals', *Biochim Biophys Acta*, 1763 (7), 723-36.
- Alston, C. L., et al. (2010), 'A novel mitochondrial tRNAGlu (MTTE) gene mutation causing chronic progressive external ophthalmoplegia at low levels of heteroplasmy in muscle', *J Neurol Sci*, 298 (1-2), 140-4.
- Alston, C. L., et al. (2017), 'The genetics and pathology of mitochondrial disease', *The Journal of pathology*, 241 (2), 236-50.
- Alston, C. L., et al. (2016), 'Biallelic Mutations in TMEM126B Cause Severe Complex I Deficiency with a Variable Clinical Phenotype', *Am J Hum Genet*, 99 (1), 217-27.
- Alston, C. L., et al. (2018), 'Bi-allelic Mutations in NDUFA6 Establish Its Role in Early-Onset Isolated Mitochondrial Complex I Deficiency', *Am J Hum Genet*, 103 (4), 592-601.
- Altmann, Richard (1894), *Die Elementarorganismen und ihre Beziehungen zu den Zellen* (Veit).
- Amunts, A., et al. (2015), 'Ribosome. The structure of the human mitochondrial ribosome', *Science*, 348 (6230), 95-98.
- Anan, Ryuichiro, et al. (1995), 'Cardiac involvement in mitochondrial diseases: a study on 17 patients with documented mitochondrial DNA defects', *Circulation*, 91 (4), 955-61.
- Anand, Ruchika, et al. (2014), 'The i-AAA protease YME1L and OMA1 cleave OPA1 to balance mitochondrial fusion and fission', *The Journal of cell biology*, 204 (6), 919-29.
- Anderson, S., et al. (1981), 'Sequence and organization of the human mitochondrial genome', *Nature*, 290 (5806), 457-65.

- Andrews, Byron, et al. (2013), 'Assembly factors for the membrane arm of human complex I', *Proceedings of the National Academy of Sciences*, 110 (47), 18934-39.
- Andrews, R. M., et al. (1999), 'Reanalysis and revision of the Cambridge reference sequence for human mitochondrial DNA', *Nat Genet*, 23 (2), 147.
- Angebault, C., et al. (2015), 'Mutation in NDUFA13/GRIM19 leads to early onset hypotonia, dyskinesia and sensorial deficiencies, and mitochondrial complex I instability', *Hum Mol Genet*, 24 (14), 3948-55.
- Angerer, H., et al. (2012), 'Tracing the tail of ubiquinone in mitochondrial complex I', *Biochim Biophys Acta*, 1817 (10), 1776-84.
- Ankel-Simons, F. and Cummins, J. M. (1996), 'Misconceptions about mitochondria and mammalian fertilization: implications for theories on human evolution', *Proc Natl Acad Sci U S A*, 93 (24), 13859-63.
- Antonicka, H., et al. (2013), 'The mitochondrial RNA-binding protein GRSF1 localizes to RNA granules and is required for posttranscriptional mitochondrial gene expression', *Cell Metab*, 17 (3), 386-98.
- Antonicka, H., et al. (2003), 'Mutations in COX10 result in a defect in mitochondrial heme A biosynthesis and account for multiple, early-onset clinical phenotypes associated with isolated COX deficiency', *Hum Mol Genet*, 12 (20), 2693-702.
- Apabhai, S., et al. (2011), 'Habitual physical activity in mitochondrial disease', *PLoS One*, 6 (7), e22294.
- Attardi, Giuseppe, Yoneda, Makoto, and Chomyn, Anne (1995), 'Complementation and segregation behavior of disease-causing mitochondrial DNA mutations in cellular model systems', *Biochimica et Biophysica Acta (BBA) - Molecular Basis of Disease*, 1271 (1), 241-48.
- Baines, H. L., et al. (2014), 'Similar patterns of clonally expanded somatic mtDNA mutations in the colon of heterozygous mtDNA mutator mice and ageing humans', *Mech Ageing Dev*, 139, 22-30.
- Baradaran, R., et al. (2013), 'Crystal structure of the entire respiratory complex I', *Nature*, 494 (7438), 443-8.
- Bates, M. G., et al. (2013), 'Defining cardiac adaptations and safety of endurance training in patients with m.3243A>G-related mitochondrial disease', *Int J Cardiol*, 168 (4), 3599-608.
- Battersby, B. J., Loredó-Ostí, J. C., and Shoubridge, E. A. (2003), 'Nuclear genetic control of mitochondrial DNA segregation', *Nat Genet*, 33 (2), 183-6.

- Bazan, S., et al. (2013), 'Cardiolipin-dependent reconstitution of respiratory supercomplexes from purified *Saccharomyces cerevisiae* complexes III and IV', *J Biol Chem*, 288 (1), 401-11.
- Belenguer, P. and Pellegrini, L. (2013), 'The dynamin GTPase OPA1: more than mitochondria?', *Biochim Biophys Acta*, 1833 (1), 176-83.
- Belevich, I., et al. (2006), 'Proton-coupled electron equilibrium in soluble and membrane-bound cytochrome c oxidase from *Paracoccus denitrificans*', *Biochemistry*, 45 (12), 4000-6.
- Bengtsson, Henrik (2017), 'matrixStats: Functions that Apply to Rows and Columns of Matrices (and to Vectors), 2018', *R package version 0.54.0*, 725.
- Benit, P., et al. (2004), 'Mutant NDUFS3 subunit of mitochondrial complex I causes Leigh syndrome', *J Med Genet*, 41 (1), 14-7.
- Benit, P., et al. (2003), 'Mutant NDUFV2 subunit of mitochondrial complex I causes early onset hypertrophic cardiomyopathy and encephalopathy', *Hum Mutat*, 21 (6), 582-6.
- Bénit, P., et al. (2001), 'Large-scale deletion and point mutations of the nuclear NDUFV1 and NDUFS1 genes in mitochondrial complex I deficiency', *American journal of human genetics*, 68 (6), 1344-52.
- Bentlage, H. A. and Attardi, G. (1996), 'Relationship of genotype to phenotype in fibroblast-derived transmitochondrial cell lines carrying the 3243 mutation associated with the MELAS encephalomyopathy: shift towards mutant genotype and role of mtDNA copy number', *Hum Mol Genet*, 5 (2), 197-205.
- Berg, Jeremy Mark (2011), *Biochemistry*, eds John L. Tymoczko and Lubert Stryer (7th ed., International ed. edn.; Basingstoke: Basingstoke : Palgrave Macmillan).
- Berger, I., et al. (2008), 'Mitochondrial complex I deficiency caused by a deleterious NDUFV1 mutation', *Ann Neurol*, 63 (3), 405-8.
- Bernier, F. P., et al. (2002), 'Diagnostic criteria for respiratory chain disorders in adults and children', *Neurology*, 59 (9), 1406-11.
- Berrisford, J. M. and Sazanov, L. A. (2009), 'Structural basis for the mechanism of respiratory complex I', *J Biol Chem*, 284 (43), 29773-83.
- Bhargava, K. and Spremulli, L. L. (2005), 'Role of the N- and C-terminal extensions on the activity of mammalian mitochondrial translational initiation factor 3', *Nucleic Acids Res*, 33 (22), 7011-8.
- Bjorkman, K., et al. (2015), 'Broad phenotypic variability in patients with complex I deficiency due to mutations in NDUFS1 and NDUFV1', *Mitochondrion*, 21, 33-40.

- Blok, M. J., et al. (2007), 'Mutations in the ND5 subunit of complex I of the mitochondrial DNA are a frequent cause of oxidative phosphorylation disease', *J Med Genet*, 44 (4), e74.
- Bogenhagen, Daniel and Clayton, David A. (1977), 'Mouse L cell mitochondrial DNA molecules are selected randomly for replication throughout the cell cycle', *Cell*, 11 (4), 719-27.
- Boggan, Róisín M., et al. (2019), 'Resolving complexity in mitochondrial disease: Towards precision medicine', *Molecular Genetics and Metabolism*.
- Borner, G. V., et al. (2000), 'Decreased aminoacylation of mutant tRNAs in MELAS but not in MERRF patients', *Hum Mol Genet*, 9 (4), 467-75.
- Bourgeron, T., et al. (1995), 'Mutation of a nuclear succinate dehydrogenase gene results in mitochondrial respiratory chain deficiency', *Nat Genet*, 11 (2), 144-9.
- Boveris, A., Oshino, N., and Chance, B. (1972), 'The cellular production of hydrogen peroxide', *Biochem J*, 128 (3), 617-30.
- Bowmaker, M., et al. (2003), 'Mammalian mitochondrial DNA replicates bidirectionally from an initiation zone', *J Biol Chem*, 278 (51), 50961-9.
- Brandt, U. (2006), 'Energy converting NADH:quinone oxidoreductase (complex I)', *Annu Rev Biochem*, 75, 69-92.
- Brown, A., et al. (2014), 'Structure of the large ribosomal subunit from human mitochondria', *Science*, 346 (6210), 718-22.
- Brown, D. T., et al. (2001), 'Random genetic drift determines the level of mutant mtDNA in human primary oocytes', *American journal of human genetics*, 68 (2), 533-36.
- Brown, W. M., George, M., Jr., and Wilson, A. C. (1979), 'Rapid evolution of animal mitochondrial DNA', *Proc Natl Acad Sci U S A*, 76 (4), 1967-71.
- Bua, E., et al. (2006), 'Mitochondrial DNA-deletion mutations accumulate intracellularly to detrimental levels in aged human skeletal muscle fibers', *Am J Hum Genet*, 79 (3), 469-80.
- Budde, S. M., et al. (2000), 'Combined enzymatic complex I and III deficiency associated with mutations in the nuclear encoded NDUFS4 gene', *Biochem Biophys Res Commun*, 275 (1), 63-8.
- Bugiani, M., et al. (2004), 'Clinical and molecular findings in children with complex I deficiency', *Biochim Biophys Acta*, 1659 (2-3), 136-47.
- Burke, R. E., et al. (1973), 'Physiological types and histochemical profiles in motor units of the cat gastrocnemius', *J Physiol*, 234 (3), 723-48.

- Calvo, S. E., Clauser, K. R., and Mootha, V. K. (2016), 'MitoCarta2.0: an updated inventory of mammalian mitochondrial proteins', *Nucleic Acids Res*, 44 (D1), D1251-7.
- Calvo, S. E., et al. (2012), 'Molecular diagnosis of infantile mitochondrial disease with targeted next-generation sequencing', *Sci Transl Med*, 4 (118), 118ra10.
- Calvo, S. E., et al. (2010), 'High-throughput, pooled sequencing identifies mutations in NUBPL and FOXRED1 in human complex I deficiency', *Nat Genet*, 42 (10), 851-8.
- Campbell, Georgia, et al. (2014), 'Dissecting the mechanisms underlying the accumulation of mitochondrial DNA deletions in human skeletal muscle', *Human molecular genetics*, 23 (17), 4612-20.
- Campos, Yolanda, et al. (1996), 'Sporadic MERRF/MELAS overlap syndrome associated with the 3243 tRNA^{Leu} (UUR) mutation of mitochondrial DNA', *Muscle & Nerve: Official Journal of the American Association of Electrodiagnostic Medicine*, 19 (2), 187-90.
- Cao, Z., et al. (2001), 'Mitochondrial DNA deletion mutations are concomitant with ragged red regions of individual, aged muscle fibers: analysis by laser-capture microdissection', *Nucleic acids research*, 29 (21), 4502-08.
- Capaldi, R. A. (1990), 'Structure and function of cytochrome c oxidase', *Annu Rev Biochem*, 59, 569-96.
- Capaldi, R. A., Marusich, M. F., and Taanman, J. W. (1995), 'Mammalian cytochrome-c oxidase: characterization of enzyme and immunological detection of subunits in tissue extracts and whole cells', *Methods Enzymol*, 260, 117-32.
- Carafoli, E. (2003), 'Historical review: mitochondria and calcium: ups and downs of an unusual relationship', *Trends Biochem Sci*, 28 (4), 175-81.
- Cardol, P., et al. (2004), 'Higher plant-like subunit composition of mitochondrial complex I from *Chlamydomonas reinhardtii*: 31 conserved components among eukaryotes', *Biochim Biophys Acta*, 1658 (3), 212-24.
- Cecchini, G. (2003), 'Function and structure of complex II of the respiratory chain', *Annu Rev Biochem*, 72, 77-109.
- Chacinska, A., et al. (2004), 'Essential role of Mia40 in import and assembly of mitochondrial intermembrane space proteins', *Embo j*, 23 (19), 3735-46.
- Chacinska, Agnieszka, et al. (2009), 'Importing mitochondrial proteins: machineries and mechanisms', *Cell*, 138 (4), 628-44.
- Chae, J. H., et al. (2007), 'A novel ND3 mitochondrial DNA mutation in three Korean children with basal ganglia lesions and complex I deficiency', *Pediatr Res*, 61 (5 Pt 1), 622-4.

- Chang, D. D. and Clayton, D. A. (1984), 'Precise identification of individual promoters for transcription of each strand of human mitochondrial DNA', *Cell*, 36 (3), 635-43.
- (1985), 'Priming of human mitochondrial DNA replication occurs at the light-strand promoter', *Proc Natl Acad Sci U S A*, 82 (2), 351-5.
- Chinnery, P. F. and Turnbull, D. M. (1997), 'Clinical features, investigation, and management of patients with defects of mitochondrial DNA', *Journal of Neurology, Neurosurgery & Psychiatry*, 63 (5), 559-63.
- Chinnery, P. F., et al. (2000), 'The spectrum of hearing loss due to mitochondrial DNA defects', *Brain*, 123 (1), 82-92.
- Chinnery, P. F., et al. (1999), 'Nonrandom tissue distribution of mutant mtDNA', *Am J Med Genet*, 85 (5), 498-501.
- Chinnery, P. F., et al. (2004), 'Risk of developing a mitochondrial DNA deletion disorder', *Lancet*, 364 (9434), 592-6.
- Chol, M., et al. (2003), 'The mitochondrial DNA G13513A MELAS mutation in the NADH dehydrogenase 5 gene is a frequent cause of Leigh-like syndrome with isolated complex I deficiency', *J Med Genet*, 40 (3), 188-91.
- Chomyn, A., et al. (2000), 'The mitochondrial myopathy, encephalopathy, lactic acidosis, and stroke-like episode syndrome-associated human mitochondrial tRNA^{Leu}(UUR) mutation causes aminoacylation deficiency and concomitant reduced association of mRNA with ribosomes', *J Biol Chem*, 275 (25), 19198-209.
- Chomyn, A., et al. (1992), 'MELAS mutation in mtDNA binding site for transcription termination factor causes defects in protein synthesis and in respiration but no change in levels of upstream and downstream mature transcripts', *Proc Natl Acad Sci U S A*, 89 (10), 4221-5.
- Ciafaloni, E., et al. (1992), 'MELAS: clinical features, biochemistry, and molecular genetics', *Ann Neurol*, 31 (4), 391-8.
- Clayton, D. A. (1982), 'Replication of animal mitochondrial DNA', *Cell*, 28 (4), 693-705.
- Cohen, J. E. and Fields, R. D. (2004), 'Extracellular calcium depletion in synaptic transmission', *Neuroscientist*, 10 (1), 12-7.
- Collet, G., et al. (2016a), 'Endothelial precursor cell-based therapy to target the pathologic angiogenesis and compensate tumor hypoxia', *Cancer Lett*, 370 (2), 345-57.
- Collet, Marie, et al. (2016b), 'High incidence and variable clinical outcome of cardiac hypertrophy due to ACAD9 mutations in childhood', *European journal of human genetics : EJHG*, 24 (8), 1112-16.

- Corona, Paola, et al. (2001), 'A novel mtDNA mutation in the ND5 subunit of complex I in two MELAS patients', *Annals of Neurology: Official Journal of the American Neurological Association and the Child Neurology Society*, 49 (1), 106-10.
- Craven, Lyndsey, et al. (2017), 'Recent Advances in Mitochondrial Disease', *Annual Review of Genomics and Human Genetics*, 18 (1), 257-75.
- Cree, L. M., et al. (2008), 'A reduction of mitochondrial DNA molecules during embryogenesis explains the rapid segregation of genotypes', *Nat Genet*, 40 (2), 249-54.
- Crimi, M., et al. (2004), 'A new mitochondrial DNA mutation in ND3 gene causing severe Leigh syndrome with early lethality', *Pediatr Res*, 55 (5), 842-6.
- D'Souza, A. R. and Minczuk, M. (2018), 'Mitochondrial transcription and translation: overview', *Essays Biochem*, 62 (3), 309-20.
- Daems, W. T. and Wisse, E. (1966), 'Shape and attachment of the cristae mitochondriales in mouse hepatic cell mitochondria', *J Ultrastruct Res*, 16 (1), 123-40.
- Damian, M. S., et al. (1995), 'Clinical spectrum of the MELAS mutation in a large pedigree', *Acta Neurol Scand*, 92 (5), 409-15.
- de Grey, A. D. (1997), 'A proposed refinement of the mitochondrial free radical theory of aging', *Bioessays*, 19 (2), 161-6.
- de Laat, P., et al. (2015), 'Obstetric complications in carriers of the m.3243A>G mutation, a retrospective cohort study on maternal and fetal outcome', *Mitochondrion*, 25, 98-103.
- de Laat, P., et al. (2012), 'Clinical features and heteroplasmy in blood, urine and saliva in 34 Dutch families carrying the m.3243A > G mutation', *J Inherit Metab Dis*, 35 (6), 1059-69.
- de Laat, Paul, et al. (2013), 'Inheritance of the m.3243A>G mutation', *JIMD reports*, 8, 47-50.
- de Laat, Paul, et al. (2016), 'Three families with 'de novo' m.3243A > G mutation', *BBA clinical*, 6, 19-24.
- De Paepe, B., et al. (2009), 'Immunohistochemical analysis of the oxidative phosphorylation complexes in skeletal muscle from patients with mitochondrial DNA encoded tRNA gene defects', *J Clin Pathol*, 62 (2), 172-6.
- De Stefani, D., et al. (2011), 'A forty-kilodalton protein of the inner membrane is the mitochondrial calcium uniporter', *Nature*, 476 (7360), 336-40.
- Delignette-Muller, Marie Laure and Dutang, Christophe (2015), 'fitdistrplus: An R package for fitting distributions', *Journal of Statistical Software*, 64 (4), 1-34.
- Denton, R. M. and McCormack, J. G. (1980), 'On the role of the calcium transport cycle in heart and other mammalian mitochondria', *FEBS Lett*, 119 (1), 1-8.

- Deschauer, Marcus, et al. (2001), 'Hearing impairment is common in various phenotypes of the mitochondrial DNA A3243G mutation', *Archives of neurology*, 58 (11), 1885-88.
- Dewulf, J. P., et al. (2016), 'Evidence of a wide spectrum of cardiac involvement due to ACAD9 mutations: Report on nine patients', *Mol Genet Metab*, 118 (3), 185-9.
- Diaz, F., et al. (2006), 'Cytochrome c oxidase is required for the assembly/stability of respiratory complex I in mouse fibroblasts', *Mol Cell Biol*, 26 (13), 4872-81.
- Diaz, F., et al. (2002), 'Human mitochondrial DNA with large deletions repopulates organelles faster than full-length genomes under relaxed copy number control', *Nucleic Acids Res*, 30 (21), 4626-33.
- Dowle, Matt and Srinivasan, Arun (2017), 'data.table: Extension of 'data.frame'. R package version 1.10.4-3'.
- Dubowitz, Victor (2007), *Muscle biopsy : a practical approach*, ed. Caroline A. Sewry (3rd ed. edn.; Edinburgh: Edinburgh : Elsevier Saunders).
- Dudek, J., Rehling, P., and van der Laan, M. (2013), 'Mitochondrial protein import: common principles and physiological networks', *Biochim Biophys Acta*, 1833 (2), 274-85.
- Dudkina, N. V., et al. (2005), 'Structure of a mitochondrial supercomplex formed by respiratory-chain complexes I and III', *Proc Natl Acad Sci U S A*, 102 (9), 3225-9.
- Dunbar, D. R., et al. (1995), 'Different cellular backgrounds confer a marked advantage to either mutant or wild-type mitochondrial genomes', *Proc Natl Acad Sci U S A*, 92 (14), 6562-6.
- Dunbar, D. R., et al. (1996), 'Complex I deficiency is associated with 3243G:C mitochondrial DNA in osteosarcoma cell hybrids', *Hum Mol Genet*, 5 (1), 123-29.
- Dunning, C. J. R., et al. (2007), 'Human CIA30 is involved in the early assembly of mitochondrial complex I and mutations in its gene cause disease', *The EMBO journal*, 26 (13), 3227-37.
- Durham, Steve E., et al. (2007), 'Normal levels of wild-type mitochondrial DNA maintain cytochrome c oxidase activity for two pathogenic mitochondrial DNA mutations but not for m.3243A-->G', *American journal of human genetics*, 81 (1), 189-95.
- Efremov, R. G., Baradaran, R., and Sazanov, L. A. (2010), 'The architecture of respiratory complex I', *Nature*, 465 (7297), 441-5.
- El-Hattab, A. W., et al. (2015), 'MELAS syndrome: Clinical manifestations, pathogenesis, and treatment options', *Mol Genet Metab*, 116 (1-2), 4-12.
- Elliott, H. R., et al. (2008), 'Pathogenic mitochondrial DNA mutations are common in the general population', *Am J Hum Genet*, 83 (2), 254-60.

- Elson, Joanna L., et al. (2007), 'Associating mitochondrial DNA variation with complex traits', *American journal of human genetics*, 80 (2), 378-83.
- Elson, Joanna L., et al. (2002), 'The length of cytochrome *c* oxidase-negative segments in muscle fibres in patients with mtDNA myopathy', *Neuromuscular Disorders*, 12 (9), 858-64.
- Endo, T. and Yamano, K. (2010), 'Transport of proteins across or into the mitochondrial outer membrane', *Biochim Biophys Acta*, 1803 (6), 706-14.
- Engel, W. K. and Cunningham, G. G. (1963), 'RAPID EXAMINATION OF MUSCLE TISSUE. AN IMPROVED TRICHOME METHOD FOR FRESH-FROZEN BIOPSY SECTIONS', *Neurology*, 13, 919-23.
- Fabrizi, G. M., et al. (1996), 'The A to G transition at nt 3243 of the mitochondrial tRNA^{Leu}(UUR) may cause an MERRF syndrome', *Journal of neurology, neurosurgery, and psychiatry*, 61 (1), 47-51.
- Falkenberg, M., Larsson, N. G., and Gustafsson, C. M. (2007), 'DNA replication and transcription in mammalian mitochondria', *Annu Rev Biochem*, 76, 679-99.
- Falkenberg, M., et al. (2002), 'Mitochondrial transcription factors B1 and B2 activate transcription of human mtDNA', *Nat Genet*, 31 (3), 289-94.
- Fassone, E. and Rahman, S. (2012), 'Complex I deficiency: clinical features, biochemistry and molecular genetics', *J Med Genet*, 49 (9), 578-90.
- Fassone, E., et al. (2011), 'Mutations in the mitochondrial complex I assembly factor NDUFAF1 cause fatal infantile hypertrophic cardiomyopathy', *J Med Genet*, 48 (10), 691-7.
- Faxen, K., et al. (2005), 'A mechanistic principle for proton pumping by cytochrome *c* oxidase', *Nature*, 437 (7056), 286-9.
- Fernandez-Moreira, D., et al. (2007), 'X-linked NDUFA1 gene mutations associated with mitochondrial encephalomyopathy', *Ann Neurol*, 61 (1), 73-83.
- Ferreira, R., et al. (2010), 'Subsarcolemmal and intermyofibrillar mitochondria proteome differences disclose functional specializations in skeletal muscle', *Proteomics*, 10 (17), 3142-54.
- Fiedorczuk, K., et al. (2016), 'Atomic structure of the entire mammalian mitochondrial complex I', *Nature*, 538 (7625), 406-10.
- Filograna, R., et al. (2019), 'Modulation of mtDNA copy number ameliorates the pathological consequences of a heteroplasmic mtDNA mutation in the mouse', *Sci Adv*, 5 (4), eaav9824.

- Fisher, N. and Rich, P. R. (2000), 'A motif for quinone binding sites in respiratory and photosynthetic systems', *J Mol Biol*, 296 (4), 1153-62.
- Fisher, R. P. and Clayton, D. A. (1988), 'Purification and characterization of human mitochondrial transcription factor 1', *Mol Cell Biol*, 8 (8), 3496-509.
- Fisher, R. P., Topper, J. N., and Clayton, D. A. (1987), 'Promoter selection in human mitochondria involves binding of a transcription factor to orientation-independent upstream regulatory elements', *Cell*, 50 (2), 247-58.
- Flierl, A., Reichmann, H., and Seibel, P. (1997), 'Pathophysiology of the MELAS 3243 transition mutation', *J Biol Chem*, 272 (43), 27189-96.
- Formosa, L. E., et al. (2018), 'Building a complex complex: Assembly of mitochondrial respiratory chain complex I', *Semin Cell Dev Biol*, 76, 154-62.
- Fornuskova, D., et al. (2008), 'The impact of mitochondrial tRNA mutations on the amount of ATP synthase differs in the brain compared to other tissues', *Biochim Biophys Acta*, 1782 (5), 317-25.
- Frederiksen, A. L., et al. (2006), 'Tissue specific distribution of the 3243A->G mtDNA mutation', *J Med Genet*, 43 (8), 671-7.
- Frey, T. G. and Mannella, C. A. (2000), 'The internal structure of mitochondria', *Trends Biochem Sci*, 25 (7), 319-24.
- Friedman, J. R., et al. (2011), 'ER tubules mark sites of mitochondrial division', *Science*, 334 (6054), 358-62.
- Friedrich, T. and Bottcher, B. (2004), 'The gross structure of the respiratory complex I: a Lego System', *Biochim Biophys Acta*, 1608 (1), 1-9.
- Fukui, H. and Moraes, C. T. (2009), 'Mechanisms of formation and accumulation of mitochondrial DNA deletions in aging neurons', *Hum Mol Genet*, 18 (6), 1028-36.
- Fuste, J. M., et al. (2010), 'Mitochondrial RNA polymerase is needed for activation of the origin of light-strand DNA replication', *Mol Cell*, 37 (1), 67-78.
- Galati, Domenico, et al. (2009), 'Role of nuclear-encoded subunit Vb in the assembly and stability of cytochrome c oxidase complex: implications in mitochondrial dysfunction and ROS production', *The Biochemical journal*, 420 (3), 439-49.
- Galkin, A., Drose, S., and Brandt, U. (2006), 'The proton pumping stoichiometry of purified mitochondrial complex I reconstituted into proteoliposomes', *Biochim Biophys Acta*, 1757 (12), 1575-81.
- Gaspari, M., et al. (2004), 'The mitochondrial RNA polymerase contributes critically to promoter specificity in mammalian cells', *Embo j*, 23 (23), 4606-14.

- Gehrig, Saskia Maria, et al. (2016), 'Altered skeletal muscle (mitochondrial) properties in patients with mitochondrial DNA single deletion myopathy', *Orphanet journal of rare diseases*, 11 (1), 105-05.
- Gerbitz, Klaus-Dieter, et al. (1995), 'Mitochondrial diabetes mellitus: a review', *Biochimica et Biophysica Acta (BBA)-Molecular Basis of Disease*, 1271 (1), 253-60.
- Ghezzi, D. and Zeviani, M. (2018), 'Human diseases associated with defects in assembly of OXPHOS complexes', *Essays Biochem*, 62 (3), 271-86.
- Ghezzi, D., et al. (2009), 'SDHAF1, encoding a LYR complex-II specific assembly factor, is mutated in SDH-defective infantile leukoencephalopathy', *Nat Genet*, 41 (6), 654-6.
- Giachin, G., et al. (2016), 'Dynamics of Human Mitochondrial Complex I Assembly: Implications for Neurodegenerative Diseases', *Front Mol Biosci*, 3, 43.
- Giesen, C., et al. (2014), 'Highly multiplexed imaging of tumor tissues with subcellular resolution by mass cytometry', *Nat Methods*, 11 (4), 417-22.
- Giles, R. E., et al. (1980), 'Maternal inheritance of human mitochondrial DNA', *Proc Natl Acad Sci U S A*, 77 (11), 6715-9.
- Gilkerson, R. W., Selker, J. M., and Capaldi, R. A. (2003), 'The cristal membrane of mitochondria is the principal site of oxidative phosphorylation', *FEBS Lett*, 546 (2-3), 355-8.
- Gillies, A. R. and Lieber, R. L. (2011), 'Structure and function of the skeletal muscle extracellular matrix', *Muscle Nerve*, 44 (3), 318-31.
- Gorman, G. S., et al. (2016), 'Mitochondrial diseases', *Nat Rev Dis Primers*, 2, 16080.
- Gorman, G. S., et al. (2015a), 'Prevalence of nuclear and mitochondrial DNA mutations related to adult mitochondrial disease', *Ann Neurol*, 77 (5), 753-9.
- Gorman, Grainne S., et al. (2015b), 'Novel MTND1 mutations cause isolated exercise intolerance, complex I deficiency and increased assembly factor expression', *Clinical science (London, England : 1979)*, 128 (12), 895-904.
- Goto, Y., Nonaka, I., and Horai, S. (1990), 'A mutation in the tRNA(Leu)(UUR) gene associated with the MELAS subgroup of mitochondrial encephalomyopathies', *Nature*, 348 (6302), 651-3.
- Goto, Y., et al. (1992), 'Mitochondrial myopathy, encephalopathy, lactic acidosis, and stroke-like episodes (MELAS): a correlative study of the clinical features and mitochondrial DNA mutation', *Neurology*, 42 (3 Pt 1), 545-50.
- Grady, J. P., et al. (2014), 'Disease progression in patients with single, large-scale mitochondrial DNA deletions', *Brain*, 137 (Pt 2), 323-34.

- Grady, J. P., et al. (2018), 'mtDNA heteroplasmy level and copy number indicate disease burden in m.3243A>G mitochondrial disease', *EMBO Mol Med*, 10 (6).
- Gray, H. and Wong, T. W. (1992), 'Purification and identification of subunit structure of the human mitochondrial DNA polymerase', *J Biol Chem*, 267 (9), 5835-41.
- Gray, M. W., Burger, G., and Lang, B. F. (1999), 'Mitochondrial evolution', *Science*, 283 (5407), 1476-81.
- Greaves, L. C., et al. (2010), 'Mitochondrial DNA defects and selective extraocular muscle involvement in CPEO', *Invest Ophthalmol Vis Sci*, 51 (7), 3340-6.
- Greaves, Laura C., et al. (2014), 'Clonal expansion of early to mid-life mitochondrial DNA point mutations drives mitochondrial dysfunction during human ageing', *PLoS genetics*, 10 (9), e1004620-e20.
- Greber, B. J., et al. (2014), 'Architecture of the large subunit of the mammalian mitochondrial ribosome', *Nature*, 505 (7484), 515-9.
- Greggio, C., et al. (2017), 'Enhanced Respiratory Chain Supercomplex Formation in Response to Exercise in Human Skeletal Muscle', *Cell Metab*, 25 (2), 301-11.
- Griffiths, E. J. and Rutter, G. A. (2009), 'Mitochondrial calcium as a key regulator of mitochondrial ATP production in mammalian cells', *Biochim Biophys Acta*, 1787 (11), 1324-33.
- Grigorieff, N. (1998), 'Three-dimensional structure of bovine NADH:ubiquinone oxidoreductase (complex I) at 2.2 Å in ice', *J Mol Biol*, 277 (5), 1033-46.
- Gu, J., et al. (2016), 'The architecture of the mammalian respirasome', *Nature*, 537 (7622), 639-43.
- Guarani, V., et al. (2015), 'QIL1 is a novel mitochondrial protein required for MICOS complex stability and cristae morphology', *Elife*, 4.
- Guerrero-Castillo, S., et al. (2017), 'The Assembly Pathway of Mitochondrial Respiratory Chain Complex I', *Cell Metab*, 25 (1), 128-39.
- Gustafsson, C. M., Falkenberg, M., and Larsson, N. G. (2016), 'Maintenance and Expression of Mammalian Mitochondrial DNA', *Annu Rev Biochem*, 85, 133-60.
- Gyllensten, U., et al. (1991), 'Paternal inheritance of mitochondrial DNA in mice', *Nature*, 352 (6332), 255-7.
- Haack, T. B., et al. (2010), 'Exome sequencing identifies ACAD9 mutations as a cause of complex I deficiency', *Nat Genet*, 42 (12), 1131-4.
- Haack, T. B., et al. (2012), 'Mutation screening of 75 candidate genes in 152 complex I deficiency cases identifies pathogenic variants in 16 genes including NDUFB9', *J Med Genet*, 49 (2), 83-9.

- Hallberg, B. M. and Larsson, N. G. (2011), 'TFAM forces mtDNA to make a U-turn', *Nat Struct Mol Biol*, 18 (11), 1179-81.
- (2014), 'Making proteins in the powerhouse', *Cell Metab*, 20 (2), 226-40.
- Hammans, SR, et al. (1995), 'The mitochondrial DNA transfer RNA Leu (UUR) A→G (3243) mutation: A clinical and genetic study', *Brain*, 118 (3), 721-34.
- Hanada, T., et al. (2001), 'Translation ability of mitochondrial tRNAs^{Ser} with unusual secondary structures in an in vitro translation system of bovine mitochondria', *Genes Cells*, 6 (12), 1019-30.
- Hanna, M. G., et al. (1998), 'MELAS: a new disease associated mitochondrial DNA mutation and evidence for further genetic heterogeneity', *J Neurol Neurosurg Psychiatry*, 65 (4), 512-7.
- Hao, H. X., et al. (2009), 'SDH5, a gene required for flavination of succinate dehydrogenase, is mutated in paraganglioma', *Science*, 325 (5944), 1139-42.
- Haque, M. E. and Spremulli, L. L. (2008), 'Roles of the N- and C-terminal domains of mammalian mitochondrial initiation factor 3 in protein biosynthesis', *J Mol Biol*, 384 (4), 929-40.
- Harel, T., et al. (2016), 'Recurrent De Novo and Biallelic Variation of ATAD3A, Encoding a Mitochondrial Membrane Protein, Results in Distinct Neurological Syndromes', *Am J Hum Genet*, 99 (4), 831-45.
- Hartmannova, H., et al. (2016), 'Acadian variant of Fanconi syndrome is caused by mitochondrial respiratory chain complex I deficiency due to a non-coding mutation in complex I assembly factor NDUFAF6', *Hum Mol Genet*, 25 (18), 4062-79.
- Hatefi, Youssef (1985), 'THE MITOCHONDRIAL ELECTRON TRANSPORT AND OXIDATIVE PHOSPHORYLATION SYSTEM', *Annual Review of Biochemistry*, 54 (1), 1015-69.
- Hawltitschek, G., et al. (1988), 'Mitochondrial protein import: identification of processing peptidase and of PEP, a processing enhancing protein', *Cell*, 53 (5), 795-806.
- Hayashi, J., et al. (1991), 'Introduction of disease-related mitochondrial DNA deletions into HeLa cells lacking mitochondrial DNA results in mitochondrial dysfunction', *Proceedings of the National Academy of Sciences of the United States of America*, 88 (23), 10614-18.
- Heide, H., et al. (2012), 'Complexome profiling identifies TMEM126B as a component of the mitochondrial complex I assembly complex', *Cell Metab*, 16 (4), 538-49.

- Herrmann, J. M., Woellhaf, M. W., and Bonnefoy, N. (2013), 'Control of protein synthesis in yeast mitochondria: the concept of translational activators', *Biochim Biophys Acta*, 1833 (2), 286-94.
- Hess, J. F., et al. (1991), 'Impairment of mitochondrial transcription termination by a point mutation associated with the MELAS subgroup of mitochondrial encephalomyopathies', *Nature*, 351 (6323), 236-9.
- Hirano, M., et al. (1992), 'Melas: an original case and clinical criteria for diagnosis', *Neuromuscul Disord*, 2 (2), 125-35.
- Hirst, J. (2013), 'Mitochondrial complex I', *Annu Rev Biochem*, 82, 551-75.
- Hirst, J. and Roessler, M. M. (2016), 'Energy conversion, redox catalysis and generation of reactive oxygen species by respiratory complex I', *Biochim Biophys Acta*, 1857 (7), 872-83.
- Hoefs, S. J., et al. (2008), 'NDUFA2 complex I mutation leads to Leigh disease', *Am J Hum Genet*, 82 (6), 1306-15.
- Hoefs, Saskia J. G., et al. (2011), 'NDUFA10 mutations cause complex I deficiency in a patient with Leigh disease', *European journal of human genetics : EJHG*, 19 (3), 270-74.
- Hollingsworth, K. G., et al. (2012), 'Cardiomyopathy is common in patients with the mitochondrial DNA m.3243A>G mutation and correlates with mutation load', *Neuromuscul Disord*, 22 (7), 592-6.
- Holt, I. J. and Reyes, A. (2012), 'Human mitochondrial DNA replication', *Cold Spring Harb Perspect Biol*, 4 (12).
- Holt, I. J., Harding, A. E., and Morgan-Hughes, J. A. (1988), 'Deletions of muscle mitochondrial DNA in patients with mitochondrial myopathies', *Nature*, 331 (6158), 717-9.
- Holt, I. J., Lorimer, H. E., and Jacobs, H. T. (2000), 'Coupled leading- and lagging-strand synthesis of mammalian mitochondrial DNA', *Cell*, 100 (5), 515-24.
- Hopkins, Philip M. (2006), 'Skeletal muscle physiology', *Continuing Education in Anaesthesia, Critical Care and Pain*, 6 (1), 1-6.
- Hoppeler, H. (1986), 'Exercise-induced ultrastructural changes in skeletal muscle', *Int J Sports Med*, 7 (4), 187-204.
- Horvath, R., et al. (2006), 'Coenzyme Q10 deficiency and isolated myopathy', *Neurology*, 66 (2), 253-5.

- Howell, N., et al. (1991), 'Leber hereditary optic neuropathy: identification of the same mitochondrial ND1 mutation in six pedigrees', *American journal of human genetics*, 49 (5), 939-50.
- Howell, Neil, et al. (2003), 'The pedigree rate of sequence divergence in the human mitochondrial genome: there is a difference between phylogenetic and pedigree rates', *American journal of human genetics*, 72 (3), 659-70.
- Hudson, Gavin, et al. (2005), 'Identification of an X-chromosomal locus and haplotype modulating the phenotype of a mitochondrial DNA disorder', *American journal of human genetics*, 77 (6), 1086-91.
- Hunte, C., Zickermann, V., and Brandt, U. (2010), 'Functional modules and structural basis of conformational coupling in mitochondrial complex I', *Science*, 329 (5990), 448-51.
- Iwasaki, N., et al. (2001), 'Prevalence of A-to-G mutation at nucleotide 3243 of the mitochondrial tRNA(Leu(UUR)) gene in Japanese patients with diabetes mellitus and end stage renal disease', *J Hum Genet*, 46 (6), 330-4.
- Iwata, S., et al. (1998), 'Complete structure of the 11-subunit bovine mitochondrial cytochrome bc₁ complex', *Science*, 281 (5373), 64-71.
- Jacobs, L. J., et al. (2006), 'The transmission of OXPHOS disease and methods to prevent this', *Hum Reprod Update*, 12 (2), 119-36.
- Janssen, A. J., et al. (2007a), 'Spectrophotometric assay for complex I of the respiratory chain in tissue samples and cultured fibroblasts', *Clin Chem*, 53 (4), 729-34.
- Janssen, G. M., Maassen, J. A., and van Den Ouweland, J. M. (1999), 'The diabetes-associated 3243 mutation in the mitochondrial tRNA(Leu(UUR)) gene causes severe mitochondrial dysfunction without a strong decrease in protein synthesis rate', *J Biol Chem*, 274 (42), 29744-8.
- Janssen, G. M., et al. (2007b), 'The A3243G tRNA^{Leu}(UUR) mutation induces mitochondrial dysfunction and variable disease expression without dominant negative acting translational defects in complex IV subunits at UUR codons', *Hum Mol Genet*, 16 (20), 2472-81.
- Jensen, P. K. (1966), 'Antimycin-insensitive oxidation of succinate and reduced nicotinamide-adenine dinucleotide in electron-transport particles. I. pH dependency and hydrogen peroxide formation', *Biochim Biophys Acta*, 122 (2), 157-66.
- Jenuth, J. P., et al. (1996), 'Random genetic drift in the female germline explains the rapid segregation of mammalian mitochondrial DNA', *Nat Genet*, 14 (2), 146-51.
- Jeppesen, T. D., et al. (2006), 'Muscle phenotype and mutation load in 51 persons with the 3243A>G mitochondrial DNA mutation', *Arch Neurol*, 63 (12), 1701-6.

- Jeppesen, Tina Dysgaard, et al. (2017), 'Mitochondrial DNA mutation load in a family with the m.8344A>G point mutation and lipomas: a case study', *Clinical case reports*, 5 (12), 2034-39.
- Johns, Donald R., Neufeld, Michael J., and Park, Raymond D. (1992), 'An ND-6 mitochondrial DNA mutation associated with leber hereditary optic neuropathy', *Biochemical and Biophysical Research Communications*, 187 (3), 1551-57.
- Jokinen, R., et al. (2010), 'Gimap3 regulates tissue-specific mitochondrial DNA segregation', *PLoS Genet*, 6 (10), e1001161.
- Jourdain, Alexis A., et al. (2013), 'GRSF1 regulates RNA processing in mitochondrial RNA granules', *Cell metabolism*, 17 (3), 399-410.
- Jun, A. S., Brown, M. D., and Wallace, D. C. (1994), 'A mitochondrial DNA mutation at nucleotide pair 14459 of the NADH dehydrogenase subunit 6 gene associated with maternally inherited Leber hereditary optic neuropathy and dystonia', *Proc Natl Acad Sci U S A*, 91 (13), 6206-10.
- Kadowaki, T., et al. (1994), 'A subtype of diabetes mellitus associated with a mutation of mitochondrial DNA', *N Engl J Med*, 330 (14), 962-8.
- Kamble, S. M., et al. (2017), 'In silico Evidence for Binding of Pentacyclic Triterpenoids to Keap1-Nrf2 Protein-Protein Binding Site', *Comb Chem High Throughput Screen*, 20 (3), 215-34.
- Kandel, J., et al. (2017), 'Mitochondrial DNA 3243A>G heteroplasmy is associated with changes in cytoskeletal protein expression and cell mechanics', *J R Soc Interface*, 14 (131).
- Kärppä, Mikko, et al. (2018), 'Mutation m.15923A>G in the MT-TT gene causes mild myopathy - case report of an adult-onset phenotype', *BMC neurology*, 18 (1), 149-49.
- Kärppä, Mikko, et al. (2005), 'Spectrum of myopathic findings in 50 patients with the 3243A>G mutation in mitochondrial DNA', *Brain*, 128 (8), 1861-69.
- Kaufmann, P., et al. (2011), 'Natural history of MELAS associated with mitochondrial DNA m.3243A>G genotype', *Neurology*, 77 (22), 1965-71.
- Kaukonen, J., et al. (2000), 'Role of adenine nucleotide translocator 1 in mtDNA maintenance', *Science*, 289 (5480), 782-5.
- Kaushal, P. S., et al. (2014), 'Cryo-EM structure of the small subunit of the mammalian mitochondrial ribosome', *Proc Natl Acad Sci U S A*, 111 (20), 7284-9.
- Kellems, R. E., Allison, V. F., and Butow, R. A. (1975), 'Cytoplasmic type 80S ribosomes associated with yeast mitochondria. IV. Attachment of ribosomes to the outer membrane of isolated mitochondria', *J Cell Biol*, 65 (1), 1-14.

- Kelly, D. P. and Scarpulla, R. C. (2004), 'Transcriptional regulatory circuits controlling mitochondrial biogenesis and function', *Genes Dev*, 18 (4), 357-68.
- Kerr, J. F., Wyllie, A. H., and Currie, A. R. (1972), 'Apoptosis: a basic biological phenomenon with wide-ranging implications in tissue kinetics', *Br J Cancer*, 26 (4), 239-57.
- King, M. P., et al. (1992), 'Defects in mitochondrial protein synthesis and respiratory chain activity segregate with the tRNA(Leu(UUR)) mutation associated with mitochondrial myopathy, encephalopathy, lactic acidosis, and strokelike episodes', *Mol Cell Biol*, 12 (2), 480-90.
- Kirby, D. M., et al. (2003), 'Low mutant load of mitochondrial DNA G13513A mutation can cause Leigh's disease', *Ann Neurol*, 54 (4), 473-8.
- Kirby, D. M., et al. (2004a), 'Mutations of the mitochondrial ND1 gene as a cause of MELAS', *J Med Genet*, 41 (10), 784-9.
- Kirby, D. M., et al. (2004b), 'NDUFS6 mutations are a novel cause of lethal neonatal mitochondrial complex I deficiency', *J Clin Invest*, 114 (6), 837-45.
- Kirino, Yohei, et al. (2005), 'Specific correlation between the wobble modification deficiency in mutant tRNAs and the clinical features of a human mitochondrial disease', *Proceedings of the National Academy of Sciences of the United States of America*, 102 (20), 7127-32.
- Kirino, Yohei, et al. (2004), 'Codon-specific translational defect caused by a wobble modification deficiency in mutant tRNA from a human mitochondrial disease', *Proceedings of the National Academy of Sciences of the United States of America*, 101 (42), 15070-75.
- Kirkwood, S. P., Munn, E. A., and Brooks, G. A. (1986), 'Mitochondrial reticulum in limb skeletal muscle', *Am J Physiol*, 251 (3 Pt 1), C395-402.
- Kobayashi, Y., et al. (1990), 'A point mutation in the mitochondrial tRNA(Leu)(UUR) gene in MELAS (mitochondrial myopathy, encephalopathy, lactic acidosis and stroke-like episodes)', *Biochem Biophys Res Commun*, 173 (3), 816-22.
- Koc, E. C. and Spremulli, L. L. (2002), 'Identification of mammalian mitochondrial translational initiation factor 3 and examination of its role in initiation complex formation with natural mRNAs', *J Biol Chem*, 277 (38), 35541-9.
- Koene, S., et al. (2012), 'Natural disease course and genotype-phenotype correlations in Complex I deficiency caused by nuclear gene defects: what we learned from 130 cases', *Journal of inherited metabolic disease*, 35 (5), 737-47.

- Koenig, M. K. (2008), 'Presentation and diagnosis of mitochondrial disorders in children', *Pediatr Neurol*, 38 (5), 305-13.
- Koga, Y., et al. (1993), 'Fine mapping of mitochondrial RNAs derived from the mtDNA region containing a point mutation associated with MELAS', *Nucleic Acids Res*, 21 (3), 657-62.
- Koga, Y., et al. (2000), 'Heterogeneous presentation in A3243G mutation in the mitochondrial tRNA(Leu(UUR)) gene', *Archives of disease in childhood*, 82 (5), 407-11.
- Korhonen, Jenny A., et al. (2004), 'Reconstitution of a minimal mtDNA replisome in vitro', *The EMBO journal*, 23 (12), 2423-29.
- Korner, C., et al. (2012), 'The C-terminal domain of Fcjl is required for formation of crista junctions and interacts with the TOB/SAM complex in mitochondria', *Mol Biol Cell*, 23 (11), 2143-55.
- Korr, H., et al. (1998), 'Mitochondrial DNA synthesis studied autoradiographically in various cell types in vivo', *Braz J Med Biol Res*, 31 (2), 289-98.
- Krebs, H. A. and Johnson, W. A. (1937), 'The role of citric acid in intermediate metabolism in animal tissues', *Enzymologia*, 4, 148-56.
- Kremer, L. S., et al. (2017), 'Genetic diagnosis of Mendelian disorders via RNA sequencing', *Nat Commun*, 8, 15824.
- Krishnan, K. J., et al. (2008), 'What causes mitochondrial DNA deletions in human cells?', *Nat Genet*, 40 (3), 275-9.
- Kruse, B., Narasimhan, N., and Attardi, G. (1989), 'Termination of transcription in human mitochondria: identification and purification of a DNA binding protein factor that promotes termination', *Cell*, 58 (2), 391-7.
- Kuhl, I., et al. (2016), 'POLRMT regulates the switch between replication primer formation and gene expression of mammalian mtDNA', *Sci Adv*, 2 (8), e1600963.
- Kunkel, T. A. and Loeb, L. A. (1981), 'Fidelity of mammalian DNA polymerases', *Science*, 213 (4509), 765.
- Lake, N. J., et al. (2016), 'Leigh syndrome: One disorder, more than 75 monogenic causes', *Ann Neurol*, 79 (2), 190-203.
- Larsson, Nils-Göran, et al. (1997), 'Down-Regulation of Mitochondrial Transcription Factor a During Spermatogenesis in Humans', *Human Molecular Genetics*, 6 (2), 185-191.
- Lazarou, M., et al. (2009), 'Assembly of mitochondrial complex I and defects in disease', *Biochim Biophys Acta*, 1793 (1), 78-88.

- Lazarou, Michael, et al. (2007), 'Analysis of the assembly profiles for mitochondrial- and nuclear-DNA-encoded subunits into complex I', *Molecular and cellular biology*, 27 (12), 4228-37.
- Lebon, S., et al. (2003), 'Recurrent de novo mitochondrial DNA mutations in respiratory chain deficiency', *J Med Genet*, 40 (12), 896-9.
- Lee, G. Y., et al. (1995), 'Identification of the ubiquinone-binding domain in QP1 of succinate-ubiquinone reductase', *J Biol Chem*, 270 (11), 6193-8.
- Lehtinen, S. K., et al. (2000), 'Genotypic stability, segregation and selection in heteroplasmic human cell lines containing np 3243 mutant mtDNA', *Genetics*, 154 (1), 363-80.
- Leman, Géraldine, et al. (2015), 'Assembly defects induce oxidative stress in inherited mitochondrial complex I deficiency', *The international journal of biochemistry & cell biology*, 65, 91-103.
- Letts, J. A., Fiedorczuk, K., and Sazanov, L. A. (2016), 'The architecture of respiratory supercomplexes', *Nature*, 537 (7622), 644-48.
- Lieber, Daniel S., et al. (2013), 'Targeted exome sequencing of suspected mitochondrial disorders', *Neurology*, 80 (19), 1762-70.
- Lieber, Richard L. (2010), *Skeletal muscle structure, function, and plasticity : the physiological basis of rehabilitation* (3rd ed.. edn.; Philadelphia, Pa. London: Philadelphia, Pa.
- London : Wlters Kluwer/Lippincott Williams & Wilkins).
- Lightowers, R. N., Rozanska, A., and Chrzanowska-Lightowers, Z. M. (2014), 'Mitochondrial protein synthesis: figuring the fundamentals, complexities and complications, of mammalian mitochondrial translation', *FEBS Lett*, 588 (15), 2496-503.
- Lightowers, R. N., et al. (1997), 'Mammalian mitochondrial genetics: heredity, heteroplasmy and disease', *Trends Genet*, 13 (11), 450-5.
- Lill, R., et al. (2012), 'The role of mitochondria in cellular iron-sulfur protein biogenesis and iron metabolism', *Biochim Biophys Acta*, 1823 (9), 1491-508.
- Ling, M., et al. (1997), 'The human mitochondrial elongation factor tu (EF-Tu) gene: cDNA sequence, genomic localization, genomic structure, and identification of a pseudogene', *Gene*, 197 (1-2), 325-36.
- Liu, X., et al. (1996), 'Induction of apoptotic program in cell-free extracts: requirement for dATP and cytochrome c', *Cell*, 86 (1), 147-57.

- Llopis, J., et al. (1998), 'Measurement of cytosolic, mitochondrial, and Golgi pH in single living cells with green fluorescent proteins', *Proc Natl Acad Sci U S A*, 95 (12), 6803-8.
- Loeffen, J., et al. (2001), 'Mutations in the complex I NDUFS2 gene of patients with cardiomyopathy and encephalomyopathy', *Ann Neurol*, 49 (2), 195-201.
- Loeffen, J. L., et al. (2000), 'Isolated complex I deficiency in children: clinical, biochemical and genetic aspects', *Hum Mutat*, 15 (2), 123-34.
- Loeffen, Jan, et al. (1998), 'The First Nuclear-Encoded Complex I Mutation in a Patient with Leigh Syndrome', *The American Journal of Human Genetics*, 63 (6), 1598-608.
- Lopez-Lluch, G., et al. (2008), 'Mitochondrial biogenesis and healthy aging', *Exp Gerontol*, 43 (9), 813-9.
- Lorenz, C., et al. (2017), 'Human iPSC-Derived Neural Progenitors Are an Effective Drug Discovery Model for Neurological mtDNA Disorders', *Cell Stem Cell*, 20 (5), 659-74.e9.
- Loschen, G., Flohe, L., and Chance, B. (1971), 'Respiratory chain linked H₂O₂ production in pigeon heart mitochondria', *FEBS Lett*, 18 (2), 261-64.
- Loson, O. C., et al. (2013), 'Fis1, Mff, MiD49, and MiD51 mediate Drp1 recruitment in mitochondrial fission', *Mol Biol Cell*, 24 (5), 659-67.
- Lucas, Antoine, et al. (2019), 'Package 'gmp''.
- Luo, S., et al. (2018), 'Biparental Inheritance of Mitochondrial DNA in Humans', *Proc Natl Acad Sci U S A*, 115 (51), 13039-44.
- Ma, J., et al. (1995), 'Cloning and sequence analysis of the cDNA for bovine mitochondrial translational initiation factor 2', *Biochim Biophys Acta*, 1261 (2), 321-4.
- Ma, L. and Spremulli, L. L. (1995), 'Cloning and sequence analysis of the human mitochondrial translational initiation factor 2 cDNA', *J Biol Chem*, 270 (4), 1859-65.
- MacIntosh, Brian R. (2003), 'Role of Calcium Sensitivity Modulation in Skeletal Muscle Performance', *Physiology*, 18 (6), 222-25.
- Mackey, D. and Howell, N. (1992), 'A variant of Leber hereditary optic neuropathy characterized by recovery of vision and by an unusual mitochondrial genetic etiology', *American journal of human genetics*, 51 (6), 1218-28.
- Macmillan, C., Lach, B., and Shoubridge, E. A. (1993), 'Variable distribution of mutant mitochondrial DNAs (tRNA(Leu[3243])) in tissues of symptomatic relatives with MELAS: the role of mitotic segregation', *Neurology*, 43 (8), 1586-90.
- Maeda, K., et al. (2016), 'Clinical Phenotype and Segregation of Mitochondrial 3243A>G Mutation in 2 Pairs of Monozygotic Twins', *JAMA Neurol*, 73 (8), 990-3.

- Mai, N., Chrzanowska-Lightowlers, Z. M., and Lightowlers, R. N. (2017), 'The process of mammalian mitochondrial protein synthesis', *Cell Tissue Res*, 367 (1), 5-20.
- Majamaa-Voltti, Kirsi, et al. (2002a), 'Cardiac abnormalities in patients with mitochondrial DNA mutation 3243A>G', *BMC cardiovascular disorders*, 2, 12-12.
- (2002b), 'Cardiac abnormalities in patients with mitochondrial DNA mutation 3243A>G', *BMC Cardiovascular Disorders*, 2 (1), 12.
- Majamaa, K., et al. (1998), 'Epidemiology of A3243G, the mutation for mitochondrial encephalomyopathy, lactic acidosis, and strokelike episodes: prevalence of the mutation in an adult population', *American journal of human genetics*, 63 (2), 447-54.
- Mancuso, M., et al. (2014), 'The m.3243A>G mitochondrial DNA mutation and related phenotypes. A matter of gender?', *J Neurol*, 261 (3), 504-10.
- Mancuso, M., et al. (2015), 'Redefining phenotypes associated with mitochondrial DNA single deletion', *J Neurol*, 262 (5), 1301-9.
- Mannella, C. A., Marko, M., and Buttle, K. (1997), 'Reconsidering mitochondrial structure: new views of an old organelle', *Trends Biochem Sci*, 22 (2), 37-8.
- Manwaring, N., et al. (2007), 'Population prevalence of the MELAS A3243G mutation', *Mitochondrion*, 7 (3), 230-3.
- Maranzana, E., et al. (2013), 'Mitochondrial respiratory supercomplex association limits production of reactive oxygen species from complex I', *Antioxid Redox Signal*, 19 (13), 1469-80.
- Margulis, L. (1971), 'Symbiosis and evolution', *Sci Am*, 225 (2), 48-57.
- Mariotti, C., et al. (1994), 'Defective respiratory capacity and mitochondrial protein synthesis in transformant cybrids harboring the tRNA(Leu(UUR)) mutation associated with maternally inherited myopathy and cardiomyopathy', *J Clin Invest*, 93 (3), 1102-7.
- Mariotti, C., et al. (1995), 'Genotype to phenotype correlations in mitochondrial encephalomyopathies associated with the A3243G mutation of mitochondrial DNA', *J Neurol*, 242 (5), 304-12.
- Martin, W. and Muller, M. (1998), 'The hydrogen hypothesis for the first eukaryote', *Nature*, 392 (6671), 37-41.
- Mattson, M. P. and Chan, S. L. (2003), 'Neuronal and glial calcium signaling in Alzheimer's disease', *Cell Calcium*, 34 (4-5), 385-97.
- McFarland, R., et al. (2004), 'De novo mutations in the mitochondrial ND3 gene as a cause of infantile mitochondrial encephalopathy and complex I deficiency', *Ann Neurol*, 55 (1), 58-64.

- McKenzie, M. and Ryan, M. T. (2010), 'Assembly factors of human mitochondrial complex I and their defects in disease', *IUBMB Life*, 62 (7), 497-502.
- McNeil, M. B. and Fineran, P. C. (2013), 'Prokaryotic assembly factors for the attachment of flavin to complex II', *Biochim Biophys Acta*, 1827 (5), 637-47.
- Mears, J. A., et al. (2011), 'Conformational changes in Dnm1 support a contractile mechanism for mitochondrial fission', *Nat Struct Mol Biol*, 18 (1), 20-6.
- Meeusen, S., McCaffery, J. M., and Nunnari, J. (2004), 'Mitochondrial fusion intermediates revealed in vitro', *Science*, 305 (5691), 1747-52.
- Meeusen, S., et al. (2006), 'Mitochondrial inner-membrane fusion and crista maintenance requires the dynamin-related GTPase Mgm1', *Cell*, 127 (2), 383-95.
- Milenkovic, Dusanka, et al. (2013), 'TWINKLE is an essential mitochondrial helicase required for synthesis of nascent D-loop strands and complete mtDNA replication', *Human Molecular Genetics*, 22 (10), 1983-93.
- Miller, F. J., et al. (2003), 'Precise determination of mitochondrial DNA copy number in human skeletal and cardiac muscle by a PCR-based assay: lack of change of copy number with age', *Nucleic Acids Res*, 31 (11), e61.
- Mimaki, M., et al. (2009), 'Different effects of novel mtDNA G3242A and G3244A base changes adjacent to a common A3243G mutation in patients with mitochondrial disorders', *Mitochondrion*, 9 (2), 115-22.
- Mishra, P., et al. (2014), 'Proteolytic cleavage of Opa1 stimulates mitochondrial inner membrane fusion and couples fusion to oxidative phosphorylation', *Cell Metab*, 19 (4), 630-41.
- Mishra, Prashant and Chan, David C. (2014), 'Mitochondrial dynamics and inheritance during cell division, development and disease', *Nature reviews. Molecular cell biology*, 15 (10), 634-46.
- Mitchell, P. (1961), 'Coupling of phosphorylation to electron and hydrogen transfer by a chemi-osmotic type of mechanism', *Nature*, 191, 144-8.
- (1975), 'The protonmotive Q cycle: a general formulation', *FEBS Lett*, 59 (2), 137-9.
- (1976), 'Possible molecular mechanisms of the protonmotive function of cytochrome systems', *J Theor Biol*, 62 (2), 327-67.
- Miyabayashi, S., et al. (1992), 'Defects of mitochondrial respiratory enzymes in cloned cells from MELAS fibroblasts', *J Inherit Metab Dis*, 15 (5), 797-802.
- Montoya, J., et al. (1982), 'Identification of initiation sites for heavy-strand and light-strand transcription in human mitochondrial DNA', *Proceedings of the National Academy of Sciences*, 79 (23), 7195.

- Moraes, C. T., et al. (1992), 'The mitochondrial tRNA(Leu(UUR)) mutation in mitochondrial encephalomyopathy, lactic acidosis, and strokelike episodes (MELAS): genetic, biochemical, and morphological correlations in skeletal muscle', *Am J Hum Genet*, 50 (5), 934-49.
- Moraes, C. T., et al. (1993a), 'Atypical clinical presentations associated with the MELAS mutation at position 3243 of human mitochondrial DNA', *Neuromuscul Disord*, 3 (1), 43-50.
- Moraes, Carlos T, et al. (1993b), 'Atypical clinical presentations associated with the MELAS mutation at position 3243 of human mitochondrial DNA', *Neuromuscular Disorders*, 3 (1), 43-50.
- Moreno-Lastres, D., et al. (2012), 'Mitochondrial complex I plays an essential role in human respirasome assembly', *Cell Metab*, 15 (3), 324-35.
- Morgan-Hughes, J. A., et al. (1995), 'Mitochondrial DNA (mtDNA) diseases: correlation of genotype to phenotype', *Biochim Biophys Acta*, 1271 (1), 135-40.
- Mossmann, D., Meisinger, C., and Vogtle, F. N. (2012), 'Processing of mitochondrial presequences', *Biochim Biophys Acta*, 1819 (9-10), 1098-106.
- Muller-Hocker, J., et al. (1992), 'Progressive loss of cytochrome c oxidase in the human extraocular muscles in ageing--a cytochemical-immunohistochemical study', *Mutat Res*, 275 (3-6), 115-24.
- Murphy, M. P. (2009), 'How mitochondria produce reactive oxygen species', *Biochem J*, 417 (1), 1-13.
- Murphy, M. P., et al. (2011), 'Unraveling the biological roles of reactive oxygen species', *Cell Metab*, 13 (4), 361-66.
- Nakamura, M., Fujiwara, Y., and Yamamoto, M. (1993), 'Homoplasmic and exclusive ND4 gene mutation in Japanese pedigrees with Leber's disease', *Invest Ophthalmol Vis Sci*, 34 (3), 488-95.
- Naviaux, R. K., et al. (1999), 'Mitochondrial DNA polymerase gamma deficiency and mtDNA depletion in a child with Alpers' syndrome', *Ann Neurol*, 45 (1), 54-8.
- Nelson, David L, Lehninger, Albert L, and Cox, Michael M (2008), *Lehninger principles of biochemistry* (Macmillan).
- Nesbitt, V., et al. (2013), 'The UK MRC Mitochondrial Disease Patient Cohort Study: clinical phenotypes associated with the m.3243A>G mutation--implications for diagnosis and management', *J Neurol Neurosurg Psychiatry*, 84 (8), 936-8.
- Ng, Yi Shiau, et al. (2016), 'Pseudo-obstruction, stroke, and mitochondrial dysfunction: A lethal combination', *Annals of neurology*, 80 (5), 686-92.

- Ngu, L. H., et al. (2012), 'A catalytic defect in mitochondrial respiratory chain complex I due to a mutation in NDUFS2 in a patient with Leigh syndrome', *Biochim Biophys Acta*, 1822 (2), 168-75.
- Nicholls, T. J. and Minczuk, M. (2014), 'In D-loop: 40 years of mitochondrial 7S DNA', *Exp Gerontol*, 56, 175-81.
- Noji, H., et al. (1997), 'Direct observation of the rotation of F1-ATPase', *Nature*, 386 (6622), 299-302.
- Nouws, J., et al. (2010), 'Acyl-CoA dehydrogenase 9 is required for the biogenesis of oxidative phosphorylation complex I', *Cell Metab*, 12 (3), 283-94.
- Nouws, Jessica, et al. (2014), 'A Patient with Complex I Deficiency Caused by a Novel ACAD9 Mutation Not Responding to Riboflavin Treatment', *JIMD reports*, 12, 37-45.
- Ogata, T. and Yamasaki, Y. (1997), 'Ultra-high-resolution scanning electron microscopy of mitochondria and sarcoplasmic reticulum arrangement in human red, white, and intermediate muscle fibers', *Anat Rec*, 248 (2), 214-23.
- Ogilvie, I., Kennaway, N. G., and Shoubridge, E. A. (2005), 'A molecular chaperone for mitochondrial complex I assembly is mutated in a progressive encephalopathy', *J Clin Invest*, 115 (10), 2784-92.
- Ojala, Deanna, Montoya, Julio, and Attardi, Giuseppe (1981), 'tRNA punctuation model of RNA processing in human mitochondria', *Nature*, 290 (5806), 470-74.
- Old, S. L. and Johnson, M. A. (1989), 'Methods of microphotometric assay of succinate dehydrogenase and cytochrome c oxidase activities for use on human skeletal muscle', *Histochem J*, 21 (9-10), 545-55.
- Orrenius, S., Zhivotovsky, B., and Nicotera, P. (2003), 'Regulation of cell death: the calcium-apoptosis link', *Nat Rev Mol Cell Biol*, 4 (7), 552-65.
- Ostergaard, E., et al. (2011), 'Respiratory chain complex I deficiency due to NDUFA12 mutations as a new cause of Leigh syndrome', *J Med Genet*, 48 (11), 737-40.
- Otera, H., et al. (2010), 'Mff is an essential factor for mitochondrial recruitment of Drp1 during mitochondrial fission in mammalian cells', *J Cell Biol*, 191 (6), 1141-58.
- Ozawa, Matsuko, Nonaka, Ikuya, and Goto, Yu-ichi (1998), 'Single muscle fiber analysis in patients with 3243 mutation in mitochondrial DNA: Comparison with the phenotype and the proportion of mutant genome', *Journal of the Neurological Sciences*, 159 (2), 170-75.
- Pacheu-Grau, D., et al. (2015), 'Cooperation between COA6 and SCO2 in COX2 maturation during cytochrome c oxidase assembly links two mitochondrial cardiomyopathies', *Cell Metab*, 21 (6), 823-33.

- Pagliarini, D. J., et al. (2008), 'A mitochondrial protein compendium elucidates complex I disease biology', *Cell*, 134 (1), 112-23.
- Palade, G. E. (1952), 'The fine structure of mitochondria', *Anat Rec*, 114 (3), 427-51.
- Palmer, C. S., et al. (2011), 'MiD49 and MiD51, new components of the mitochondrial fission machinery', *EMBO Rep*, 12 (6), 565-73.
- Parikh, S., et al. (2015), 'Diagnosis and management of mitochondrial disease: a consensus statement from the Mitochondrial Medicine Society', *Genet Med*, 17 (9), 689-701.
- Park, H., Davidson, E., and King, M. P. (2003), 'The pathogenic A3243G mutation in human mitochondrial tRNA^{Leu}(UUR) decreases the efficiency of aminoacylation', *Biochemistry*, 42 (4), 958-64.
- Perales-Clemente, E., et al. (2010), 'Five entry points of the mitochondrially encoded subunits in mammalian complex I assembly', *Mol Cell Biol*, 30 (12), 3038-47.
- Petruzzella, V., et al. (2001), 'A nonsense mutation in the NDUFS4 gene encoding the 18 kDa (AQDQ) subunit of complex I abolishes assembly and activity of the complex in a patient with Leigh-like syndrome', *Hum Mol Genet*, 10 (5), 529-35.
- Petruzzella, V., et al. (2004), 'Cerebellar ataxia as atypical manifestation of the 3243A>G MELAS mutation', *Clin Genet*, 65 (1), 64-5.
- Petruzzella, Vittorla, et al. (1994), 'Extremely high levels of mutant mtDNAs co-localize with cytochrome c oxidase-negative ragged-red fibers in patients harboring a point mutation at nt 3243', *Human molecular genetics*, 3 (3), 449-54.
- Pickett, Sarah J., et al. (2018), 'Phenotypic heterogeneity in m.3243A>G mitochondrial disease: The role of nuclear factors', *Annals of clinical and translational neurology*, 5 (3), 333-45.
- Piekutowska-Abramczuk, D., et al. (2018), 'NDUFB8 Mutations Cause Mitochondrial Complex I Deficiency in Individuals with Leigh-like Encephalomyopathy', *Am J Hum Genet*, 102 (3), 460-67.
- Pierce, G. F., et al. (1991), 'Role of platelet-derived growth factor in wound healing', *J Cell Biochem*, 45 (4), 319-26.
- Pitceathly, R. D., Rahman, S., and Hanna, M. G. (2012), 'Single deletions in mitochondrial DNA--molecular mechanisms and disease phenotypes in clinical practice', *Neuromuscul Disord*, 22 (7), 577-86.
- Plutino, Morgane, et al. (2018), 'Targeted next generation sequencing with an extended gene panel does not impact variant detection in mitochondrial diseases', *BMC Medical Genetics*, 19 (1), 57.

- Pogoryelov, D., et al. (2009), 'High-resolution structure of the rotor ring of a proton-dependent ATP synthase', *Nat Struct Mol Biol*, 16 (10), 1068-73.
- Porteous, W. K., et al. (1998), 'Bioenergetic consequences of accumulating the common 4977-bp mitochondrial DNA deletion', *Eur J Biochem*, 257 (1), 192-201.
- Puigserver, P., et al. (1998), 'A cold-inducible coactivator of nuclear receptors linked to adaptive thermogenesis', *Cell*, 92 (6), 829-39.
- Quinlan, C. L., et al. (2012), 'Mitochondrial complex II can generate reactive oxygen species at high rates in both the forward and reverse reactions', *J Biol Chem*, 287 (32), 27255-64.
- Raap, A. K., et al. (2012), 'Non-random mtDNA segregation patterns indicate a metastable heteroplasmic segregation unit in m.3243A>G cybrid cells', *PLoS One*, 7 (12), e52080.
- Rahman, Shamima, et al. (2000), 'Cytochrome oxidase immunohistochemistry: clues for genetic mechanisms', *Brain*, 123 (3), 591-600.
- Rebello, A. P., Dillon, L. M., and Moraes, C. T. (2011), 'Mitochondrial DNA transcription regulation and nucleoid organization', *J Inherit Metab Dis*, 34 (4), 941-51.
- Rehling, P., et al. (2003), 'Protein insertion into the mitochondrial inner membrane by a twin-pore translocase', *Science*, 299 (5613), 1747-51.
- Richter, C., Park, J. W., and Ames, B. N. (1988), 'Normal oxidative damage to mitochondrial and nuclear DNA is extensive', *Proc Natl Acad Sci U S A*, 85 (17), 6465-7.
- Rieske, J. S. (1976), 'Composition, structure, and function of complex III of the respiratory chain', *Biochim Biophys Acta*, 456 (2), 195-247.
- Riezman, H., et al. (1983), 'The outer membrane of yeast mitochondria: isolation of outside-out sealed vesicles', *Embo j*, 2 (7), 1105-11.
- Rikimaru, M., et al. (2012), 'Taurine ameliorates impaired the mitochondrial function and prevents stroke-like episodes in patients with MELAS', *Intern Med*, 51 (24), 3351-7.
- Ringel, R., et al. (2011), 'Structure of human mitochondrial RNA polymerase', *Nature*, 478 (7368), 269-73.
- Ripple, M. O., Kim, N., and Springett, R. (2013), 'Mammalian complex I pumps 4 protons per 2 electrons at high and physiological proton motive force in living cells', *J Biol Chem*, 288 (8), 5374-80.
- Robberson, D. L., Kasamatsu, H., and Vinograd, J. (1972), 'Replication of mitochondrial DNA. Circular replicative intermediates in mouse L cells', *Proc Natl Acad Sci U S A*, 69 (3), 737-41.

- Roberti, M., et al. (2006), 'MTERF3, the most conserved member of the mTERF-family, is a modular factor involved in mitochondrial protein synthesis', *Biochim Biophys Acta*, 1757 (9-10), 1199-206.
- Rocha, M. C., et al. (2015), 'A novel immunofluorescent assay to investigate oxidative phosphorylation deficiency in mitochondrial myopathy: understanding mechanisms and improving diagnosis', *Scientific reports*, 5, 15037-37.
- Rocha, M. C., et al. (2018), 'Pathological mechanisms underlying single large-scale mitochondrial DNA deletions', *Ann Neurol*, 83 (1), 115-30.
- Rorbach, J., et al. (2008), 'The human mitochondrial ribosome recycling factor is essential for cell viability', *Nucleic Acids Res*, 36 (18), 5787-99.
- Ross, J. M. (2011), 'Visualization of mitochondrial respiratory function using cytochrome c oxidase/succinate dehydrogenase (COX/SDH) double-labeling histochemistry', *J Vis Exp*, (57), e3266.
- Rossi, C. S. and Lehninger, A. L. (1964), 'STOICHIOMETRY OF RESPIRATORY STIMULATION, ACCUMULATION OF CA⁺⁺ AND PHOSPHATE, AND OXIDATIVE PHOSPHORYLATION IN RAT LIVER MITOCHONDRIA', *J Biol Chem*, 239, 3971-80.
- Rossignol, R., et al. (2003), 'Mitochondrial threshold effects', *Biochem J*, 370 (Pt 3), 751-62.
- Rossmannith, W. and Karwan, R. M. (1998), 'Characterization of human mitochondrial RNase P: novel aspects in tRNA processing', *Biochem Biophys Res Commun*, 247 (2), 234-41.
- Rubin, M. S. and Tzagoloff, A. (1973), 'Assembly of the mitochondrial membrane system. X. Mitochondrial synthesis of three of the subunit proteins of yeast cytochrome oxidase', *J Biol Chem*, 248 (12), 4275-9.
- Ryan, M. T., Wagner, R., and Pfanner, N. (2000), 'The transport machinery for the import of preproteins across the outer mitochondrial membrane', *Int J Biochem Cell Biol*, 32 (1), 13-21.
- Rygiel, Karolina A., Picard, Martin, and Turnbull, Doug M. (2016), 'The ageing neuromuscular system and sarcopenia: a mitochondrial perspective', *The Journal of physiology*, 594 (16), 4499-512.
- Saada, Ann, et al. (2009), 'Mutations in NDUFAF3 (C3ORF60), encoding an NDUFAF4 (C6ORF66)-interacting complex I assembly protein, cause fatal neonatal mitochondrial disease', *American journal of human genetics*, 84 (6), 718-27.
- Sabharwal, S. S. and Schumacker, P. T. (2014), 'Mitochondrial ROS in cancer: initiators, amplifiers or an Achilles' heel?', *Nat Rev Cancer*, 14 (11), 709-21.

- Sacconi, Sabrina, et al. (2008), 'A functionally dominant mitochondrial DNA mutation', *Human molecular genetics*, 17 (12), 1814-20.
- Sanchez-Caballero, L., Guerrero-Castillo, S., and Nijtmans, L. (2016), 'Unraveling the complexity of mitochondrial complex I assembly: A dynamic process', *Biochim Biophys Acta*, 1857 (7), 980-90.
- Sanger, F., Nicklen, S., and Coulson, A. R. (1977), 'DNA sequencing with chain-terminating inhibitors', *Proceedings of the National Academy of Sciences of the United States of America*, 74 (12), 5463-67.
- Santorelli, F. M., et al. (1997), 'Identification of a novel mutation in the mtDNA ND5 gene associated with MELAS', *Biochem Biophys Res Commun*, 238 (2), 326-8.
- Sarzi, Emmanuelle, et al. (2007), 'A novel recurrent mitochondrial DNA mutation in ND3 gene is associated with isolated complex I deficiency causing Leigh syndrome and dystonia', *American journal of medical genetics Part A*, 143 (1), 33-41.
- Sasarman, F., Antonicka, H., and Shoubridge, E. A. (2008), 'The A3243G tRNA^{Leu}(UUR) MELAS mutation causes amino acid misincorporation and a combined respiratory chain assembly defect partially suppressed by overexpression of EFTu and EFG2', *Hum Mol Genet*, 17 (23), 3697-707.
- Sazanov, L. A. (2015), 'A giant molecular proton pump: structure and mechanism of respiratory complex I', *Nat Rev Mol Cell Biol*, 16 (6), 375-88.
- Sazanov, L. A. and Hinchliffe, P. (2006), 'Structure of the hydrophilic domain of respiratory complex I from *Thermus thermophilus*', *Science*, 311 (5766), 1430-6.
- Schaefer, A. M., et al. (2006), 'Mitochondrial disease in adults: a scale to monitor progression and treatment', *Neurology*, 66 (12), 1932-4.
- Schaefer, A. M., et al. (2008), 'Prevalence of mitochondrial DNA disease in adults', *Ann Neurol*, 63 (1), 35-9.
- Schagger, H. and Pfeiffer, K. (2000), 'Supercomplexes in the respiratory chains of yeast and mammalian mitochondria', *Embo j*, 19 (8), 1777-83.
- (2001), 'The ratio of oxidative phosphorylation complexes I-V in bovine heart mitochondria and the composition of respiratory chain supercomplexes', *J Biol Chem*, 276 (41), 37861-7.
- Schatz, G. and Dobberstein, B. (1996), 'Common principles of protein translocation across membranes', *Science*, 271 (5255), 1519-26.
- Scherz-Shouval, R., et al. (2007), 'Reactive oxygen species are essential for autophagy and specifically regulate the activity of Atg4', *Embo j*, 26 (7), 1749-60.

- Schiaffino, S., et al. (1989), 'Three myosin heavy chain isoforms in type 2 skeletal muscle fibres', *J Muscle Res Cell Motil*, 10 (3), 197-205.
- Schiffer, Steffen, Rösch, Sylvia, and Marchfelder, Anita (2002), 'Assigning a function to a conserved group of proteins: the tRNA 3'-processing enzymes', *The EMBO journal*, 21 (11), 2769-77.
- Schmidt, O., Pfanner, N., and Meisinger, C. (2010), 'Mitochondrial protein import: from proteomics to functional mechanisms', *Nat Rev Mol Cell Biol*, 11 (9), 655-67.
- Schon, E. A., DiMauro, S., and Hirano, M. (2012), 'Human mitochondrial DNA: roles of inherited and somatic mutations', *Nat Rev Genet*, 13 (12), 878-90.
- Schon, E. A., et al. (1989), 'A direct repeat is a hotspot for large-scale deletion of human mitochondrial DNA', *Science*, 244 (4902), 346-9.
- Schuelke, M., et al. (1999), 'Mutant NDUFB1 subunit of mitochondrial complex I causes leukodystrophy and myoclonic epilepsy', *Nat Genet*, 21 (3), 260-1.
- Schulz, C., Schendzielorz, A., and Rehling, P. (2015), 'Unlocking the presequence import pathway', *Trends Cell Biol*, 25 (5), 265-75.
- Schwartz, M. and Vissing, J. (2002), 'Paternal inheritance of mitochondrial DNA', *N Engl J Med*, 347 (8), 576-80.
- Sciacco, M. and Bonilla, E. (1996), 'Cytochemistry and immunocytochemistry of mitochondria in tissue sections', *Methods Enzymol*, 264, 509-21.
- Sciacco, M., et al. (1994), 'Distribution of wild-type and common deletion forms of mtDNA in normal and respiration-deficient muscle fibers from patients with mitochondrial myopathy', *Hum Mol Genet*, 3 (1), 13-9.
- Scott, Iain and Youle, Richard J. (2010), 'Mitochondrial fission and fusion', *Essays in biochemistry*, 47, 85-98.
- Sena, L. A., et al. (2013), 'Mitochondria are required for antigen-specific T cell activation through reactive oxygen species signaling', *Immunity*, 38 (2), 225-36.
- Shanske, S., et al. (2004), 'Varying loads of the mitochondrial DNA A3243G mutation in different tissues: implications for diagnosis', *Am J Med Genet A*, 130a (2), 134-7.
- Shanske, S., et al. (2008), 'The G13513A mutation in the ND5 gene of mitochondrial DNA as a common cause of MELAS or Leigh syndrome: evidence from 12 cases', *Arch Neurol*, 65 (3), 368-72.
- Shi, Y., et al. (2012), 'Mammalian transcription factor A is a core component of the mitochondrial transcription machinery', *Proc Natl Acad Sci U S A*, 109 (41), 16510-5.
- Shoffner, J. M., et al. (1990), 'Myoclonic epilepsy and ragged-red fiber disease (MERRF) is associated with a mitochondrial DNA tRNA(Lys) mutation', *Cell*, 61 (6), 931-7.

- Shoubridge, E A (1998), 'Mitochondrial encephalomyopathies', *Current opinion in neurology*, 11 (5), 491-96.
- Shoubridge, E. A. (1995), 'Segregation of mitochondrial DNAs carrying a pathogenic point mutation (tRNA(Leu3243)) in cybrid cells', *Biochem Biophys Res Commun*, 213 (1), 189-95.
- Shoubridge, E. A. and Wai, T. (2007), 'Mitochondrial DNA and the mammalian oocyte', *Curr Top Dev Biol*, 77, 87-111.
- Shoubridge, Eric A. (2001), 'Cytochrome c oxidase deficiency', *American Journal of Medical Genetics*, 106 (1), 46-52.
- Shutt, T. E. and Gray, M. W. (2006), 'Bacteriophage origins of mitochondrial replication and transcription proteins', *Trends Genet*, 22 (2), 90-5.
- Sickmann, A., et al. (2003), 'The proteome of *Saccharomyces cerevisiae* mitochondria', *Proc Natl Acad Sci U S A*, 100 (23), 13207-12.
- Simard, Marie-Lune, et al. (2018), 'A novel histochemistry assay to assess and quantify focal cytochrome c oxidase deficiency', *The Journal of pathology*, 245 (3), 311-23.
- Singh, G., Lott, M. T, and Wallace, D. C (1989), 'A mitochondrial DNA mutation as a cause of Leber's hereditary optic neuropathy', *New England Journal of Medicine*, 320 (20), 1300-05.
- Sjostrand, F. S. (1953), 'Electron microscopy of mitochondria and cytoplasmic double membranes', *Nature*, 171 (4340), 30-2.
- Skladal, Daniela, Halliday, Jane, and Thorburn, David R. (2003), 'Minimum birth prevalence of mitochondrial respiratory chain disorders in children', *Brain*, 126 (8), 1905-12.
- Smeitink, J., van den Heuvel, L., and DiMauro, S. (2001), 'The genetics and pathology of oxidative phosphorylation', *Nat Rev Genet*, 2 (5), 342-52.
- Smerdu, V., et al. (2005), 'Identification of myosin heavy chain I, IIa and IIx in canine skeletal muscles by an electrophoretic and immunoblotting study', *Cells Tissues Organs*, 180 (2), 106-16.
- Smirnova, E., et al. (2001), 'Dynamin-related protein Drp1 is required for mitochondrial division in mammalian cells', *Mol Biol Cell*, 12 (8), 2245-56.
- Sofou, K., et al. (2018), 'Phenotype-genotype correlations in Leigh syndrome: new insights from a multicentre study of 96 patients', *J Med Genet*, 55 (1), 21-27.
- Sofou, Kalliopi, et al. (2014), 'A multicenter study on Leigh syndrome: disease course and predictors of survival', *Orphanet Journal of Rare Diseases*, 9 (1), 52.

- Soleimanpour-Lichaei, Hamid Reza, et al. (2007), 'mtRF1a is a human mitochondrial translation release factor decoding the major termination codons UAA and UAG', *Molecular cell*, 27 (5), 745-57.
- Song, Shiwei, et al. (2005), 'DNA precursor asymmetries in mammalian tissue mitochondria and possible contribution to mutagenesis through reduced replication fidelity', *Proceedings of the National Academy of Sciences of the United States of America*, 102 (14), 4990.
- Song, Z., et al. (2007), 'OPA1 processing controls mitochondrial fusion and is regulated by mRNA splicing, membrane potential, and Yme1L', *J Cell Biol*, 178 (5), 749-55.
- Soto, I. C., et al. (2012), 'Biogenesis and assembly of eukaryotic cytochrome c oxidase catalytic core', *Biochim Biophys Acta*, 1817 (6), 883-97.
- Sparaco, M., et al. (1995), 'Myoclonic epilepsy with ragged-red fibers (MERRF): an immunohistochemical study of the brain', *Brain Pathol*, 5 (2), 125-33.
- Spelbrink, J. N., et al. (2001), 'Human mitochondrial DNA deletions associated with mutations in the gene encoding Twinkle, a phage T7 gene 4-like protein localized in mitochondria', *Nat Genet*, 28 (3), 223-31.
- Sperl, W., et al. (2015), 'The spectrum of pyruvate oxidation defects in the diagnosis of mitochondrial disorders', *J Inherit Metab Dis*, 38 (3), 391-403.
- Spiegel, Ronen, et al. (2009), 'Mutated NDUFS6 is the cause of fatal neonatal lactic acidemia in Caucasus Jews', *European journal of human genetics : EJHG*, 17 (9), 1200-03.
- Spinazzola, A., et al. (2006), 'MPV17 encodes an inner mitochondrial membrane protein and is mutated in infantile hepatic mitochondrial DNA depletion', *Nat Genet*, 38 (5), 570-5.
- St-Jean-Pelletier, F., et al. (2017), 'The impact of ageing, physical activity, and pre-frailty on skeletal muscle phenotype, mitochondrial content, and intramyocellular lipids in men', *J Cachexia Sarcopenia Muscle*, 8 (2), 213-28.
- Stehling, O. and Lill, R. (2013), 'The role of mitochondria in cellular iron-sulfur protein biogenesis: mechanisms, connected processes, and diseases', *Cold Spring Harb Perspect Biol*, 5 (8), a011312.
- Stewart, J. B. and Chinnery, P. F. (2015), 'The dynamics of mitochondrial DNA heteroplasmy: implications for human health and disease', *Nat Rev Genet*, 16 (9), 530-42.
- Straub, S. P., et al. (2016), 'Dynamic organization of the mitochondrial protein import machinery', *Biol Chem*, 397 (11), 1097-114.

- Stroud, D. A., et al. (2016), 'Accessory subunits are integral for assembly and function of human mitochondrial complex I', *Nature*, 538 (7623), 123-26.
- Sugiana, C., et al. (2008), 'Mutation of C20orf7 disrupts complex I assembly and causes lethal neonatal mitochondrial disease', *Am J Hum Genet*, 83 (4), 468-78.
- Sun, F., et al. (2005), 'Crystal structure of mitochondrial respiratory membrane protein complex II', *Cell*, 121 (7), 1043-57.
- Susin, S. A., et al. (1999), 'Molecular characterization of mitochondrial apoptosis-inducing factor', *Nature*, 397 (6718), 441-6.
- Sutovsky, P., et al. (2000), 'Ubiquitinated sperm mitochondria, selective proteolysis, and the regulation of mitochondrial inheritance in mammalian embryos', *Biol Reprod*, 63 (2), 582-90.
- Suzuki, Susumu, et al. (2003), 'Clinical features of diabetes mellitus with the mitochondrial DNA 3243 (A–G) mutation in Japanese: Maternal inheritance and mitochondria-related complications', *Diabetes Research and Clinical Practice*, 59 (3), 207-17.
- Suzuki, T., et al. (2002), 'Taurine as a constituent of mitochondrial tRNAs: new insights into the functions of taurine and human mitochondrial diseases', *Embo j*, 21 (23), 6581-9.
- Swalwell, H., et al. (2011), 'Respiratory chain complex I deficiency caused by mitochondrial DNA mutations', *Eur J Hum Genet*, 19 (7), 769-75.
- Szabo, I. and Zoratti, M. (2014), 'Mitochondrial channels: ion fluxes and more', *Physiol Rev*, 94 (2), 519-608.
- Takemoto, C., et al. (1995), 'The ability of bovine mitochondrial transfer RNAMet to decode AUG and AUA codons', *Biochimie*, 77 (1-2), 104-8.
- Tang, S., et al. (2011), 'Mitochondrial DNA polymerase gamma mutations: an ever expanding molecular and clinical spectrum', *J Med Genet*, 48 (10), 669-81.
- Tanji, N., et al. (2001), 'Adefovir nephrotoxicity: possible role of mitochondrial DNA depletion', *Hum Pathol*, 32 (7), 734-40.
- Taylor, R. W. and Turnbull, D. M. (2005), 'Mitochondrial DNA mutations in human disease', *Nat Rev Genet*, 6 (5), 389-402.
- Taylor, R. W., et al. (2003), 'A homoplasmic mitochondrial transfer ribonucleic acid mutation as a cause of maternally inherited hypertrophic cardiomyopathy', *J Am Coll Cardiol*, 41 (10), 1786-96.
- Taylor, R. W., et al. (2014), 'Use of whole-exome sequencing to determine the genetic basis of multiple mitochondrial respiratory chain complex deficiencies', *Jama*, 312 (1), 68-77.

- Thompson, K., et al. (2019), 'Recent advances in understanding the molecular genetic basis of mitochondrial disease', *J Inherit Metab Dis*.
- Tiranti, V., et al. (1997), 'Identification of the gene encoding the human mitochondrial RNA polymerase (h-mtRPOL) by cyberscreening of the Expressed Sequence Tags database', *Hum Mol Genet*, 6 (4), 615-25.
- Tiranti, V., et al. (1998), 'Mutations of SURF-1 in Leigh disease associated with cytochrome c oxidase deficiency', *Am J Hum Genet*, 63 (6), 1609-21.
- Tokunaga, M., et al. (1994), 'Single muscle fiber analysis of mitochondrial myopathy, encephalopathy, lactic acidosis, and stroke-like episodes (MELAS)', *Ann Neurol*, 35 (4), 413-9.
- Tondera, D., et al. (2005), 'The mitochondrial protein MTP18 contributes to mitochondrial fission in mammalian cells', *J Cell Sci*, 118 (Pt 14), 3049-59.
- Tondera, D., et al. (2004), 'Knockdown of MTP18, a novel phosphatidylinositol 3-kinase-dependent protein, affects mitochondrial morphology and induces apoptosis', *J Biol Chem*, 279 (30), 31544-55.
- Triepels, R., et al. (1998), 'The nuclear-encoded human NADH:ubiquinone oxidoreductase NDUFA8 subunit: cDNA cloning, chromosomal localization, tissue distribution, and mutation detection in complex-I-deficient patients', *Hum Genet*, 103 (5), 557-63.
- Triepels, R. H., et al. (1999), 'Leigh syndrome associated with a mutation in the NDUFS7 (PSST) nuclear encoded subunit of complex I', *Ann Neurol*, 45 (6), 787-90.
- Tsukihara, T., et al. (1996), 'The whole structure of the 13-subunit oxidized cytochrome c oxidase at 2.8 Å', *Science*, 272 (5265), 1136-44.
- Turrens, J. F. (2003), 'Mitochondrial formation of reactive oxygen species', *J Physiol*, 552 (Pt 2), 335-44.
- Turrens, J. F. and Boveris, A. (1980), 'Generation of superoxide anion by the NADH dehydrogenase of bovine heart mitochondria', *Biochem J*, 191 (2), 421-7.
- Ugalde, C., et al. (2007), 'Mutated ND2 impairs mitochondrial complex I assembly and leads to Leigh syndrome', *Mol Genet Metab*, 90 (1), 10-4.
- Ugalde, C., et al. (2003), 'Impaired complex I assembly in a Leigh syndrome patient with a novel missense mutation in the ND6 gene', *Ann Neurol*, 54 (5), 665-9.
- van den Bosch, B. J., et al. (2012), 'Defective NDUFA9 as a novel cause of neonatally fatal complex I disease', *J Med Genet*, 49 (1), 10-5.
- van den Ouweland, J. M., et al. (1992), 'Mutation in mitochondrial tRNA(Leu)(UUR) gene in a large pedigree with maternally transmitted type II diabetes mellitus and deafness', *Nat Genet*, 1 (5), 368-71.

- Van Goethem, G., et al. (2001), 'Mutation of POLG is associated with progressive external ophthalmoplegia characterized by mtDNA deletions', *Nat Genet*, 28 (3), 211-2.
- van Rahden, Vanessa A., et al. (2015), 'Mutations in NDUFB11, encoding a complex I component of the mitochondrial respiratory chain, cause microphthalmia with linear skin defects syndrome', *American journal of human genetics*, 96 (4), 640-50.
- van Rahden, Vanessa A, et al. (2015), 'Mutations in NDUFB11, Encoding a Complex I Component of the Mitochondrial Respiratory Chain, Cause Microphthalmia with Linear Skin Defects Syndrome', *The American Journal of Human Genetics*, 96 (4), 640-50.
- Verhaak, Christianne, et al. (2016), 'Quality of life, fatigue and mental health in patients with the m.3243A > G mutation and its correlates with genetic characteristics and disease manifestation', *Orphanet journal of rare diseases*, 11, 25-25.
- Vilarinho, L., et al. (1997), 'The mitochondrial A3243G mutation presenting as severe cardiomyopathy', *J Med Genet*, 34 (7), 607-9.
- Villinger, Saskia, et al. (2010), 'Functional dynamics in the voltage-dependent anion channel', *Proceedings of the National Academy of Sciences of the United States of America*, 107 (52), 22546-51.
- Vincent, Amy E., et al. (2016a), 'Mitochondrial dysfunction in myofibrillar myopathy', *Neuromuscular disorders : NMD*, 26 (10), 691-701.
- Vincent, Amy E., et al. (2016b), 'Dysferlin mutations and mitochondrial dysfunction', *Neuromuscular Disorders*, 26 (11), 782-88.
- Vincent, Amy E., et al. (2018), 'Subcellular origin of mitochondrial DNA deletions in human skeletal muscle', *Annals of neurology*, 84 (2), 289-301.
- Vinothkumar, K. R., Zhu, J., and Hirst, J. (2014), 'Architecture of mammalian respiratory complex I', *Nature*, 515 (7525), 80-84.
- Virbasius, J. V. and Scarpulla, R. C. (1994), 'Activation of the human mitochondrial transcription factor A gene by nuclear respiratory factors: a potential regulatory link between nuclear and mitochondrial gene expression in organelle biogenesis', *Proc Natl Acad Sci U S A*, 91 (4), 1309-13.
- Vogel, F., et al. (2006), 'Dynamic subcompartmentalization of the mitochondrial inner membrane', *J Cell Biol*, 175 (2), 237-47.
- Vogel, R. O., Smeitink, J. A., and Nijtmans, L. G. (2007), 'Human mitochondrial complex I assembly: a dynamic and versatile process', *Biochim Biophys Acta*, 1767 (10), 1215-27.

- Vogtle, F. N., et al. (2009), 'Global analysis of the mitochondrial N-proteome identifies a processing peptidase critical for protein stability', *Cell*, 139 (2), 428-39.
- Wai, T. and Langer, T. (2016), 'Mitochondrial Dynamics and Metabolic Regulation', *Trends Endocrinol Metab*, 27 (2), 105-17.
- Wai, T., et al. (2010), 'The role of mitochondrial DNA copy number in mammalian fertility', *Biol Reprod*, 83 (1), 52-62.
- Wallace, D. C. (1992), 'Mitochondrial genetics: a paradigm for aging and degenerative diseases?', *Science*, 256 (5057), 628-32.
- Wallace, D. C., et al. (1988), 'Mitochondrial DNA mutation associated with Leber's hereditary optic neuropathy', *Science*, 242 (4884), 1427-30.
- Walther, D. M., et al. (2009), 'Signals in bacterial beta-barrel proteins are functional in eukaryotic cells for targeting to and assembly in mitochondria', *Proc Natl Acad Sci U S A*, 106 (8), 2531-6.
- Wang, B., et al. (2017), 'A Novel Potentially Causative Variant of NDUFAF7 Revealed by Mutation Screening in a Chinese Family With Pathologic Myopia', *Invest Ophthalmol Vis Sci*, 58 (10), 4182-92.
- Wang, C. and Youle, R. J. (2009), 'The role of mitochondria in apoptosis*', *Annu Rev Genet*, 43, 95-118.
- Wang, X. (2001), 'The expanding role of mitochondria in apoptosis', *Genes Dev*, 15 (22), 2922-33.
- Wang, Y. and Bogenhagen, D. F. (2006), 'Human mitochondrial DNA nucleoids are linked to protein folding machinery and metabolic enzymes at the mitochondrial inner membrane', *J Biol Chem*, 281 (35), 25791-802.
- Wanrooij, S., et al. (2008), 'Human mitochondrial RNA polymerase primes lagging-strand DNA synthesis in vitro', *Proc Natl Acad Sci U S A*, 105 (32), 11122-7.
- Ward J, Joe H (1963), 'Hierarchical grouping to optimize an objective function', *Journal of the American statistical association*, 58 (301), 236-44.
- Watanabe, Kimitsuna (2010), 'Unique features of animal mitochondrial translation systems. The non-universal genetic code, unusual features of the translational apparatus and their relevance to human mitochondrial diseases', *Proceedings of the Japan Academy. Series B, Physical and biological sciences*, 86 (1), 11-39.
- Watt, Ian N., et al. (2010), 'Bioenergetic cost of making an adenosine triphosphate molecule in animal mitochondria', *Proceedings of the National Academy of Sciences*, 107 (39), 16823.

- Weidner, Uwe, et al. (1993), 'The gene locus of the proton-translocating NADH: ubiquinone oxidoreductase in *Escherichia coli*: organization of the 14 genes and relationship between the derived proteins and subunits of mitochondrial complex I', *Journal of molecular biology*, 233 (1), 109-22.
- West, A. P., Shadel, G. S., and Ghosh, S. (2011), 'Mitochondria in innate immune responses', *Nat Rev Immunol*, 11 (6), 389-402.
- Westermann, B. (2010), 'Mitochondrial fusion and fission in cell life and death', *Nat Rev Mol Cell Biol*, 11 (12), 872-84.
- (2012), 'Bioenergetic role of mitochondrial fusion and fission', *Biochim Biophys Acta*, 1817 (10), 1833-8.
- Wickham, Hadley (2011), 'The Split-Apply-Combine Strategy for Data Analysis', *Journal of Statistical Software; Vol 1, Issue 1 (2011)*.
- (2016), *ggplot2: elegant graphics for data analysis* (Springer).
- Wilson, K. S. and Prochaska, L. J. (1990), 'Phospholipid vesicles containing bovine heart mitochondrial cytochrome c oxidase and subunit III-deficient enzyme: analysis of respiratory control and proton translocating activities', *Arch Biochem Biophys*, 282 (2), 413-20.
- Wirth, C., et al. (2016), 'Structure and function of mitochondrial complex I', *Biochim Biophys Acta*, 1857 (7), 902-14.
- Wittenhagen, Lisa M and Kelley, Shana O (2002), 'Dimerization of a pathogenic human mitochondrial tRNA', *Nature Structural & Molecular Biology*, 9 (8), 586.
- Wortmann, S. B., et al. (2015), 'Whole exome sequencing of suspected mitochondrial patients in clinical practice', *J Inherit Metab Dis*, 38 (3), 437-43.
- Wu, C. K., et al. (2001), 'The 2.0 Å structure of human ferrochelatase, the terminal enzyme of heme biosynthesis', *Nat Struct Biol*, 8 (2), 156-60.
- Wu, M., et al. (2016), 'Structure of Mammalian Respiratory Supercomplex I₁III₂IV₁', *Cell*, 167 (6), 1598-609.e10.
- Xia, D., et al. (1997), 'Crystal structure of the cytochrome bc₁ complex from bovine heart mitochondria', *Science*, 277 (5322), 60-6.
- Yakubovskaya, E., et al. (2010), 'Helix unwinding and base flipping enable human MTERF1 to terminate mitochondrial transcription', *Cell*, 141 (6), 982-93.
- Yang, M. Y., et al. (2002), 'Biased incorporation of ribonucleotides on the mitochondrial L-strand accounts for apparent strand-asymmetric DNA replication', *Cell*, 111 (4), 495-505.

- Yasukawa, T., et al. (2000), 'Modification defect at anticodon wobble nucleotide of mitochondrial tRNAs(Leu)(UUR) with pathogenic mutations of mitochondrial myopathy, encephalopathy, lactic acidosis, and stroke-like episodes', *J Biol Chem*, 275 (6), 4251-7.
- Yasukawa, Takehiro, et al. (2006), 'Replication of vertebrate mitochondrial DNA entails transient ribonucleotide incorporation throughout the lagging strand', *The EMBO journal*, 25 (22), 5358-71.
- Yatsuga, S., et al. (2012), 'MELAS: a nationwide prospective cohort study of 96 patients in Japan', *Biochim Biophys Acta*, 1820 (5), 619-24.
- Yen, M. Y., et al. (2002), 'Leber's hereditary optic neuropathy--the spectrum of mitochondrial DNA mutations in Chinese patients', *Jpn J Ophthalmol*, 46 (1), 45-51.
- Yokota, Mutsumi, et al. (2015), 'Mitochondrial respiratory dysfunction caused by a heteroplasmic mitochondrial DNA mutation blocks cellular reprogramming', *Human Molecular Genetics*, 24 (16), 4698-709.
- Yokoyama, S., et al. (1985), 'Molecular mechanism of codon recognition by tRNA species with modified uridine in the first position of the anticodon', *Proc Natl Acad Sci U S A*, 82 (15), 4905-9.
- Yoneda, M., et al. (1992), 'Marked replicative advantage of human mtDNA carrying a point mutation that causes the MELAS encephalomyopathy', *Proceedings of the National Academy of Sciences of the United States of America*, 89 (23), 11164-68.
- Yu-Wai-Man, P., et al. (2009), 'Inherited mitochondrial optic neuropathies', *J Med Genet*, 46 (3), 145-58.
- Yu-Wai-Man, P., et al. (2003), 'The epidemiology of Leber hereditary optic neuropathy in the North East of England', *Am J Hum Genet*, 72 (2), 333-9.
- Yu, C. A., et al. (1999), 'Structure and reaction mechanisms of multifunctional mitochondrial cytochrome bc1 complex', *Biofactors*, 9 (2-4), 103-9.
- Zerbes, R. M., et al. (2012), 'Role of MINOS in mitochondrial membrane architecture: cristae morphology and outer membrane interactions differentially depend on mitofilin domains', *J Mol Biol*, 422 (2), 183-91.
- Zeviani, M., et al. (1988), 'Deletions of mitochondrial DNA in Kearns-Sayre syndrome', *Neurology*, 38 (9), 1339-46.
- Zhang, Y. and Spremulli, L. L. (1998), 'Identification and cloning of human mitochondrial translational release factor 1 and the ribosome recycling factor', *Biochim Biophys Acta*, 1443 (1-2), 245-50.

- Zhu, J., Vinothkumar, K. R., and Hirst, J. (2016), 'Structure of mammalian respiratory complex I', *Nature*, 536 (7616), 354-58.
- Zhu, Z., et al. (1998), 'SURF1, encoding a factor involved in the biogenesis of cytochrome c oxidase, is mutated in Leigh syndrome', *Nat Genet*, 20 (4), 337-43.
- Zickermann, V., et al. (2015), 'Structural biology. Mechanistic insight from the crystal structure of mitochondrial complex I', *Science*, 347 (6217), 44-9.
- Zierz, C. M., Joshi, P. R., and Zierz, S. (2015), 'Frequencies of myohistological mitochondrial changes in patients with mitochondrial DNA deletions and the common m.3243A>G point mutation', *Neuropathology*, 35 (2), 130-6.
- Zollo, Ornella, Tiranti, Valeria, and Sondheimer, Neal (2012), 'Transcriptional requirements of the distal heavy-strand promoter of mtDNA', *Proceedings of the National Academy of Sciences*, 109 (17), 6508.